

# Density Model for Fin Whale (*Balaenoptera physalus*) for the U.S. East Coast: Supplementary Report

## Model Version 12.1

Duke University Marine Geospatial Ecology Laboratory\*

2023-05-27


## Citation

When citing our methodology or results generally, please cite Roberts et al. (2016, 2023). The complete references appear at the end of this document. We are preparing a new article for a peer-reviewed journal that will eventually replace those. Until that is published, those are the best general citations.

When citing this model specifically, please use this reference:

Roberts JJ, Yack TM, Cañadas A, Fujioka E, Halpin PN, Barco SG, Boisseau O, Chavez-Rosales S, Cole TVN, Cotter MP, Cummings EW, Davis GE, DiGiovanni Jr. RA, Garrison LP, Gowan TA, Jackson KA, Kenney RD, Khan CB, Lockhart GG, Lomac-MacNair KS, McAlarney RJ, McLellan WA, Mullin KD, Nowacek DP, O'Brien O, Pabst DA, Palka DL, Quintana-Rizzo E, Redfern JV, Rickard ME, White M, Whitt AD, Zoidis AM (2022) Density Model for Fin Whale (*Balaenoptera physalus*) for the U.S. East Coast, Version 12.1, 2023-05-27, and Supplementary Report. Marine Geospatial Ecology Laboratory, Duke University, Durham, North Carolina.

## Copyright and License

 This document and the accompanying results are © 2023 by the Duke University Marine Geospatial Ecology Laboratory and are licensed under a [Creative Commons Attribution 4.0 International License](https://creativecommons.org/licenses/by/4.0/).

## Model Version History

---

Version	Date	Description
1	2013-05-10	Initial version.

---

---

\*For questions or to offer feedback please contact Jason Roberts ([jason.roberts@duke.edu](mailto:jason.roberts@duke.edu)) and Tina Yack ([tina.yack@duke.edu](mailto:tina.yack@duke.edu))



(continued)

---

Version	Date	Description
2	2014-03-01	Switched from four seasonal models to two. Reformulated density model using a Horvitz-Thompson estimator. Eliminated GAM for group size (consequence of above). Added group size as a candidate covariate in detection functions (benefit of above). Added survey ID as a candidate covariate in NOAA NARWSS detection functions. Took more care in selecting right-truncation distances. Fitted models with contemporaneous predictors, for comparison to climatological. Switched SST and SST fronts predictors from NOAA Pathfinder to GHRSSST CMC0.2deg L4. Changed SST fronts algorithm to use Canny operator instead of Cayula-Cornillon. Switched winds predictors from SCOW to CCMP (SCOW only gives climatol. estimates.) Added DistToEddy predictors, based on Chelton et al. (2011) eddy database. Added cumulative VGPM predictors, summing productivity for 45, 90, and 180 days. Added North Atlantic Oscillation (NAO) predictor; included 3 and 6 month lags. Transformed predictors more carefully, to better minimize leverage of outliers. Implemented hybrid hierarchical-forward / exhaustive model selection procedure. Model selection procedure better avoids concurrency between predictors. Allowed GAMs to select between multiple formulations of dynamic predictors. Adjusted land mask to eliminate additional estuaries and hard-to-predict cells.
3	2014-05-20	Fixed bug in temporal variability plots. Density models unchanged.
4	2013-06-02	Added Reclassification of Ambiguous Sightings section, which was accidentally omitted. Density models unchanged.
5	2014-09-02	Added surveys: NJ-DEP, Virginia Aquarium, NARWSS 2013, UNCW 2013. Extended study area up Scotian Shelf. Added SEAPODYM predictors. Switched to mgcv estimation of Tweedie p parameter (family=tw()).
6	2014-10-18	Switched to a single season model. Added Palka (2006) survey-specific $g(0)$ estimates. Updated distance to eddy predictors using Chelton et al.'s 2014 database. Removed distance to eddy and wind speed predictors. Fixed missing pixels in several climatological predictors, which led to not all segments being utilized. Eliminated Cape Cod Bay subregion.
7	2014-11-03	Fixed error in $g(0)$ for NEFSC Abel-J Binocular Surveys: previously used 0.87; changed to correct value, 0.32, and refitted the model. Updated documentation.
8	2014-11-10	Reconfigured detection hierarchy and adjusted NARWSS detection functions based on additional information from Tim Cole. Removed CumVGPM180 predictor. Updated documentation.
9	2014-12-03	Fixed bug that applied the wrong detection function to segments NE_narwss_1999_widgeon_hapo dataset. Refitted model. Updated documentation.
9.1	2015-02-02	Updated the documentation. No changes to the model.
9.2	2015-05-14	Updated calculation of CVs. Switched density rasters to logarithmic breaks. No changes to the model.
9.3	2015-09-26	Updated the documentation. No changes to the model.
9.4	2016-04-21	Switched calculation of monthly 5% and 95% confidence interval rasters to the method used to produce the year-round rasters. (We intended this to happen in version 9.2 but I did not implement it properly.) No changes to the other rasters or the model itself. Model files released as supplementary information to Roberts et al. (2016).
10	2017-06-01	Began update to Roberts et al. (2015) model. Introduced new surveys from AMAPPS, NARWSS, UNCW, VAMSC, and the SEUS NARW teams. Updated modeling methodology. Refitted detection functions and spatial models from scratch using new and reprocessed covariates. Model released as part of a scheduled update to the U.S. Navy Marine Species Density Database (NMSDD).
11	2018-04-22	Discovered that model version 10 erroneously excluded ambiguous "fin or sei whale" sightings classified as fin whales. Refitted the model with them included. The functional form of the resulting model was essentially the same but deviance explained rose from 36% to 40%. Predicted density showed a similar spatiotemporal pattern but total abundance rose about 15%, reflecting the additional sightings introduced into the model. Model released as part of a scheduled update to the U.S. Navy Marine Species Density Database (NMSDD).

*(continued)*

---

Version	Date	Description
12	2022-06-20	This model is a major update over the prior version, with substantial additional data, improved statistical methods, and an increased spatial resolution. It was released as part of the final delivery of the U.S. Navy Marine Species Density Database (NMSDD) for the Atlantic Fleet Testing and Training (AFTT) Phase IV Environmental Impact Statement. Several new collaborators joined and contributed survey data: New York State Department of Environmental Conservation, TetraTech, HDR, and Marine Conservation Research. We incorporated additional surveys from all continuing and new collaborators through the end of 2020. (Because some environmental covariates were only available through 2019, certain models only extend through 2019.) We increased the spatial resolution to 5 km and, at NOAA's request, we extended the model further inshore from New York through Maine. We reformulated and refitted all detection functions and spatial models. We updated all environmental covariates to newer products, when available, and added several covariates to the set of candidates. For models that incorporated dynamic covariates, we estimated model uncertainty using a new method that accounts for both model parameter error and temporal variability.
12.1	2023-05-27	Completed the supplementary report documenting the details of this model. The model itself was not changed.

---

# 1 Survey Data

We built this model from data collected between 1998-2020 (Table 1, Figure 1). In keeping with our primary strategy for the 2022 modeling cycle, we excluded data prior to 1998 in order to utilize biological covariates derived from satellite ocean color observations, which were only available for a few months before 1998. We restricted the model to survey transects with sea states of Beaufort 5 or less (for a few surveys we used Beaufort 4 or less) for both aerial and shipboard surveys. We also excluded transects with poor weather or visibility for surveys that reported those conditions.

Table 1: Survey effort and observations considered for this model. Effort is tallied as the cumulative length of on-effort transects. Observations are the number of groups and individuals encountered while on effort. Off effort observations and those lacking an estimate of group size or distance to the group were excluded.

Institution	Program	Period	Effort		Observations	
			1000s km	Groups	Individuals	Mean Group Size
<b>Aerial Surveys</b>						
HDR	Navy Norfolk Canyon	2018-2019	11	19	30	1.6
NEAq	CNM	2017-2020	2	15	16	1.1
NEAq	MMS-WEA	2017-2020	37	51	93	1.8
NEAq	NLPSC	2011-2015	43	75	126	1.7
NEFSC	AMAPPS	2010-2019	89	131	158	1.2
NEFSC	NARWSS	2003-2020	484	2,192	3,213	1.5
NEFSC	Pre-AMAPPS	1999-2008	46	144	175	1.2
NJDEP	NJEBS	2008-2009	11	1	1	1.0
NYS-DEC/TT	NYBWM	2017-2020	77	82	149	1.8
SEFSC	AMAPPS	2010-2020	114	28	38	1.4
SEFSC	MATS	2002-2005	27	6	13	2.2
UNCW	MidA Bottlenose	2002-2002	17	1	2	2.0
UNCW	Navy Cape Hatteras	2011-2017	34	5	7	1.4
UNCW	Navy Jacksonville	2009-2017	92	0	0	
UNCW	Navy Norfolk Canyon	2015-2017	14	8	9	1.1
UNCW	Navy Onslow Bay	2007-2011	49	1	1	1.0
UNCW	SEUS NARW EWS	2005-2008	114	12	31	2.6
VAMSC	MD DNR WEA	2013-2015	16	8	13	1.6
VAMSC	Navy VACAPES	2016-2017	19	1	2	2.0
VAMSC	VA CZM WEA	2012-2015	21	11	27	2.5
		<b>Total</b>	<b>1,319</b>	<b>2,791</b>	<b>4,104</b>	<b>1.5</b>
<b>Shipboard Surveys</b>						
MCR	SOTW Visual	2012-2019	9	19	29	1.5
NEFSC	AMAPPS	2011-2016	16	259	365	1.4
NEFSC	Pre-AMAPPS	1998-2007	14	137	190	1.4
NJDEP	NJEBS	2008-2009	14	24	35	1.5
SEFSC	AMAPPS	2011-2016	17	5	7	1.4
SEFSC	Pre-AMAPPS	1998-2006	30	11	15	1.4
		<b>Total</b>	<b>99</b>	<b>455</b>	<b>641</b>	<b>1.4</b>
		<b>Grand Total</b>	<b>1,417</b>	<b>3,246</b>	<b>4,745</b>	<b>1.5</b>

Table 2: Institutions that contributed surveys used in this model.

Institution	Full Name
HDR	HDR, Inc.
MCR	Marine Conservation Research
NEAq	New England Aquarium
NEFSC	NOAA Northeast Fisheries Science Center
NJDEP	New Jersey Department of Environmental Protection
NYS-DEC/TT	New York State Department of Environmental Conservation and Tetra Tech, Inc.

Table 2: Institutions that contributed surveys used in this model. *(continued)*

Institution	Full Name
SEFSC	NOAA Southeast Fisheries Science Center
UNCW	University of North Carolina Wilmington
VAMSC	Virginia Aquarium & Marine Science Center

Table 3: Descriptions and references for survey programs used in this model.

Program	Description	References
AMAPPS	Atlantic Marine Assessment Program for Protected Species	Palka et al. (2017), Palka et al. (2021)
CNM	Northeast Canyons Marine National Monument Aerial Surveys	Redfern et al. (2021)
MATS	Mid-Atlantic Tursiops Surveys	
MD DNR WEA	Aerial Surveys of the Maryland Wind Energy Area	Barco et al. (2015)
MidA Bottlenose	Mid-Atlantic Onshore/Offshore Bottlenose Dolphin Surveys	Torres et al. (2005)
MMS-WEA	Marine Mammal Surveys of the MA and RI Wind Energy Areas	Quintana-Rizzo et al. (2021), O'Brien et al. (2022)
NARWSS	North Atlantic Right Whale Sighting Surveys	Cole et al. (2007)
Navy Cape Hatteras	Aerial Surveys of the Navy's Cape Hatteras Study Area	McLellan et al. (2018)
Navy Jacksonville	Aerial Surveys of the Navy's Jacksonville Study Area	Foley et al. (2019)
Navy Norfolk Canyon	Aerial Surveys of the Navy's Norfolk Canyon Study Area	Cotter (2019), McAlarney et al. (2018)
Navy Onslow Bay	Aerial Surveys of the Navy's Onslow Bay Study Area	Read et al. (2014)
Navy VACAPES	Aerial Survey Baseline Monitoring in the Continental Shelf Region of the VACAPES OPAREA	Mallette et al. (2017)
NJEBS	New Jersey Ecological Baseline Study	Geo-Marine, Inc. (2010), Whitt et al. (2015)
NLPSC	Northeast Large Pelagic Survey Collaborative Aerial Surveys	Leiter et al. (2017), Stone et al. (2017)
NYBWM	New York Bight Whale Monitoring Surveys	Zoidis et al. (2021)
Pre-AMAPPS	Pre-AMAPPS Marine Mammal Abundance Surveys	Mullin and Fulling (2003), Garrison et al. (2010), Palka (2006)
SEUS NARW EWS	Southeast U.S. Right Whale Early Warning System Surveys	
SOTW Visual	R/V Song of the Whale Visual Surveys	Ryan et al. (2013)
VA CZM WEA	Virginia CZM Wind Energy Area Surveys	Mallette et al. (2014), Mallette et al. (2015)

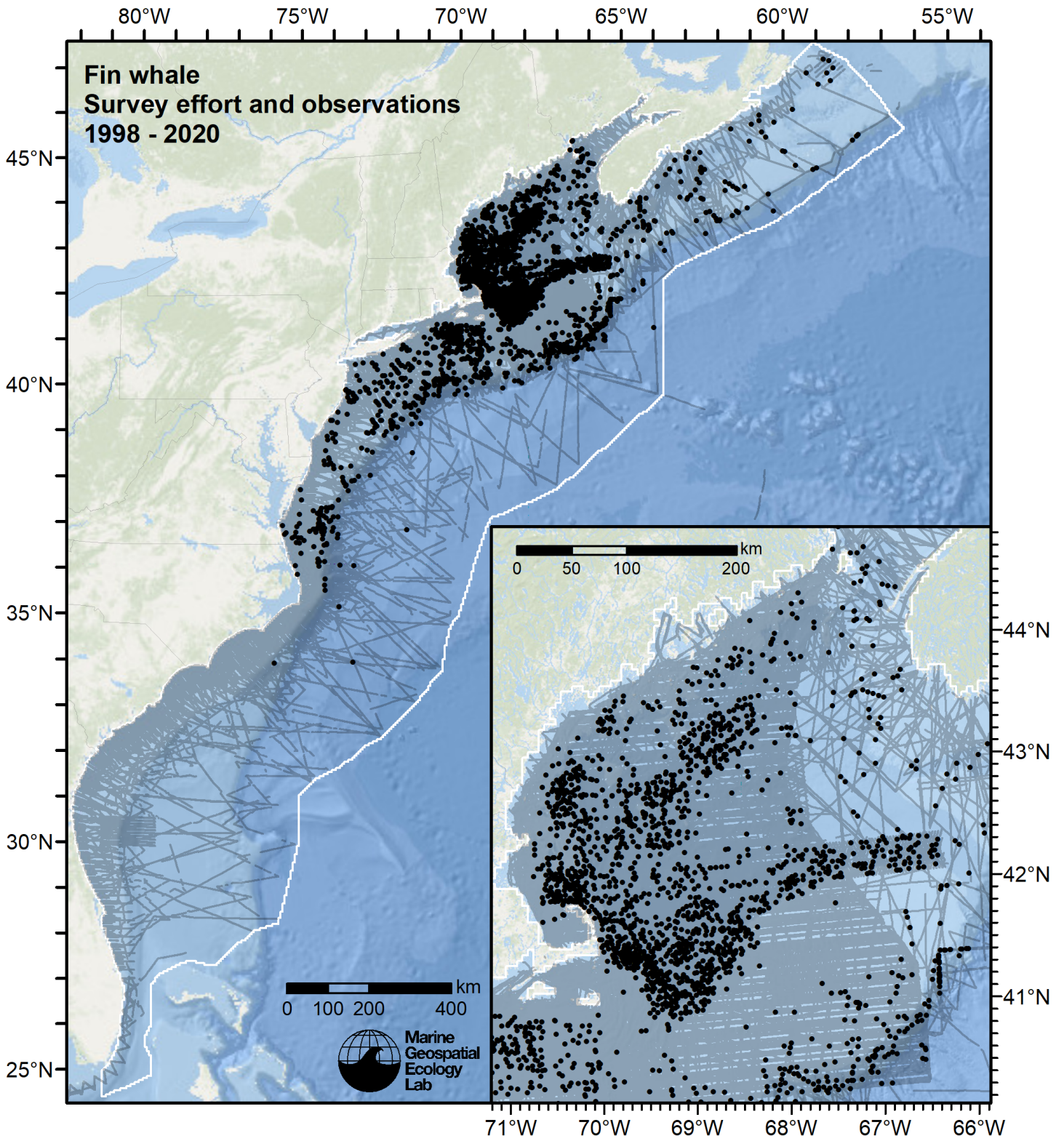


Figure 1: Survey effort and fin whale observations available for density modeling, after detection functions were applied, and excluded segments and truncated observations were removed.

## 2 Classification of Ambiguous Sightings

Observers occasionally experience difficulty identifying species, due to poor sighting conditions or phenotypic similarities between the possible choices. For example, observers may not always be able to distinguish fin whales from sei whales due their similar size and shape. When this happens, observers will report an ambiguous identification, such as “fin or sei whale”. In our density models, we handled ambiguous identifications in three ways:

1. For sightings with very generic identifications such as “large whale”, we discarded the sightings. These sightings represented a clear minority when compared to those with definitive species identifications, but they are uncounted animals and our density models may therefore underestimate density to some degree.
2. For sightings of certain taxa in which a large majority of identifications were ambiguous (e.g. “unidentified pilot whale”) rather than specific (e.g. “short-finned pilot whale” or “long-finned pilot whale”), it was not tractable to model the individual species so we modeled the generic taxon instead.
3. For sightings that reported an ambiguous identification of two species (e.g. “fin or sei whale”) that are known to exhibit different habitat preferences or typically occur in different group sizes, and for which we had sufficient number of definitive sightings of both species, we first fitted a predictive model that classified the ambiguous sightings into one species or the other and then included the resulting classified sightings in the density models for each of the two species.

This section describes how we classified the third category of ambiguous sightings reported as “Fin or sei whale” into one species or the other.

For the predictive model, we used the cforest classifier (Hothorn et al. 2006), an elaboration of the classic random forest classifier (Breiman 2001). First, we trained a binary classifier using the sightings that reported definitive species identifications (“fin whale” and “sei whale”). To increase the range of sampling of the classification model’s covariates, the training data may have included additional surveys not considered for the density model, as well as transects from outside the spatial and temporal extents of the density model. Only on-effort sightings were used. We used the species ID as the response variable and environmental variables as covariates.

We used receiver operating characteristic (ROC) curve analysis to select a threshold for classifying the probabilistic predictions of species identifications made by the model into a binary result of one species or another. For the classification threshold, we selected the value that maximized the Youden index (Perkins and Schisterman 2006). Then, for all sightings reporting the ambiguous identification, we classified each as either one species or the other by processing the covariate values observed for it through the fitted model. We then included the classified sightings in the detection functions and density models. The sightings reported elsewhere in this document incorporate both the definitive sightings and the classified sightings, unless otherwise noted.

### 2.1 Classification Model

MODEL SUMMARY:

=====

Random Forest using Conditional Inference Trees

Number of trees: 1000

Response: factor(OriginalScientificName)

Inputs: ClimChl, ClimDistToFront063, ClimEKE, ClimMnkEpi, ClimPP\_CAFE, ClimSST\_CMC, ClimTKE, DayOfYear, Depth, DistTo300m, DistToShore, Slope

Number of observations: 4256

Number of variables tried at each split: 5

Estimated predictor variable importance (conditional = FALSE):

Importance

ClimMnkEpi 0.03845

DayOfYear 0.03699

ClimSST\_CMC 0.03159

ClimPP\_CAFE 0.01901  
 ClimEKE 0.01862  
 Depth 0.01456  
 DistToShore 0.01381  
 DistTo300m 0.01144  
 ClimChl 0.01138  
 ClimDistToFront063 0.00799  
 Slope 0.00751  
 ClimTKE 0.00736

MODEL PERFORMANCE SUMMARY:  
 =====

Statistics calculated from the training data.

Area under the ROC curve (auc) = 0.949  
 Mean cross-entropy (mxe) = 0.310  
 Precision-recall break-even point (prbe) = 0.922  
 Root-mean square error (rmse) = 0.307

User-specified cutoff = 0.565

Confusion matrix for that cutoff:

	Actual Balaenoptera physalus	Actual Balaenoptera borealis	Total
Predicted Balaenoptera physalus	2823	239	3062
Predicted Balaenoptera borealis	240	954	1194
Total	3063	1193	4256

Model performance statistics for that cutoff:

Accuracy (acc) = 0.887  
 Error rate (err) = 0.113  
 Rate of positive predictions (rpp) = 0.719  
 Rate of negative predictions (rnp) = 0.281  
  
 True positive rate (tpr, or sensitivity) = 0.922  
 False positive rate (fpr, or fallout) = 0.200  
 True negative rate (tnr, or specificity) = 0.800  
 False negative rate (fnr, or miss) = 0.078  
  
 Positive prediction value (ppv, or precision) = 0.922  
 Negative prediction value (npv) = 0.799  
 Prediction-conditioned fallout (pcfall) = 0.078  
 Prediction-conditioned miss (pcmiss) = 0.201  
  
 Matthews correlation coefficient (mcc) = 0.721  
 Odds ratio (odds) = 46.952  
 SAR = 0.714  
  
 Cohen's kappa (K) = 0.721



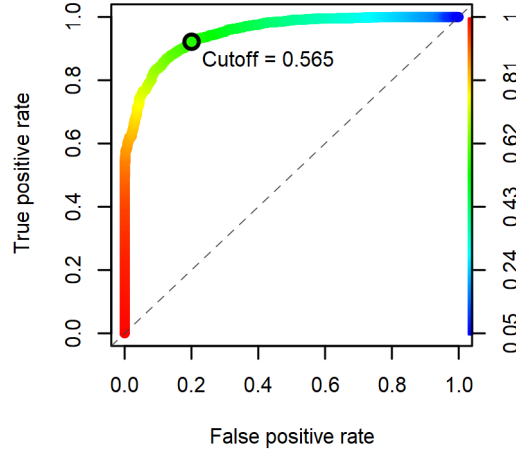


Figure 2: Receiver operating characteristic (ROC) curve summarizing the predictive performance of the ambiguous sighting classification model.

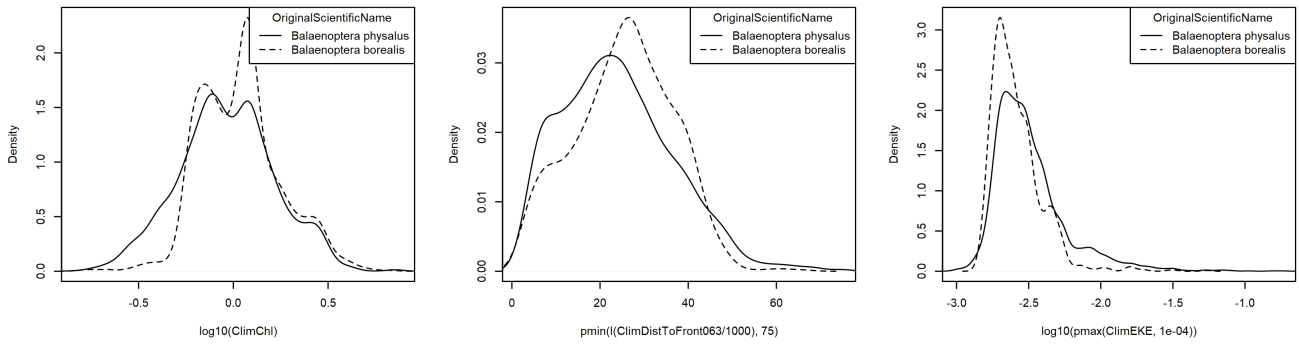
Table 4: Covariates used in the ambiguous sighting classification model.

Covariate	Description
ClimChl	Climatological monthly mean chlorophyll a concentration ( $\text{mg m}^{-3}$ ) from Copernicus GlobColour (Garnesson et al. (2019)), provided by E.U. Copernicus Marine Service (product OCEANCOLOUR_GLO_CHL_L4_REP_OBSERVATIONS_009_082)
ClimDistToFront063	Climatological monthly mean distance (km) to the closest sea surface temperature front detected in daily GHRSSST Level 4 CMC0.2deg and CMC0.1deg images (Brasnett (2008); Canada Meteorological Center (2012); Meissner et al. (2016); Canada Meteorological Center (2016)) with MGET’s implementation of the Canny edge detector (Roberts et al. (2010); Canny (1986))
ClimEKE	Climatological monthly mean eddy kinetic energy ( $\text{m}^2 \text{s}^{-2}$ ) derived from Aviso Ssalto/Duacs global gridded L4 reprocessed geostrophic currents, produced and distributed by E.U. Copernicus Marine Service. doi: <a href="https://doi.org/10.48670/moi-00148">10.48670/moi-00148</a>
ClimMnkEpi	Climatological monthly mean micronekton biomass available in the epipelagic zone, expressed as wet weight ( $\text{g m}^{-2}$ ), from SEAPODYM (Lehodey et al. (2008); Lehodey et al. (2015)), provided by E.U. Copernicus Marine Service. doi: <a href="https://doi.org/10.48670/moi-00020">10.48670/moi-00020</a> . Computed as the sum of the SEAPODYM mnkc_epi, mnkc_mumeso, and mnkc_hmlmeso variables.
ClimPP_CAFE	Climatological monthly mean net primary productivity ( $\text{mg C m}^{-2} \text{day}^{-1}$ ) from the Carbon, Absorption, and Fluorescence Euphotic-resolving (CAFE) model (Silsbe et al. (2016))
ClimSST_CMC	Climatological monthly mean sea surface temperature ( $^{\circ}\text{C}$ ) from GHRSSST Level 4 CMC0.2deg and CMC0.1deg (Brasnett (2008); Canada Meteorological Center (2012); Meissner et al. (2016); Canada Meteorological Center (2016))
ClimTKE	Climatological monthly mean total kinetic energy ( $\text{m}^2 \text{s}^{-2}$ ) derived from Aviso Ssalto/Duacs global gridded L4 reprocessed geostrophic currents, produced and distributed by E.U. Copernicus Marine Service. doi: <a href="https://doi.org/10.48670/moi-00148">10.48670/moi-00148</a>
DayOfYear	Days elapsed since the start of the year
Depth	Depth (m) of the seafloor, from SRTM30_PLUS (Becker et al. (2009))
DistTo300m	Distance (km) to the 300m isobath, derived from SRTM30_PLUS (Becker et al. (2009))
DistToShore	Distance (km) to shore excluding Bermuda and Sable Island, derived from SRTM30_PLUS (Becker et al. (2009))

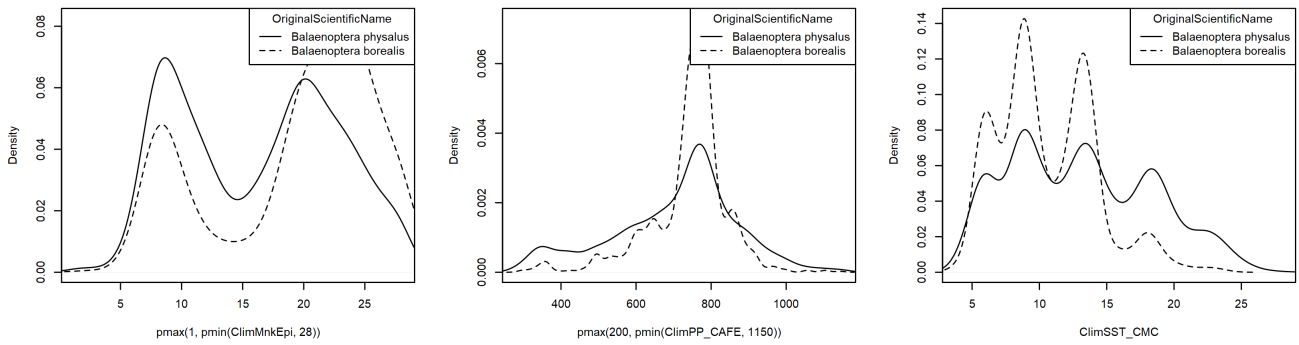


Table 4: Covariates used in the ambiguous sighting classification model. (*continued*)

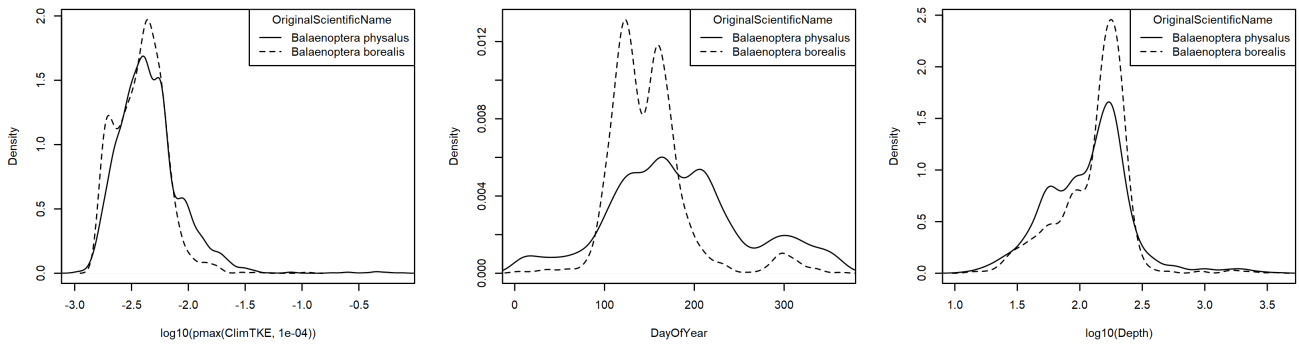
Covariate	Description
Slope	Slope (percent rise) of the seafloor, derived from SRTM30_PLUS (Becker et al. (2009))



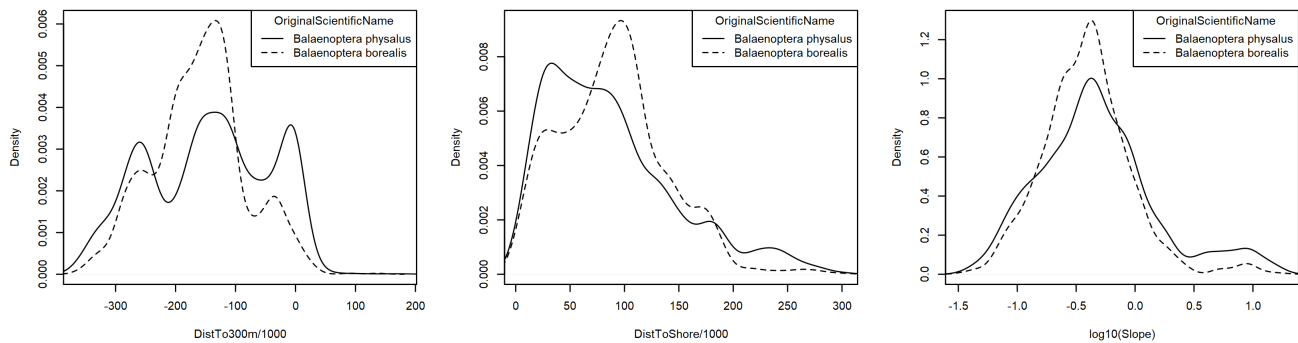
(a) Chlorophyll a concentration (mg m<sup>-3</sup>) (b) Climatological distance to SST front (km) (c) Climatological eddy kinetic energy (m<sup>2</sup> s<sup>-2</sup>)



(d) Climatological epipelagic micronekton biomass (g m<sup>-2</sup>) (e) Climatological net primary productivity (mg C m<sup>-2</sup> day<sup>-1</sup>) (CAFE model) (f) Climatological sea surface temperature (°C)



(g) Climatological total kinetic energy (m<sup>2</sup> s<sup>-2</sup>) (h) Day of year (i) Seafloor depth (m)



(j) Distance to 300m isobath (km) (k) Distance to shore (km) (l) Seafloor slope (percent rise)

Figure 3: Density histograms showing the per-species distribution of each covariate in the ambiguous sighting classification model. When a covariate exhibits a substantially different distribution for each species, it is a good candidate for differentiating the species. Transforms and other treatments are indicated in axis labels.  $\log_{10}$  indicates the covariate was  $\log_{10}$  transformed.  $\text{pmax}$  and  $\text{pmin}$  indicate the covariate's minimum and maximum values, respectively, were Winsorized to the values shown.  $/1000$  indicates meters were transformed to kilometers for interpretation convenience.

## 2.2 Classifications Performed

Table 5: Summary of the definitive sightings used to train the classification model, the ambiguous sightings to which the model was applied, and their resulting classifications. To increase the range of sampling of the classification model’s covariates, the training data may have included additional surveys not considered for the density model, as well as transects from outside the spatial and temporal extents of the density model. Only on-effort sightings were used.

Institution	Program	Definitive			Classified	
		B. physalus	B. borealis	Ambiguous	B. physalus	B. borealis
<b>Aerial Surveys</b>						
FWRI	SEUS NARW EWS	3	0	0	0	0
HDR	Navy Norfolk Canyon	32	6	0	0	0
NEAq	CNM	16	2	0	0	0
NEAq	MMS-WEA	51	24	6	4	2
NEAq	NLPSC	68	21	10	9	1
NEFSC	AMAPPS	110	15	29	26	3
NEFSC	NARWSS	1,972	1,086	663	398	265
NEFSC	Pre-AMAPPS	208	8	39	37	2
NJDEP	NJEBS	1	0	0	0	0
NYS-DEC/TT	NYBWM	161	3	0	0	0
SEFSC	AMAPPS	36	0	0	0	0
SEFSC	MATS	6	0	0	0	0
UNCW	MidA Bottlenose	1	0	0	0	0
UNCW	Navy Cape Hatteras	9	0	0	0	0
UNCW	Navy Norfolk Canyon	9	0	0	0	0
UNCW	Navy Onslow Bay	1	0	0	0	0
UNCW	SEUS NARW EWS	12	0	0	0	0
VAMSC	MD DNR WEA	16	0	0	0	0
VAMSC	Navy VACAPES	1	0	0	0	0
VAMSC	VA CZM WEA	11	0	0	0	0
WLT/SSA/CMARI	SEUS NARW EWS	2	0	0	0	0
	<b>Total</b>	<b>2,726</b>	<b>1,165</b>	<b>747</b>	<b>474</b>	<b>273</b>
<b>Shipboard Surveys</b>						
MCR	SOTW Visual	5	2	0	0	0
NEFSC	AMAPPS	219	16	50	48	2
NEFSC	Pre-AMAPPS	69	10	96	96	0
NJDEP	NJEBS	26	0	0	0	0
SEFSC	AMAPPS	7	0	0	0	0
SEFSC	Pre-AMAPPS	11	0	0	0	0
	<b>Total</b>	<b>337</b>	<b>28</b>	<b>146</b>	<b>144</b>	<b>2</b>
	<b>Grand Total</b>	<b>3,063</b>	<b>1,193</b>	<b>893</b>	<b>618</b>	<b>275</b>

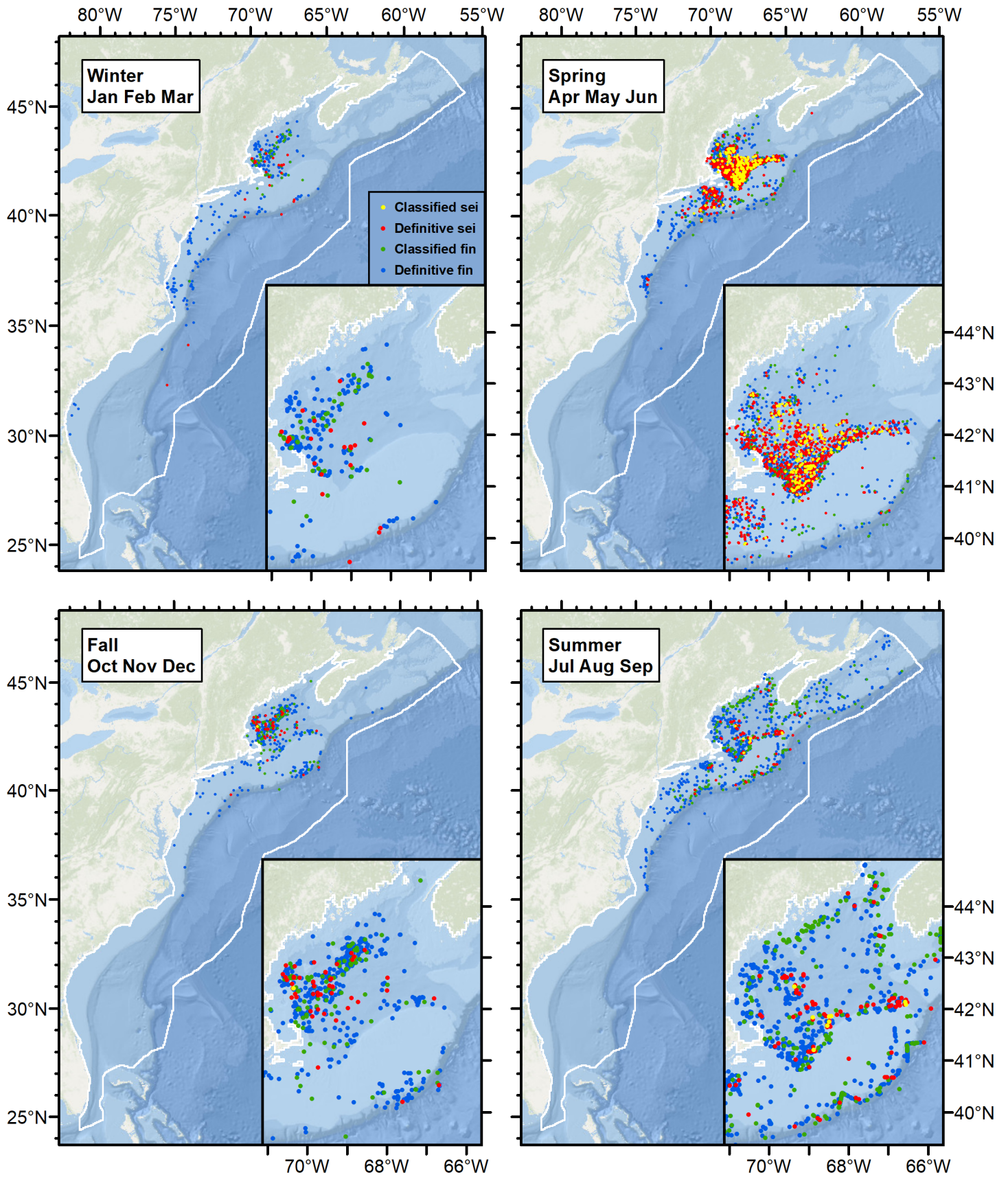


Figure 4: Definitive sightings used to train the model and ambiguous sightings classified by the model.

## 3 Detection Functions

### 3.1 With a Taxonomic Covariate

We fitted the detection functions in this section to pools of species with similar detectability characteristics and used the taxonomic identification as a covariate (ScientificName) to account for differences between them. We consulted the literature and observer teams to determine appropriate poolings. We usually employed this approach to boost the counts of observations in the detection functions, which increased the chance that other covariates such as Beaufort sea state could be used to account for differences in observing conditions. When defining the taxonomic covariate, we sometimes had too few observations of species to allocate each of them their own level of the covariate and had to group them together, again consulting the literature and observers for advice on species similarity. Also, when species were observed frequently enough to be allocated their own levels but statistical tests indicated no significant difference between the levels, we usually grouped them together into a single level.

### 3.1.1 Large Whales

#### 3.1.1.1 Aerial Surveys

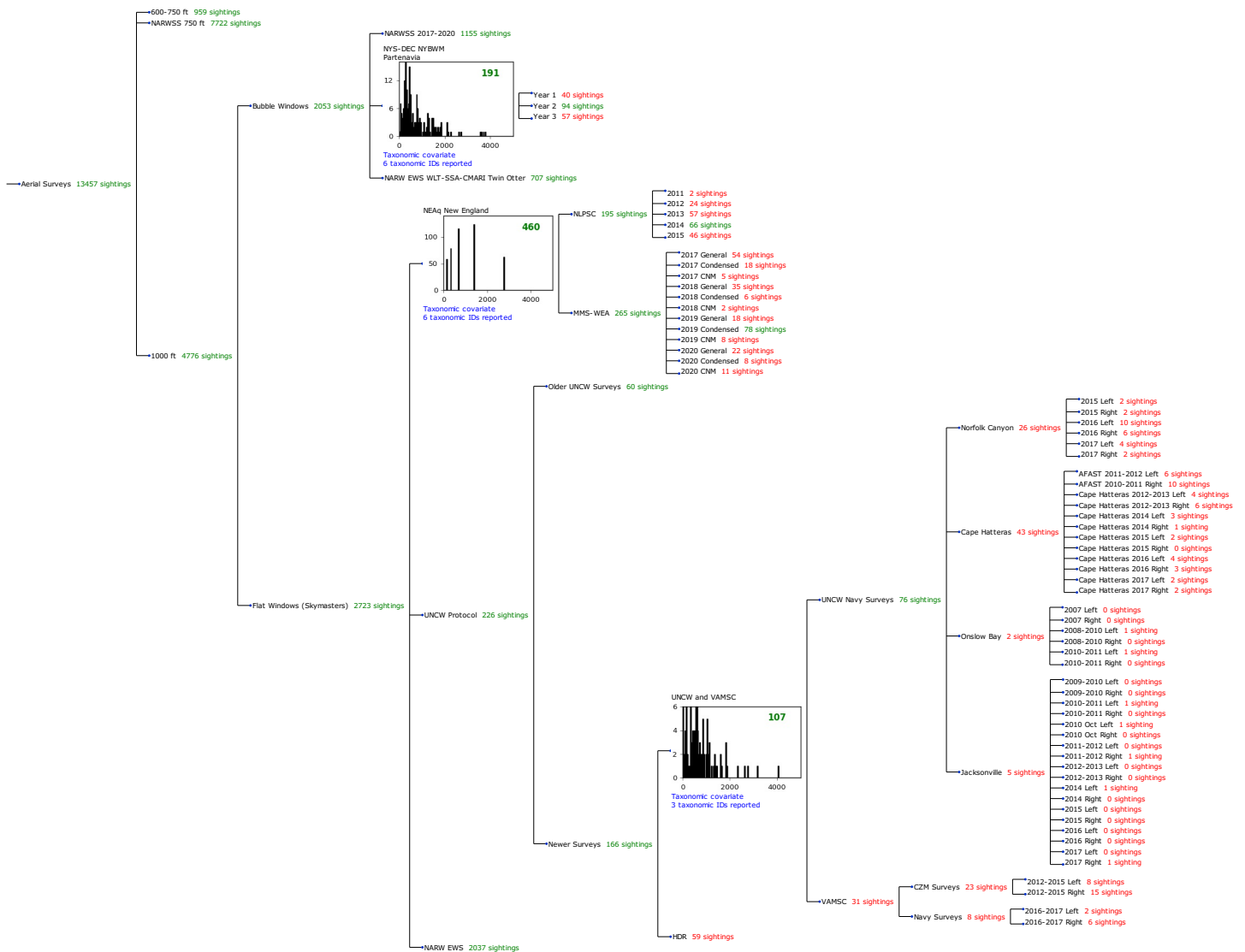


Figure 5: Detection hierarchy for aerial surveys, showing how they were pooled during detectability modeling, for detection functions that pooled multiple taxa and used a taxonomic covariate to account for differences between them. Each histogram represents a detection function and summarizes the perpendicular distances of observations that were pooled to fit it, prior to truncation. Observation counts, also prior to truncation, are shown in green when they met the recommendation of Buckland et al. (2001) that detection functions utilize at least 60 sightings, and red otherwise. For rare taxa, it was not always possible to meet this recommendation, yielding higher statistical uncertainty. During the spatial modeling stage of the analysis, effective strip widths were computed for each survey using the closest detection function above it in the hierarchy (i.e. moving from right to left in the figure). Surveys that do not have a detection function above them in this figure were either addressed by a detection function presented in a different section of this report, or were omitted from the analysis.

##### 3.1.1.1.1 NYS-DEC NYBWM Partenavia

After right-truncating observations greater than 2100 m and left-truncating observations less than 125 m (Figure 7), we fitted the detection function to the 172 observations that remained (Table 6). The selected detection function (Figure 6) used a hazard rate key function with OriginalScientificName (Figure 8), Season (Figure 9) and SurveyID (Figure 10) as covariates.

Table 6: Observations used to fit the NYS-DEC NYBWM Partenavia detection function.

ScientificName	n
Balaenoptera borealis	2
Balaenoptera musculus	2
Balaenoptera physalus	82
Eubalaena glacialis	12
Megaptera novaeangliae	57
Physeter macrocephalus	17
<b>Total</b>	<b>172</b>

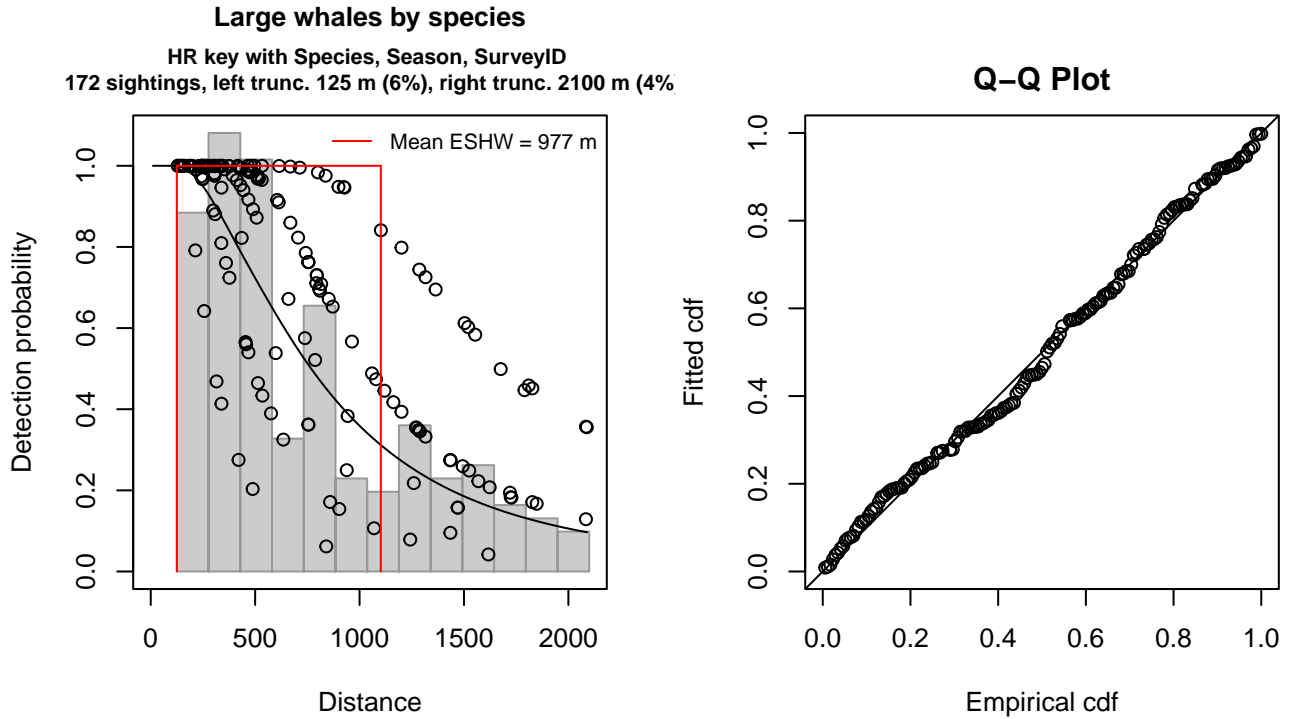


Figure 6: NYS-DEC NYBWM Partenavia detection function and Q-Q plot showing its goodness of fit.

Statistical output for this detection function:

Summary for ds object

Number of observations : 172  
 Distance range : 125 - 2100  
 AIC : 2521.205

Detection function:

Hazard-rate key function

Detection function parameters

Scale coefficient(s):

	estimate	se
(Intercept)	5.5563867	0.3693793
OriginalScientificNameHumpback, Right	0.4977955	0.2125828
SeasonSpring	0.7279337	0.2896812
SeasonSummer	0.7542217	0.2477951
SurveyIDYears 2-3	0.4837030	0.2648931

Shape coefficient(s):

	estimate	se
(Intercept)	0.8485132	0.197714

	Estimate	SE	CV
Average p	0.4075964	0.06072428	0.1489814
N in covered region	421.9860458	68.23264910	0.1616941

Distance sampling Cramer-von Mises test (unweighted)  
 Test statistic = 0.068137 p = 0.763045

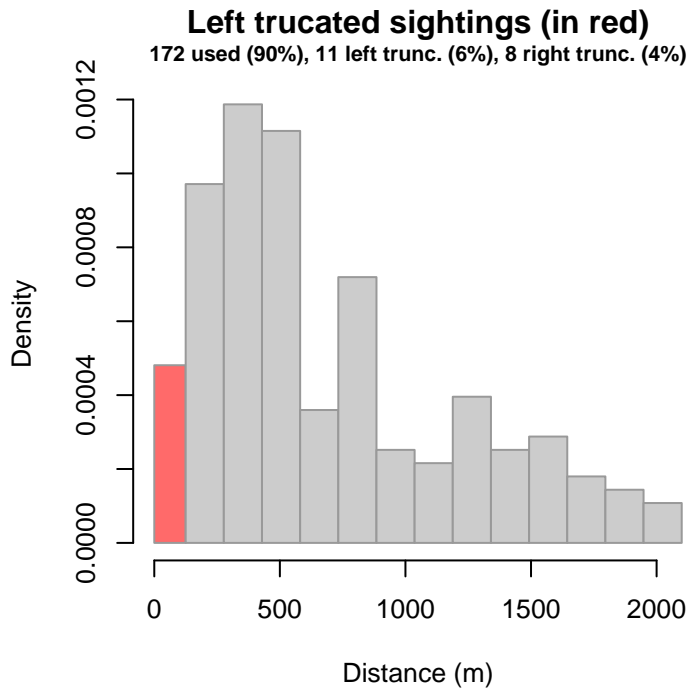


Figure 7: Density histogram of observations used to fit the NYS-DEC NYBWM Partenavia detection function, with the left-most bar showing observations at distances less than 125 m, which were left-truncated and excluded from the analysis [Buckland et al. (2001)]. (This bar may be very short if there were very few left-truncated sightings, or very narrow if the left truncation distance was very small; in either case it may not appear red.)



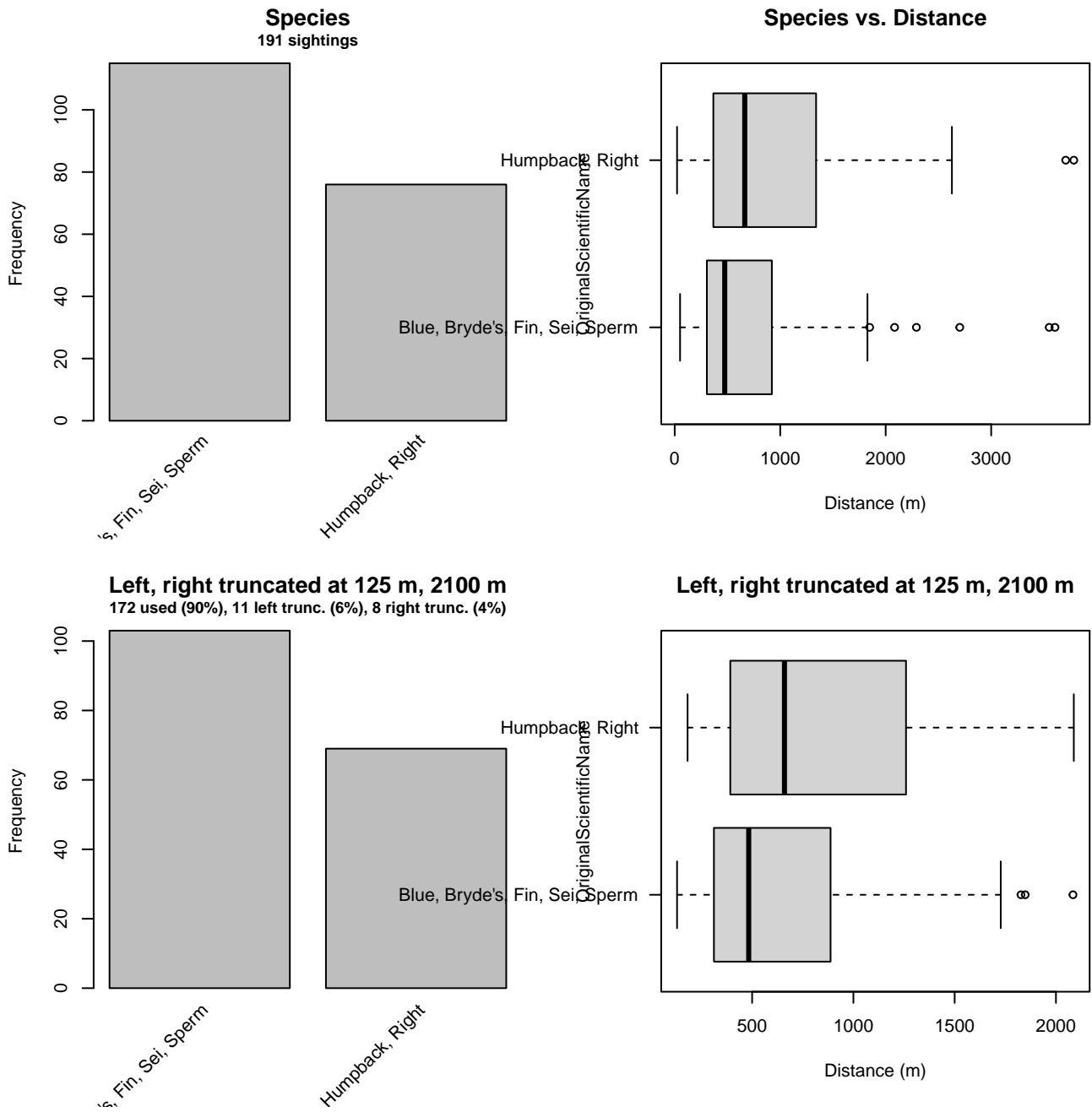


Figure 8: Distribution of the OriginalScientificName covariate before (top row) and after (bottom row) observations were truncated to fit the NYS-DEC NYBWM Partenavia detection function.

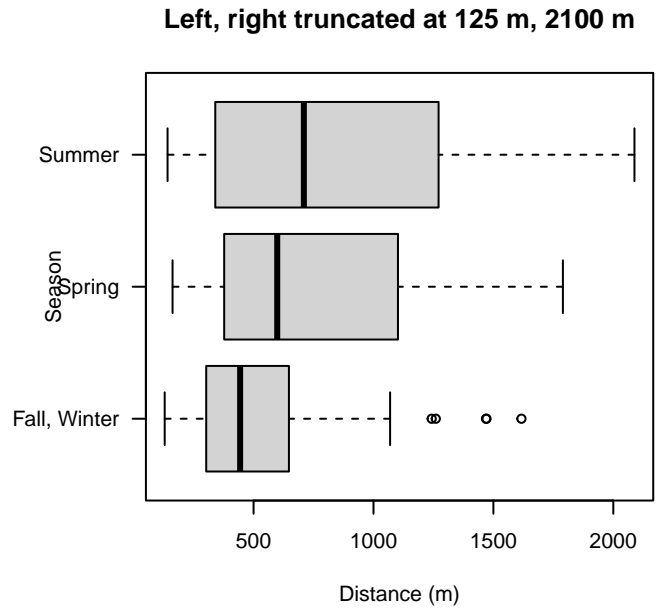
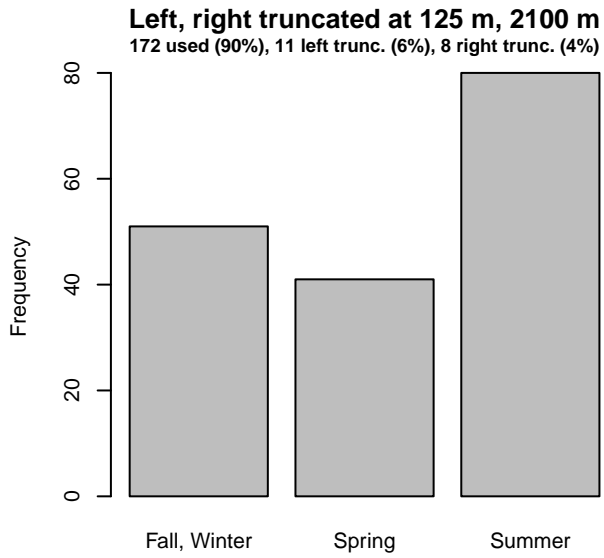
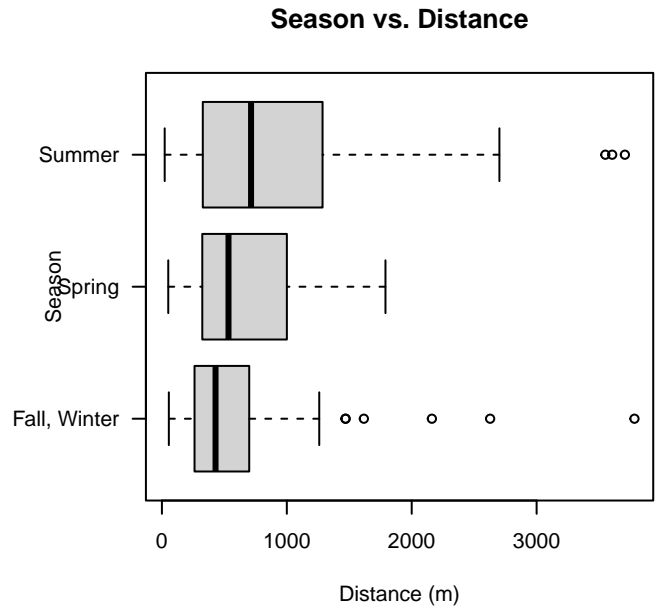
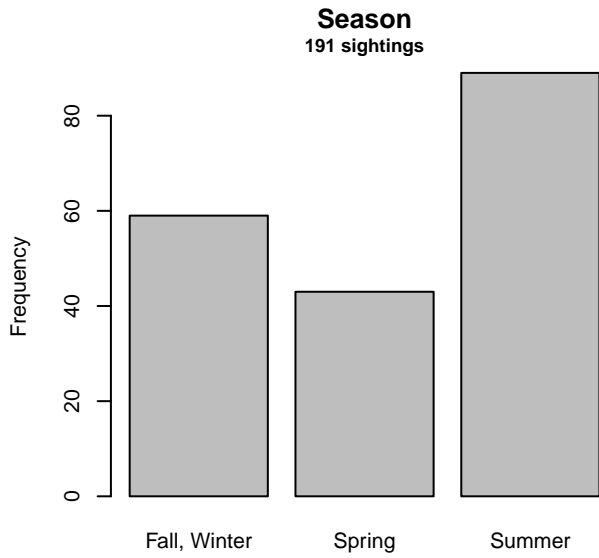


Figure 9: Distribution of the Season covariate before (top row) and after (bottom row) observations were truncated to fit the NYS-DEC NYBWM Partenavia detection function.

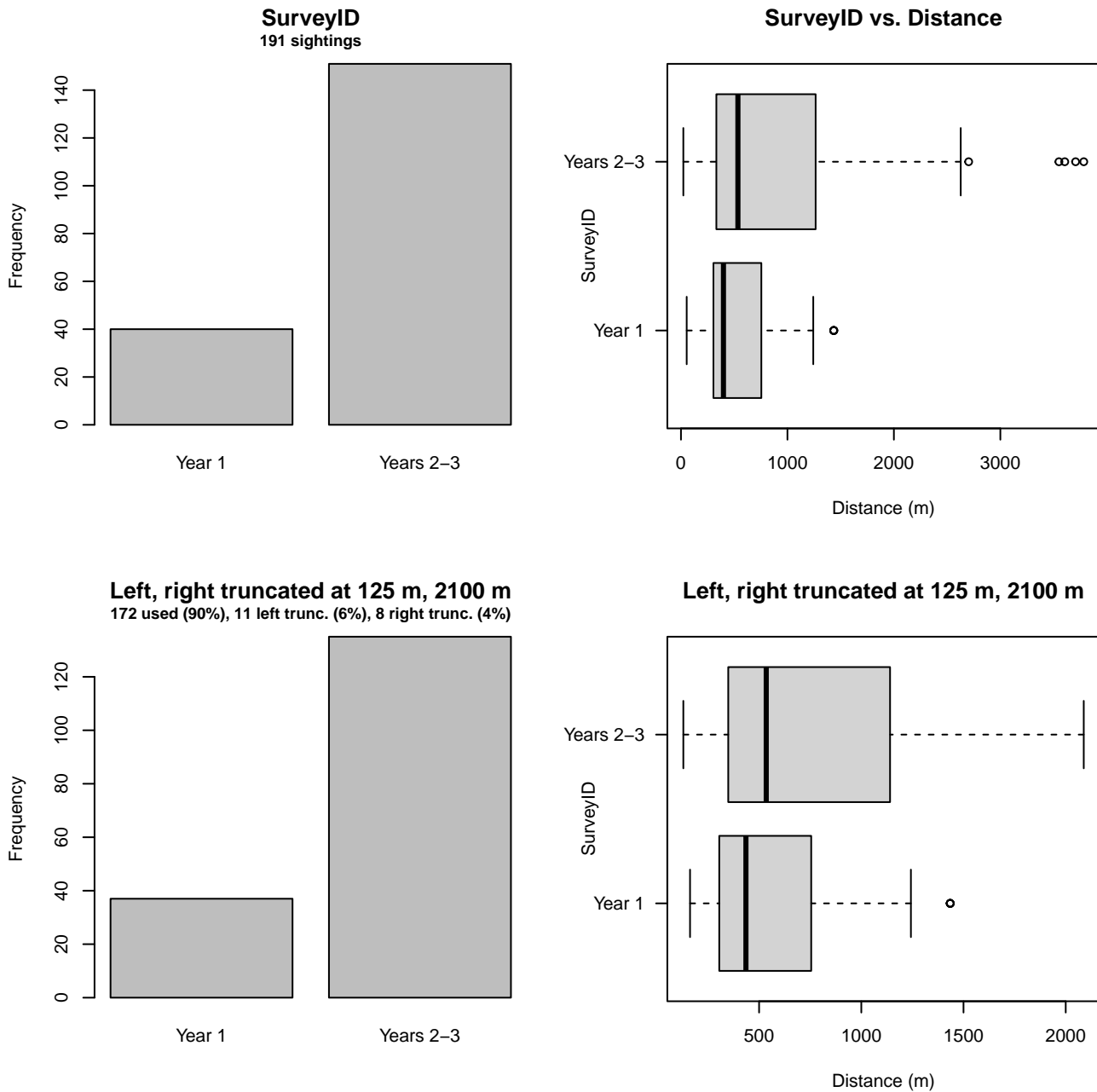


Figure 10: Distribution of the SurveyID covariate before (top row) and after (bottom row) observations were truncated to fit the NYS-DEC NYBWM Partenavia detection function.

### 3.1.1.1.2 NEAq New England

After right-truncating observations greater than 3704 m and left-truncating observations less than 71 m (Figure 12), we fitted the detection function to the 441 observations that remained (Table 7). The selected detection function (Figure 11) used a half normal key function with Beaufort (Figure 13), Glare (Figure 14) and OriginalScientificName (Figure 15) as covariates.

Table 7: Observations used to fit the NEAq New England detection function.

ScientificName	n
Balaenoptera borealis	44
Balaenoptera musculus	2
Balaenoptera physalus	128
Eubalaena glacialis	146
Megaptera novaeangliae	112
Physeter macrocephalus	9
<b>Total</b>	<b>441</b>

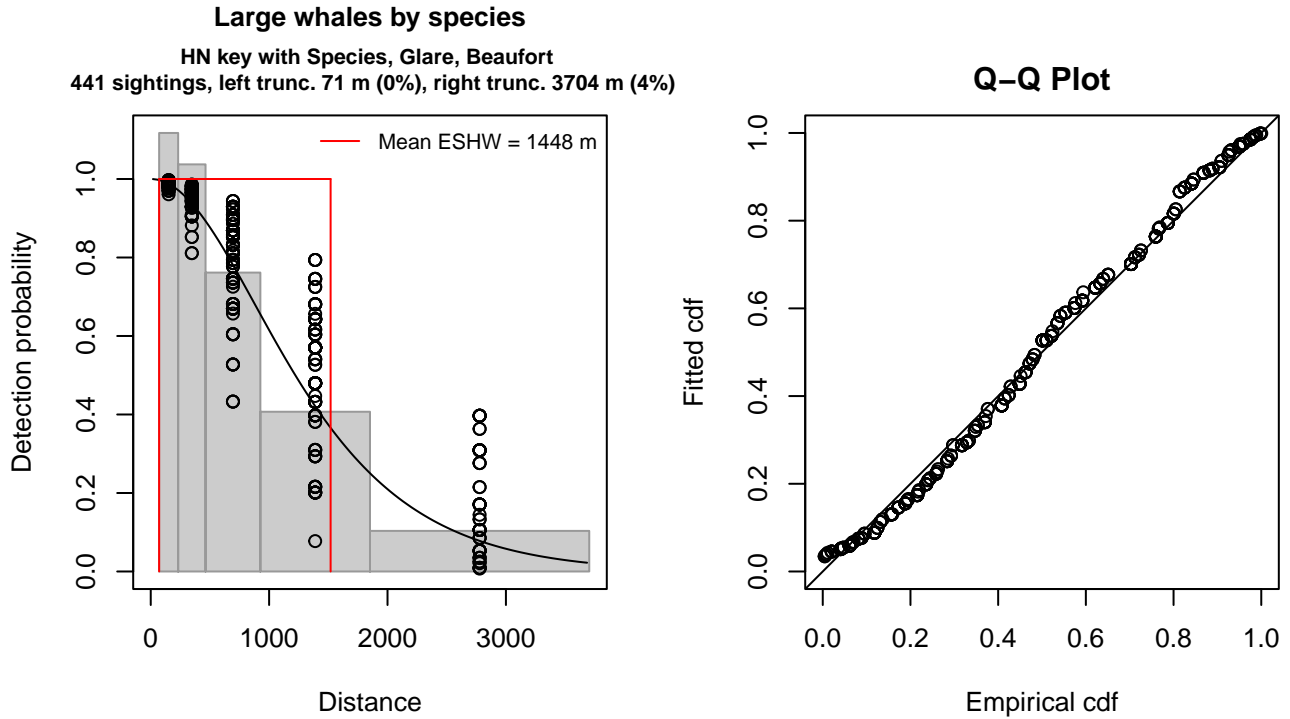


Figure 11: NEAq New England detection function and Q-Q plot showing its goodness of fit.

Statistical output for this detection function:

Summary for ds object

Number of observations : 441  
 Distance range : 71 - 3704  
 AIC : 1351.833

Detection function:

Half-normal key function

Detection function parameters

Scale coefficient(s):

	estimate	se
(Intercept)	6.4199373	0.11956192
OriginalScientificNameHumpback	0.1198260	0.10455078
OriginalScientificNameRight	-0.1344891	0.09839291
GlareSevere	0.3449677	0.16999750
GlareSlight, Moderate	0.3904627	0.09774396
Beaufort2	0.3680223	0.09867329
Beaufort3-4	0.6919932	0.12929768

	Estimate	SE	CV
Average p	0.3618698	0.01608762	0.04445694
N in covered region	1218.6704246	72.16746829	0.05921820

Distance sampling Cramer-von Mises test (unweighted)  
 Test statistic = 0.341945 p = 0.103421

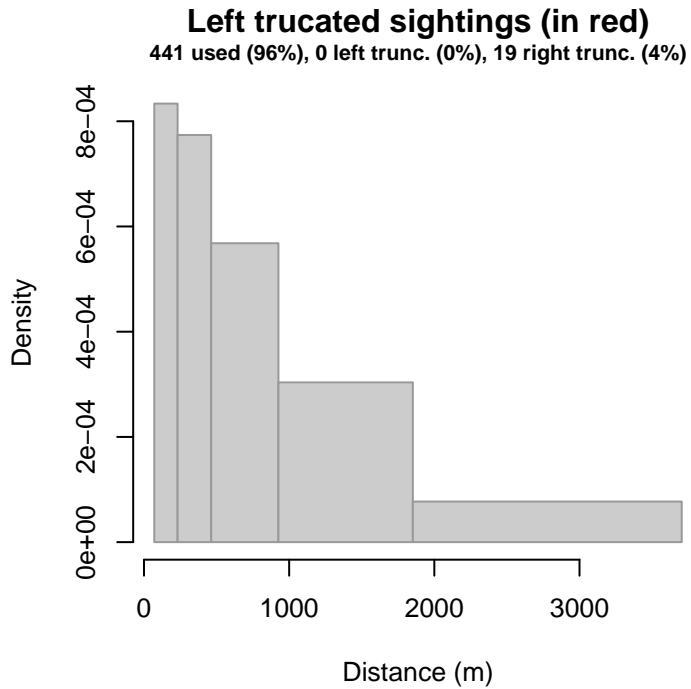


Figure 12: Density histogram of observations used to fit the NEAq New England detection function, with the left-most bar showing observations at distances less than 71 m, which were left-truncated and excluded from the analysis [Buckland et al. (2001)]. (This bar may be very short if there were very few left-truncated sightings, or very narrow if the left truncation distance was very small; in either case it may not appear red.)

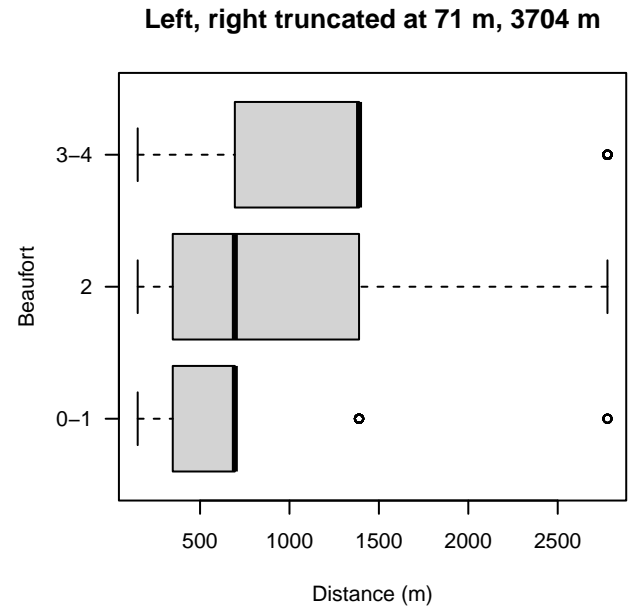
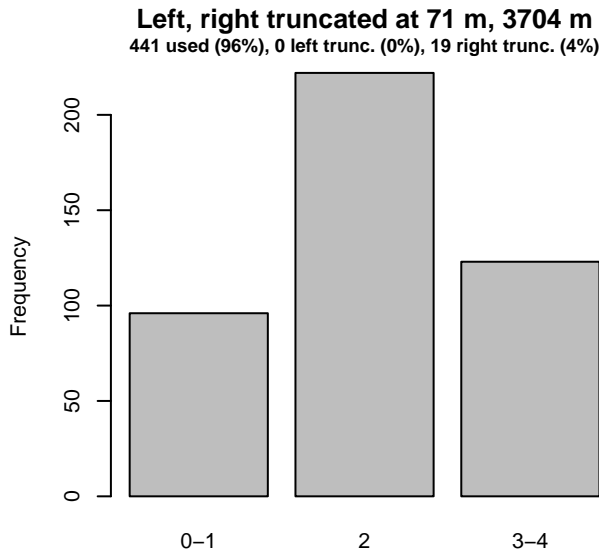
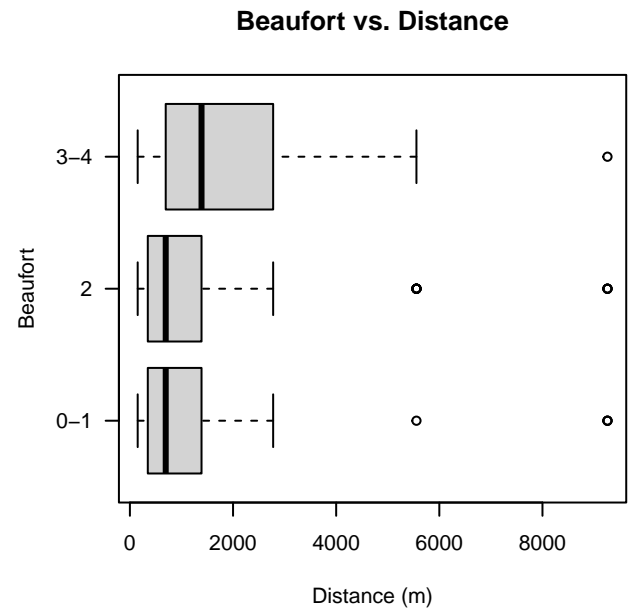
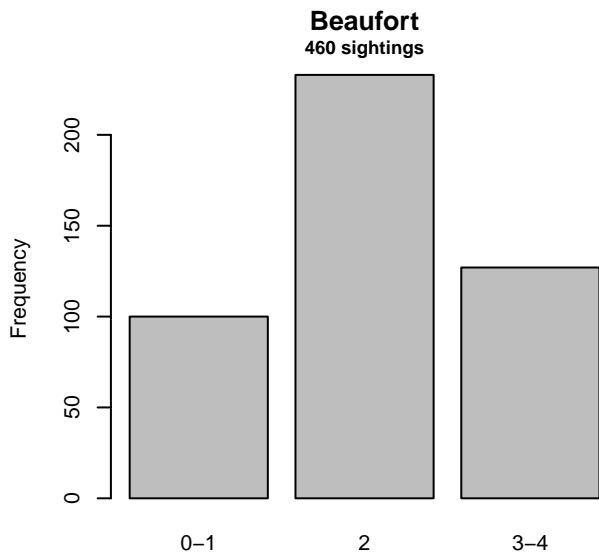


Figure 13: Distribution of the Beaufort covariate before (top row) and after (bottom row) observations were truncated to fit the NEAq New England detection function.

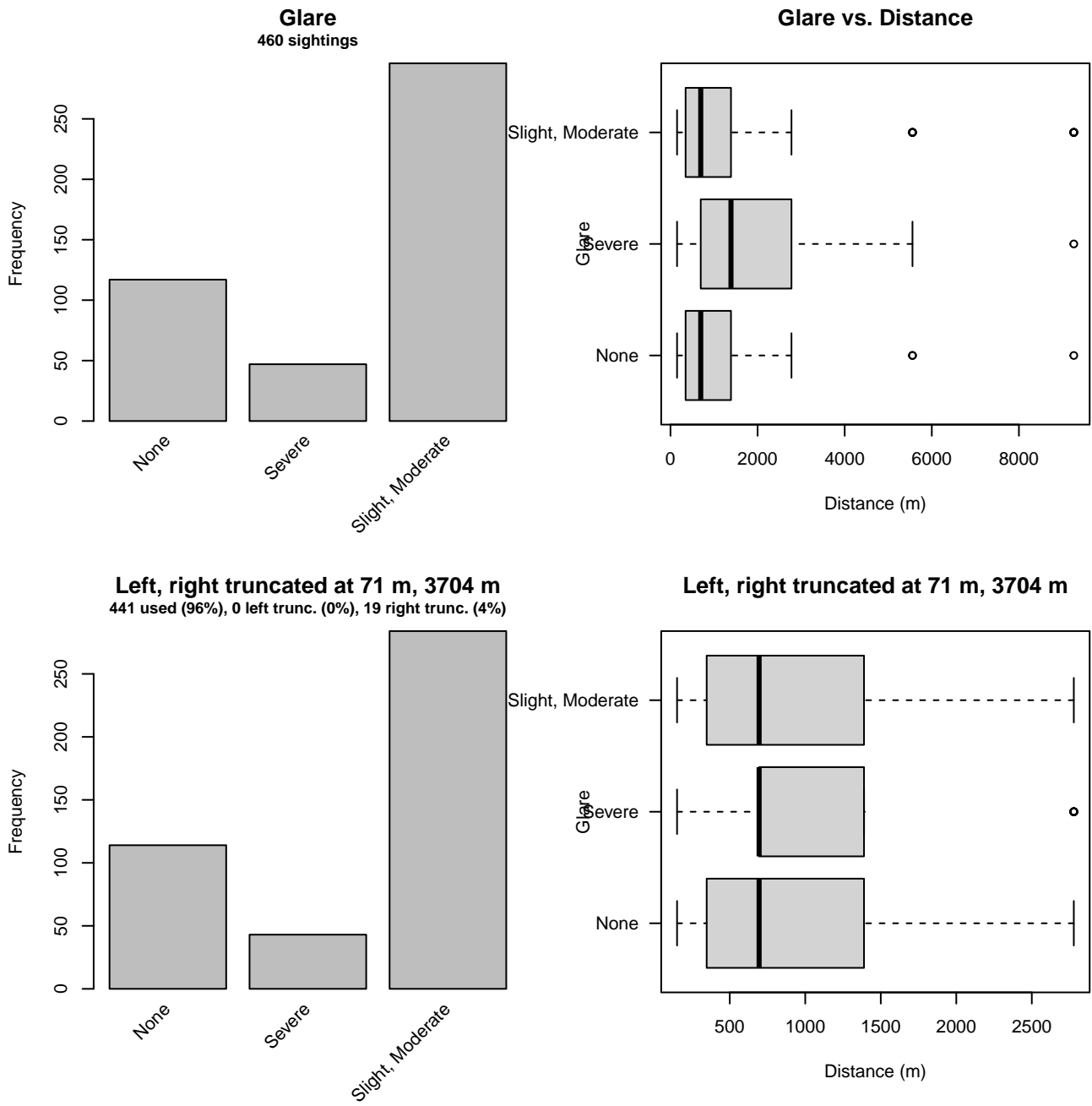


Figure 14: Distribution of the Glare covariate before (top row) and after (bottom row) observations were truncated to fit the NEAq New England detection function.

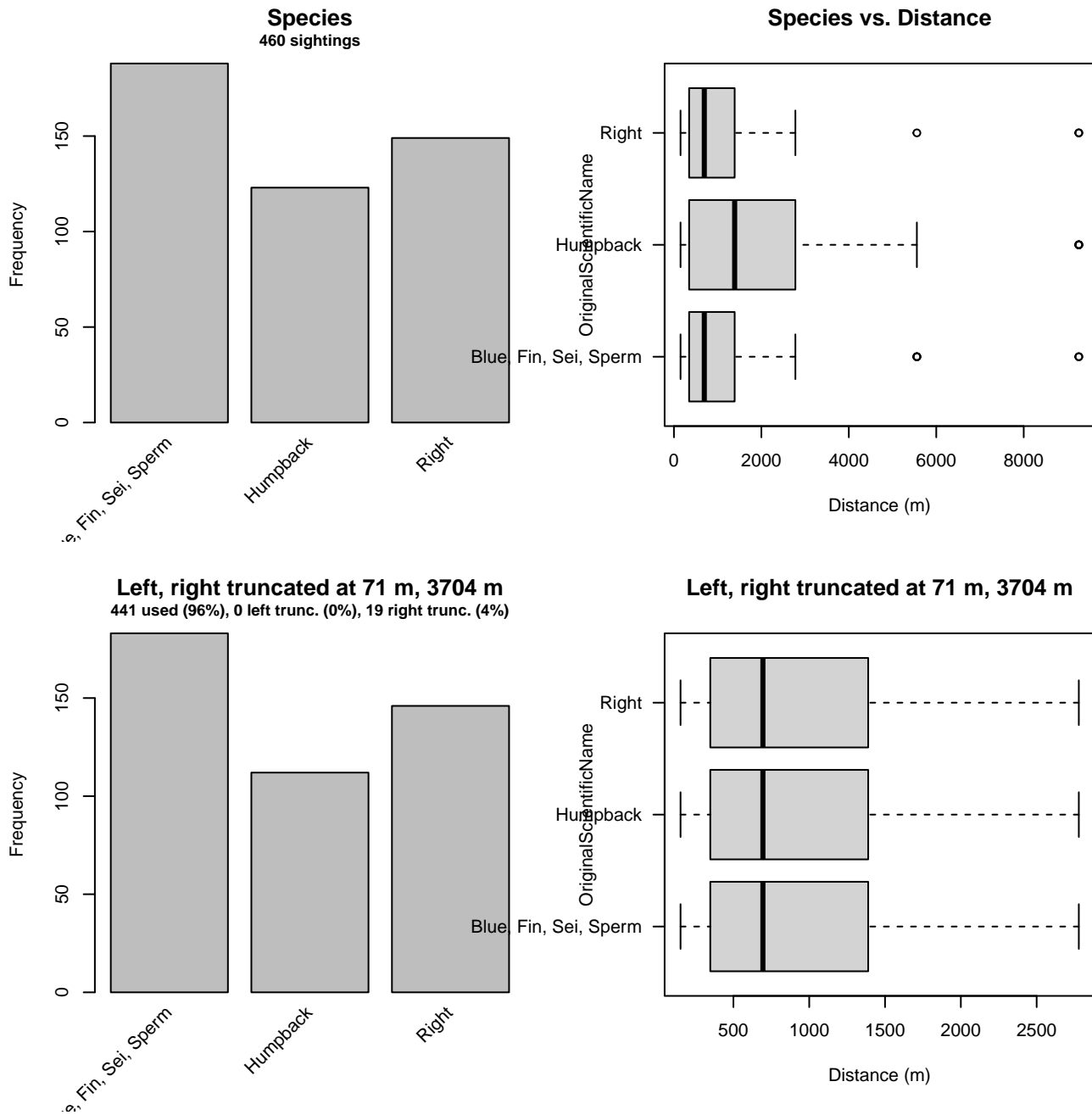


Figure 15: Distribution of the OriginalScientificName covariate before (top row) and after (bottom row) observations were truncated to fit the NEAq New England detection function.

### 3.1.1.1.3 UNCW and VAMSC

After right-truncating observations greater than 2000 m, we fitted the detection function to the 100 observations that remained (Table 8). The selected detection function (Figure 16) used a hazard rate key function with OriginalScientificName (Figure 17) as a covariate.



Table 8: Observations used to fit the UNCW and VAMSC detection function.

ScientificName	n
Balaenoptera physalus	27
Megaptera novaeangliae	31
Physeter macrocephalus	42
<b>Total</b>	<b>100</b>

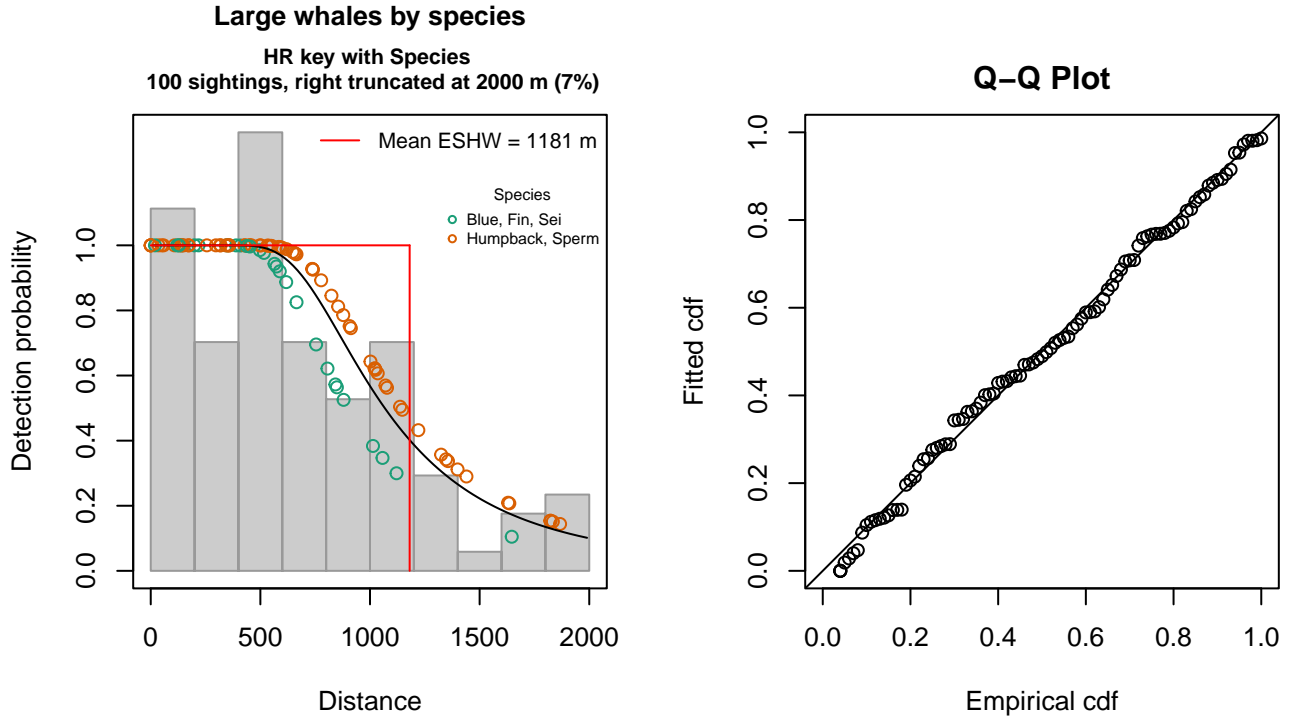


Figure 16: UNCW and VAMSC detection function and Q-Q plot showing its goodness of fit.

Statistical output for this detection function:

Summary for ds object

Number of observations : 100  
 Distance range : 0 - 2000  
 AIC : 1484.772

Detection function:  
 Hazard-rate key function

Detection function parameters

Scale coefficient(s):

	estimate	se
(Intercept)	6.6826489	0.2197841
OriginalScientificNameHumpback, Sperm	0.2371163	0.2278764

Shape coefficient(s):

	estimate	se
(Intercept)	1.11195	0.3071042

	Estimate	SE	CV
Average p	0.5857436	0.05399642	0.0921844
N in covered region	170.7231622	19.23003142	0.1126387

Distance sampling Cramer-von Mises test (unweighted)  
 Test statistic = 0.036117 p = 0.952042

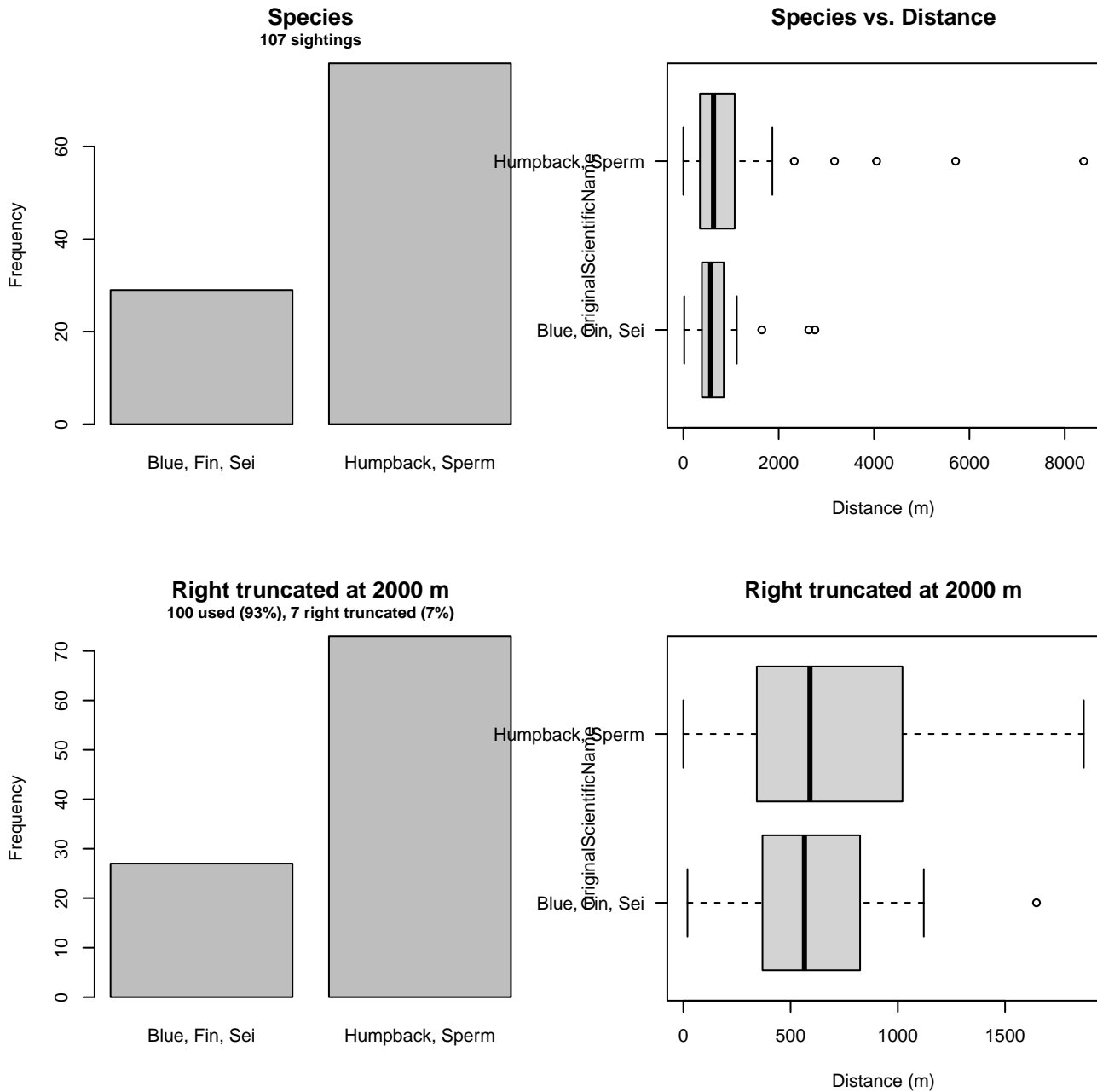


Figure 17: Distribution of the OriginalScientificName covariate before (top row) and after (bottom row) observations were truncated to fit the UNCW and VAMSC detection function.

### 3.1.1.2 Shipboard Surveys

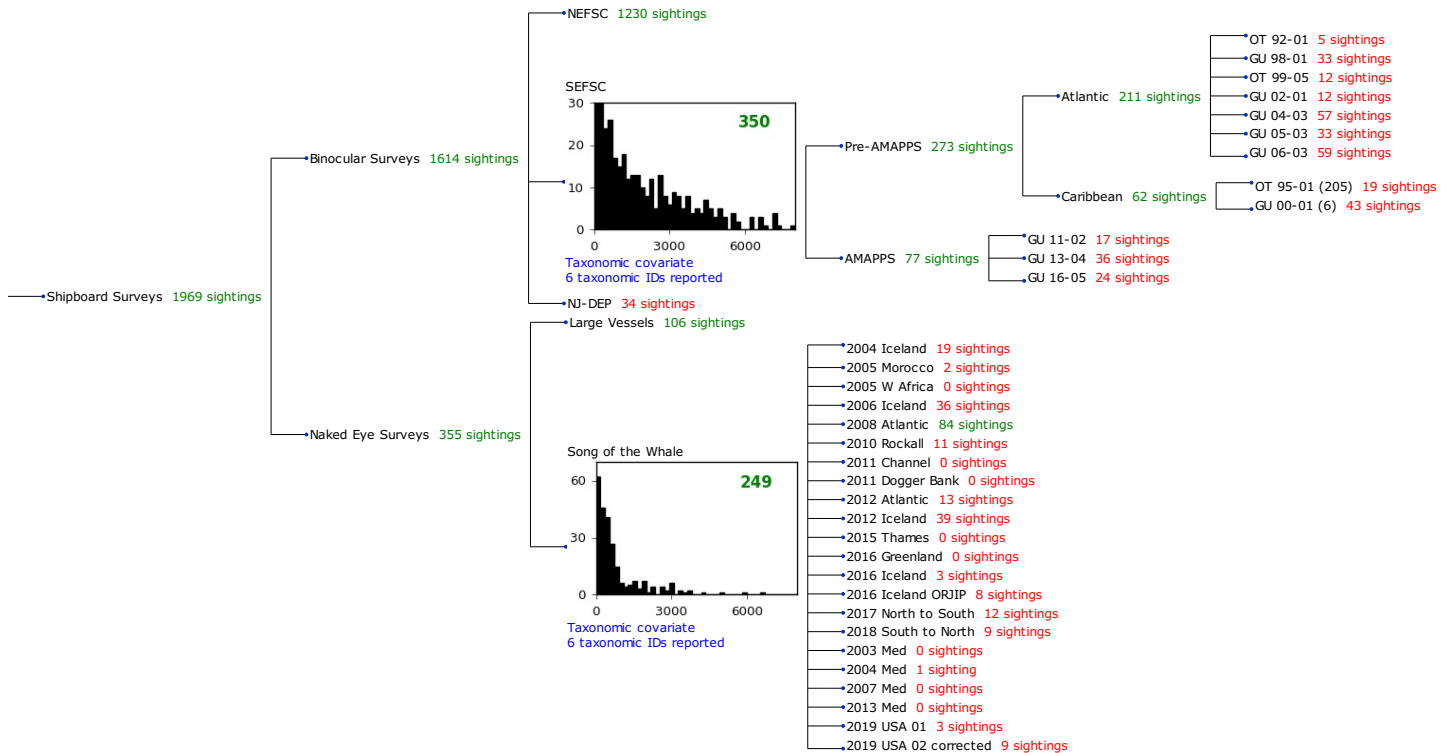


Figure 18: Detection hierarchy for shipboard surveys, showing how they were pooled during detectability modeling, for detection functions that pooled multiple taxa and used a taxonomic covariate to account for differences between them. Each histogram represents a detection function and summarizes the perpendicular distances of observations that were pooled to fit it, prior to truncation. Observation counts, also prior to truncation, are shown in green when they met the recommendation of Buckland et al. (2001) that detection functions utilize at least 60 sightings, and red otherwise. For rare taxa, it was not always possible to meet this recommendation, yielding higher statistical uncertainty. During the spatial modeling stage of the analysis, effective strip widths were computed for each survey using the closest detection function above it in the hierarchy (i.e. moving from right to left in the figure). Surveys that do not have a detection function above them in this figure were either addressed by a detection function presented in a different section of this report, or were omitted from the analysis.

#### 3.1.1.2.1 SEFSC

After right-truncating observations greater than 6000 m, we fitted the detection function to the 332 observations that remained (Table 9). The selected detection function (Figure 19) used a hazard rate key function with Beaufort (Figure 20), OriginalScientificName (Figure 21) and Program (Figure 22) as covariates.

Table 9: Observations used to fit the SEFSC detection function.

ScientificName	n
Balaenoptera borealis/edeni	3
Balaenoptera edeni	10
Balaenoptera physalus	17
Eubalaena glacialis	2
Megaptera novaeangliae	32
Physeter macrocephalus	268
<b>Total</b>	<b>332</b>

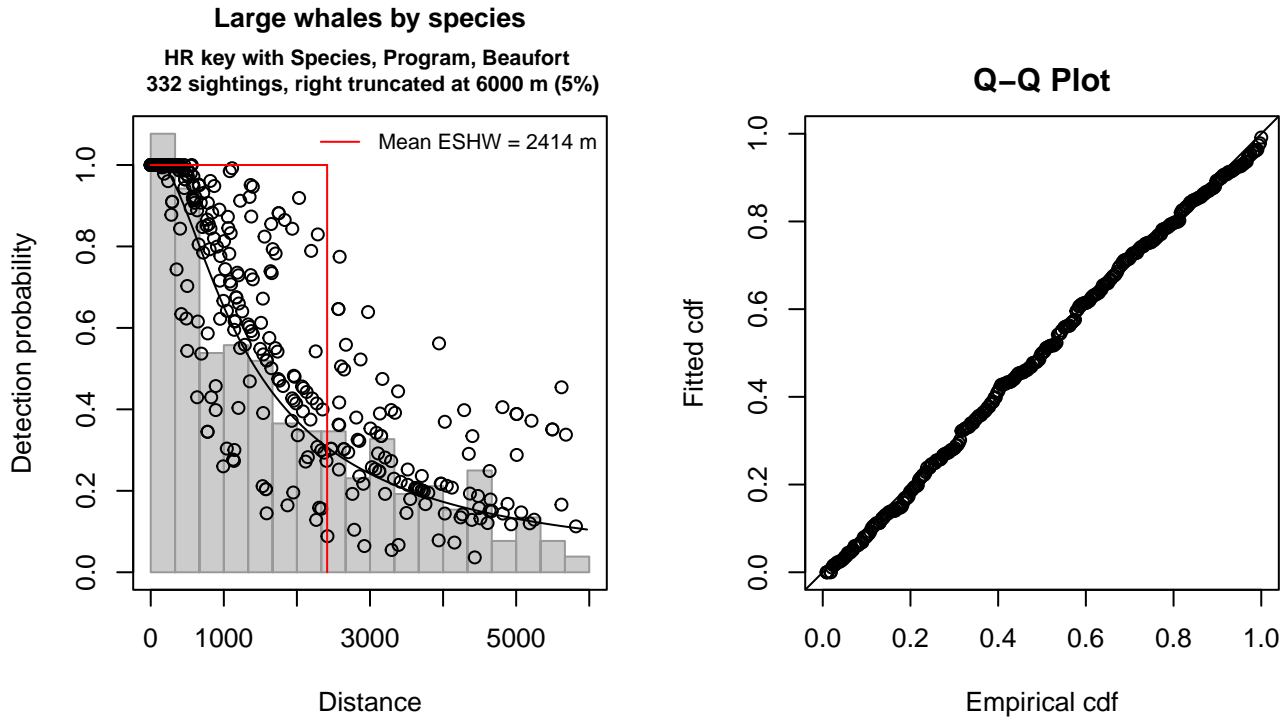


Figure 19: SEFSC detection function and Q-Q plot showing its goodness of fit.

Statistical output for this detection function:

Summary for ds object

Number of observations : 332  
 Distance range : 0 - 6000  
 AIC : 5604.674

Detection function:

Hazard-rate key function

Detection function parameters

Scale coefficient(s):

	estimate	se
(Intercept)	7.4794246	0.4929618
OriginalScientificNameSperm	0.7957413	0.3448895
ProgramAtlantic Pre-AMAPPS	-0.7295682	0.3154763
ProgramCaribbean	-0.7773443	0.4064337
Beaufort	-0.1322436	0.1039800

Shape coefficient(s):

	estimate	se
(Intercept)	0.3345999	0.1370809

	Estimate	SE	CV
Average p	0.3546416	0.03786854	0.1067797
N in covered region	936.1563072	108.72789053	0.1161429

Distance sampling Cramer-von Mises test (unweighted)

Test statistic = 0.055285 p = 0.843624

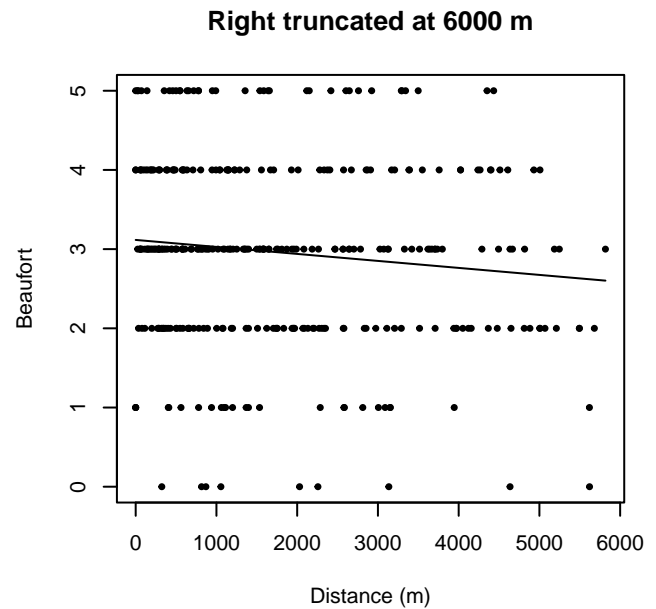
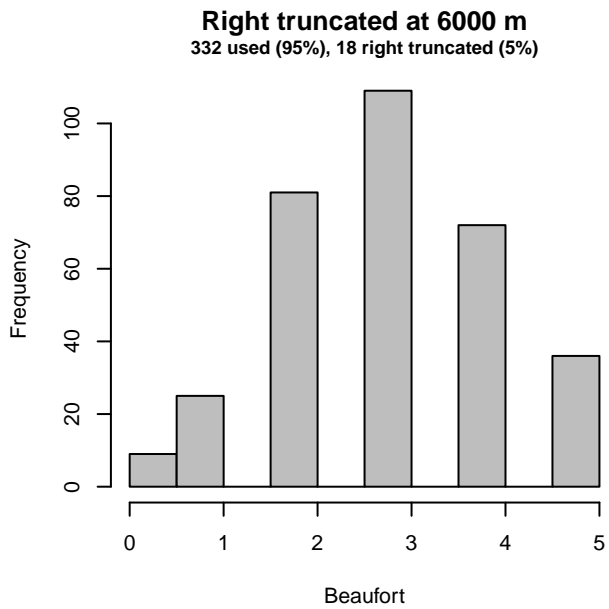
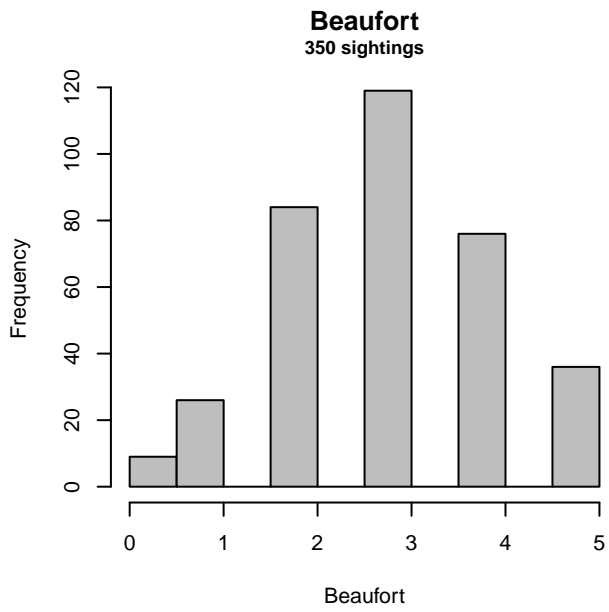


Figure 20: Distribution of the Beaufort covariate before (top row) and after (bottom row) observations were truncated to fit the SEFSC detection function.

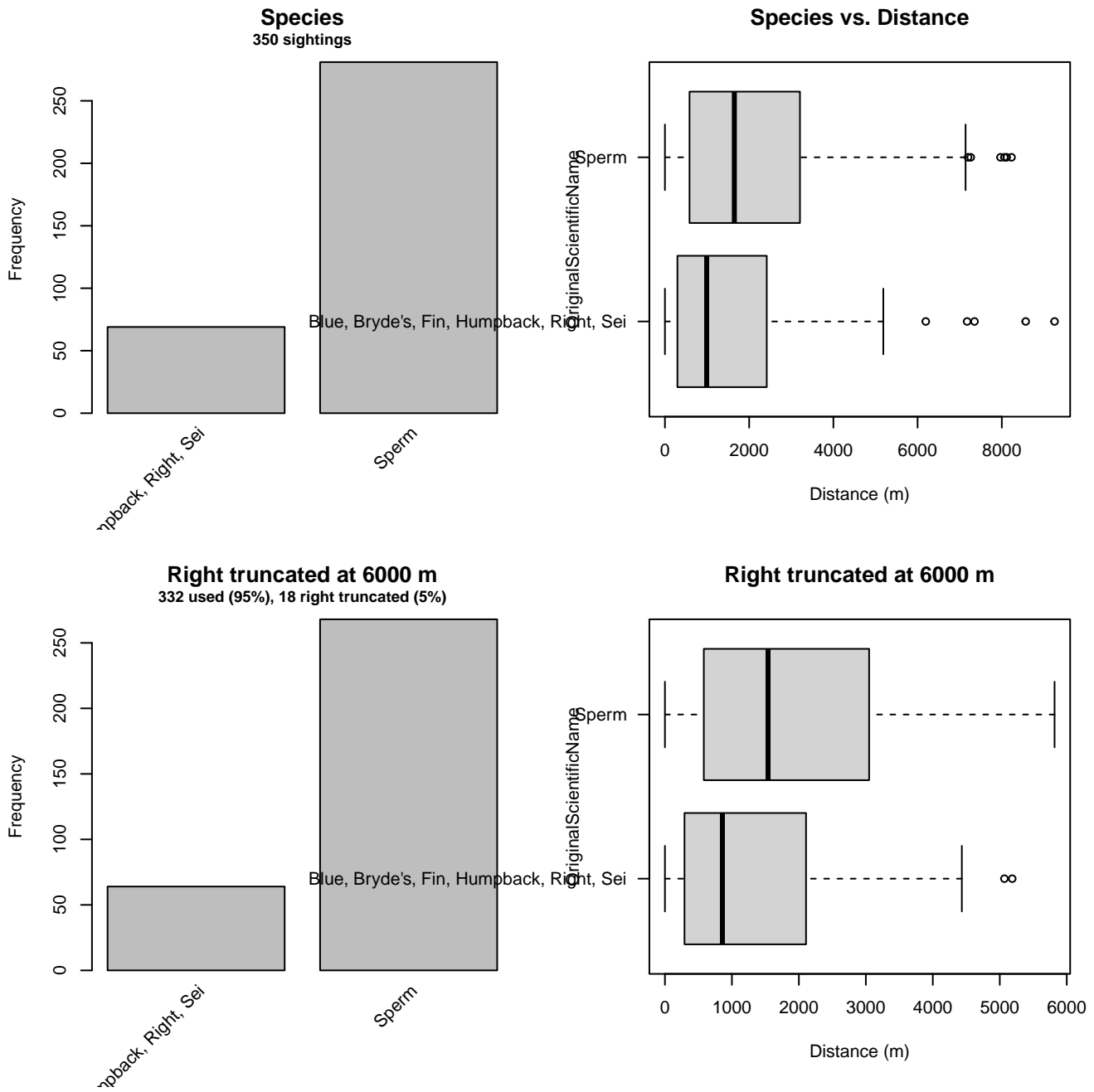


Figure 21: Distribution of the OriginalScientificName covariate before (top row) and after (bottom row) observations were truncated to fit the SEFSC detection function.

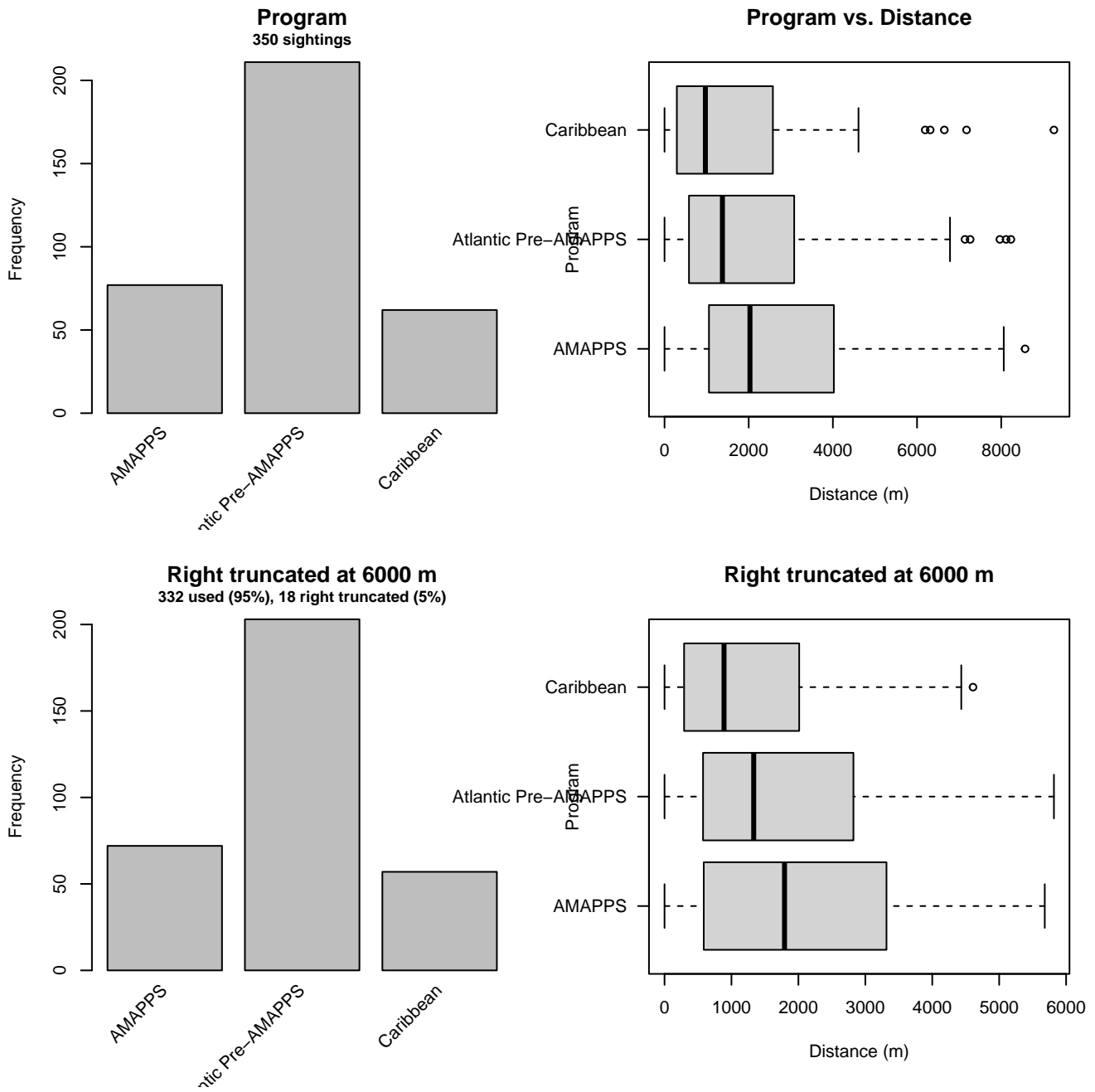


Figure 22: Distribution of the Program covariate before (top row) and after (bottom row) observations were truncated to fit the SEFSC detection function.

### 3.1.1.2.2 Song of the Whale

After right-truncating observations greater than 3000 m, we fitted the detection function to the 239 observations that remained (Table 10). The selected detection function (Figure 23) used a hazard rate key function with Glare (Figure 24), OriginalScientificName (Figure 25) and WeatherCode (Figure 26) as covariates.

Table 10: Observations used to fit the Song of the Whale detection function.

ScientificName	n
Balaenoptera borealis	13
Balaenoptera edeni	7
Balaenoptera musculus	8
Balaenoptera physalus	27
Megaptera novaeangliae	69
Physeter macrocephalus	115
<b>Total</b>	<b>239</b>

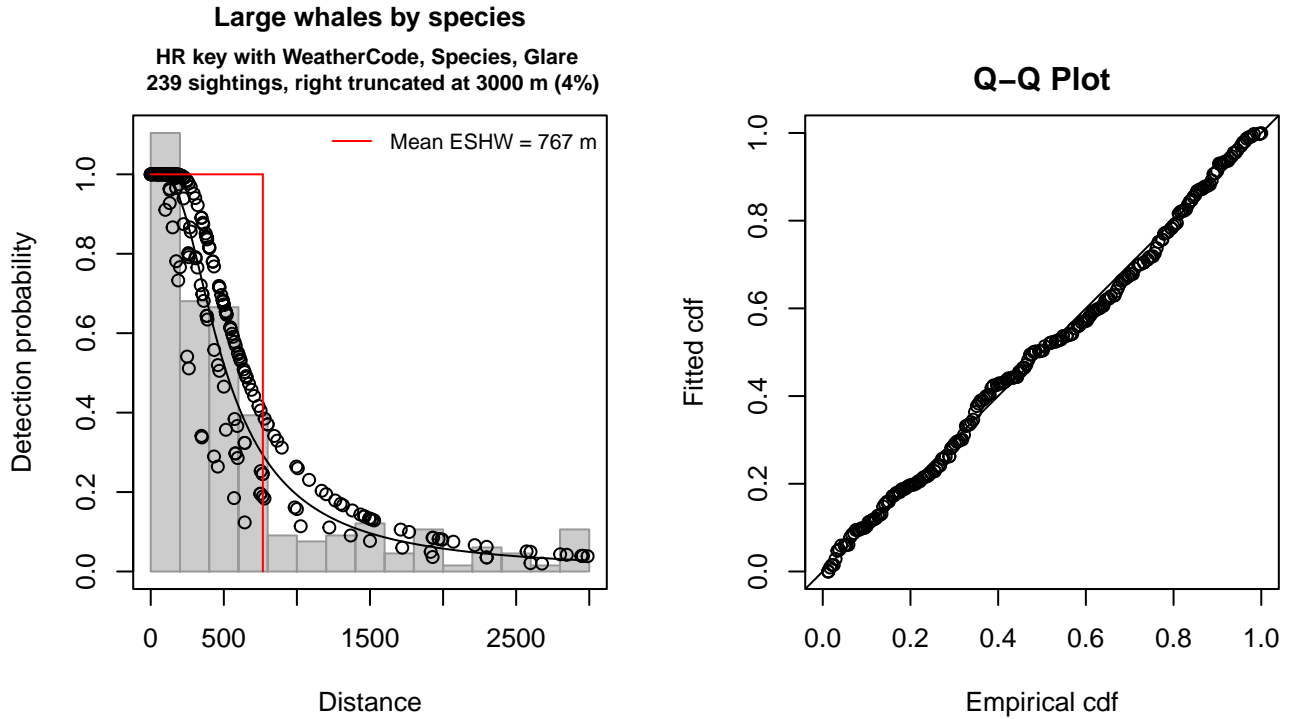


Figure 23: Song of the Whale detection function and Q-Q plot showing its goodness of fit.

Statistical output for this detection function:

Summary for ds object

Number of observations : 239  
 Distance range : 0 - 3000  
 AIC : 3547.931

Detection function:

Hazard-rate key function

Detection function parameters

Scale coefficient(s):

	estimate	se
(Intercept)	5.9647631	0.2274130
WeatherCodeHaze	-0.8889445	0.5747918
OriginalScientificNameHumpback, Sperm	0.3084029	0.2238350
GlareSevere	-0.4670165	0.2579856

Shape coefficient(s):

estimate	se
----------	----



(Intercept) 0.6276528 0.09675212

	Estimate	SE	CV
Average p	0.2409962	0.02414927	0.100206
N in covered region	991.7170380	114.27753421	0.115232

Distance sampling Cramer-von Mises test (unweighted)  
 Test statistic = 0.073160 p = 0.732317

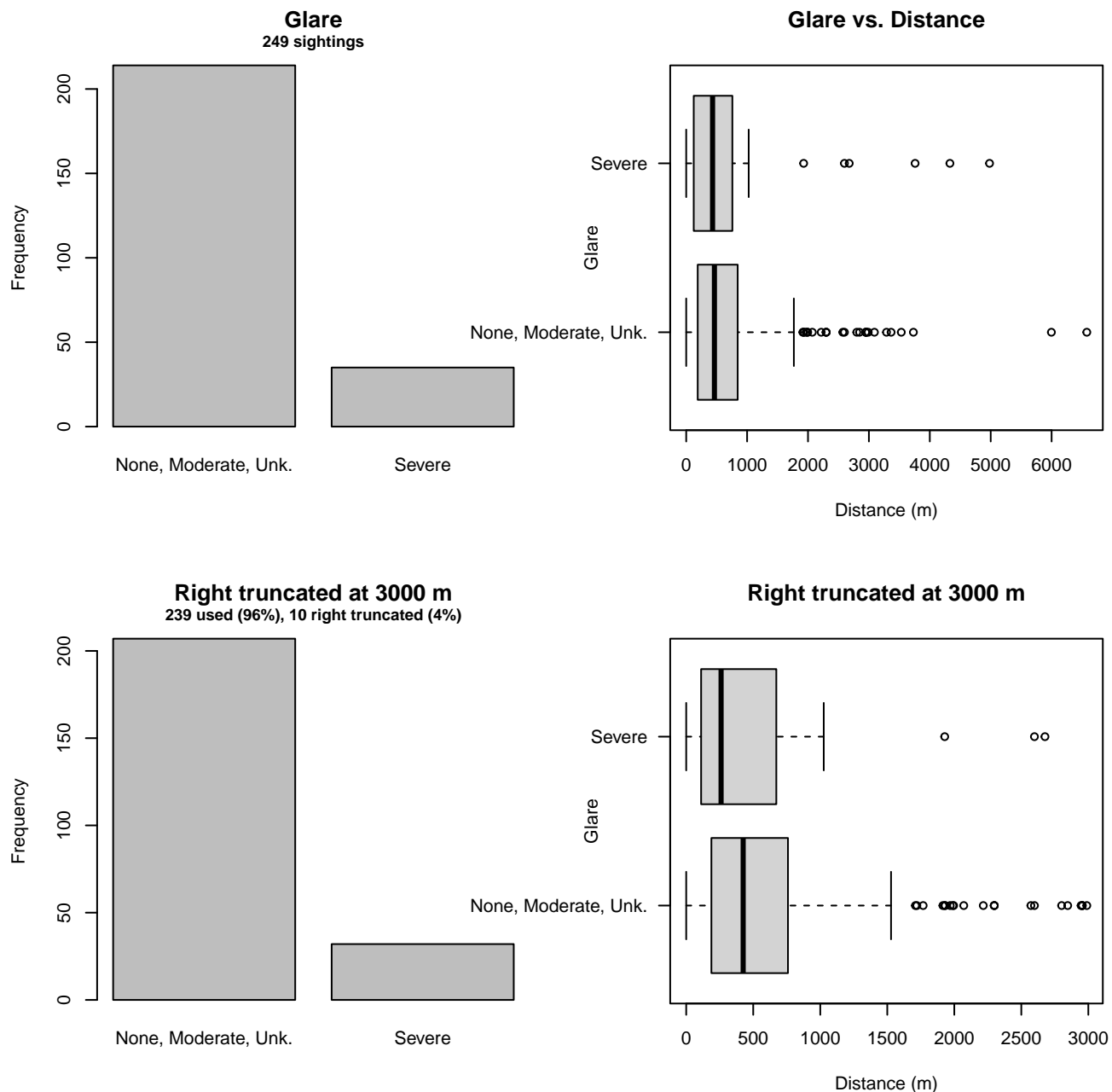


Figure 24: Distribution of the Glare covariate before (top row) and after (bottom row) observations were truncated to fit the Song of the Whale detection function.

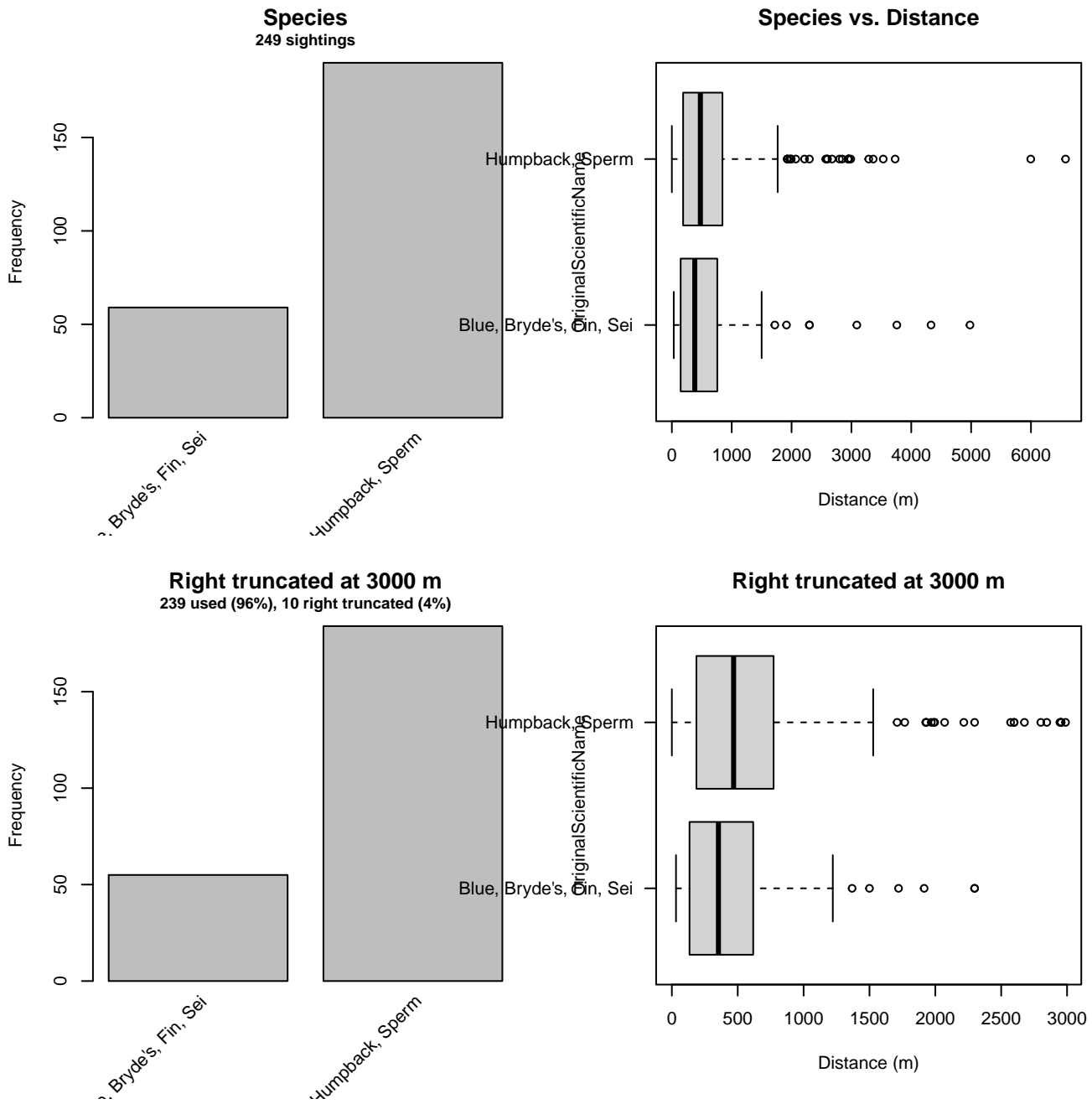


Figure 25: Distribution of the OriginalScientificName covariate before (top row) and after (bottom row) observations were truncated to fit the Song of the Whale detection function.

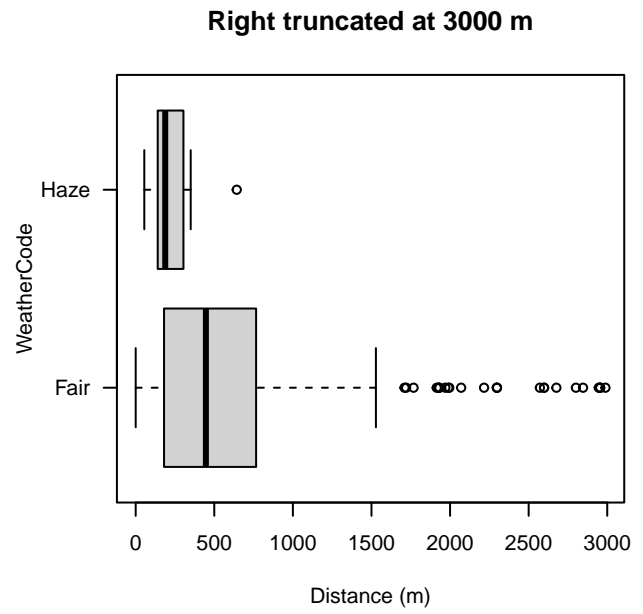
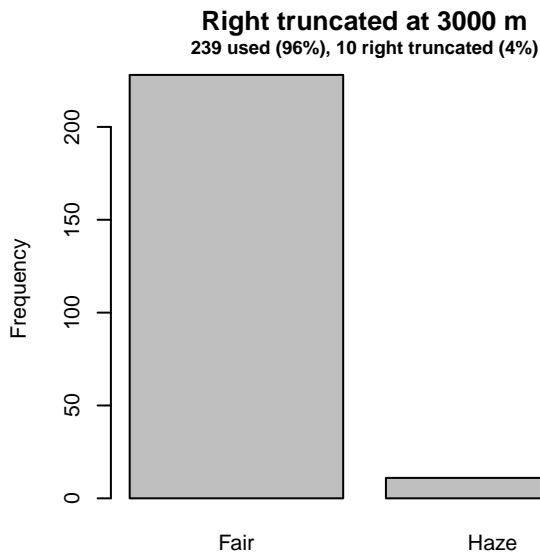
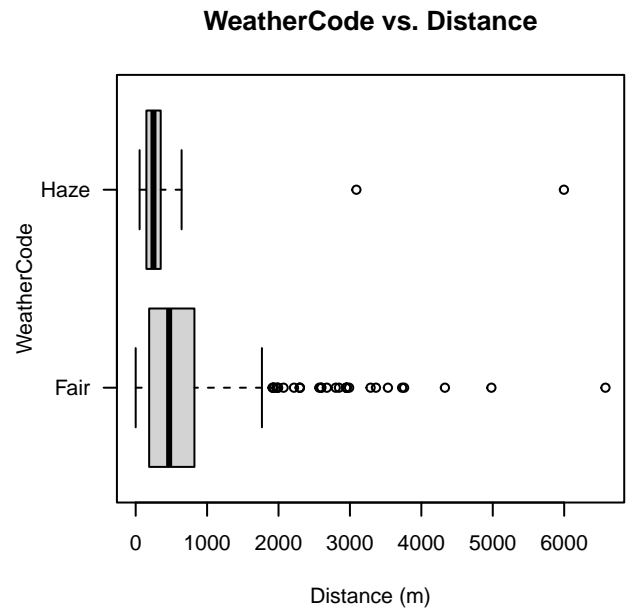
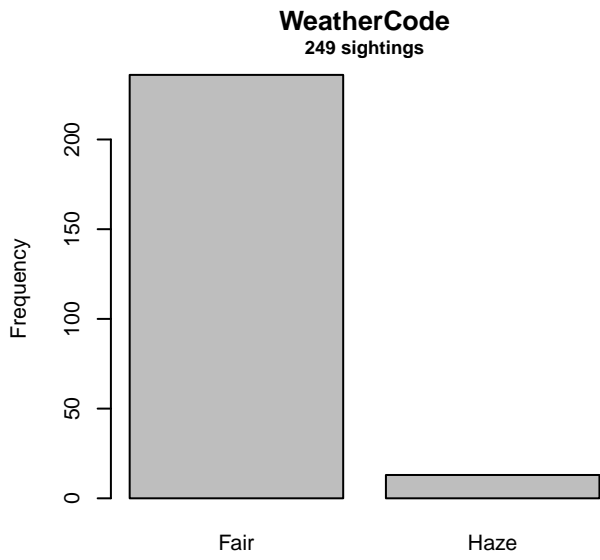


Figure 26: Distribution of the WeatherCode covariate before (top row) and after (bottom row) observations were truncated to fit the Song of the Whale detection function.

### 3.1.2 Large Whales (second group)

#### 3.1.2.1 Aerial Surveys

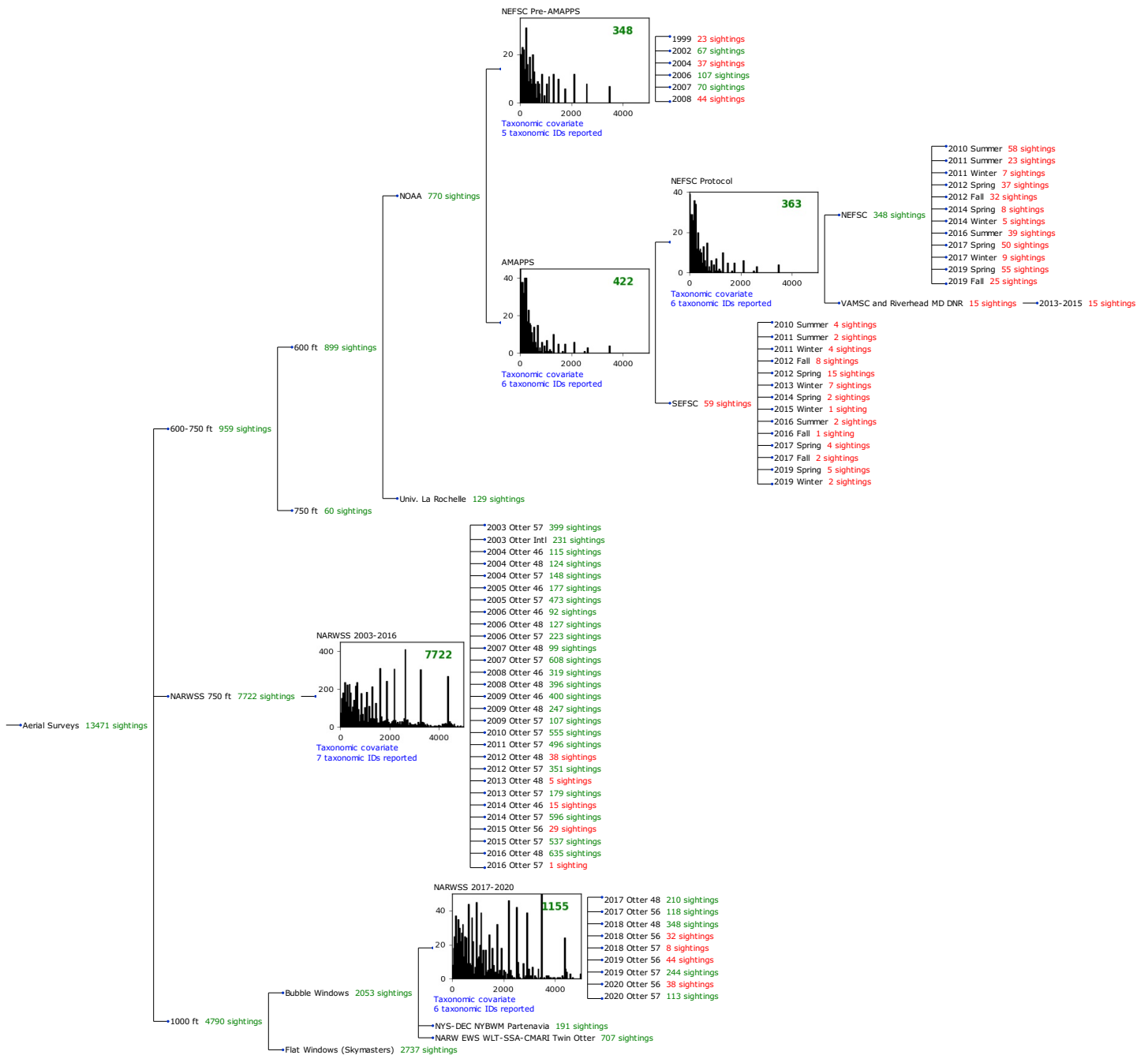


Figure 27: Detection hierarchy for aerial surveys, showing how they were pooled during detectability modeling, for detection functions that pooled multiple taxa and used a taxonomic covariate to account for differences between them. Each histogram represents a detection function and summarizes the perpendicular distances of observations that were pooled to fit it, prior to truncation. Observation counts, also prior to truncation, are shown in green when they met the recommendation of Buckland et al. (2001) that detection functions utilize at least 60 sightings, and red otherwise. For rare taxa, it was not always possible to meet this recommendation, yielding higher statistical uncertainty. During the spatial modeling stage of the analysis, effective strip widths were computed for each survey using the closest detection function above it in the hierarchy (i.e. moving from right to left in the figure). Surveys that do not have a detection function above them in this figure were either addressed by a detection function presented in a different section of this report, or were omitted from the analysis.

### 3.1.2.1.1 NEFSC Pre-AMAPPS

After right-truncating observations greater than 1500 m, we fitted the detection function to the 312 observations that remained (Table 11). The selected detection function (Figure 28) used a hazard rate key function with Beaufort (Figure 29) and ScientificName (Figure 30) as covariates.

Table 11: Observations used to fit the NEFSC Pre-AMAPPS detection function.

ScientificName	n
Blue, Fin, Sei, Sperm	170
Humpback, Right	142
<b>Total</b>	<b>312</b>

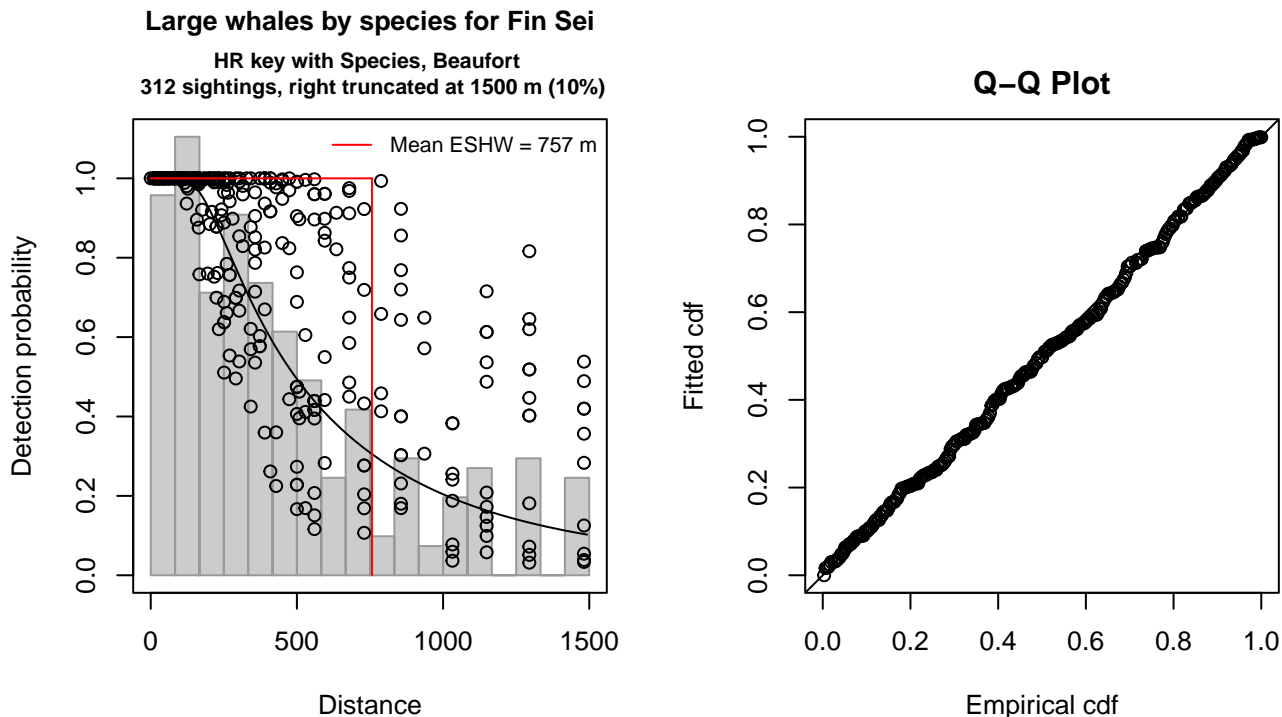


Figure 28: NEFSC Pre-AMAPPS detection function and Q-Q plot showing its goodness of fit.

Statistical output for this detection function:

Summary for ds object

Number of observations : 312  
 Distance range : 0 - 1500  
 AIC : 4376.913

Detection function:  
 Hazard-rate key function

Detection function parameters  
 Scale coefficient(s):

	estimate	se
(Intercept)	5.1153004	0.25110719
ScientificNameHumpback, Right	0.8493800	0.16417511
Beaufort	0.3206412	0.08719038

Shape coefficient(s):

estimate se  
 (Intercept) 0.7821505 0.1268451

	Estimate	SE	CV
Average p	0.4255304	0.0322576	0.07580562
N in covered region	733.2025745	64.9225054	0.08854648

Distance sampling Cramer-von Mises test (unweighted)  
 Test statistic = 0.034598 p = 0.958737

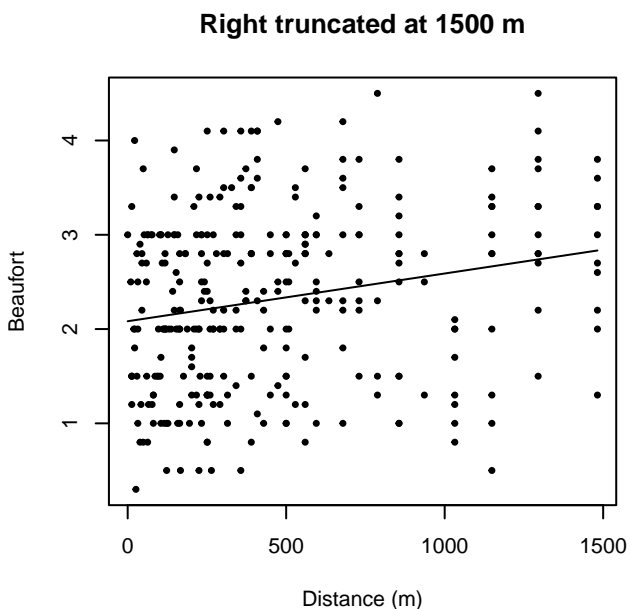
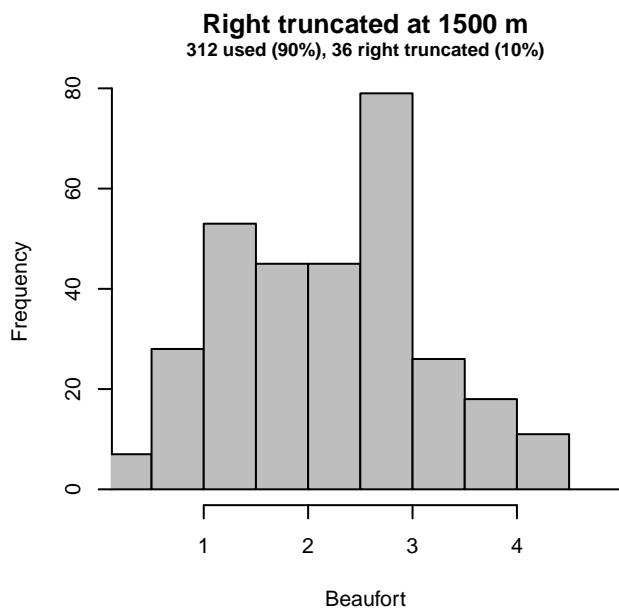
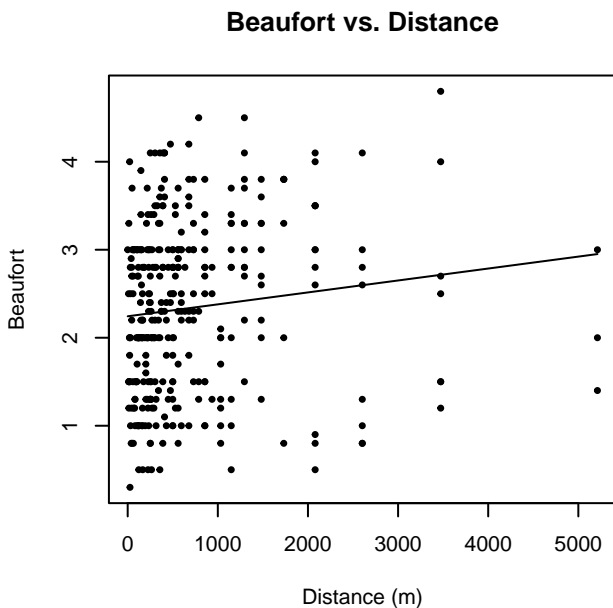
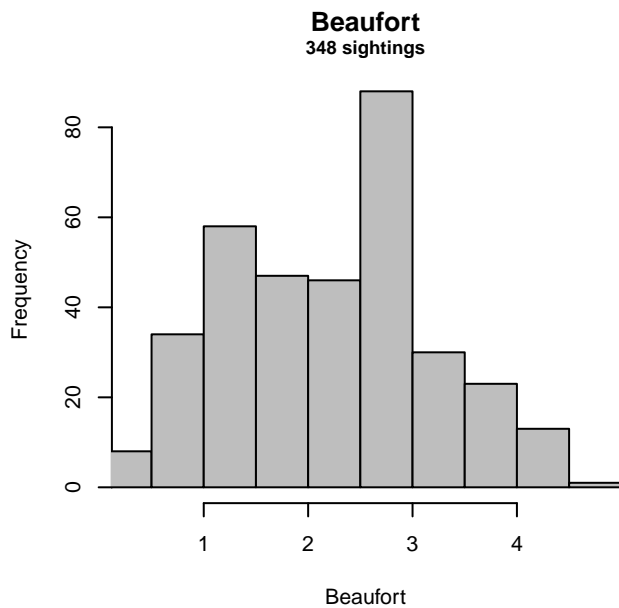


Figure 29: Distribution of the Beaufort covariate before (top row) and after (bottom row) observations were truncated to fit the NEFSC Pre-AMAPPS detection function.

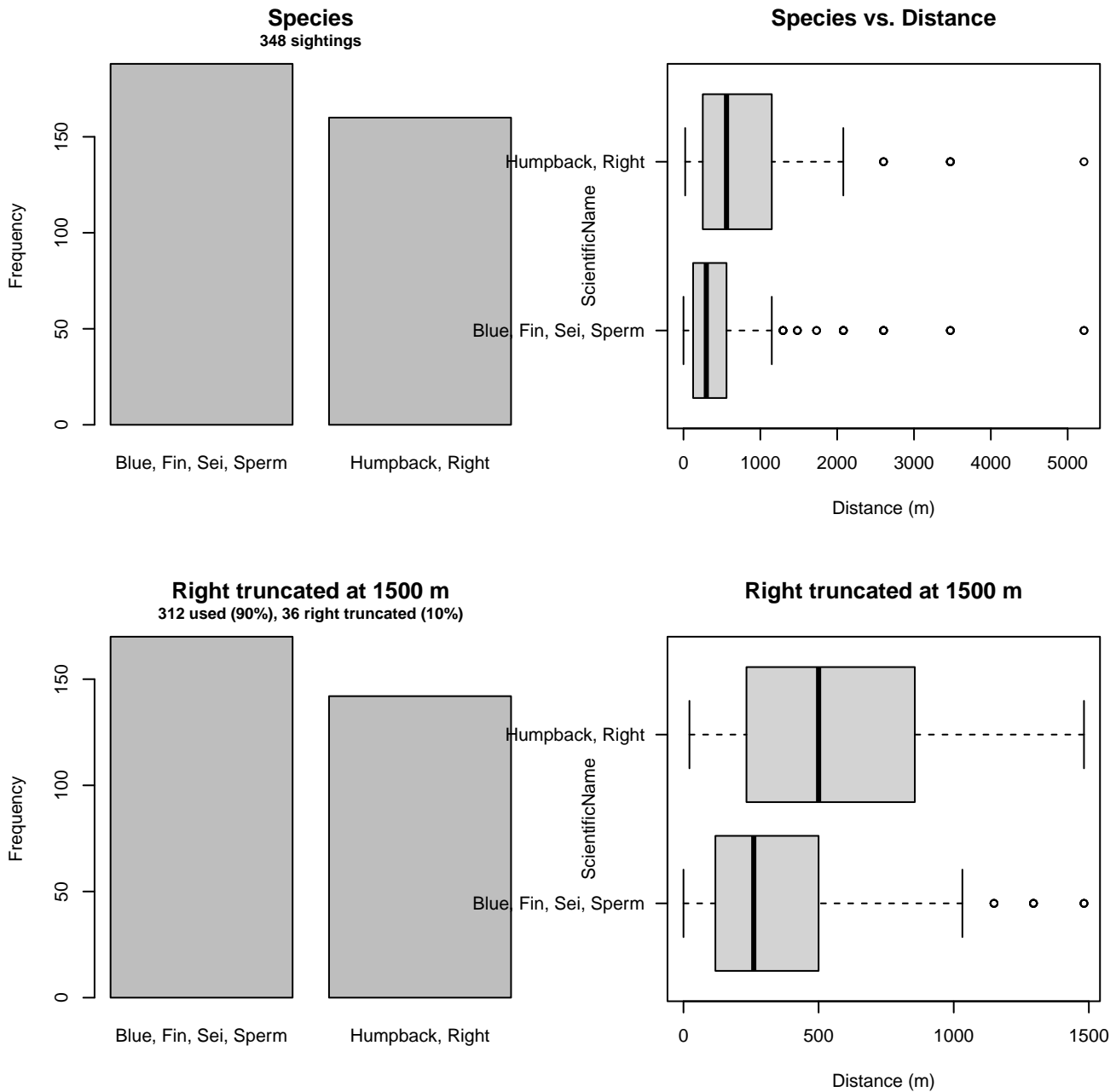


Figure 30: Distribution of the ScientificName covariate before (top row) and after (bottom row) observations were truncated to fit the NEFSC Pre-AMAPPS detection function.

### 3.1.2.1.2 NEFSC AMAPPS Protocol

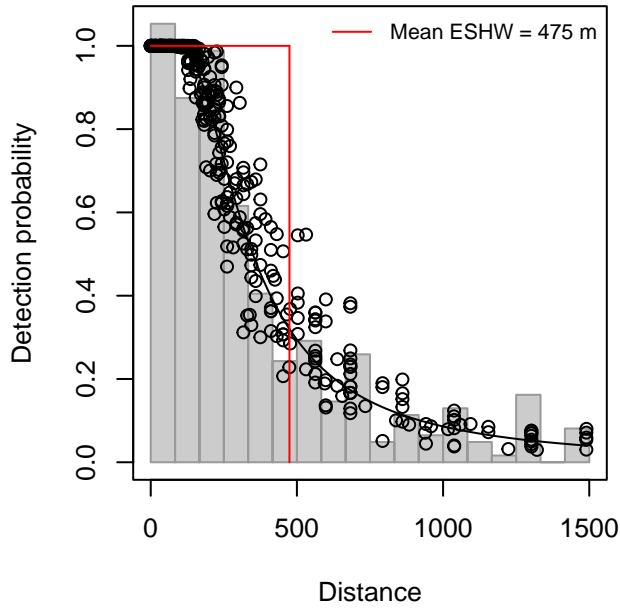
After right-truncating observations greater than 1500 m, we fitted the detection function to the 342 observations that remained (Table 12). The selected detection function (Figure 31) used a hazard rate key function with Beaufort (Figure 32), ScientificName (Figure 33) and Season (Figure 34) as covariates.

Table 12: Observations used to fit the NEFSC AMAPPS Protocol detection function.

ScientificName	n
Blue, Fin, Sei, Sperm	169
Humpback, Right	173
<b>Total</b>	<b>342</b>

### Large whales by species for Fin Sei

HR key with Season, Species, Beaufort  
342 sightings, right truncated at 1500 m (6%)



### Q-Q Plot

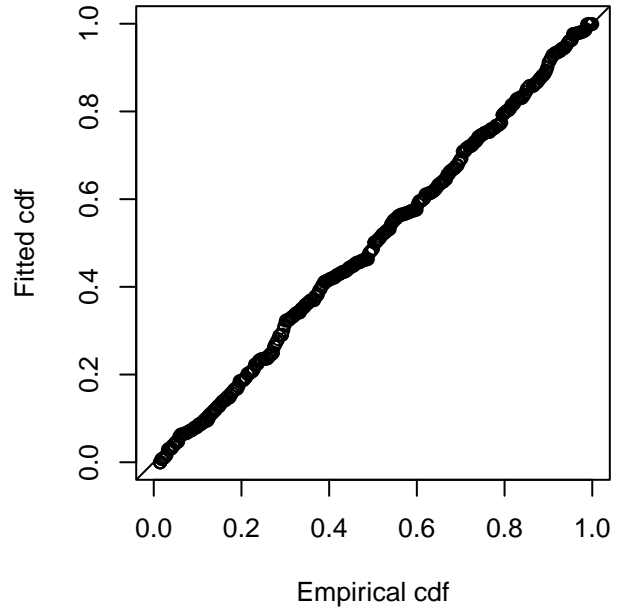


Figure 31: NEFSC AMAPPS Protocol detection function and Q-Q plot showing its goodness of fit.

Statistical output for this detection function:

Summary for ds object

Number of observations : 342  
Distance range : 0 - 1500  
AIC : 4680.051

Detection function:

Hazard-rate key function

Detection function parameters

Scale coefficient(s):

	estimate	se
(Intercept)	5.4141136	0.28874273
SeasonSummer, Fall, Winter	-0.2958446	0.16505718
ScientificNameHumpback, Right	0.1935469	0.15017530
Beaufort	0.1447199	0.08488516

Shape coefficient(s):

	estimate	se
(Intercept)	0.6850132	0.09386195

	Estimate	SE	CV
Average p	0.3078245	0.02296861	0.07461592
N in covered region	1111.0225351	96.96112333	0.08727197

Distance sampling Cramer-von Mises test (unweighted)

Test statistic = 0.052545 p = 0.860677



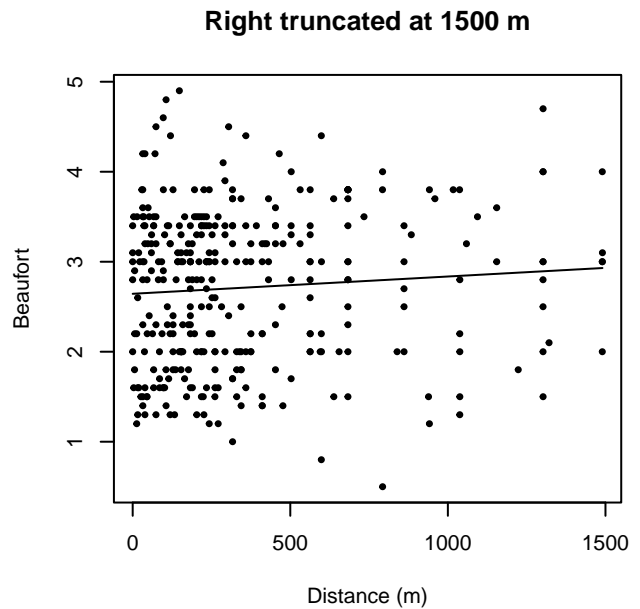
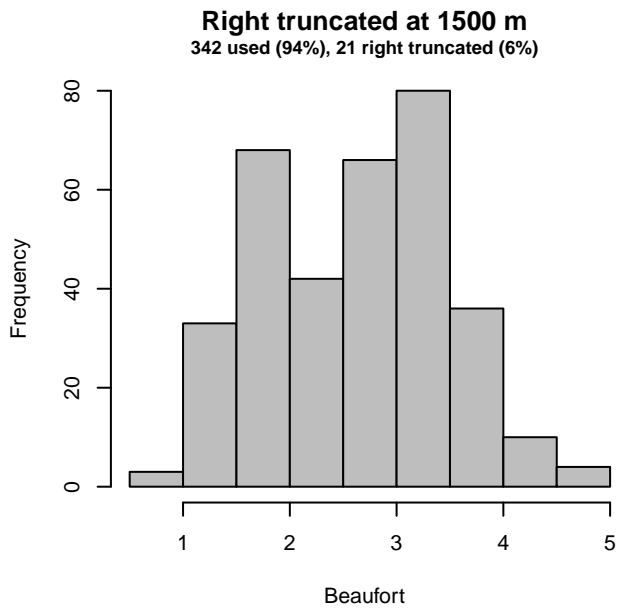
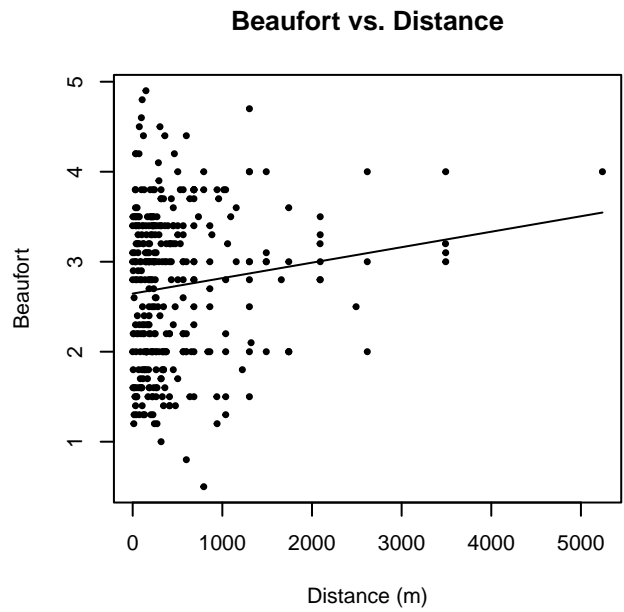
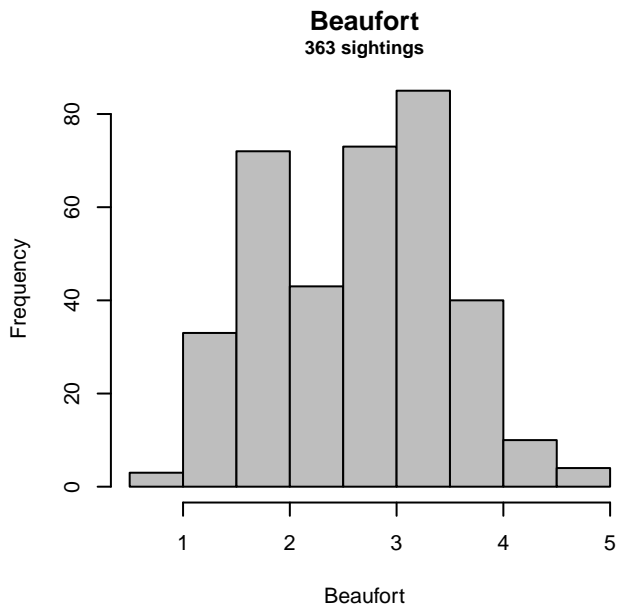


Figure 32: Distribution of the Beaufort covariate before (top row) and after (bottom row) observations were truncated to fit the NEFSC AMAPPS Protocol detection function.

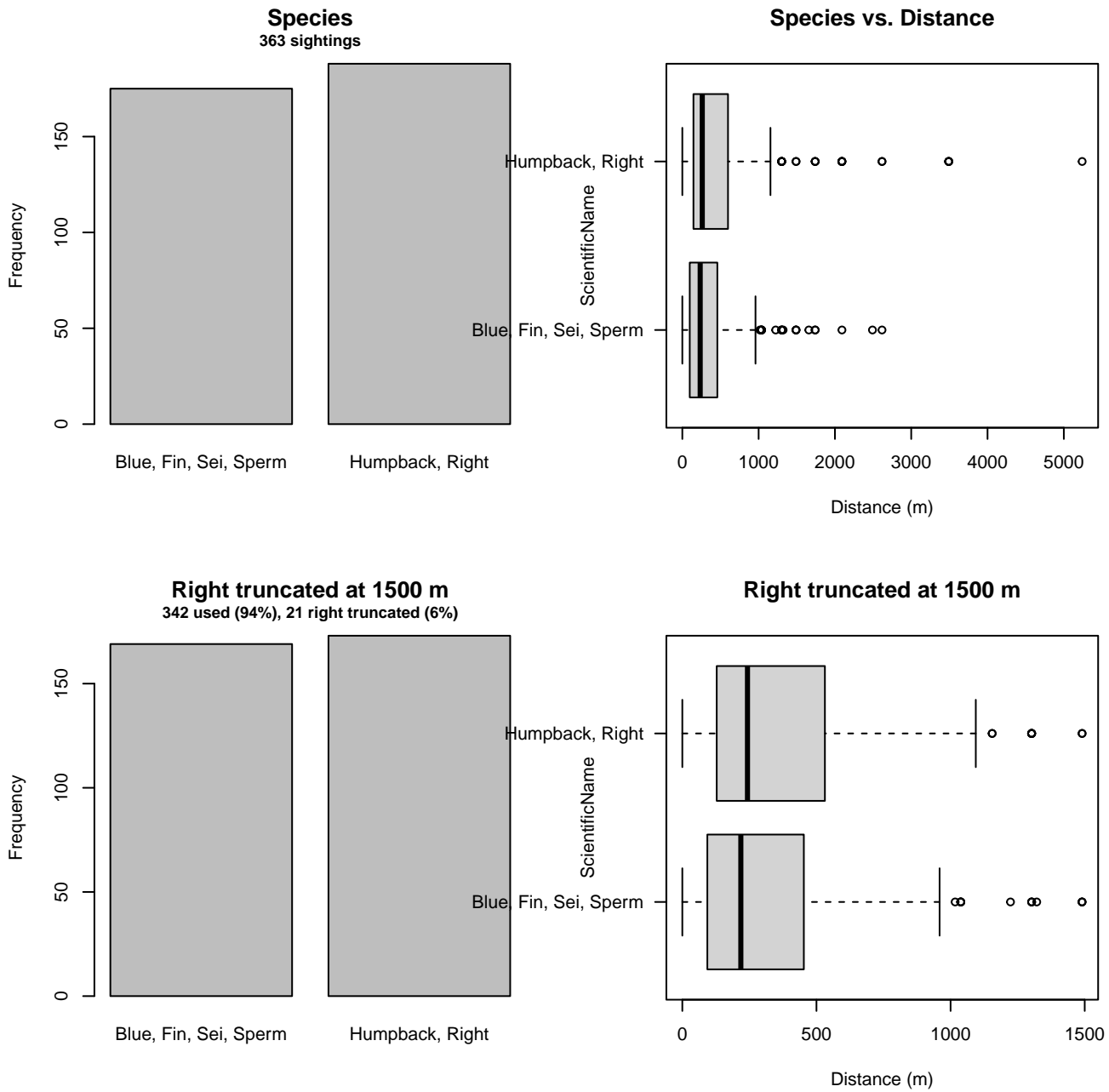


Figure 33: Distribution of the ScientificName covariate before (top row) and after (bottom row) observations were truncated to fit the NEFSC AMAPPS Protocol detection function.

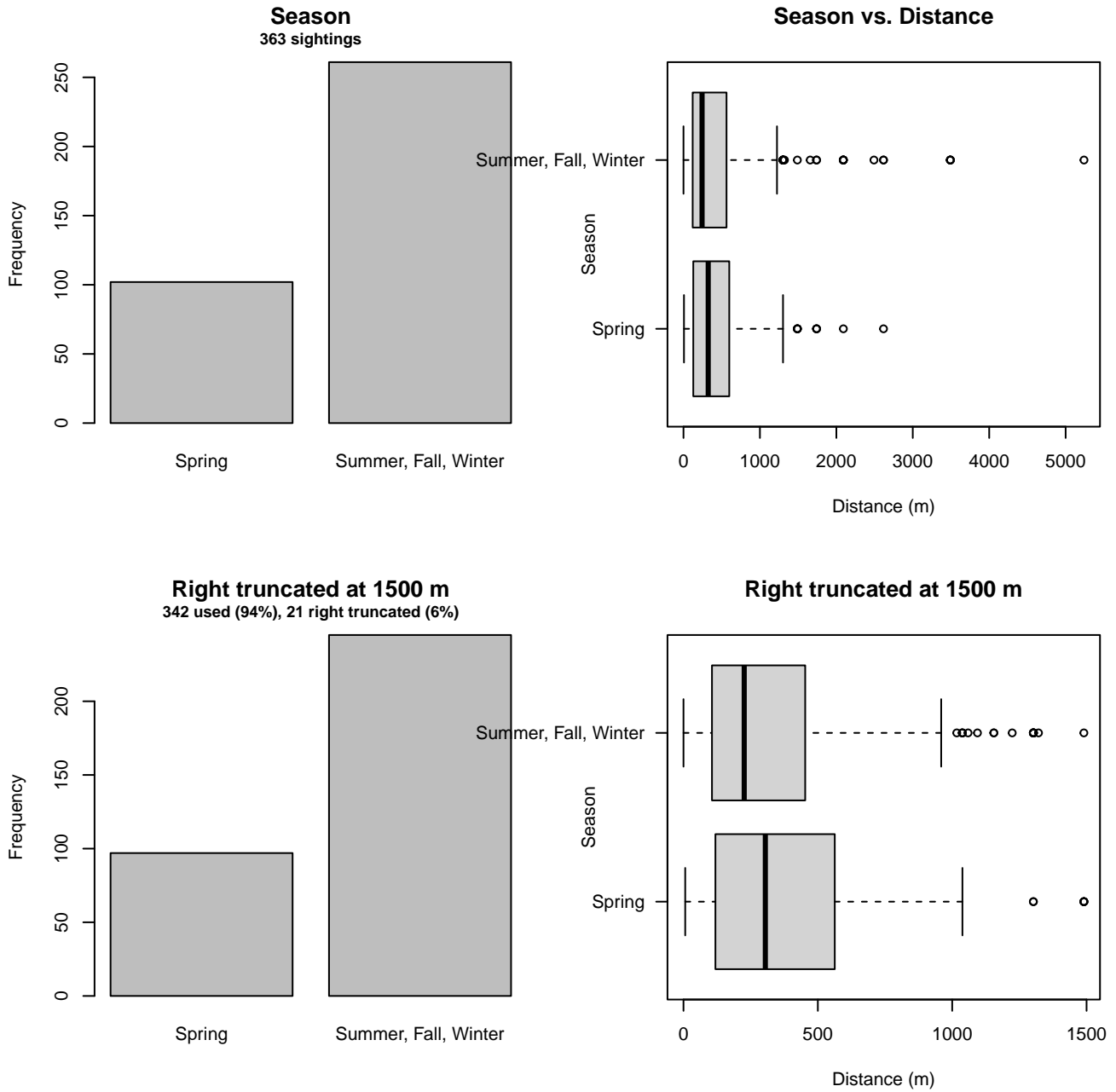


Figure 34: Distribution of the Season covariate before (top row) and after (bottom row) observations were truncated to fit the NEFSC AMAPPS Protocol detection function.

### 3.1.2.1.3 AMAPPS

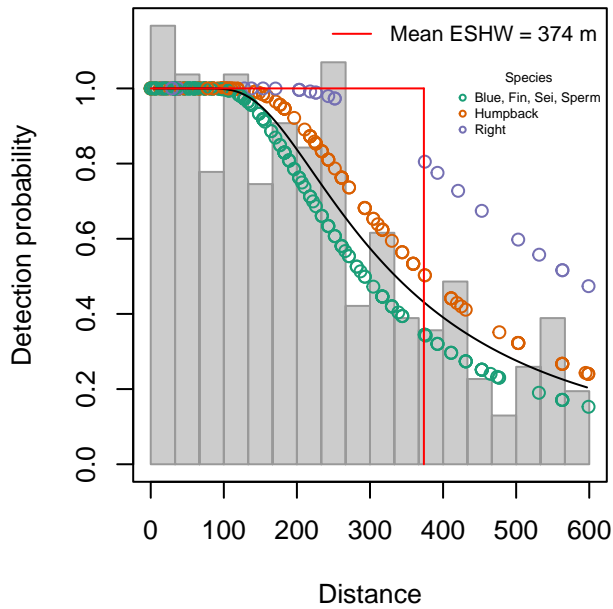
After right-truncating observations greater than 600 m, we fitted the detection function to the 341 observations that remained (Table 13). The selected detection function (Figure 35) used a hazard rate key function with ScientificName (Figure 36) as a covariate.

Table 13: Observations used to fit the AMAPPS detection function.

ScientificName	n
Blue, Fin, Sei, Sperm	178
Humpback	137
Right	26
<b>Total</b>	<b>341</b>

## Large whales by species for Fin Sei

HR key with Species  
341 sightings, right truncated at 600 m (19%)



## Q-Q Plot

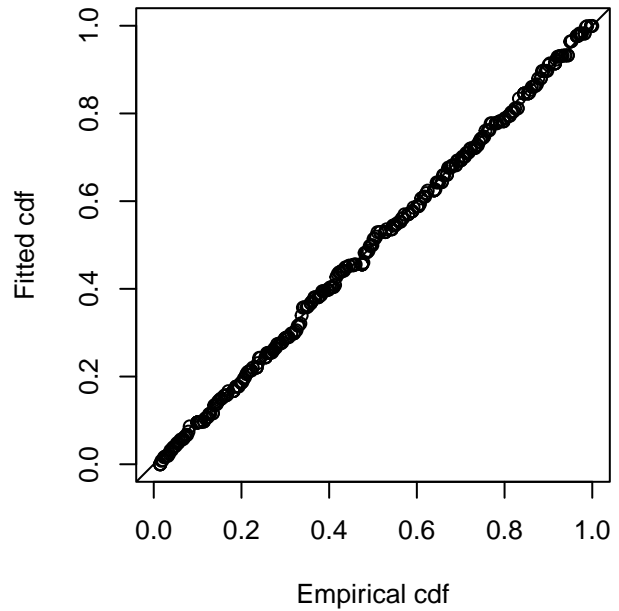


Figure 35: AMAPPS detection function and Q-Q plot showing its goodness of fit.

Statistical output for this detection function:

Summary for ds object

Number of observations : 341  
Distance range : 0 - 600  
AIC : 4284.044

Detection function:

Hazard-rate key function

Detection function parameters

Scale coefficient(s):

	estimate	se
(Intercept)	5.4948745	0.1470359
ScientificNameHumpback	0.2526859	0.1796647
ScientificNameRight	0.6784369	0.3879710

Shape coefficient(s):

	estimate	se
(Intercept)	0.6905331	0.1975579

	Estimate	SE	CV
Average p	0.6139761	0.04048736	0.06594289
N in covered region	555.3962176	41.21446559	0.07420732

Distance sampling Cramer-von Mises test (unweighted)

Test statistic = 0.027885 p = 0.982585

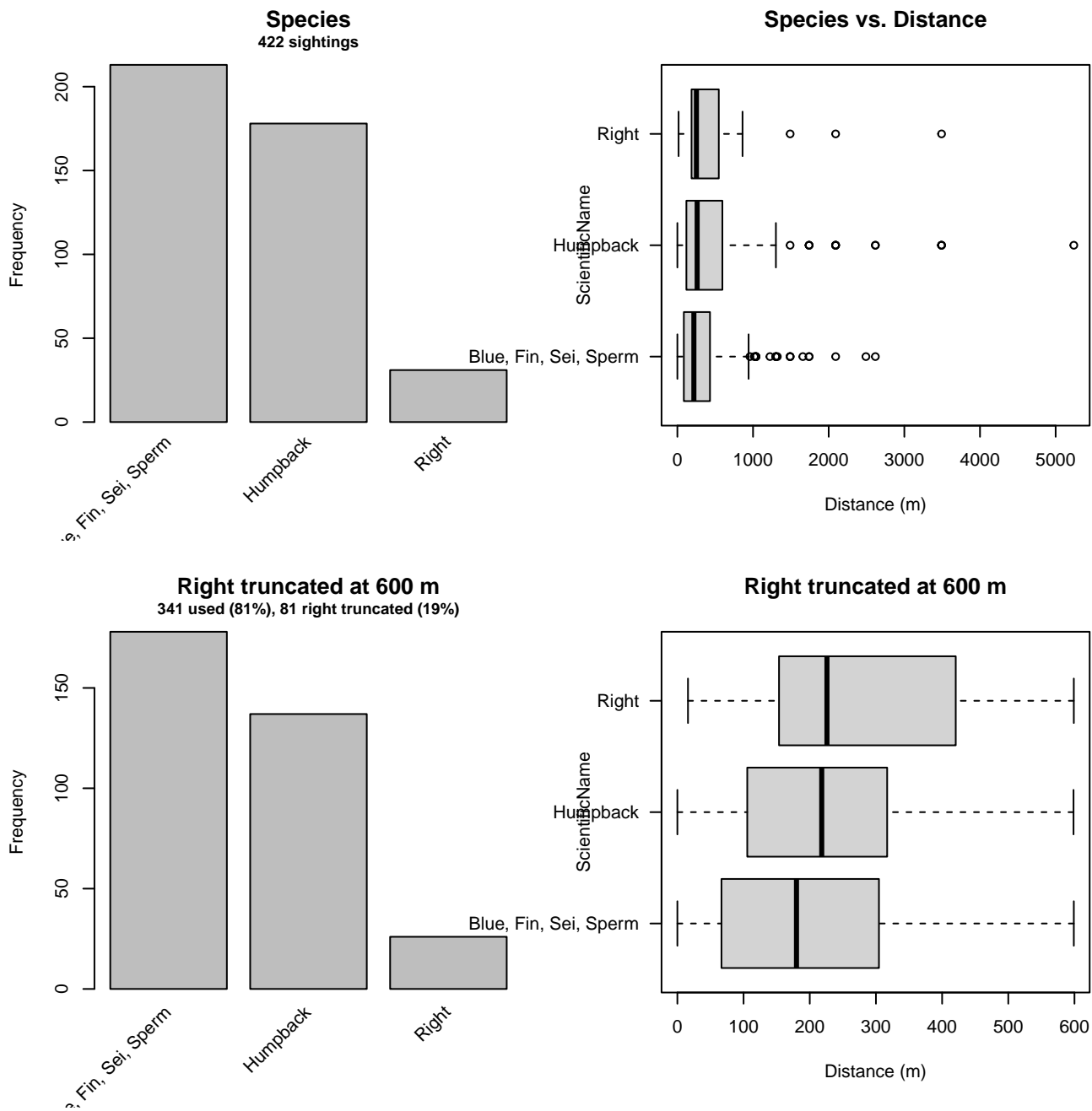


Figure 36: Distribution of the ScientificName covariate before (top row) and after (bottom row) observations were truncated to fit the AMAPPS detection function.

#### 3.1.2.1.4 NARWSS 2003-2016

After right-truncating observations greater than 5236 m, we fitted the detection function to the 7315 observations that remained (Table 14). The selected detection function (Figure 37) used a hazard rate key function with Beaufort (Figure 38), Glare (Figure 39), ScientificName (Figure 40) and Visibility (Figure 41) as covariates.

Table 14: Observations used to fit the NARWSS 2003-2016 detection function.

ScientificName	n
Blue, Fin, Sei, Sperm	3084
Humpback	2890
Right, Bowhead	1341
<b>Total</b>	<b>7315</b>

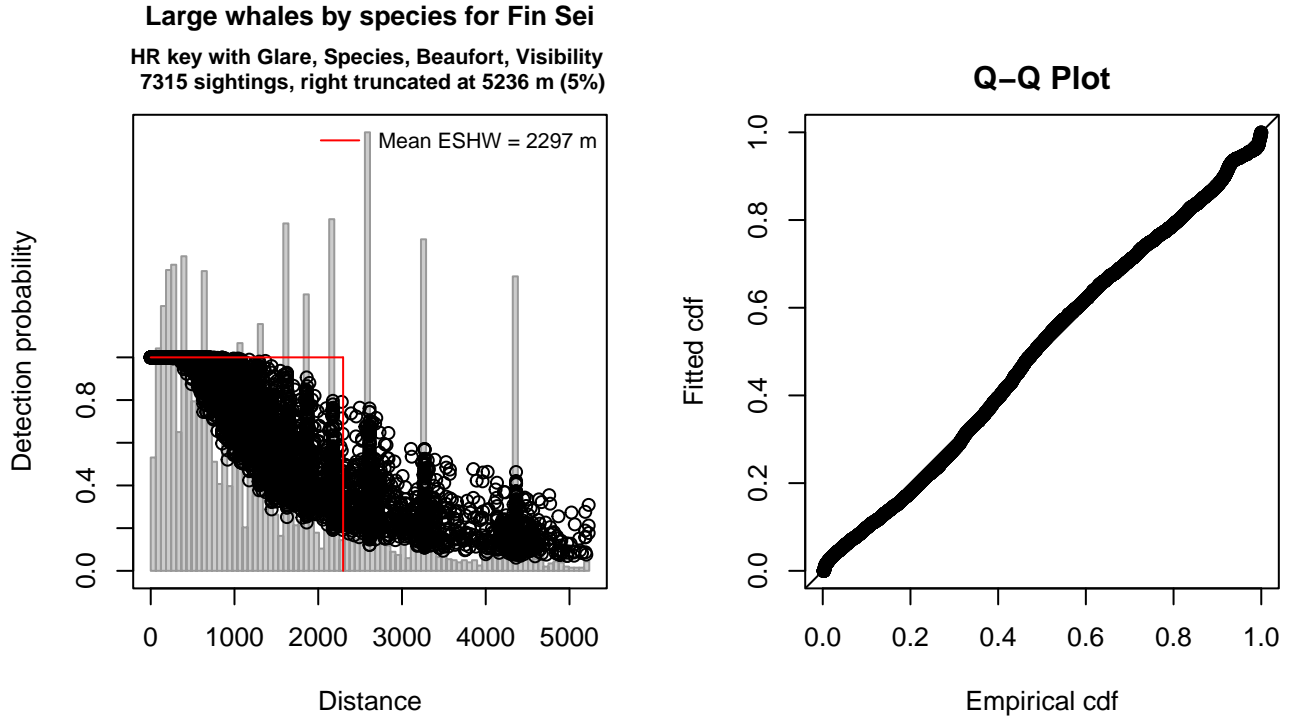


Figure 37: NARWSS 2003-2016 detection function and Q-Q plot showing its goodness of fit.

Statistical output for this detection function:

Summary for ds object

Number of observations : 7315  
 Distance range : 0 - 5236  
 AIC : 121560.3

Detection function:

Hazard-rate key function

Detection function parameters

Scale coefficient(s):

	estimate	se
(Intercept)	6.532231399	0.095753398
GlareSevere	0.418817117	0.059020446
ScientificNameHumpback	0.392288899	0.046225103
ScientificNameRight, Bowhead	0.123395135	0.057328635
Beaufort	0.099396384	0.022096321
Visibility	0.007659624	0.002242667

Shape coefficient(s):

	estimate	se
(Intercept)	0.4861478	0.03138397

	Estimate	SE	CV
Average p	4.220665e-01	7.456216e-03	0.01766597
N in covered region	1.733139e+04	3.437425e+02	0.01983352

Distance sampling Cramer-von Mises test (unweighted)  
 Test statistic = 1.731302 p = 0.000052

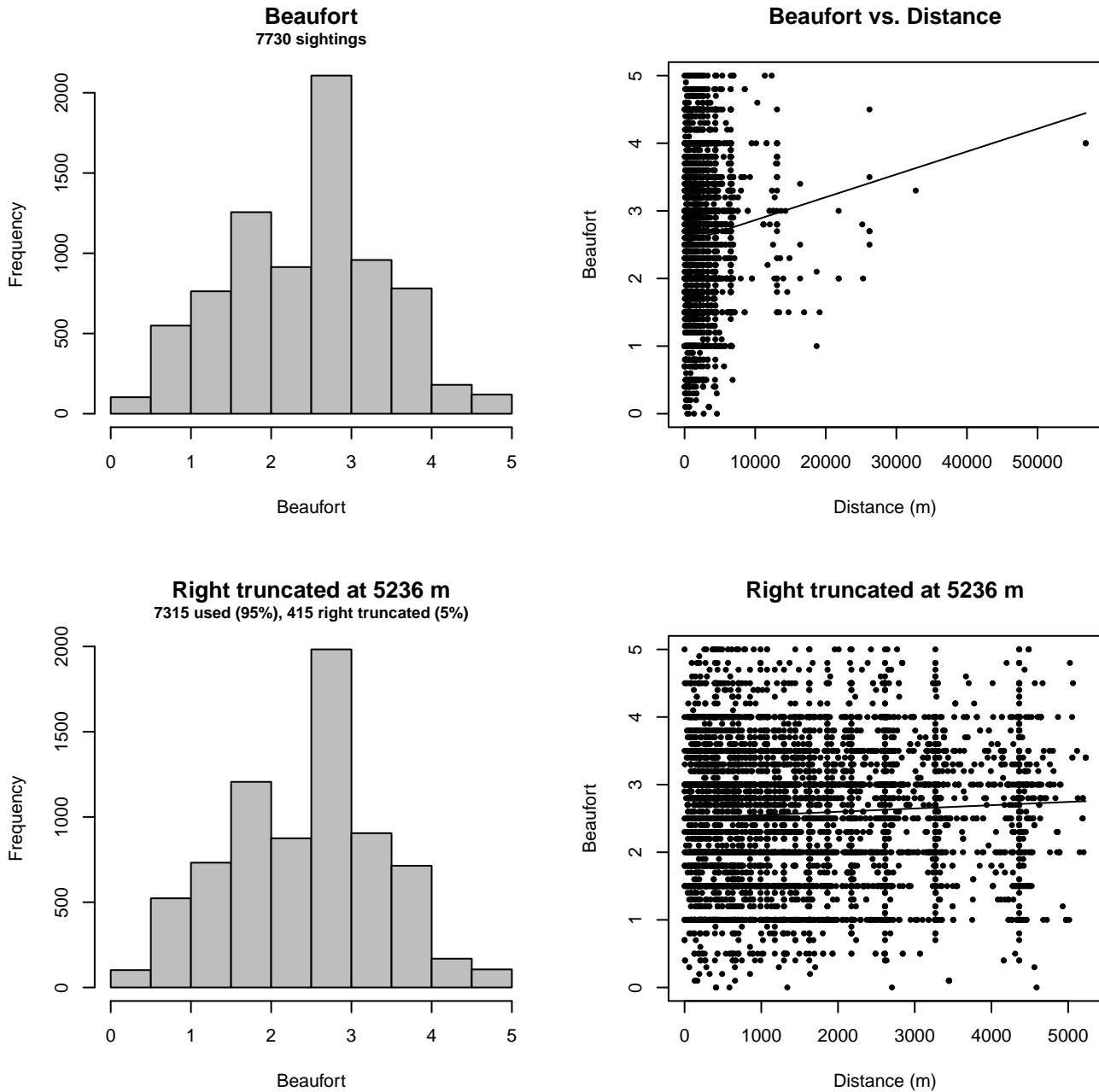


Figure 38: Distribution of the Beaufort covariate before (top row) and after (bottom row) observations were truncated to fit the NARWSS 2003-2016 detection function.

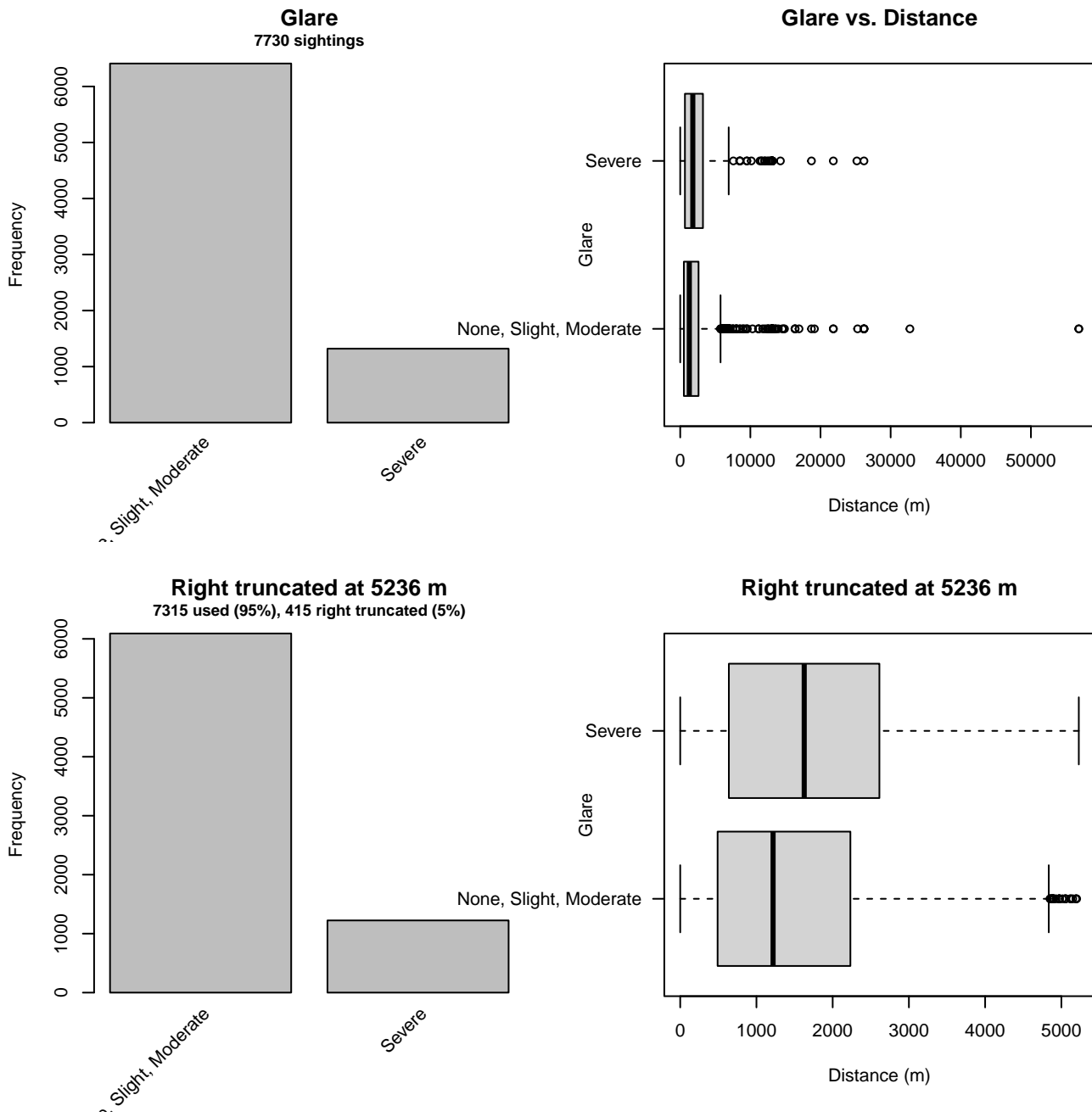


Figure 39: Distribution of the Glare covariate before (top row) and after (bottom row) observations were truncated to fit the NARWSS 2003-2016 detection function.



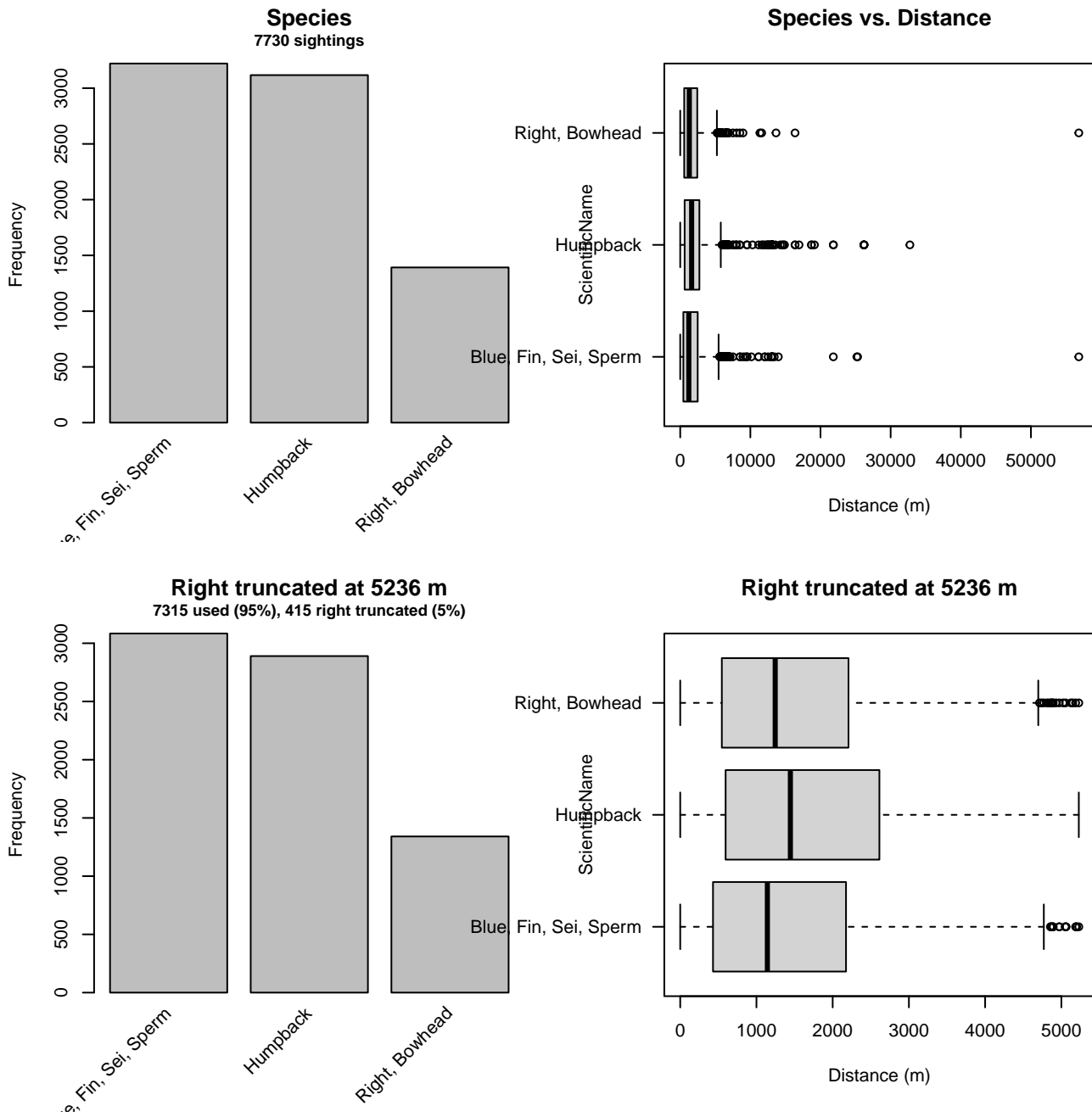


Figure 40: Distribution of the ScientificName covariate before (top row) and after (bottom row) observations were truncated to fit the NARWSS 2003-2016 detection function.

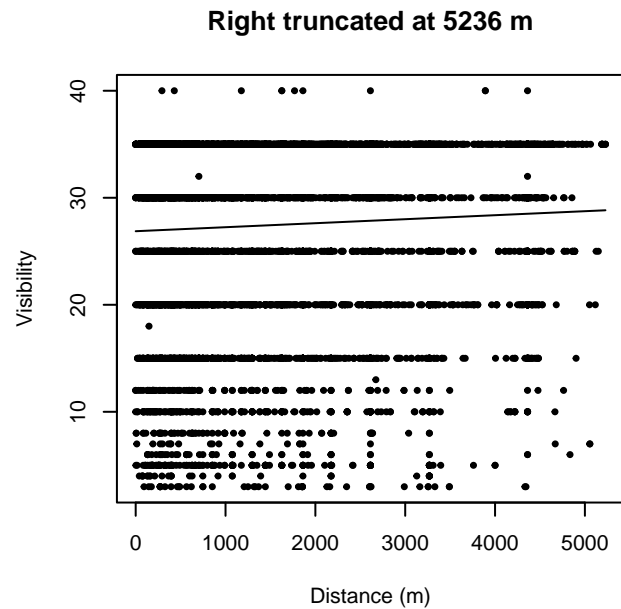
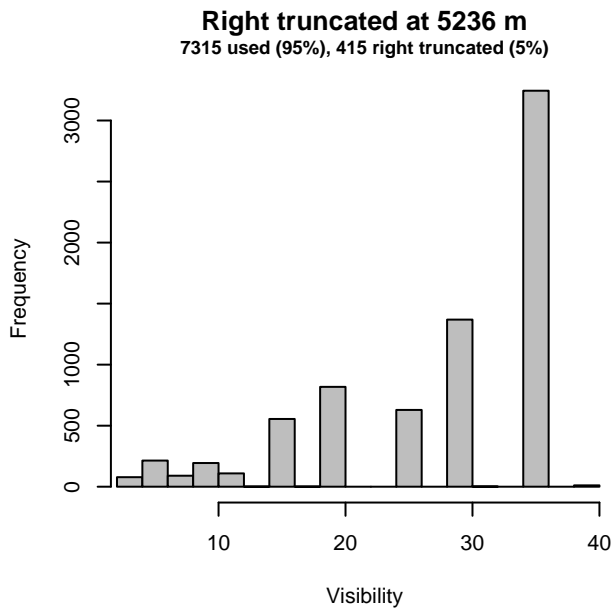
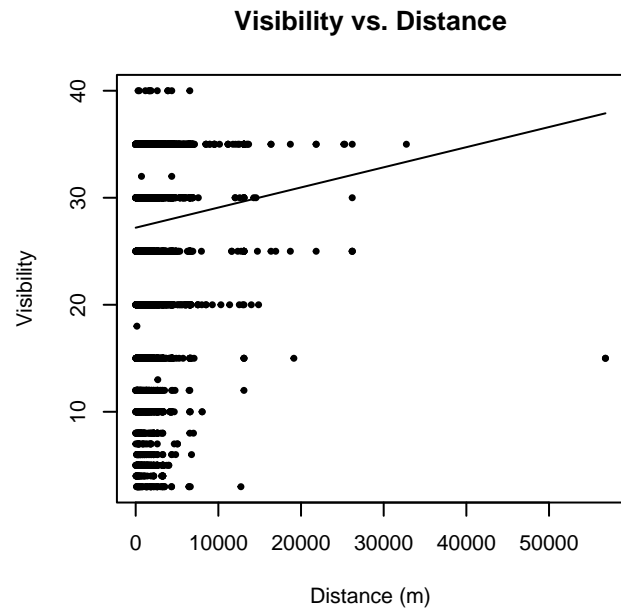
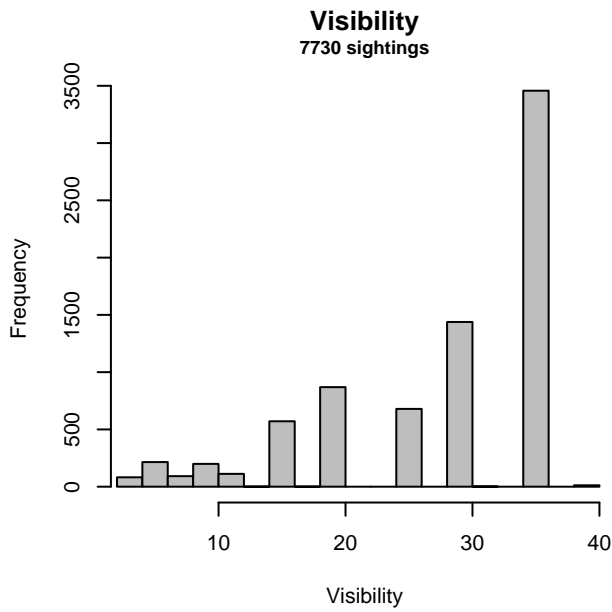


Figure 41: Distribution of the Visibility covariate before (top row) and after (bottom row) observations were truncated to fit the NARWSS 2003-2016 detection function.

### 3.1.2.1.5 NARWSS 2017-2020

After right-truncating observations greater than 5236 m, we fitted the detection function to the 1088 observations that remained (Table 15). The selected detection function (Figure 42) used a hazard rate key function with QualityCode (Figure 43) and ScientificName (Figure 44) as covariates.

Table 15: Observations used to fit the NARWSS 2017-2020 detection function.

ScientificName	n
Blue, Bowhead, Fin, Right, Sperm	510
Humpback	402
Sei, Bryde's	176
<b>Total</b>	<b>1088</b>

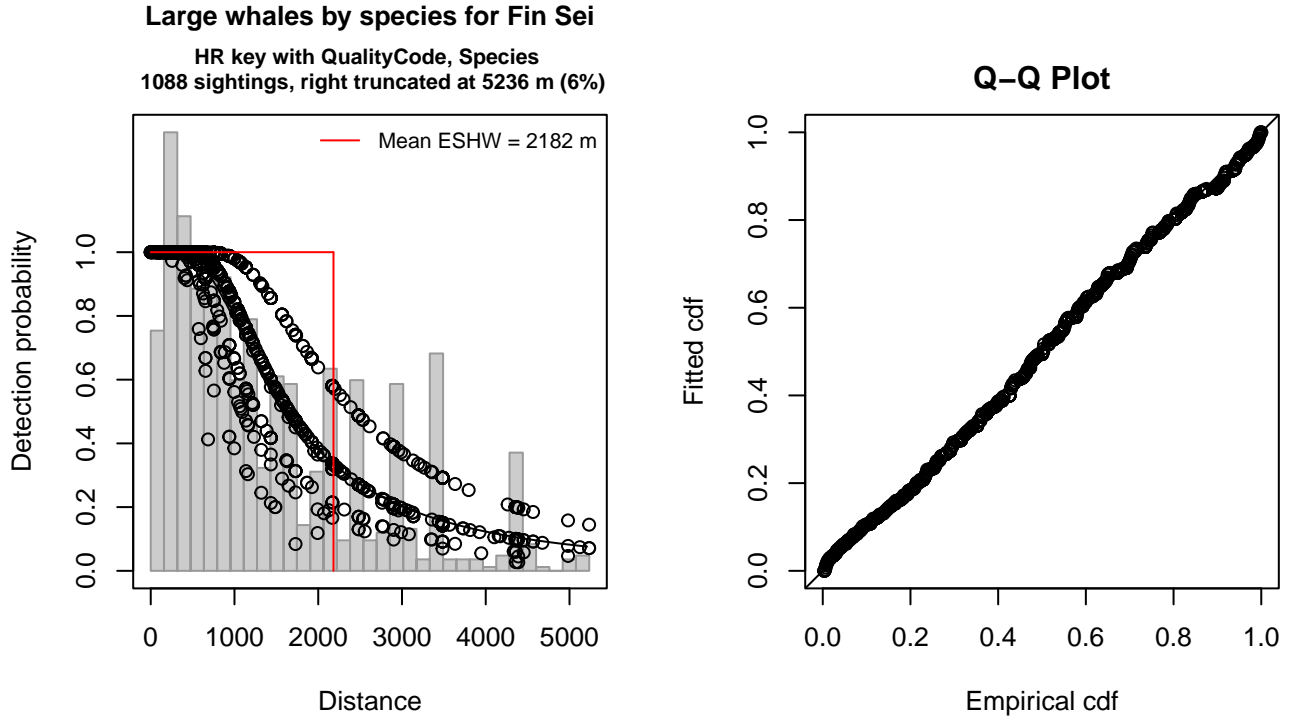


Figure 42: NARWSS 2017-2020 detection function and Q-Q plot showing its goodness of fit.

Statistical output for this detection function:

Summary for ds object

Number of observations : 1088  
 Distance range : 0 - 5236  
 AIC : 17919.96

Detection function:  
 Hazard-rate key function

Detection function parameters

Scale coefficient(s):

	estimate	se
(Intercept)	7.2235234	0.08269456
QualityCodeGood	-0.4184817	0.11743936
QualityCodeModerate	-0.7472672	0.45781582
ScientificNameHumpback	0.3855596	0.09754242
ScientificNameSei, Bryde's	-0.2722542	0.12297203

Shape coefficient(s):

	estimate	se
(Intercept)	0.6646987	0.07157793

	Estimate	SE	CV
Average p	0.3945574	0.01634594	0.04142856
N in covered region	2757.5202964	132.04989012	0.04788719

Distance sampling Cramer-von Mises test (unweighted)  
 Test statistic = 0.162876 p = 0.352620

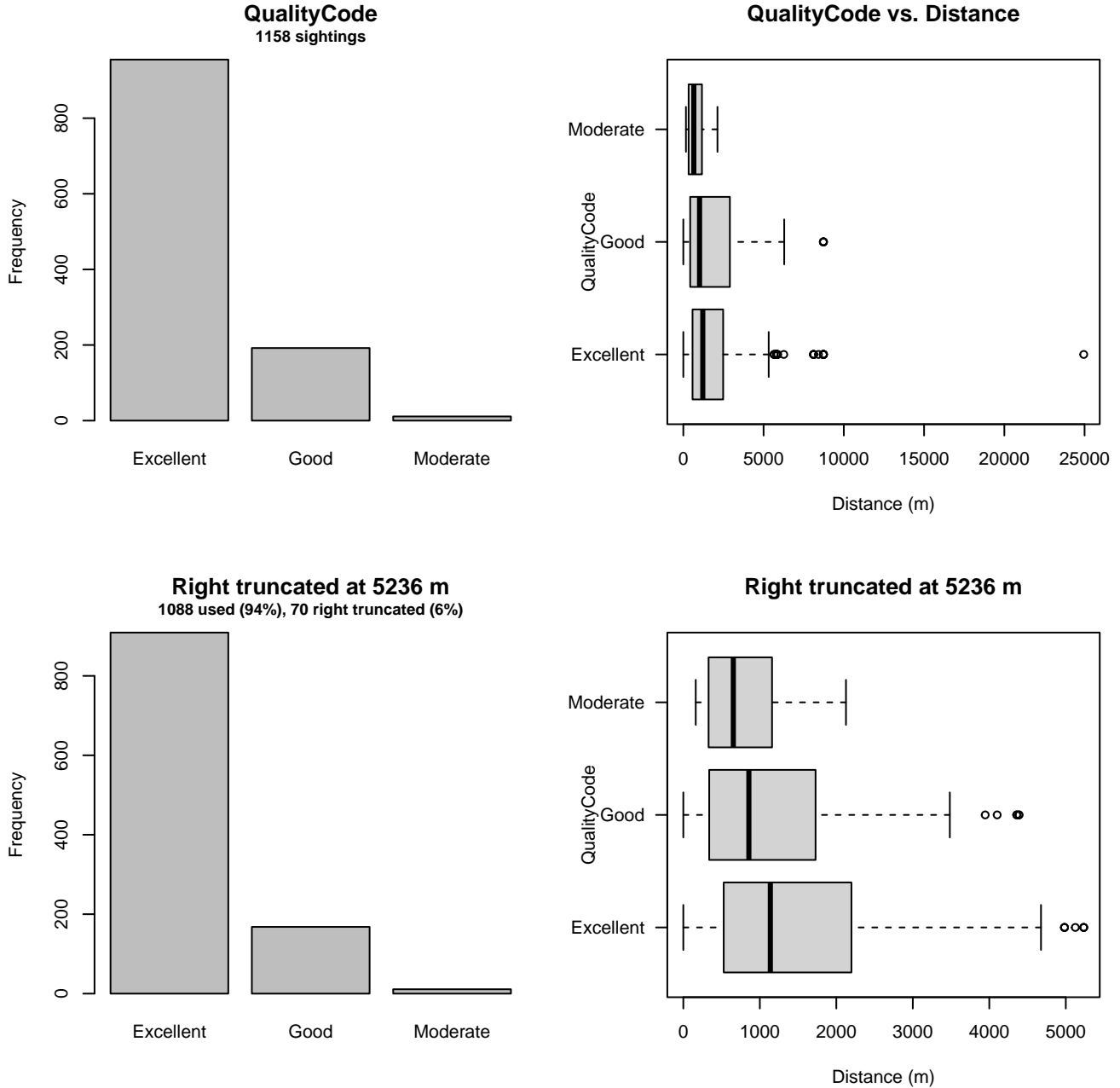


Figure 43: Distribution of the QualityCode covariate before (top row) and after (bottom row) observations were truncated to fit the NARWSS 2017-2020 detection function.

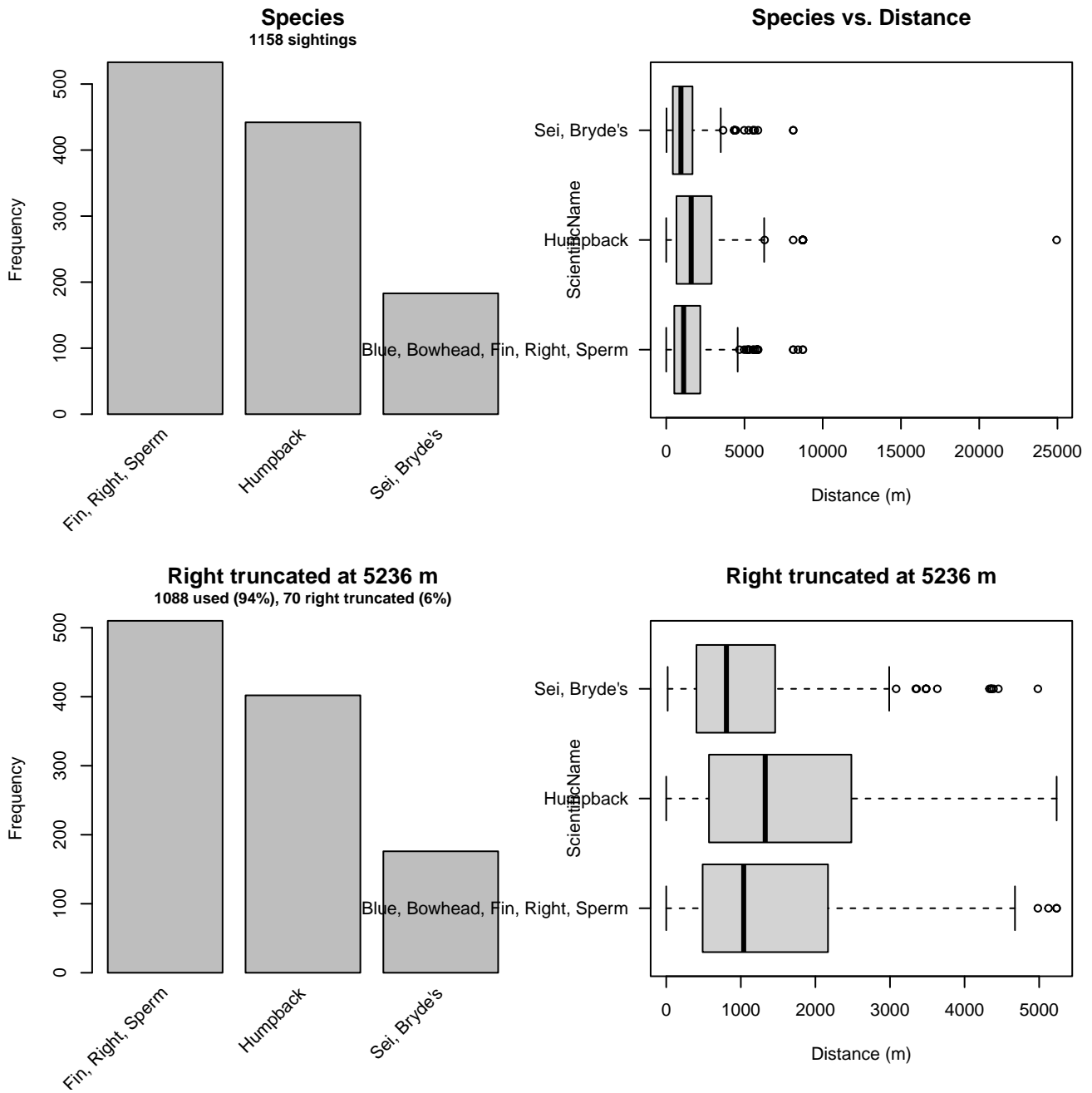


Figure 44: Distribution of the ScientificName covariate before (top row) and after (bottom row) observations were truncated to fit the NARWSS 2017-2020 detection function.

### 3.1.2.2 Shipboard Surveys

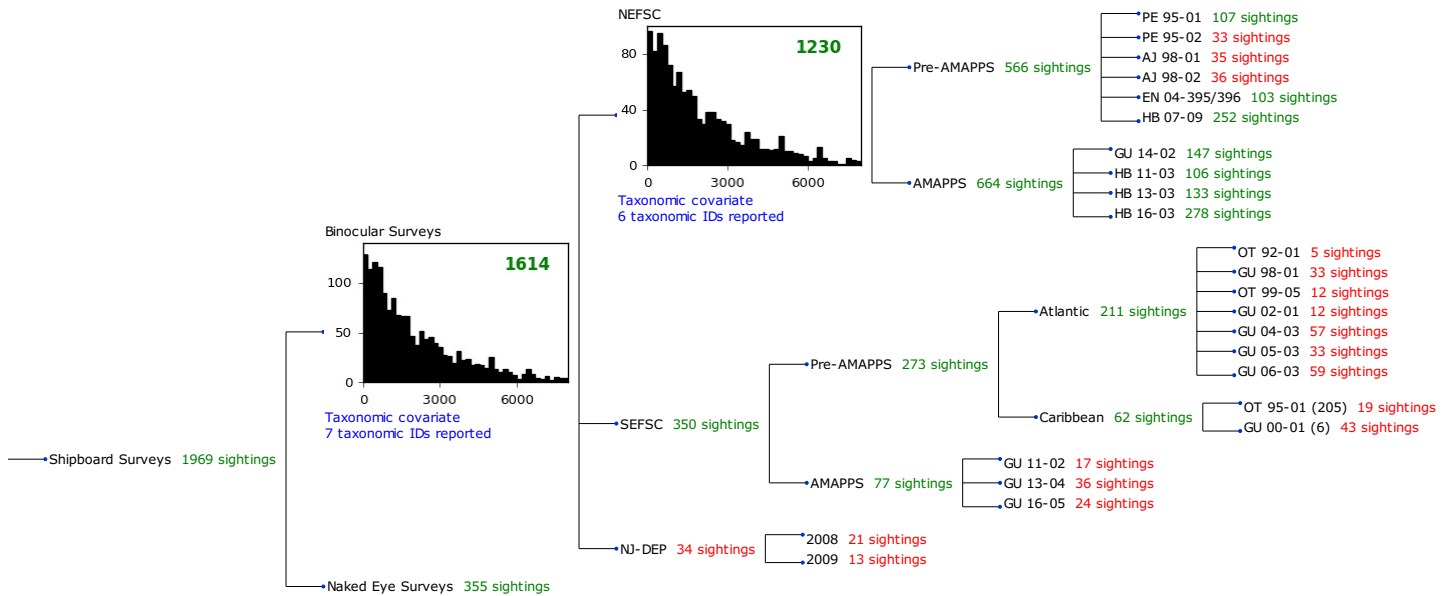


Figure 45: Detection hierarchy for shipboard surveys, showing how they were pooled during detectability modeling, for detection functions that pooled multiple taxa and used a taxonomic covariate to account for differences between them. Each histogram represents a detection function and summarizes the perpendicular distances of observations that were pooled to fit it, prior to truncation. Observation counts, also prior to truncation, are shown in green when they met the recommendation of Buckland et al. (2001) that detection functions utilize at least 60 sightings, and red otherwise. For rare taxa, it was not always possible to meet this recommendation, yielding higher statistical uncertainty. During the spatial modeling stage of the analysis, effective strip widths were computed for each survey using the closest detection function above it in the hierarchy (i.e. moving from right to left in the figure). Surveys that do not have a detection function above them in this figure were either addressed by a detection function presented in a different section of this report, or were omitted from the analysis.

#### 3.1.2.2.1 NEFSC

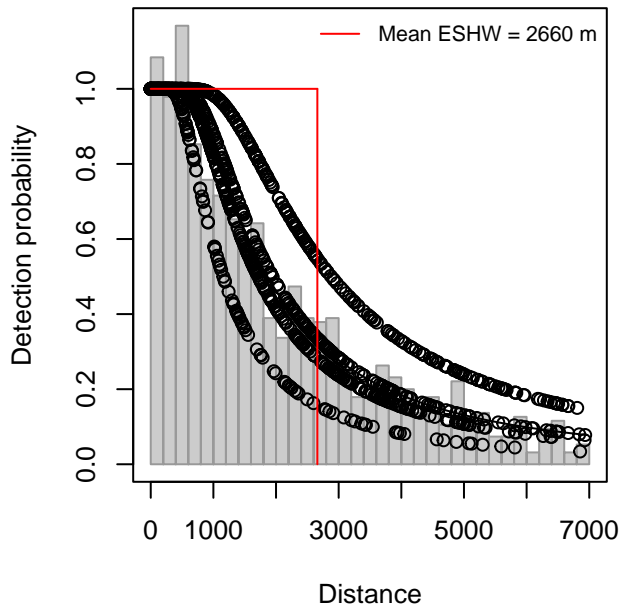
After right-truncating observations greater than 7000 m, we fitted the detection function to the 1201 observations that remained (Table 16). The selected detection function (Figure 46) used a hazard rate key function with Program (Figure 47) and ScientificName (Figure 48) as covariates.

Table 16: Observations used to fit the NEFSC detection function.

ScientificName	n
Blue, Fin, Right, Sei	452
Humpback, Sperm	749
<b>Total</b>	<b>1201</b>

## Large whales by species for Fin Sei

HR key with Program, Species  
1201 sightings, right truncated at 7000 m (2%)



## Q-Q Plot

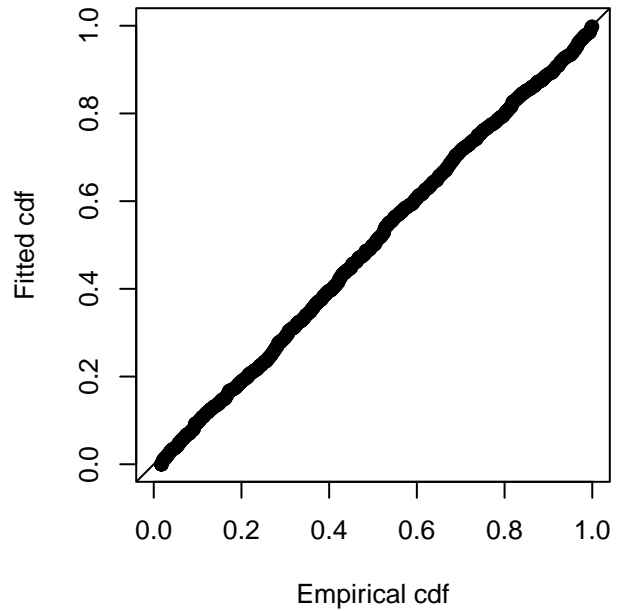


Figure 46: NEFSC detection function and Q-Q plot showing its goodness of fit.

Statistical output for this detection function:

Summary for ds object

Number of observations : 1201  
Distance range : 0 - 7000  
AIC : 20465.31

Detection function:

Hazard-rate key function

Detection function parameters

Scale coefficient(s):

	estimate	se
(Intercept)	7.3545852	0.10172378
ProgramMarine Mammal Abundance Surveys	-0.5171427	0.09909896
ScientificNameHumpback, Sperm	0.3937321	0.10074438

Shape coefficient(s):

	estimate	se
(Intercept)	0.5222304	0.06599629

	Estimate	SE	CV
Average p	0.3611076	0.01603822	0.04441397
N in covered region	3325.8788088	166.96697837	0.05020236

Distance sampling Cramer-von Mises test (unweighted)

Test statistic = 0.099680 p = 0.586443

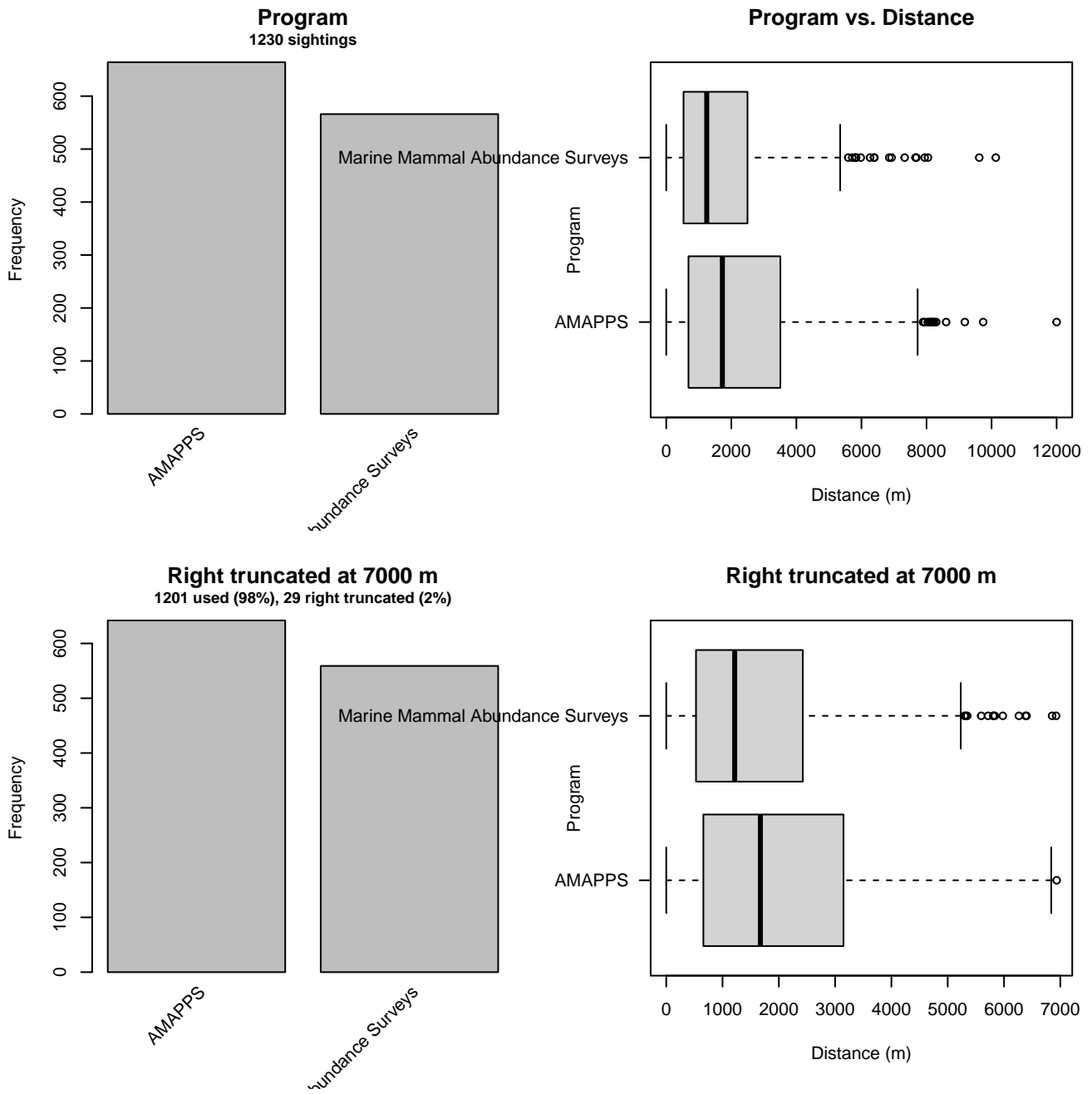


Figure 47: Distribution of the Program covariate before (top row) and after (bottom row) observations were truncated to fit the NEFSC detection function.



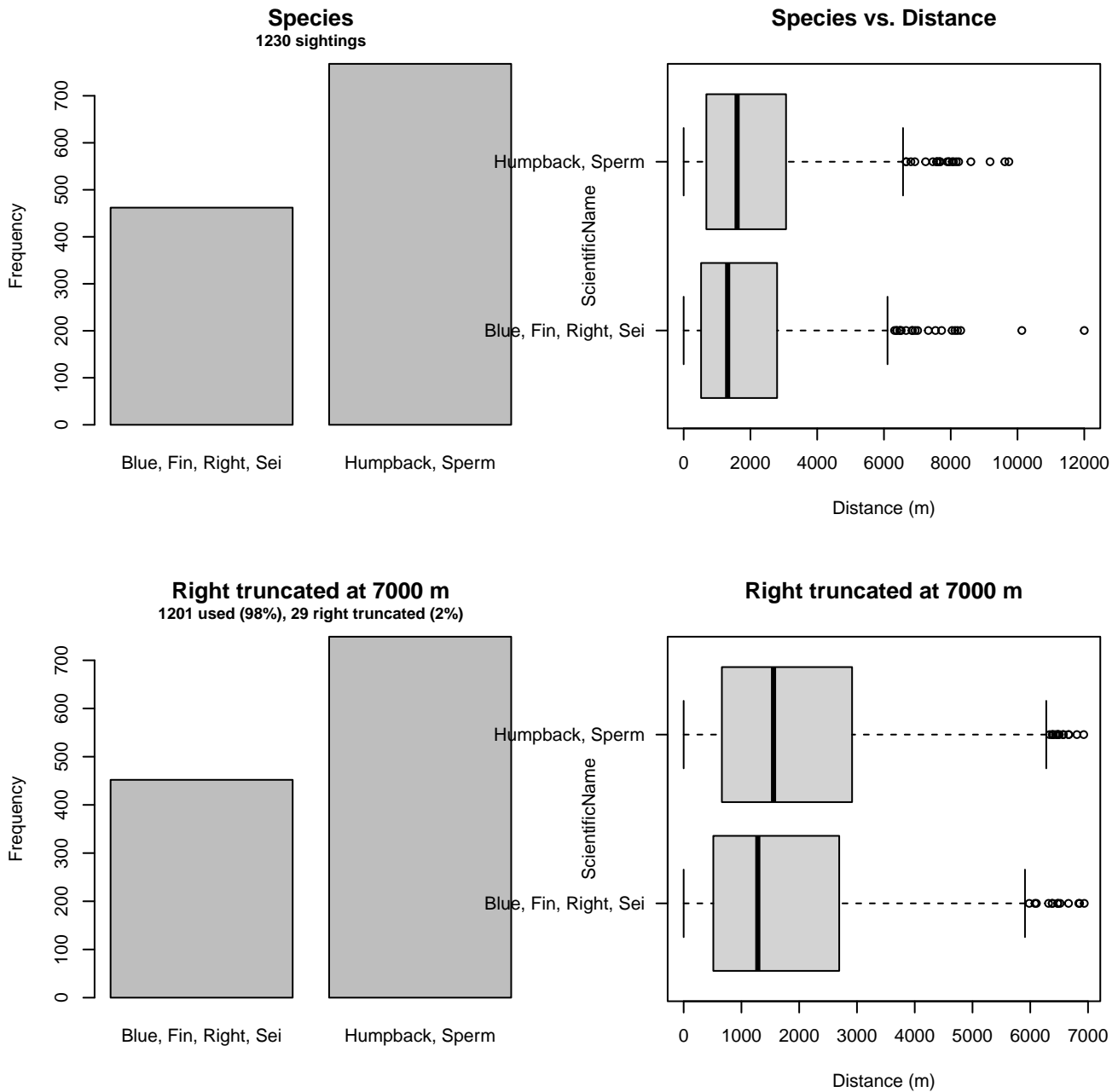


Figure 48: Distribution of the ScientificName covariate before (top row) and after (bottom row) observations were truncated to fit the NEFSC detection function.

### 3.1.2.2.2 Binocular Surveys

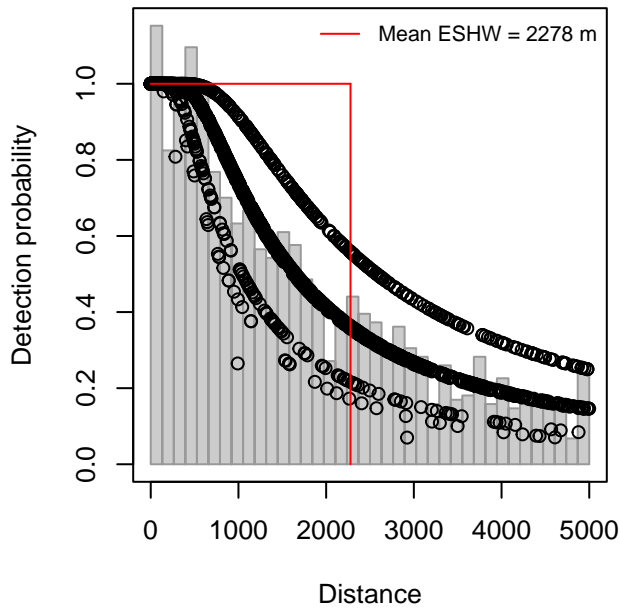
After right-truncating observations greater than 5000 m, we fitted the detection function to the 1471 observations that remained (Table 17). The selected detection function (Figure 49) used a hazard rate key function with Program (Figure 50) and ScientificName (Figure 51) as covariates.

Table 17: Observations used to fit the Binocular Surveys detection function.

ScientificName	n
Blue, Bryde's, Fin, Right, Sei	481
Humpback, Sperm	990
<b>Total</b>	<b>1471</b>

## Large whales by species for Fin Sei

HR key with Program, Species  
1471 sightings, right truncated at 5000 m (9%)



## Q-Q Plot

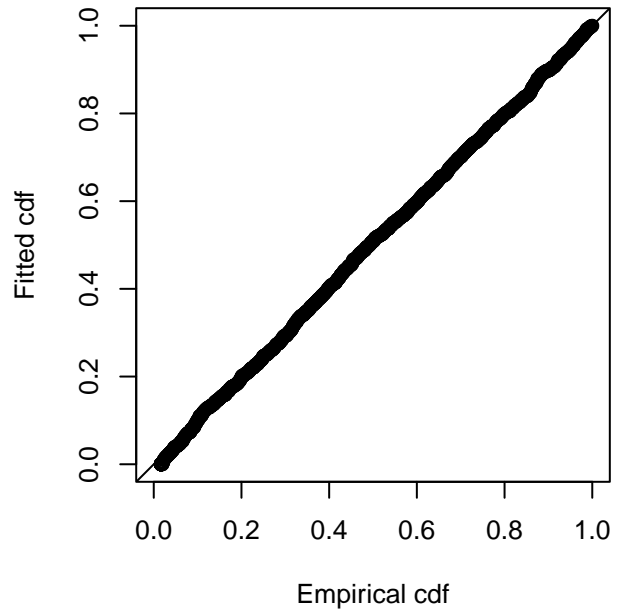


Figure 49: Binocular Surveys detection function and Q-Q plot showing its goodness of fit.

Statistical output for this detection function:

Summary for ds object

Number of observations : 1471  
Distance range : 0 - 5000  
AIC : 24501.67

Detection function:

Hazard-rate key function

Detection function parameters

Scale coefficient(s):

	estimate	se
(Intercept)	7.1184872	0.1313642
ProgramAtlantic Pre-AMAPPS	-0.4445467	0.1304985
ProgramCaribbean	-1.1012861	0.3025140
ScientificNameHumpback, Sperm	0.4613393	0.1338556

Shape coefficient(s):

	estimate	se
(Intercept)	0.2893248	0.07461625

	Estimate	SE	CV
Average p	0.4374109	0.02107636	0.04818435
N in covered region	3362.9703944	175.27854744	0.05212016

Distance sampling Cramer-von Mises test (unweighted)

Test statistic = 0.042713 p = 0.918683

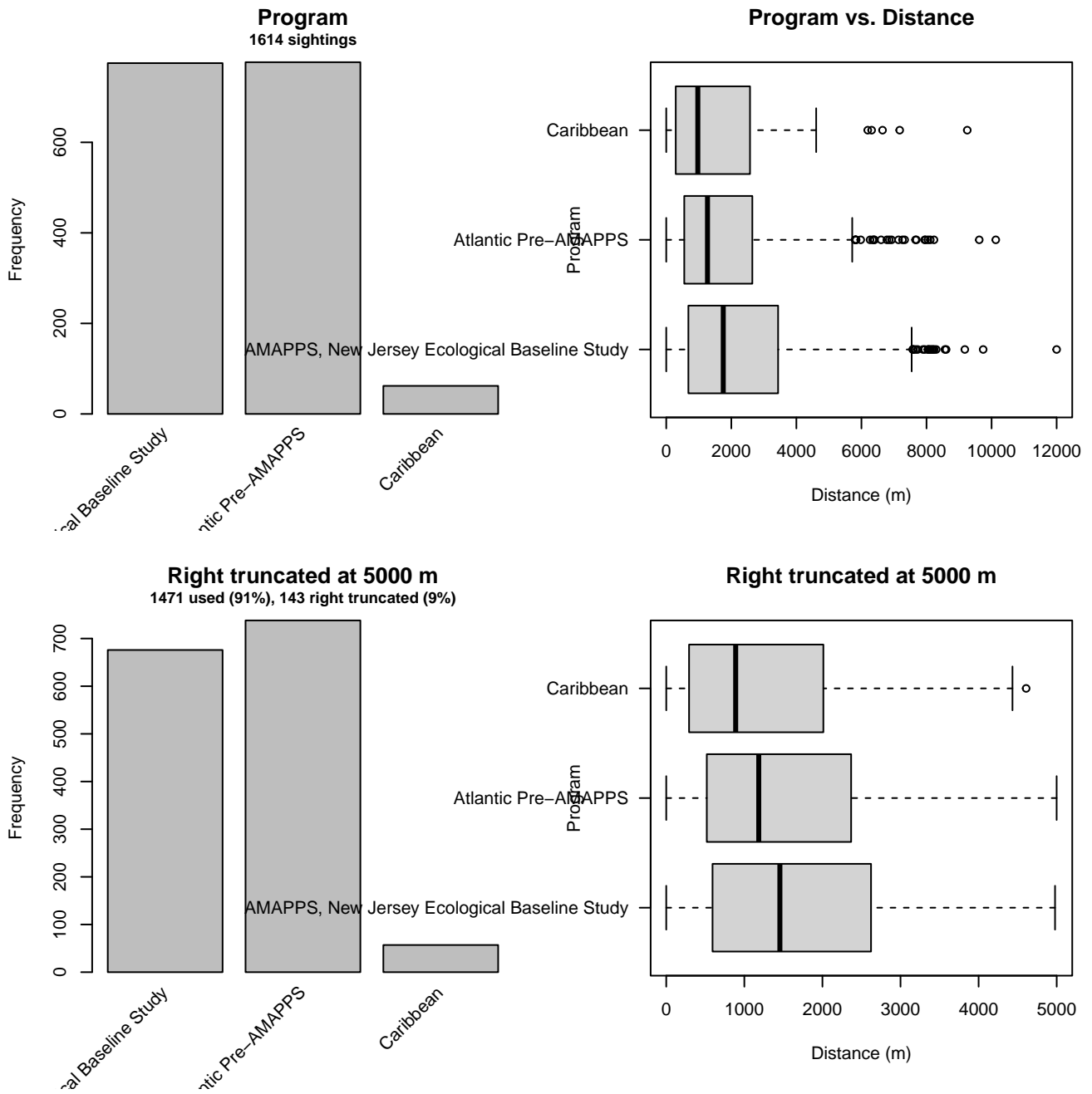


Figure 50: Distribution of the Program covariate before (top row) and after (bottom row) observations were truncated to fit the Binocular Surveys detection function.

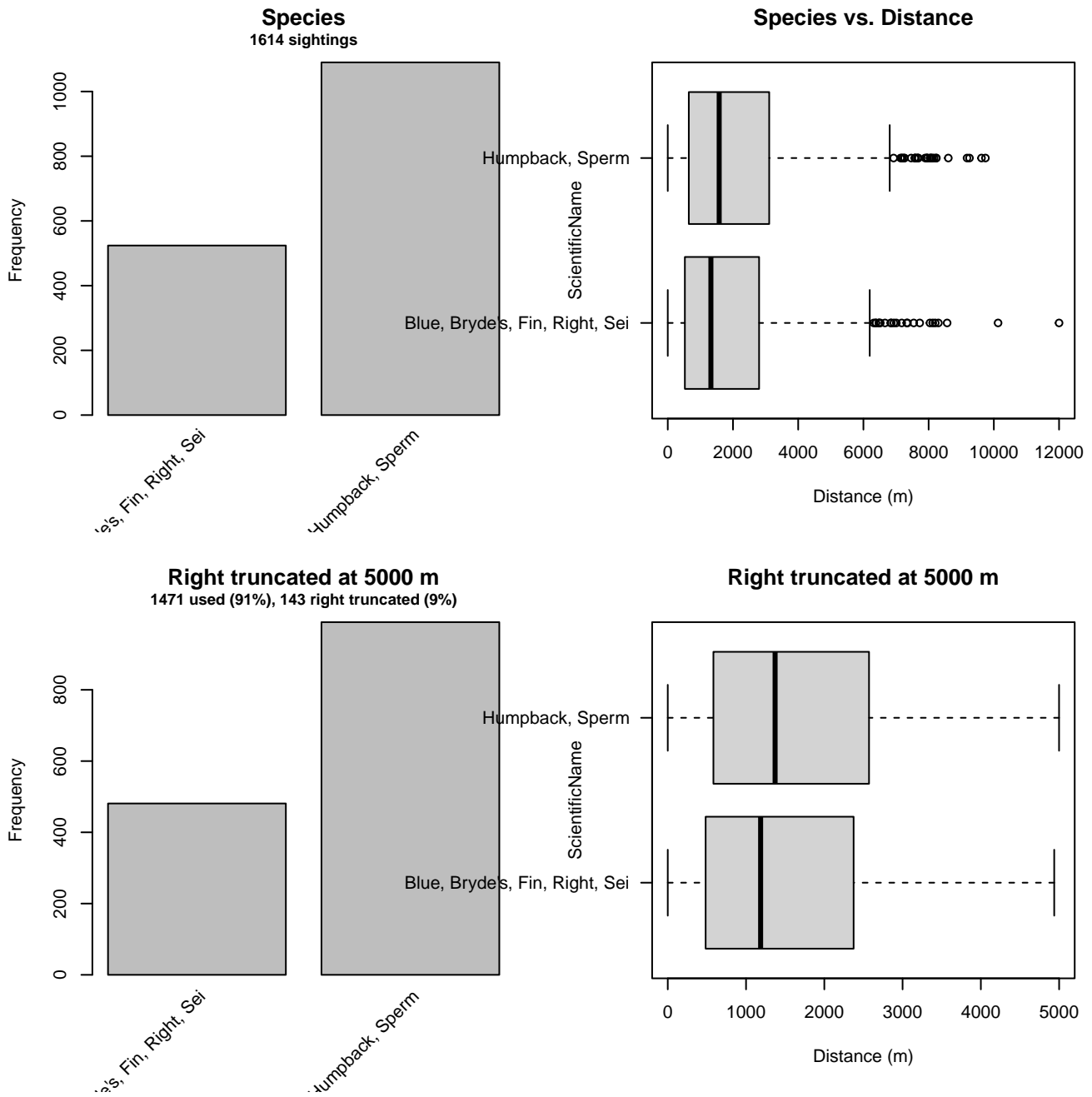


Figure 51: Distribution of the ScientificName covariate before (top row) and after (bottom row) observations were truncated to fit the Binocular Surveys detection function.

### 3.2 Without a Taxonomic Covariate

We fitted the detection functions in this section to pools of species with similar detectability characteristics but could not use a taxonomic identification as a covariate to account for differences between them. We usually took this approach after trying the taxonomic covariate and finding it had insufficient statistical power to be retained. We also resorted to it when the focal taxon being modeled had too few observations to be allocated its own taxonomic covariate level and was too poorly known for us to confidently determine which other taxa we could group it with.

### 3.2.1 Aerial Surveys

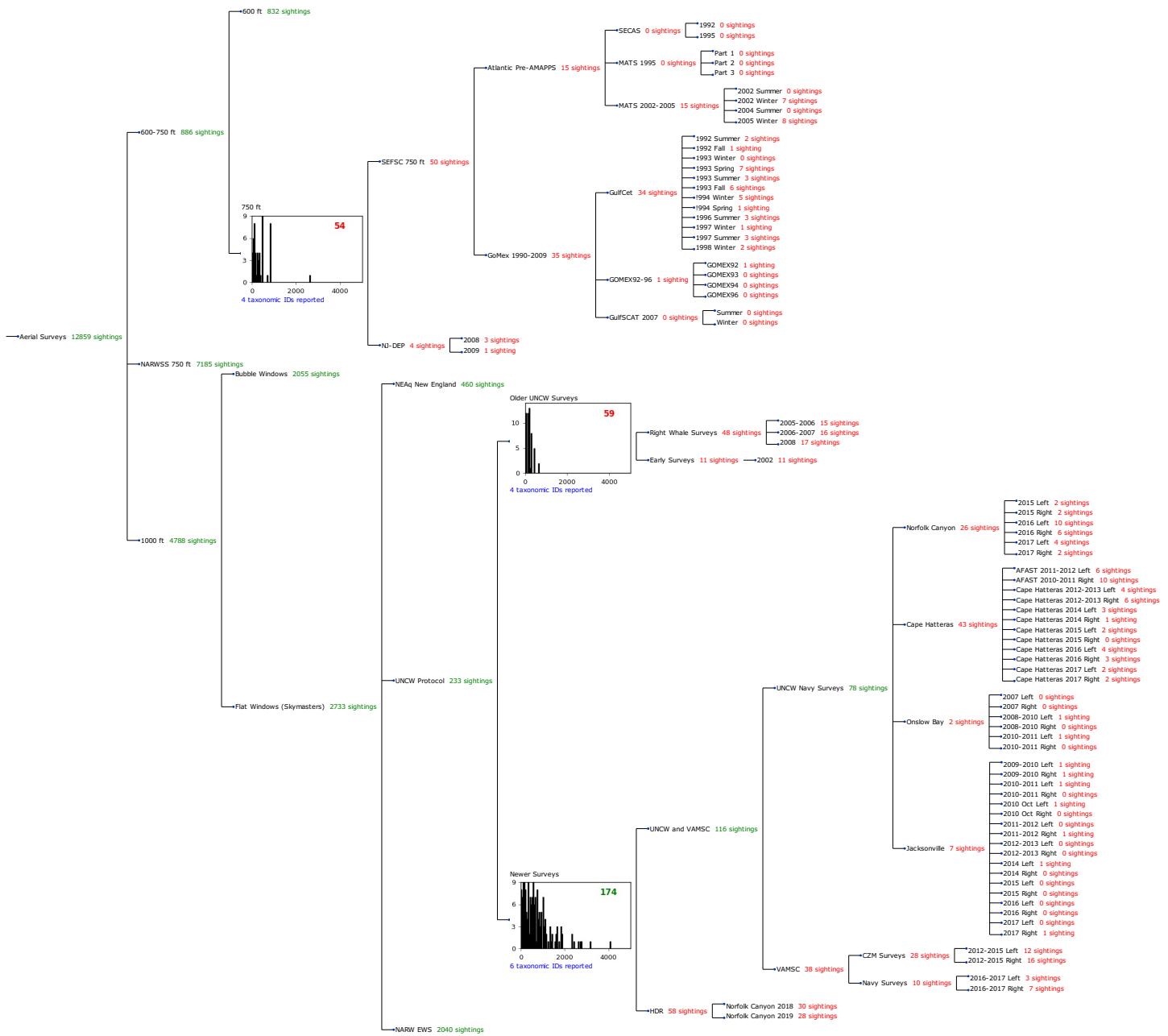


Figure 52: Detection hierarchy for aerial surveys, showing how they were pooled during detectability modeling, for detection functions that pooled multiple taxa but could not use a taxonomic covariate to account for differences between them. Each histogram represents a detection function and summarizes the perpendicular distances of observations that were pooled to fit it, prior to truncation. Observation counts, also prior to truncation, are shown in green when they met the recommendation of Buckland et al. (2001) that detection functions utilize at least 60 sightings, and red otherwise. For rare taxa, it was not always possible to meet this recommendation, yielding higher statistical uncertainty. During the spatial modeling stage of the analysis, effective strip widths were computed for each survey using the closest detection function above it in the hierarchy (i.e. moving from right to left in the figure). Surveys that do not have a detection function above them in this figure were either addressed by a detection function presented in a different section of this report, or were omitted from the analysis.

#### 3.2.1.1 750 ft

After right-truncating observations greater than 1297 m, we fitted the detection function to the 53 observations that remained (Table 18). The selected detection function (Figure 53) used a hazard rate key function with no covariates.

Table 18: Observations used to fit the 750 ft detection function.

ScientificName	n
Balaenoptera physalus	8
Eubalaena glacialis	5
Megaptera novaeangliae	7
Physeter macrocephalus	33
<b>Total</b>	<b>53</b>

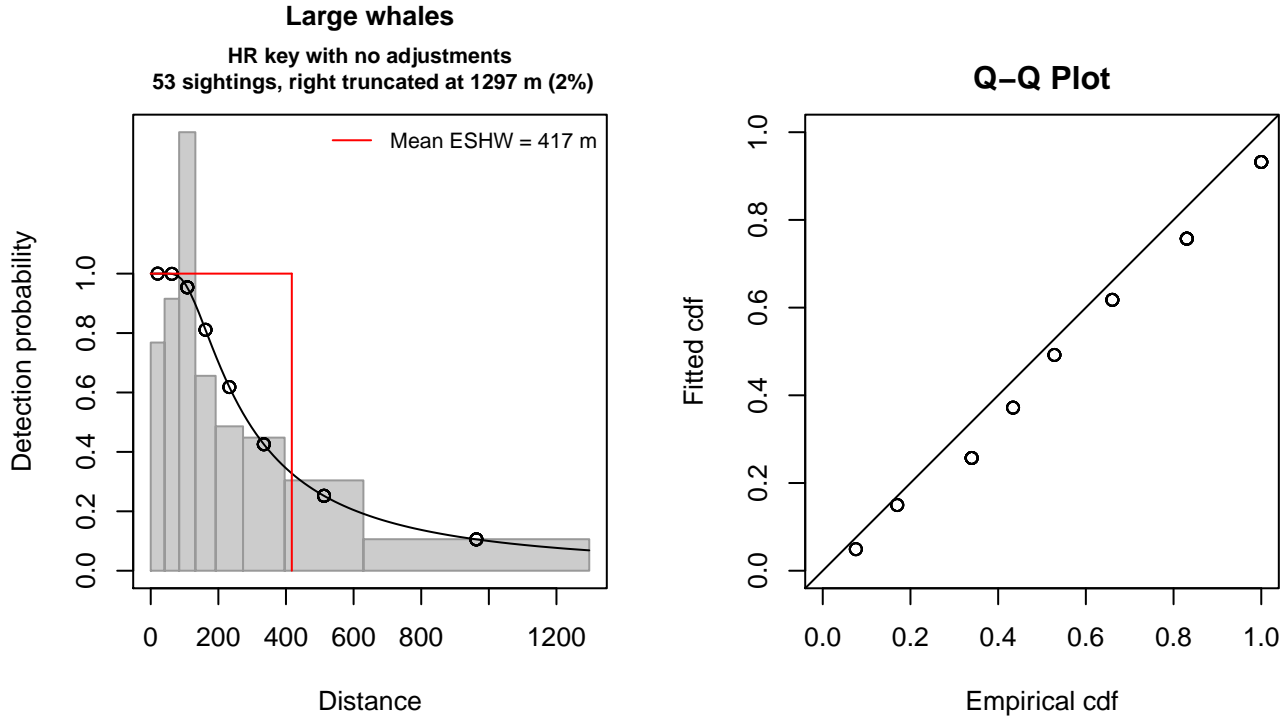


Figure 53: 750 ft detection function and Q-Q plot showing its goodness of fit.

Statistical output for this detection function:

Summary for ds object

Number of observations : 53  
 Distance range : 0 - 1297  
 AIC : 222.2921

Detection function:

Hazard-rate key function

Detection function parameters

Scale coefficient(s):

	estimate	se
(Intercept)	5.423929	0.4460729

Shape coefficient(s):

	estimate	se
(Intercept)	0.4163623	0.3128171

	Estimate	SE	CV
Average p	0.321688	0.07665669	0.2382951
N in covered region	164.755912	43.46025892	0.2637857

Distance sampling Cramer-von Mises test (unweighted)  
 Test statistic = 0.101698 p = 0.576612

### 3.2.1.2 Older UNCW Surveys

After right-truncating observations greater than 838 m, we fitted the detection function to the 59 observations that remained (Table 19). The selected detection function (Figure 54) used a hazard rate key function with Beaufort (Figure 55) as a covariate.

Table 19: Observations used to fit the Older UNCW Surveys detection function.

ScientificName	n
Balaenoptera physalus	13
Eubalaena glacialis	24
Megaptera novaeangliae	13
Physeter macrocephalus	9
<b>Total</b>	<b>59</b>

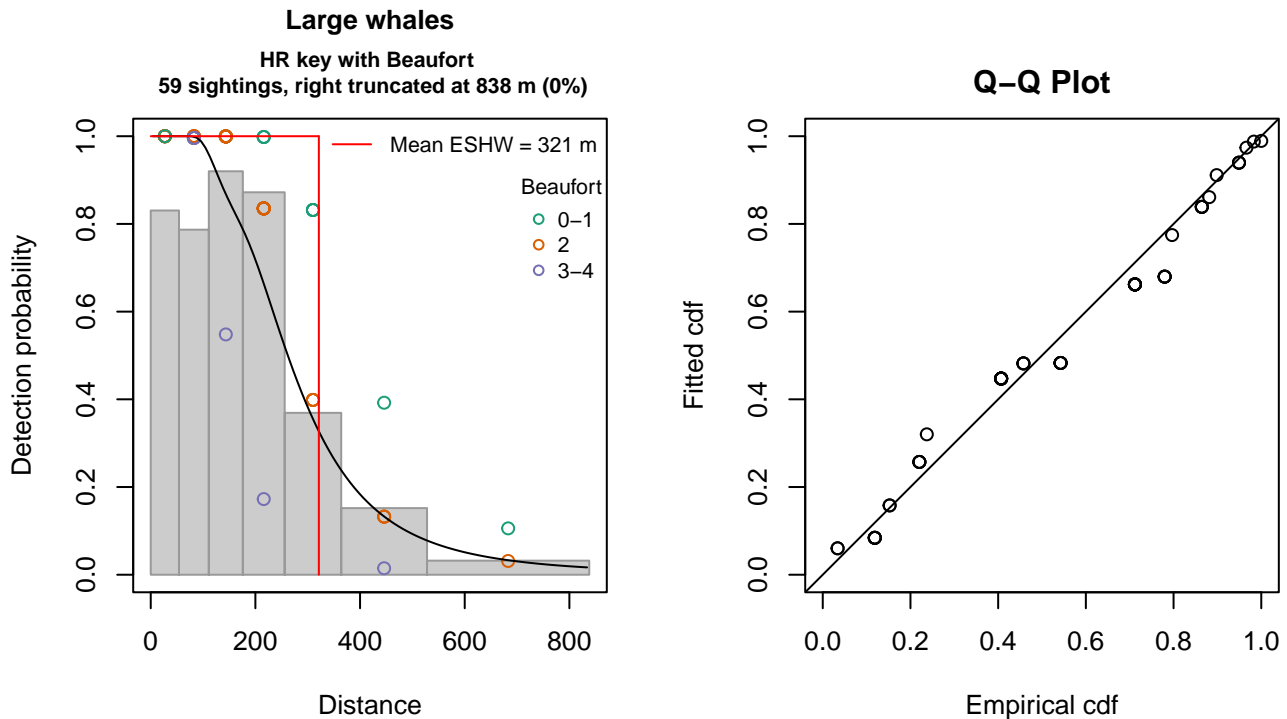


Figure 54: Older UNCW Surveys detection function and Q-Q plot showing its goodness of fit.

Statistical output for this detection function:

```
Summary for ds object
Number of observations : 59
Distance range       : 0 - 838
AIC                  : 218.1082
```

```
Detection function:
Hazard-rate key function
```

```
Detection function parameters
Scale coefficient(s):
```

	estimate	se
(Intercept)	5.9013957	0.2950158
Beaufort2	-0.3578033	0.3134356
Beaufort3-4	-1.0008354	0.3877033

Shape coefficient(s):

	estimate	se
(Intercept)	1.254247	0.2627137

	Estimate	SE	CV
Average p	0.3508662	0.04814793	0.1372259
N in covered region	168.1552636	29.31126242	0.1743107

Distance sampling Cramer-von Mises test (unweighted)  
Test statistic = 0.291522 p = 0.142842



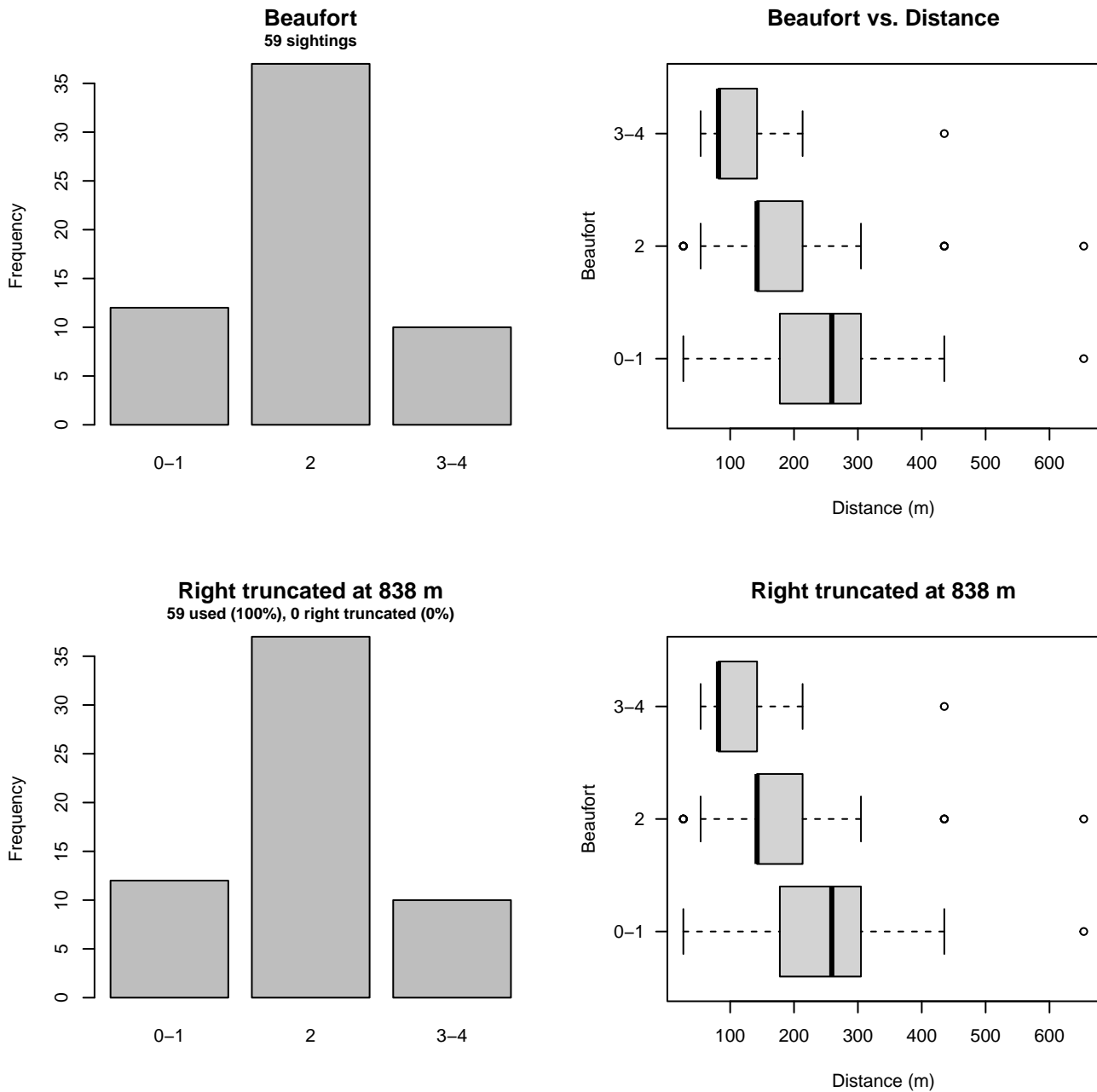


Figure 55: Distribution of the Beaufort covariate before (top row) and after (bottom row) observations were truncated to fit the Older UNCW Surveys detection function.

### 3.2.1.3 Newer Surveys

After right-truncating observations greater than 2000 m, we fitted the detection function to the 164 observations that remained (Table 20). The selected detection function (Figure 56) used a half normal key function with Beaufort (Figure 57) as a covariate.

Table 20: Observations used to fit the Newer Surveys detection function.

ScientificName	n
Balaenoptera borealis	3
Balaenoptera musculus	1
Balaenoptera physalus	48
Eubalaena glacialis	11
Megaptera novaeangliae	40
Physeter macrocephalus	61
<b>Total</b>	<b>164</b>

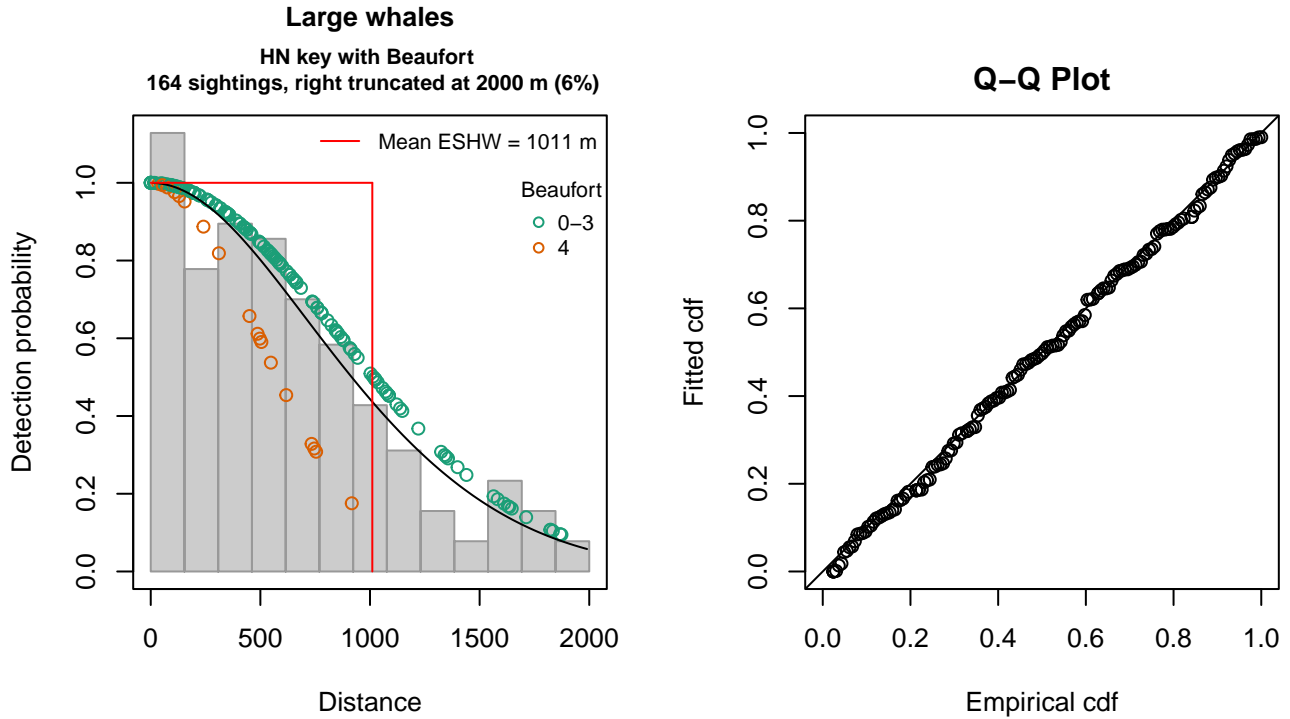


Figure 56: Newer Surveys detection function and Q-Q plot showing its goodness of fit.

Statistical output for this detection function:

Summary for ds object

Number of observations : 164  
 Distance range : 0 - 2000  
 AIC : 2414.311

Detection function:

Half-normal key function

Detection function parameters

Scale coefficient(s):

	estimate	se
(Intercept)	6.7601346	0.07305226
Beaufort4	-0.5625984	0.24677736

	Estimate	SE	CV
Average p	0.4908118	0.03341248	0.06807595
N in covered region	334.1403290	29.56205574	0.08847198

Distance sampling Cramer-von Mises test (unweighted)  
 Test statistic = 0.025201 p = 0.989164

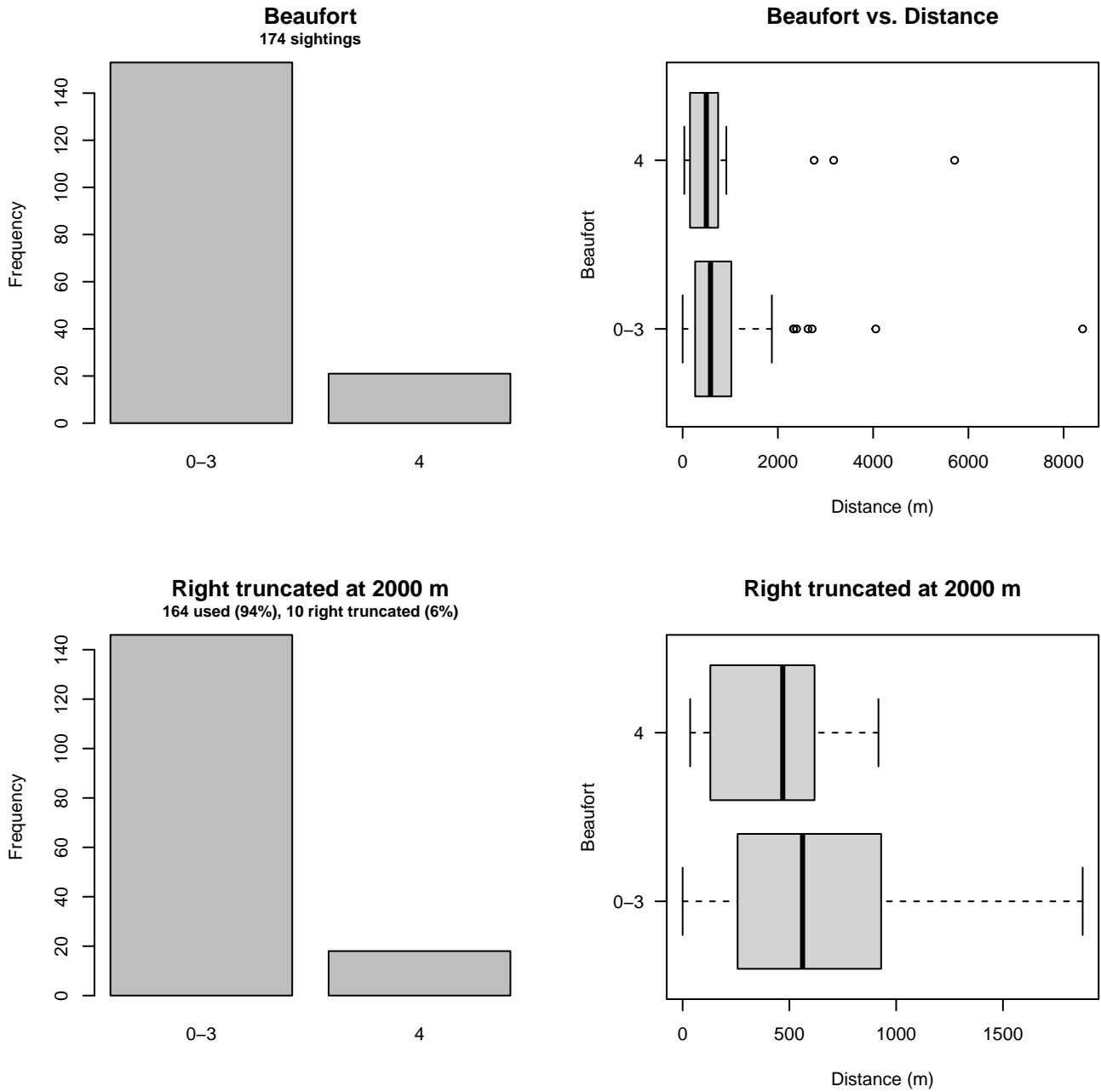


Figure 57: Distribution of the Beaufort covariate before (top row) and after (bottom row) observations were truncated to fit the Newer Surveys detection function.

### 3.2.2 Shipboard Surveys

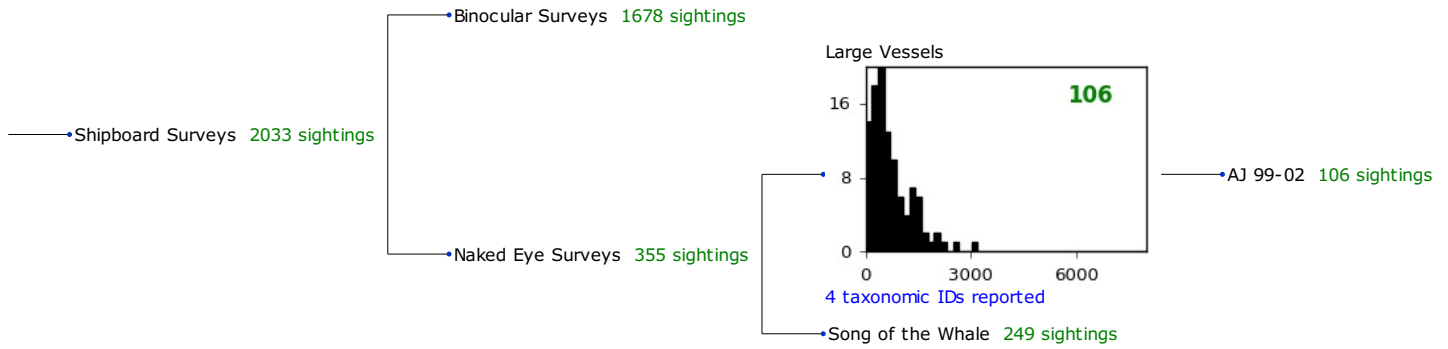


Figure 58: Detection hierarchy for shipboard surveys, showing how they were pooled during detectability modeling, for detection functions that pooled multiple taxa but could not use a taxonomic covariate to account for differences between them. Each histogram represents a detection function and summarizes the perpendicular distances of observations that were pooled to fit it, prior to truncation. Observation counts, also prior to truncation, are shown in green when they met the recommendation of Buckland et al. (2001) that detection functions utilize at least 60 sightings, and red otherwise. For rare taxa, it was not always possible to meet this recommendation, yielding higher statistical uncertainty. During the spatial modeling stage of the analysis, effective strip widths were computed for each survey using the closest detection function above it in the hierarchy (i.e. moving from right to left in the figure). Surveys that do not have a detection function above them in this figure were either addressed by a detection function presented in a different section of this report, or were omitted from the analysis.

#### 3.2.2.1 Large Vessels

After right-truncating observations greater than 2000 m, we fitted the detection function to the 102 observations that remained (Table 21). The selected detection function (Figure 59) used a hazard rate key function with no covariates.

Table 21: Observations used to fit the Large Vessels detection function.

ScientificName	n
Balaenoptera borealis	2
Balaenoptera borealis/physalus	53
Eubalaena glacialis	10
Megaptera novaeangliae	37
<b>Total</b>	<b>102</b>

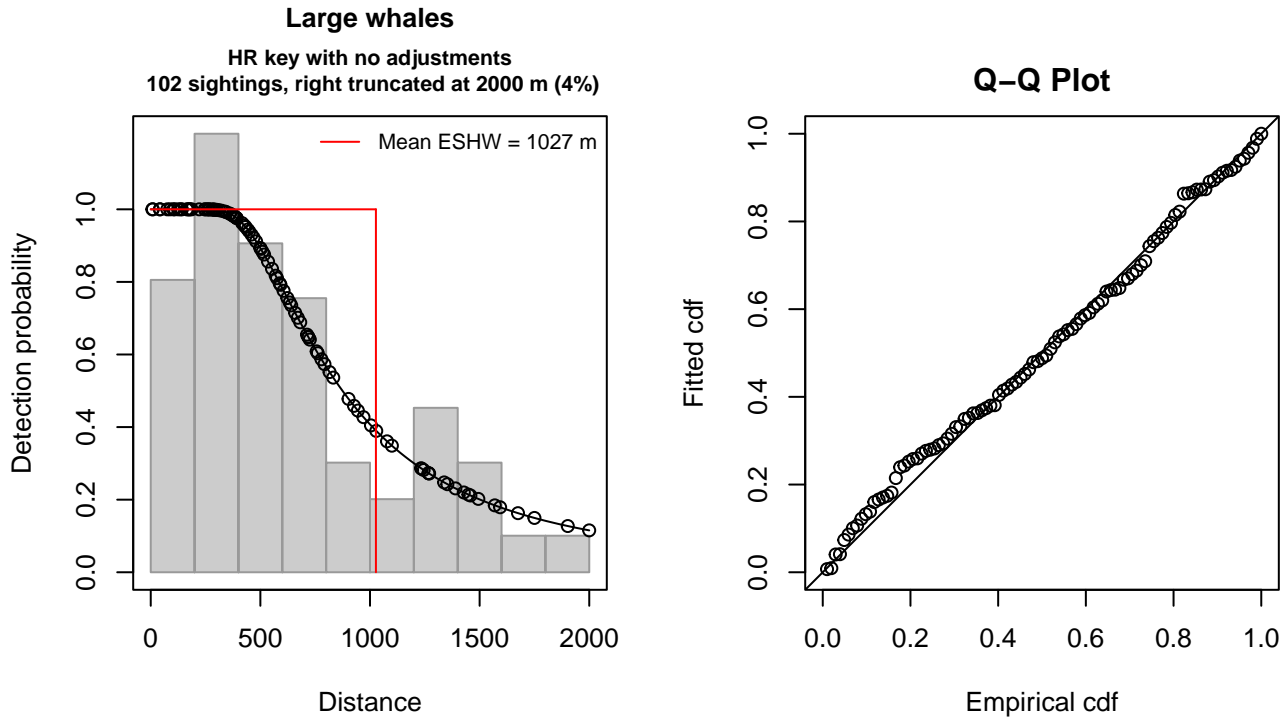


Figure 59: Large Vessels detection function and Q-Q plot showing its goodness of fit.

Statistical output for this detection function:

Summary for ds object

Number of observations : 102  
 Distance range : 0 - 2000  
 AIC : 1511.039

Detection function:  
 Hazard-rate key function

Detection function parameters  
 Scale coefficient(s):  

	estimate	se
(Intercept)	6.598567	0.2138084

Shape coefficient(s):  

	estimate	se
(Intercept)	0.7389469	0.2835546

	Estimate	SE	CV
Average p	0.5134925	0.06353129	0.1237239
N in covered region	198.6396966	28.14611852	0.1416943

Distance sampling Cramer-von Mises test (unweighted)  
 Test statistic = 0.063071 p = 0.794652

## 4 Bias Corrections

Density surface modeling methodology uses *distance sampling* (Buckland et al. 2001) to model the probability that an observer on a line transect survey will detect an animal given the perpendicular distance to it from the transect line. Distance sampling assumes that detection probability is 1 when perpendicular distance is 0. When this assumption is not

met, detection probability is biased high, leading to an underestimation of density and abundance. This is known as the  $g_0 < 1$  problem, where  $g_0$  refers to the detection probability at distance 0. Modelers often try to address this problem by estimating  $g_0$  empirically and dividing it into estimated density or abundance, thereby correcting those estimates to account for the animals that were presumed missed.

Two important sources of bias for visual surveys are known as *availability bias*, in which an animal was present on the transect line but impossible to detect, e.g. because it was under water, and *perception bias*, in which an animal was present and available but not noticed, e.g. because of its small size or cryptic coloration or behavior (Marsh and Sinclair 1989). Modelers often estimate the influence of these two sources of bias on detection probability independently, yielding two estimates of  $g_0$ , hereafter referred to as  $g_{0A}$  and  $g_{0P}$ , and multiply them together to obtain a final, combined estimate:  $g_0 = g_{0A} \cdot g_{0P}$ .

Our overall approach was to perform this correction on a per-observation basis, to have the flexibility to account for many factors such as platform type, surveyor institution, group size, group composition (e.g. singleton, mother-calf pair, or surface active group), and geographic location (e.g. feeding grounds vs. calving grounds). The level of complexity of the corrections varied by species according to the amount of information available, with North Atlantic right whale having the most elaborate corrections, derived from a substantial set of publications documenting its behavior, and various lesser known odontocetes having corrections based only on platform type (aerial or shipboard), derived from comparatively sparse information. Here we document the corrections used for fin whale.

## 4.1 Aerial Surveys

Palka et al. (2021) developed perception bias corrections using two team, mark recapture distance sampling (MRDS) methodology (Burt et al. 2014) for aerial surveys conducted in 2010-2017 by NOAA NEFSC and SEFSC during the AMAPPS program. These were the only extant perception bias estimates developed from aerial surveys used in our analysis, aside from estimates developed earlier by Palka and colleagues (Palka 2006; Palka et al. 2017). Those earlier efforts utilized older methods and less data than their 2021 analysis, so we applied the Palka et al. (2021) estimates to all aerial survey programs (Table 22).

We applied Palka’s estimate for NEFSC to all programs other than SEFSC on the basis that those programs employed a similar visual scanning protocol that allowed observers to scan from the trackline up to the horizon, while SEFSC’s protocol generally limited scanning only up to  $50^\circ$  from the trackline, resulting in a smaller effective strip width. UNCW’s earlier surveys were an exception, for which detection distances were much closer to SEFSC’s for most species, so we applied Palka’s SEFSC estimate.

We caution that it is possible that perception bias was different on the other aerial programs, as they often used different aircraft, flew at different altitudes, and were staffed by different personnel. Of particular concern are that many programs flew Cessna 337 Skymasters, which had flat windows, while NOAA flew de Havilland Twin Otters, which had bubble windows, which likely afforded a better view of the transect line and therefore might have required less of a correction than the Skymasters. Correcting the other programs using NOAA’s estimate as we have done is likely to yield less bias than leaving them uncorrected, but we urge all programs to undertake their own efforts to estimate perception bias, as resources allow.

We estimated availability bias corrections using the Laake et al. (1997) estimator and dive intervals reported by Palka et al. (2017) (Table 23). To estimate time in view, needed by the Laake estimator, we used results reported by Robertson et al. (2015), rescaled linearly for each survey program according to its target altitude and speed. We caution that Robertson’s analysis was done for a de Havilland Twin Otter, which may have a different field of view than that of the other aircraft used here, which mainly comprised Cessna 337 Skymasters with flat windows but also a Partenavia P-68 with bubble windows (on the NYS-DEC/TT surveys). However, we note that McLellan et al. (2018) conducted a sensitivity analysis on the influence of the length of the “window of opportunity” to view beaked whales from a Cessna Skymaster on their final density estimates and found that they varied by only a few thousandths of an animal per kilometer when the window of opportunity more than doubled. Still, we urge additional program-specific research into estimation of availability bias.

To address the influence of group size on availability bias, we applied the group availability estimator of McLellan et al. (2018) on a per-observation basis. Following Palka et al. (2021), who also used that method, we assumed that individuals in the group dived asynchronously. The resulting  $g_{0A}$  corrections ranged from about 0.33 to 1 (Figure 60). We caution that the assumption of asynchronous diving can lead to an underestimation of density and abundance if diving is actually synchronous; see McLellan et al. (2018) for an exploration of this effect. However, if future research finds that this species conducts synchronous dives and characterizes the degree of synchronicity, the model can be updated to account for this knowledge.

Table 22: Perception bias corrections for fin whale applied to aerial surveys.

Surveys	Group Size	$g_{0P}$	$g_{0P}$ Source
SEFSC, UNCW 2002-2008	< 3	0.86	Palka et al. (2021): SEFSC
All others	< 3	0.67	Palka et al. (2021): NEFSC
All	$\geq 3$	1.00	Assumed

Table 23: Surface and dive intervals for fin whale used to estimate availability bias corrections.

Surface Interval (s)	Dive Interval (s)	Source
51.7	173.5	Palka et al. (2017)

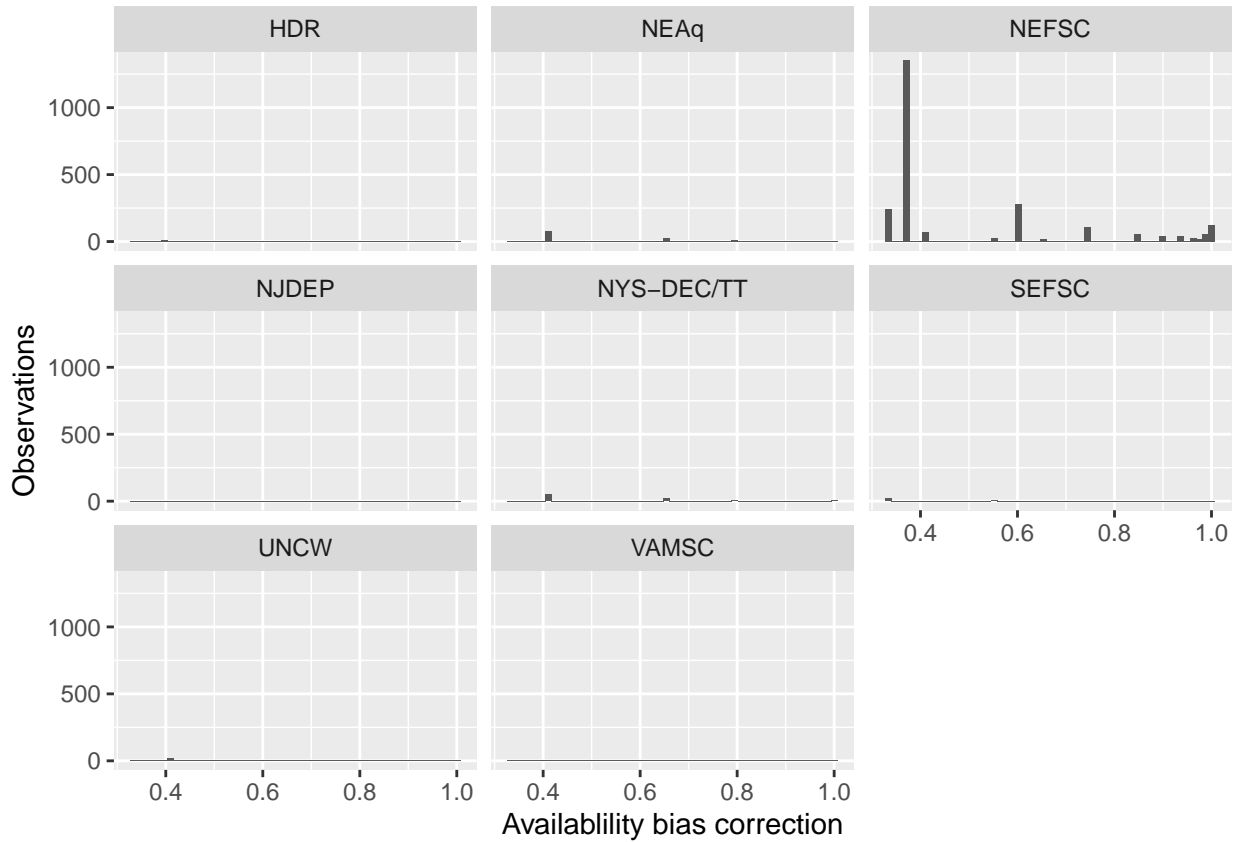


Figure 60: Availability bias corrections for fin whale for aerial surveys, by institution.

## 4.2 Shipboard Surveys

Most of the shipboard surveys in our analysis used high-power (25x150), pedestal-mounted binoculars. Similar to aerial surveys, Palka et al. (2021) developed perception bias corrections using two team, MRDS methodology (Burt et al. 2014) for high-power binocular surveys conducted in 2010-2017 by NOAA NEFSC and SEFSC during the AMAPPS program. These were the only extant perception bias estimates developed from high-power binocular surveys used in our analysis, aside from estimates developed earlier by Palka and colleagues (Palka 2006; Palka et al. 2017). Those earlier efforts utilized older methods and less data than their 2021 analysis, so we applied the Palka et al. (2021) estimates to all shipboard surveys that searched with high-power binoculars (Table 24).

A few surveys used naked eyes rather than high-power binoculars. For the one NEFSC naked eye survey (AJ 99-02) used in our analysis, we used the estimate developed for this survey by Palka (2006). For the surveys conducted by MCR on R/V Song of the Whale, for which a program-specific estimate was not available, we used the estimate from Cañadas et al. (2021). Given that the dive interval of this species (Table 23) was short relative to the amount of time a given patch of water

remained in view to shipboard observers, we assumed that no availability bias correction was needed ( $g_{0A} = 1$ ), following Palka et al. (2021), except for the MCR surveys, for which Cañadas et al. (2021) prepared an estimate that was slightly lower ( $g_{0A} = 0.99$ ).

Table 24: Perception and availability bias corrections for fin whale applied to shipboard surveys.

Surveys	Searching Method	Group Size	$g_{0P}$	$g_{0P}$ Source	$g_{0A}$	$g_{0A}$ Source
NEFSC, NJDEP	Binoculars	Any	0.48	Palka et al. (2021): NEFSC	1.00	Assumed
SEFSC	Binoculars	Any	0.57	Palka et al. (2021): SEFSC	1.00	Assumed
NEFSC (AJ 99-02)	Naked eye	Any	0.48	Palka et al. (2006)	1.00	Assumed
MCR	Naked eye	Any	0.72	Cañadas et al. (2021)	0.99	Cañadas et al. (2021)

## 5 Density Model

Surveys conducted from 1978-1989 reported that fin whales were the most frequently sighted large whale on the U.S. continental shelf north of Cape Hatteras and were present throughout this region during all four seasons (Winn 1982; Hain et al. 1992). Despite their prevalence, little is known about fin whale migration patterns. Similar to other baleen whales, they may undertake seasonal migrations north to feed and south to breed, but these patterns have not been described in the literature. Hain et al. (1992), using data from CeTAP and subsequent surveys of the U.S. east coast in the 1980s, reported markedly decreased fin whale abundance in fall compared to spring and summer. A 2015 review of the global distributions of fin whales noted that fin whale breeding areas were still unknown, and that while modern scientific studies and historic whaling records indicate that fin whales are more common at high latitudes in summer than in winter, some remain in higher (colder) latitudes in winter and lower (warmer) latitudes in summer (Edwards et al. 2015). These authors concluded that fin whales likely do not conduct long-distance seasonal migrations to tropical latitudes like humpback whales. Instead, some may remain at high latitudes year-round, while others may make short migrations, or something more complicated.

More recently, passive acoustic monitoring has confirmed the year-round presence of fin whale across much of the eastern seaboard. In a large synthesis of passive acoustic monitoring data collected from Florida to the Davis Strait for the period 2004-2014, Davis et al. (2020) reported that fin whales were detected nearly continuously from Virginia through eastern Greenland throughout the year. Delarue et al. (2022) reported a general uniformity in the acoustic occurrence of fin whales across waters of eastern Canada, with a greater acoustic presence in late spring and early summer, but with “non-negligible” numbers of fin whales remaining in their study area in winter. Kowarski et al. (2022), in a study of recordings collected on the outer continental shelf in the southeast U.S., reported that south of Wilmington, North Carolina, fin whale occurrence generally decreased with decreasing latitude, and that the months of peak presence were November through February.

The surveys incorporated into our model, spanning 1998-2020 (see Section 1), reported over 3200 sightings, ranging from southern North Carolina to the northern edge of the study area (Figure 1). Given the ubiquity of fin whales throughout our study area and the lack of evidence for a migration in which a large segment of the population would be expected to switch habitat preferences (as with migratory humpback whales), our approach to modeling fin whales was to fit a single model to all data, as we have done in prior iterations of this model, and rely on dynamic habitat covariates such as sea surface temperature to drive seasonal changes in fin whale density.

The model selection procedure was straightforward. When ranked by REML score (Wood 2011), the highest ranked models with climatological covariates slightly outranked those with contemporaneous covariates and explained slightly more deviance. We selected the highest ranked climatological model, which included eight terms (Table 25), four with static covariates and four with dynamic covariates. The functional relationship for depth (Figure 64) indicated a positive effect between 10-100 m, no effect between 100-300 m, and a negative effect <10m and >300m. Avoidance of the most inshore areas was indicated by the relationship fitted to fetch, which turned negative below 33 km. Two distance to isobath covariates were retained. Distance to 125 m peaked at a distance of zero, indicating highest positive influence on density right at the isobath, with the range of positive influence extending from 25 km up-slope of the isobath to 50 km down-slope. Distance to the 300 m isobath showed a wiggly but rising relationship that peaked at 25 km beyond the isobath, where we Winsorized the covariate due to relatively sparse sampling beyond the shelf break. Together, these static relationships indicate a preference for a wide range of depths across the continental shelf, with an avoidance of shallow, inshore waters, and highest densities along the edges of banks and the shelf itself.

A positive effect was indicated for surface temperatures between 7-24 °C, with a peak at 21 °C, likely reflecting peak density during summer months in waters north of the Gulf Stream. The relationship with bottom temperature peaked at 5 °C, indicating a preference for northern waters, particularly in deep areas of the shelf, such as basins of the Gulf of Maine and



Scotian Shelf. A positive effect was fitted for a broad range of epipelagic micronekton biomasses, except for the lowest biomasses, corresponding to waters south of Cape Hatteras. Finally, the relationship with distance to SST fronts wiggled around zero but dropped beyond about 45 km from fronts, indicating an avoidance of areas far from fronts, but the magnitude of this effect was weak.

### 5.1 Final Model

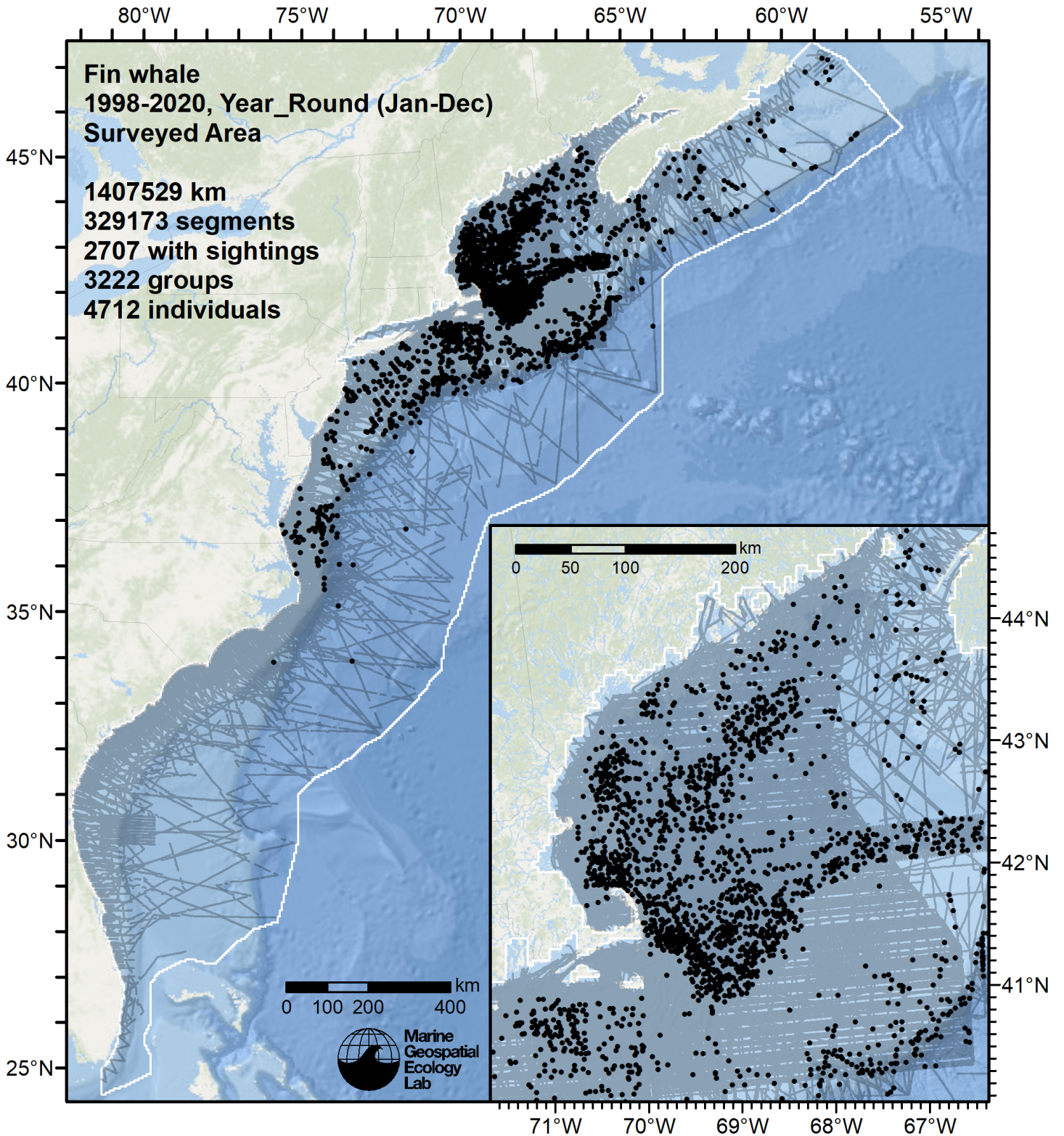


Figure 61: Survey segments used to fit the model. Black points indicate segments with observations.

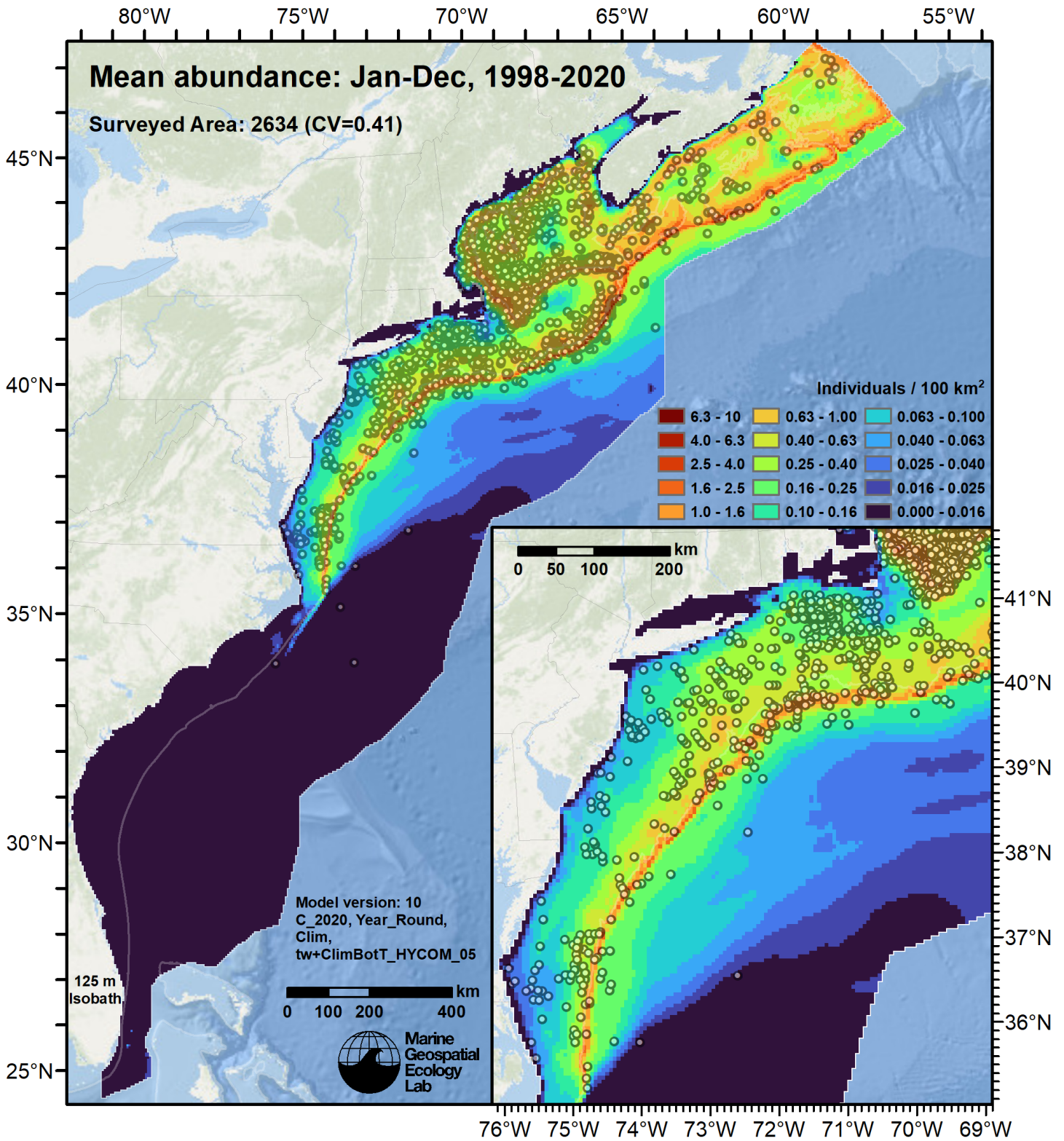


Figure 62: Fin whale mean density for the indicated period, as predicted by the model. Open circles indicate segments with observations. Mean total abundance and its coefficient of variation (CV) are given in the subtitle. Variance was estimated with the analytic approach given by Miller et al. (2022), Appendix S1, and accounts both for uncertainty in model parameter estimates and for seasonal variability in dynamic covariates but not interannual variability in them, as these covariates were monthly climatological averages.



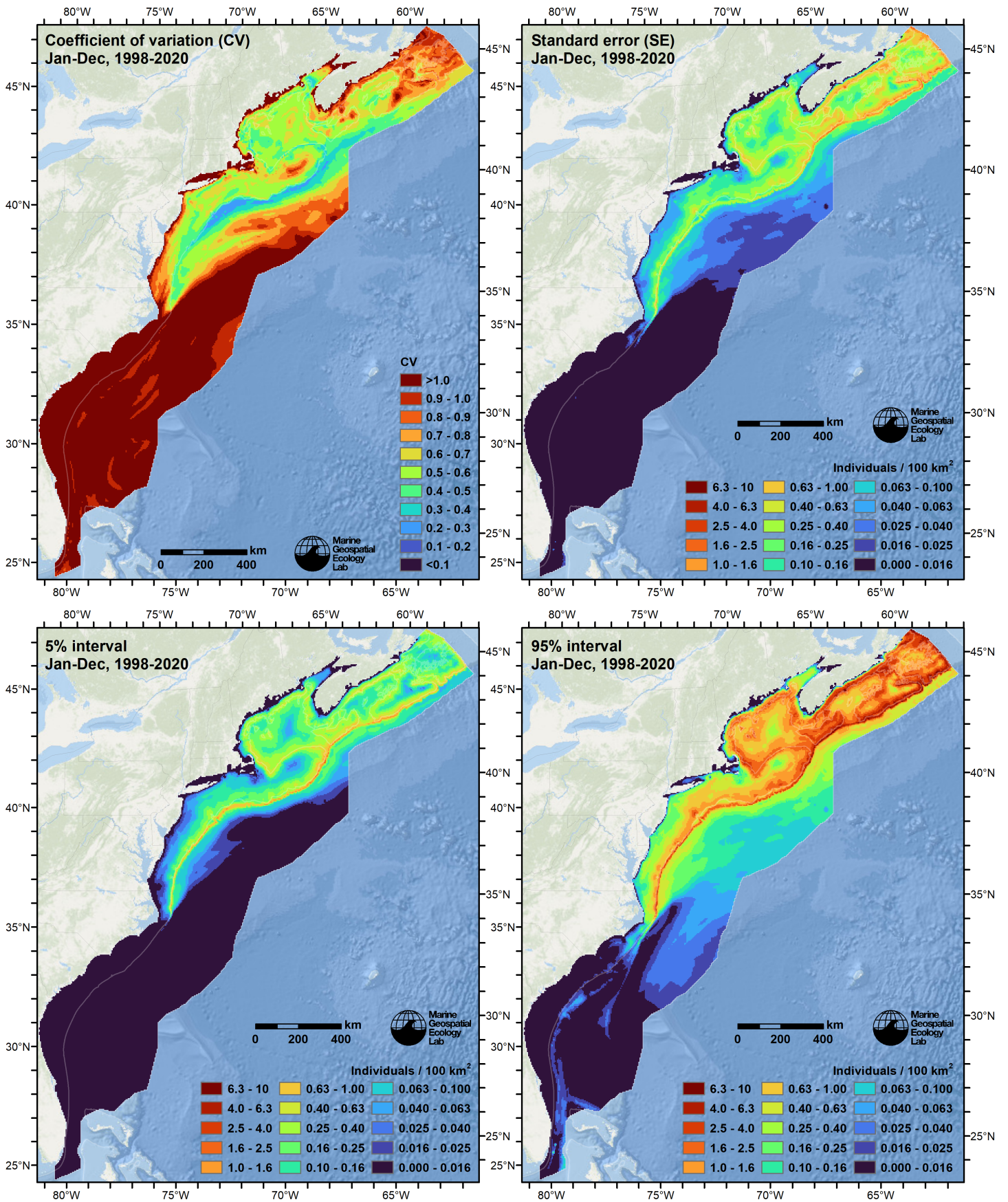


Figure 63: Uncertainty statistics for the fin whale mean density surface (Figure 62) predicted by the model. Variance was estimated with the analytic approach given by Miller et al. (2022), Appendix S1, and accounts both for uncertainty in model parameter estimates and for seasonal variability in dynamic covariates but not interannual variability in them, as these covariates were monthly climatological averages.

Statistical output for this model:

Family: Tweedie(p=1.144)

Link function: log

Formula:

```
IndividualsCorrected ~ offset(log(SegmentArea)) + s(pmax(15,
  Fetch_50km), bs = "ts") + s(log10(pmax(3, pmin(Depth, 4000))),
  bs = "ts") + s(pmax(-75, pmin(I(DistTo125m/1000), 75)), bs = "ts") +
  s(pmax(-400, pmin(I(DistTo300m/1000), 25)), bs = "ts") +
  s(pmax(3, pmin(ClimSST_CMC, 30)), bs = "ts") + s(pmax(3,
  pmin(ClimBotT_HYCOM, 25)), bs = "ts") + s(pmin(I(ClimDistToFront105/1000),
  75), bs = "ts") + s(pmax(1, pmin(ClimMnkEpi, 27)), bs = "ts")
```

Parametric coefficients:

```
Estimate Std. Error t value Pr(>|t|)
(Intercept) -21.7856 0.1598 -136.3 <2e-16 ***
```

---

Signif. codes: 0 '\*\*\*' 0.001 '\*\*' 0.01 '\*' 0.05 '.' 0.1 ' ' 1

Approximate significance of smooth terms:

	edf	Ref.df	F	p-value
s(pmax(15, Fetch_50km))	4.786	9	5.033	<2e-16 ***
s(log10(pmax(3, pmin(Depth, 4000))))	7.347	9	11.114	<2e-16 ***
s(pmax(-75, pmin(I(DistTo125m/1000), 75)))	6.352	9	17.092	<2e-16 ***
s(pmax(-400, pmin(I(DistTo300m/1000), 25)))	7.972	9	18.326	<2e-16 ***
s(pmax(3, pmin(ClimSST_CMC, 30)))	6.965	9	20.464	<2e-16 ***
s(pmax(3, pmin(ClimBotT_HYCOM, 25)))	6.440	9	33.254	<2e-16 ***
s(pmin(I(ClimDistToFront105/1000), 75))	7.871	9	7.986	<2e-16 ***
s(pmax(1, pmin(ClimMnkEpi, 27)))	7.737	9	16.404	<2e-16 ***

---

Signif. codes: 0 '\*\*\*' 0.001 '\*\*' 0.01 '\*' 0.05 '.' 0.1 ' ' 1

R-sq.(adj) = 0.0201 Deviance explained = 16.8%

-REML = 18917 Scale est. = 7.1996 n = 329173

Method: REML Optimizer: outer newton

full convergence after 14 iterations.

Gradient range [-4.880345e-05,1.72887e-05]

(score 18916.68 & scale 7.199615).

Hessian positive definite, eigenvalue range [1.449145,21157.77].

Model rank = 73 / 73

Basis dimension (k) checking results. Low p-value (k-index<1) may indicate that k is too low, especially if edf is close to k'.

	k'	edf	k-index	p-value
s(pmax(15, Fetch_50km))	9.00	4.79	0.89	0.960
s(log10(pmax(3, pmin(Depth, 4000))))	9.00	7.35	0.85	0.035 *
s(pmax(-75, pmin(I(DistTo125m/1000), 75)))	9.00	6.35	0.82	0.015 *
s(pmax(-400, pmin(I(DistTo300m/1000), 25)))	9.00	7.97	0.85	0.050 *
s(pmax(3, pmin(ClimSST_CMC, 30)))	9.00	6.97	0.86	0.080 .
s(pmax(3, pmin(ClimBotT_HYCOM, 25)))	9.00	6.44	0.85	0.015 *
s(pmin(I(ClimDistToFront105/1000), 75))	9.00	7.87	0.87	0.055 .
s(pmax(1, pmin(ClimMnkEpi, 27)))	9.00	7.74	0.82	<2e-16 ***

---

Signif. codes: 0 '\*\*\*' 0.001 '\*\*' 0.01 '\*' 0.05 '.' 0.1 ' ' 1

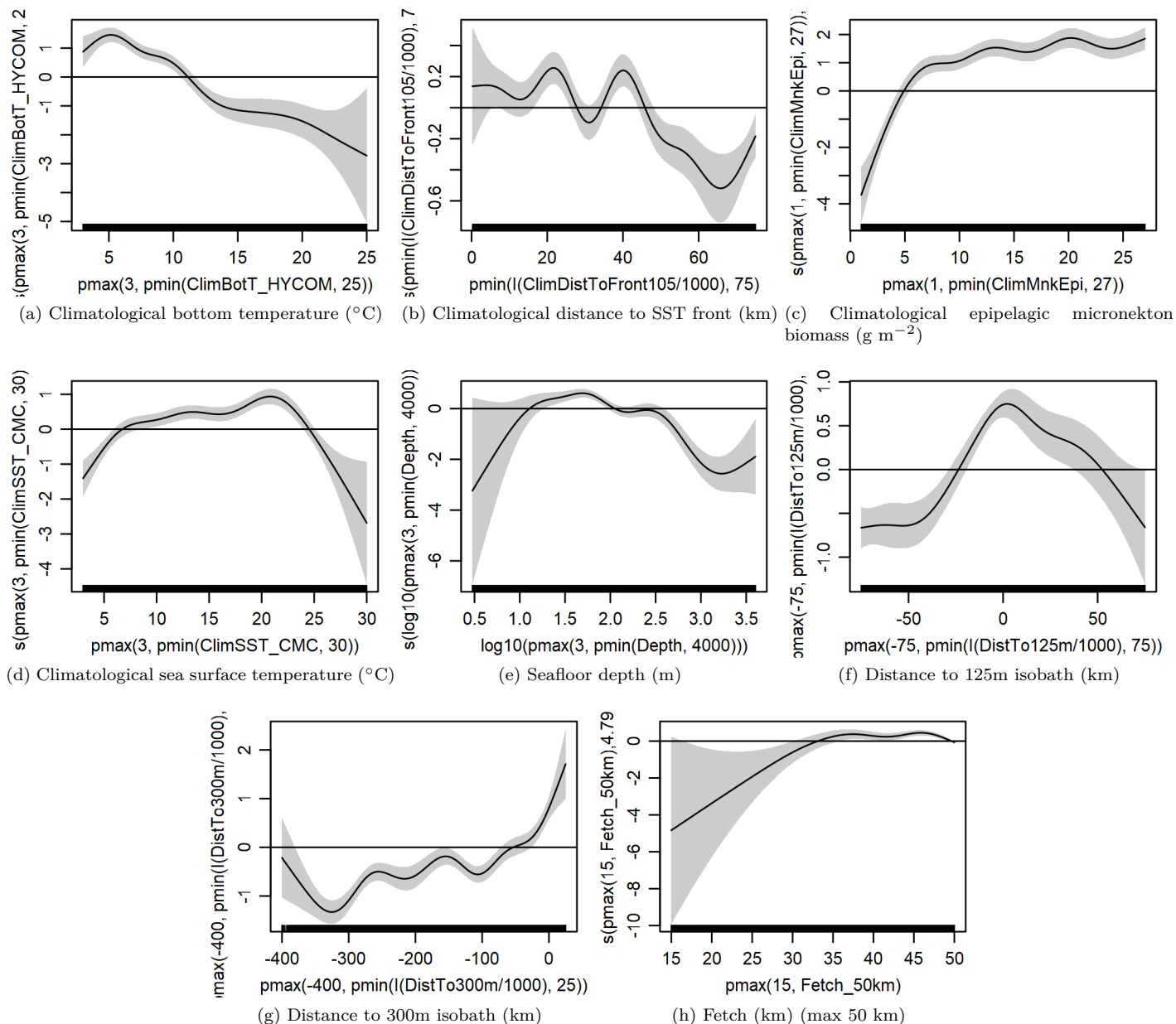


Figure 64: Functional plots for the final model. Transforms and other treatments are indicated in axis labels.  $\log_{10}$  indicates the covariate was  $\log_{10}$  transformed.  $pmax$  and  $pmin$  indicate the covariate's minimum and maximum values, respectively, were Winsorized to the values shown. Winsorization was used to prevent runaway extrapolations during prediction when covariates exceeded sampled ranges, or for ecological reasons, depending on the covariate.  $/1000$  indicates meters were transformed to kilometers for interpretation convenience.

Table 25: Covariates used in the final model.

Covariate	Description
ClimBotT_HYCOM	Climatological monthly mean bottom temperature ( $^{\circ}\text{C}$ ) from the HYCOM GOFs 3.1 1/12 $^{\circ}$ ocean model (Chassignet et al. (2009))
ClimDistToFront105	Climatological monthly mean distance (km) to the closest sea surface temperature front detected in daily GHRSSST Level 4 CMC0.2deg and CMC0.1deg images (Brasnett (2008); Canada Meteorological Center (2012); Meissner et al. (2016); Canada Meteorological Center (2016)) with MGET's implementation of the Canny edge detector (Roberts et al. (2010); Canny (1986))

Table 25: Covariates used in the final model. (continued)

Covariate	Description
ClimMnkEpi	Climatological monthly mean micronekton biomass available in the epipelagic zone, expressed as wet weight ( $\text{g m}^{-2}$ ), from SEAPODYM (Lehodey et al. (2008); Lehodey et al. (2015)), provided by E.U. Copernicus Marine Service. doi: <a href="https://doi.org/10.48670/moi-00020">10.48670/moi-00020</a> . Computed as the sum of the SEAPODYM <code>mnkc_epi</code> , <code>mnkc_mumeso</code> , and <code>mnkc_hmlmeso</code> variables.
ClimSST_CMC	Climatological monthly mean sea surface temperature ( $^{\circ}\text{C}$ ) from GHRSSST Level 4 CMC0.2deg and CMC0.1deg (Brasnett (2008); Canada Meteorological Center (2012); Meissner et al. (2016); Canada Meteorological Center (2016))
Depth	Depth (m) of the seafloor, from SRTM30_PLUS (Becker et al. (2009))
DistTo125m	Distance (km) to the 125m isobath, derived from SRTM30_PLUS (Becker et al. (2009))
DistTo300m	Distance (km) to the 300m isobath, derived from SRTM30_PLUS (Becker et al. (2009))
Fetch_50km	Fetch (km): mean distance to shore averaged over 16 radial directions, limited to a maximum of 50 km

## 5.2 Diagnostic Plots

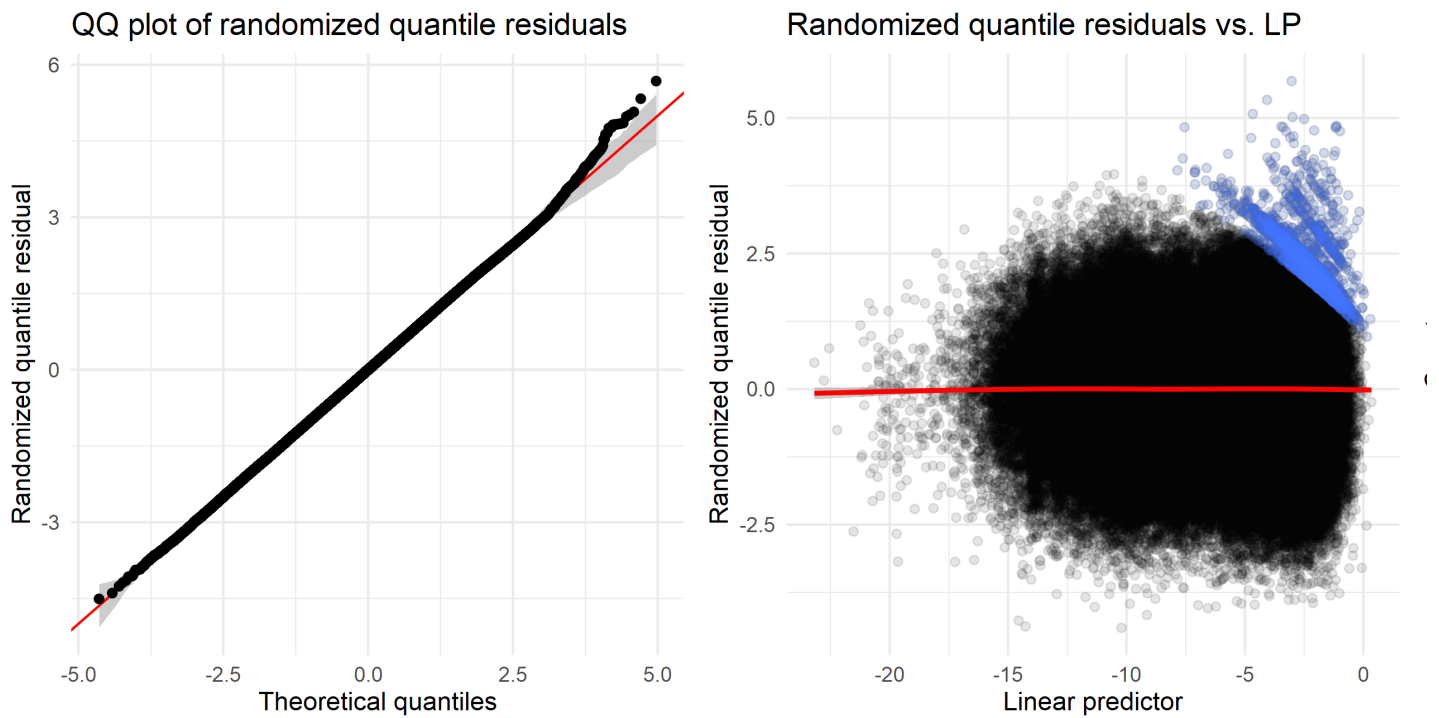


Figure 65: Residual plots for the final model.

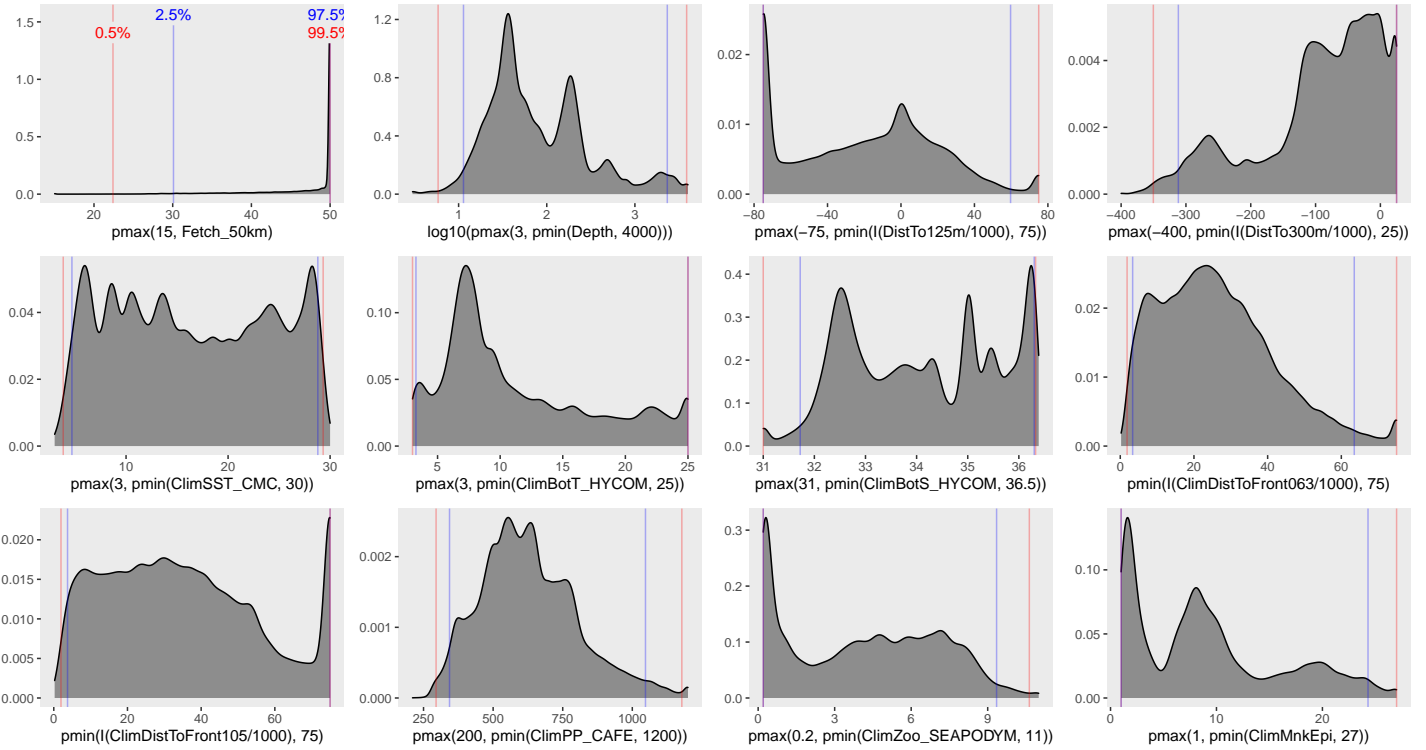


Figure 66: Density histograms showing the distributions of the covariates considered during the final model selection step. The final model may have included only a subset of the covariates shown here (see Figure 64), and additional covariates may have been considered in preceding selection steps. Red and blue lines enclose 99% and 95% of the distributions, respectively. Transforms and other treatments are indicated in axis labels.  $\log_{10}$  indicates the covariate was  $\log_{10}$  transformed.  $pmax$  and  $pmin$  indicate the covariate's minimum and maximum values, respectively, were Winsorized to the values shown. Winsorization was used to prevent runaway extrapolations during prediction when covariates exceeded sampled ranges, or for ecological reasons, depending on the covariate.  $/1000$  indicates meters were transformed to kilometers for interpretation convenience.

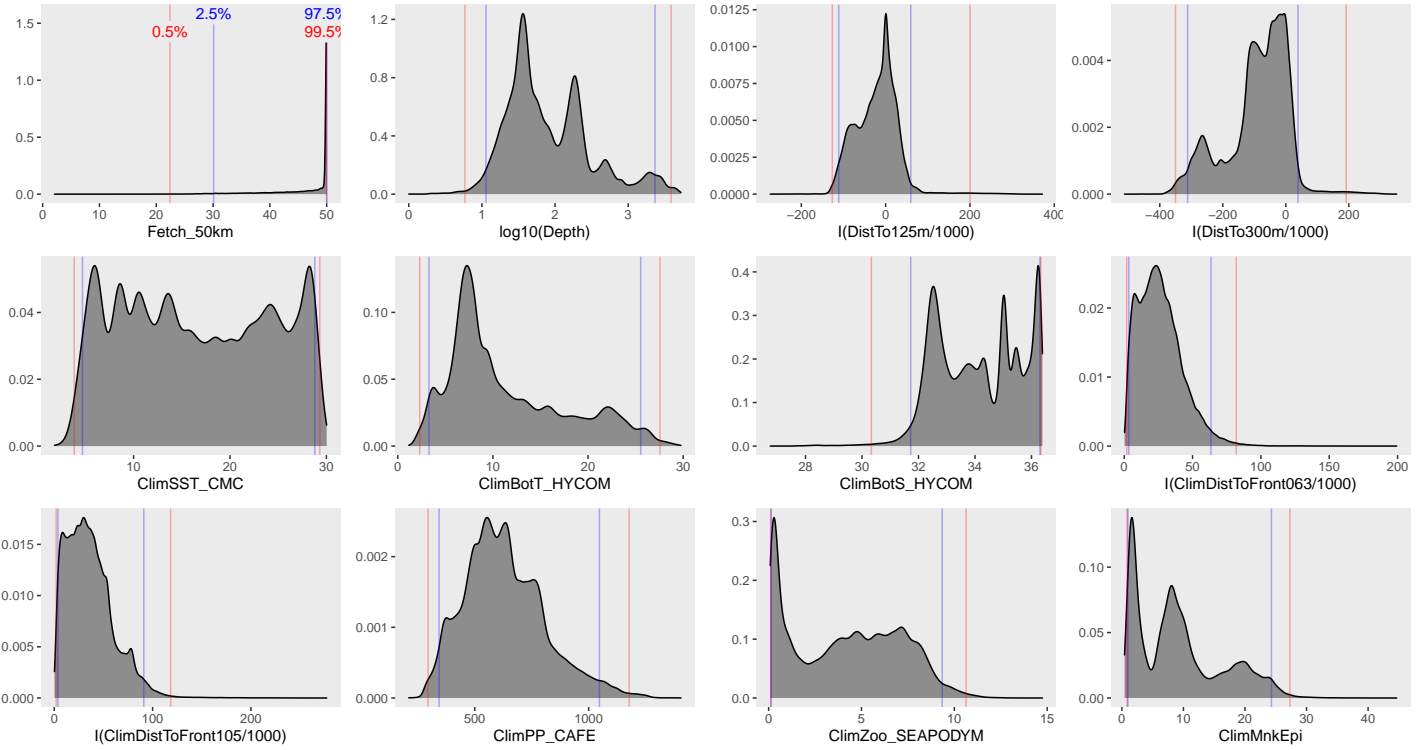


Figure 67: Density histograms shown in Figure 66 replotted without Winsorization, to show the full range of sampling represented by survey segments.



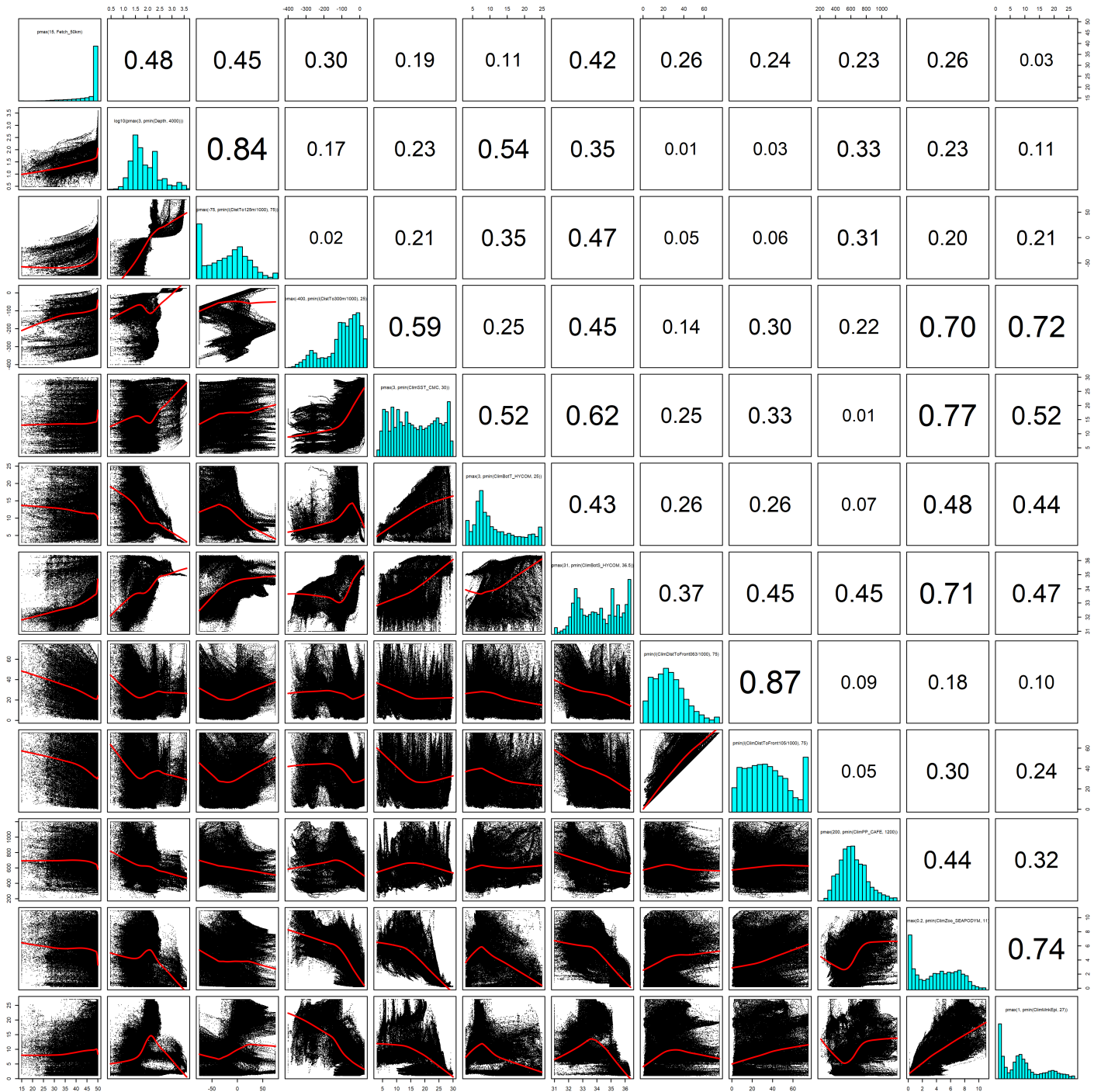


Figure 68: Scatterplot matrix of the covariates considered during the final model selection step. The final model may have included only a subset of the covariates shown here (see Figure 64), and additional covariates may have been considered in preceding selection steps. Covariates are transformed and Winsorized as shown in Figure 66. This plot is used to check simple correlations between covariates (via pairwise Pearson coefficients above the diagonal) and visually inspect for concavity (via scatterplots and red lowest curves below the diagonal).

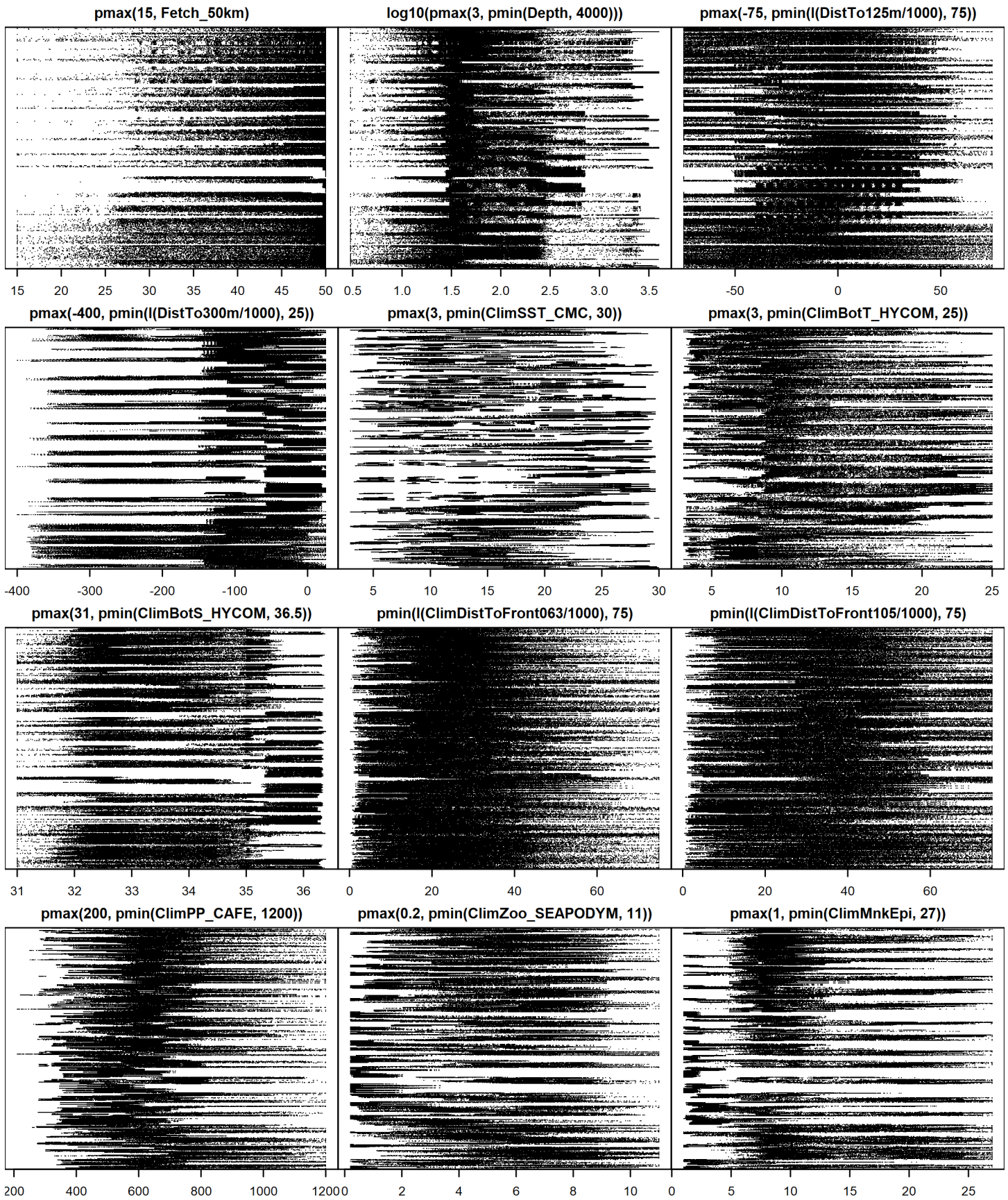


Figure 69: Dotplot of the covariates considered during the final model selection step. The final model may have included only a subset of the covariates shown here (see Figure 64), and additional covariates may have been considered in preceding selection steps. Covariates are transformed and Winsorized as shown in Figure 66. This plot is used to check for suspicious patterns and outliers in the data. Points are ordered vertically by segment ID, sequentially in time.

## 5.3 Extrapolation Diagnostics

### 5.3.1 Univariate Extrapolation

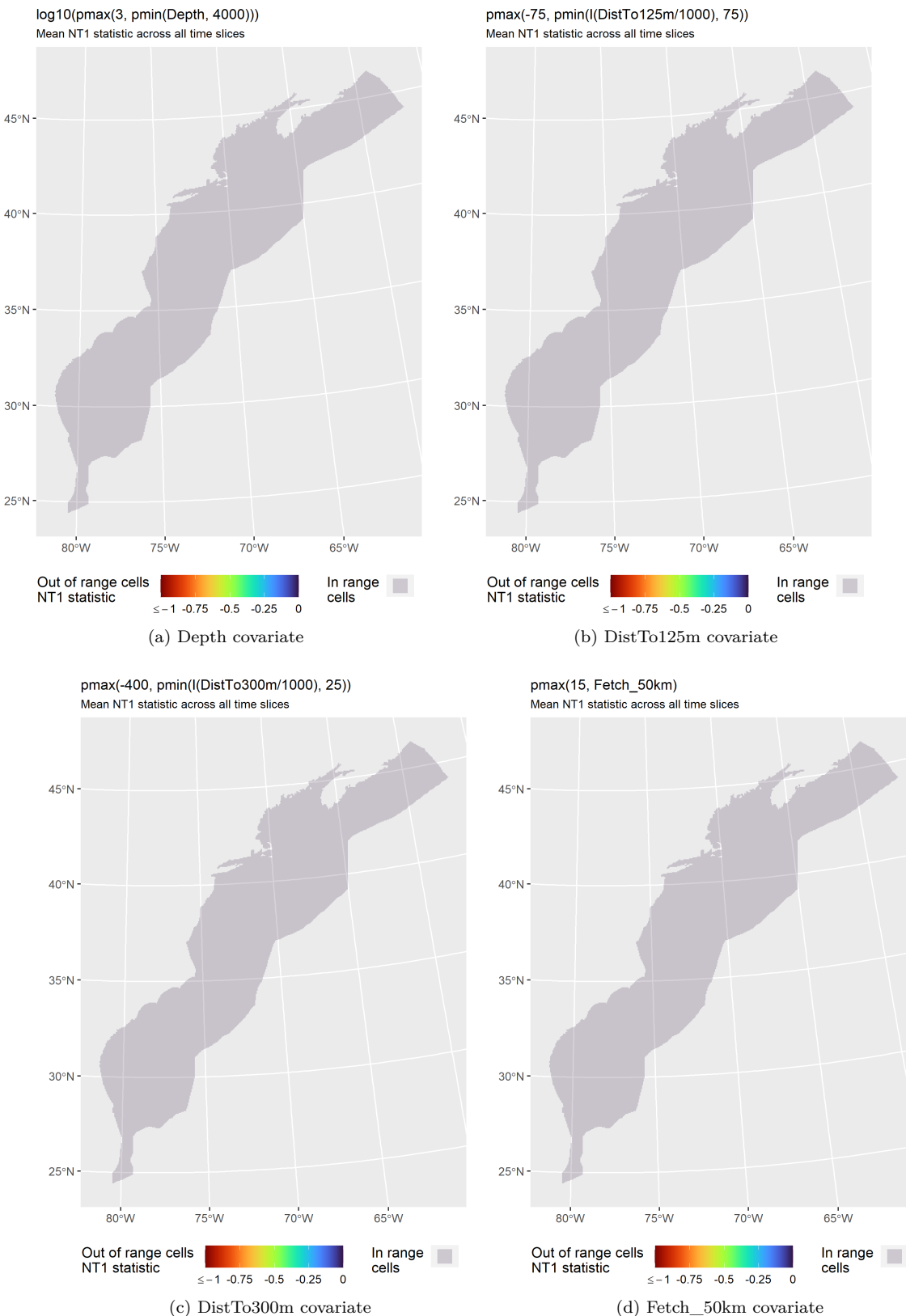


Figure 70: NT1 statistic (Mesgaran et al. (2014)) for static covariates used in the model. Areas outside the sampled range of a covariate appear in color, indicating univariate extrapolation of that covariate occurred there. Areas within the sampled range appear in gray, indicating it did not occur.

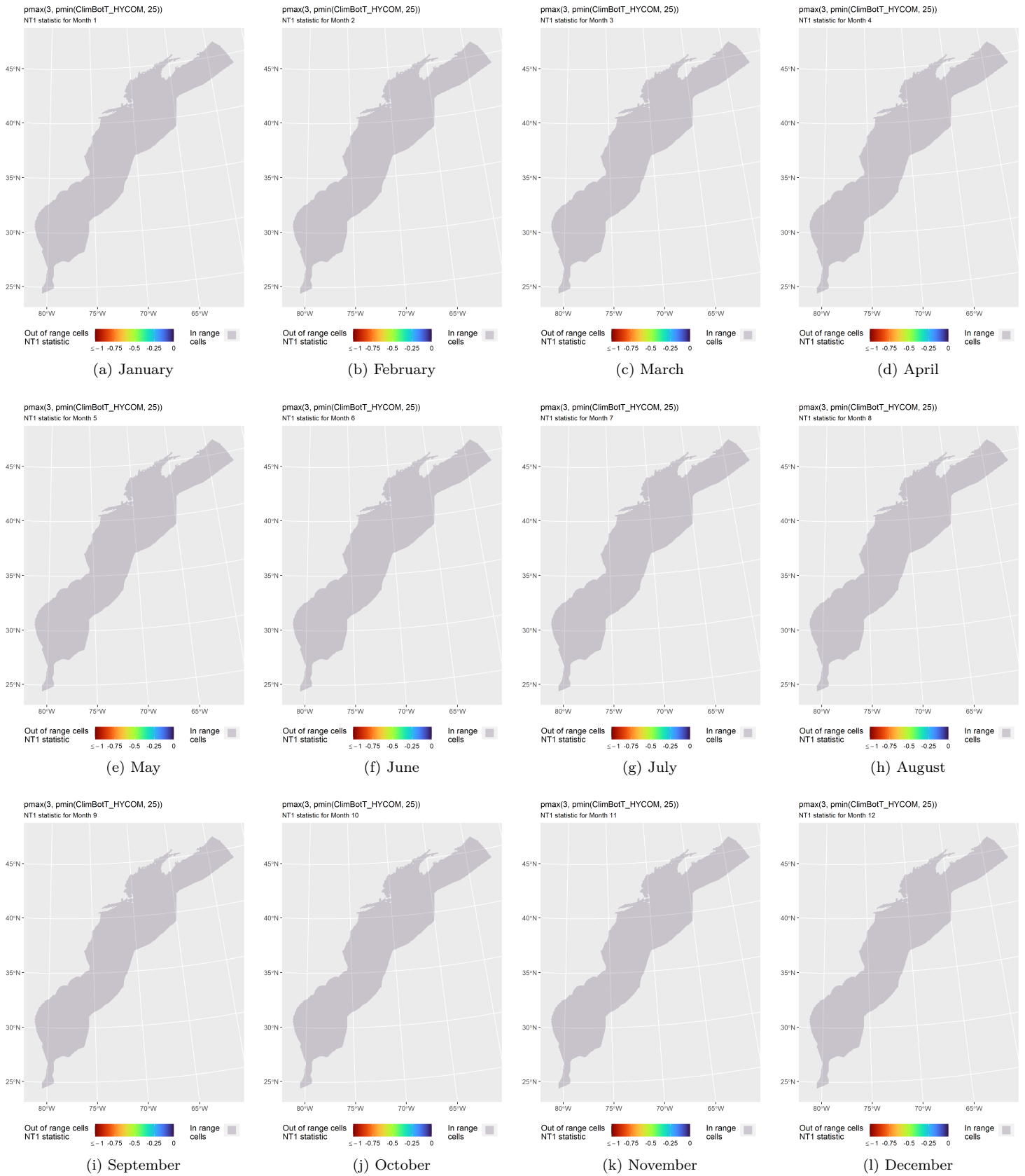


Figure 71: NT1 statistic (Mesgaran et al. (2014)) for the ClimBotT\_HYCOM covariate in the model. Areas outside the sampled range of a covariate appear in color, indicating univariate extrapolation of that covariate occurred there during the month. Areas within the sampled range appear in gray, indicating it did not occur.

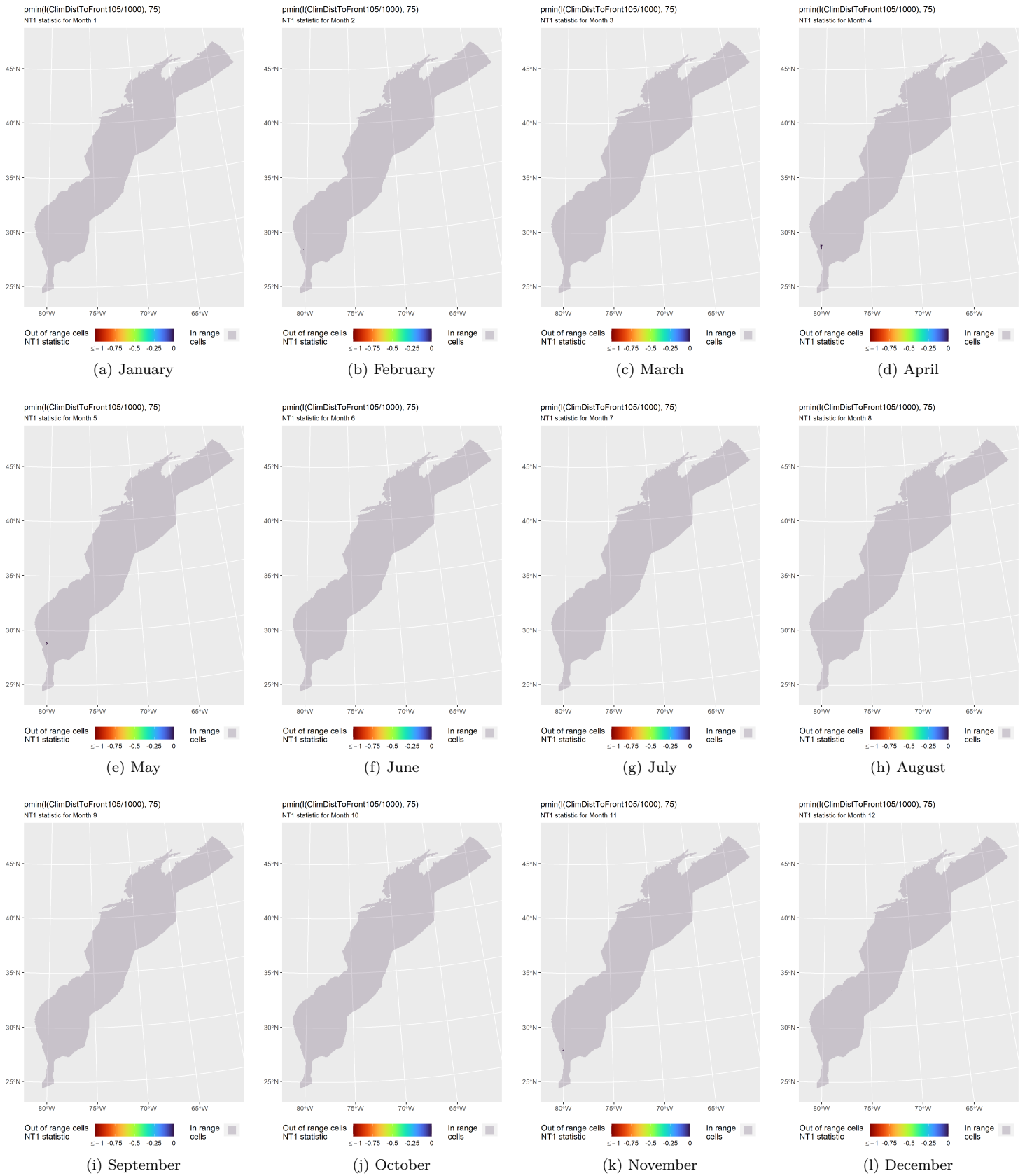


Figure 72: NT1 statistic (Mesgaran et al. (2014)) for the ClimDistToFront105 covariate in the model. Areas outside the sampled range of a covariate appear in color, indicating univariate extrapolation of that covariate occurred there during the month. Areas within the sampled range appear in gray, indicating it did not occur.

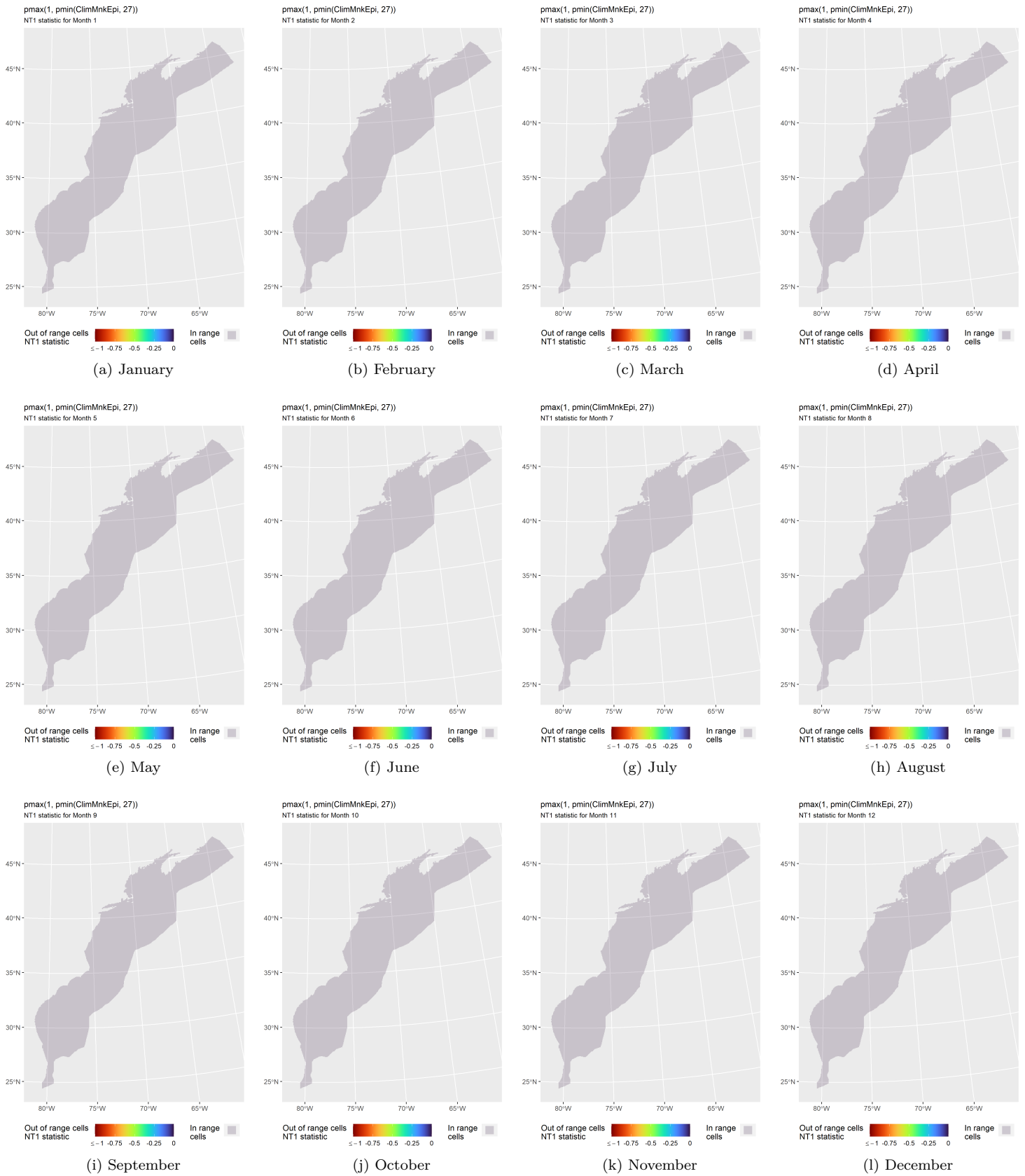


Figure 73: NT1 statistic (Mesgaran et al. (2014)) for the ClimMnkEpi covariate in the model. Areas outside the sampled range of a covariate appear in color, indicating univariate extrapolation of that covariate occurred there during the month. Areas within the sampled range appear in gray, indicating it did not occur.



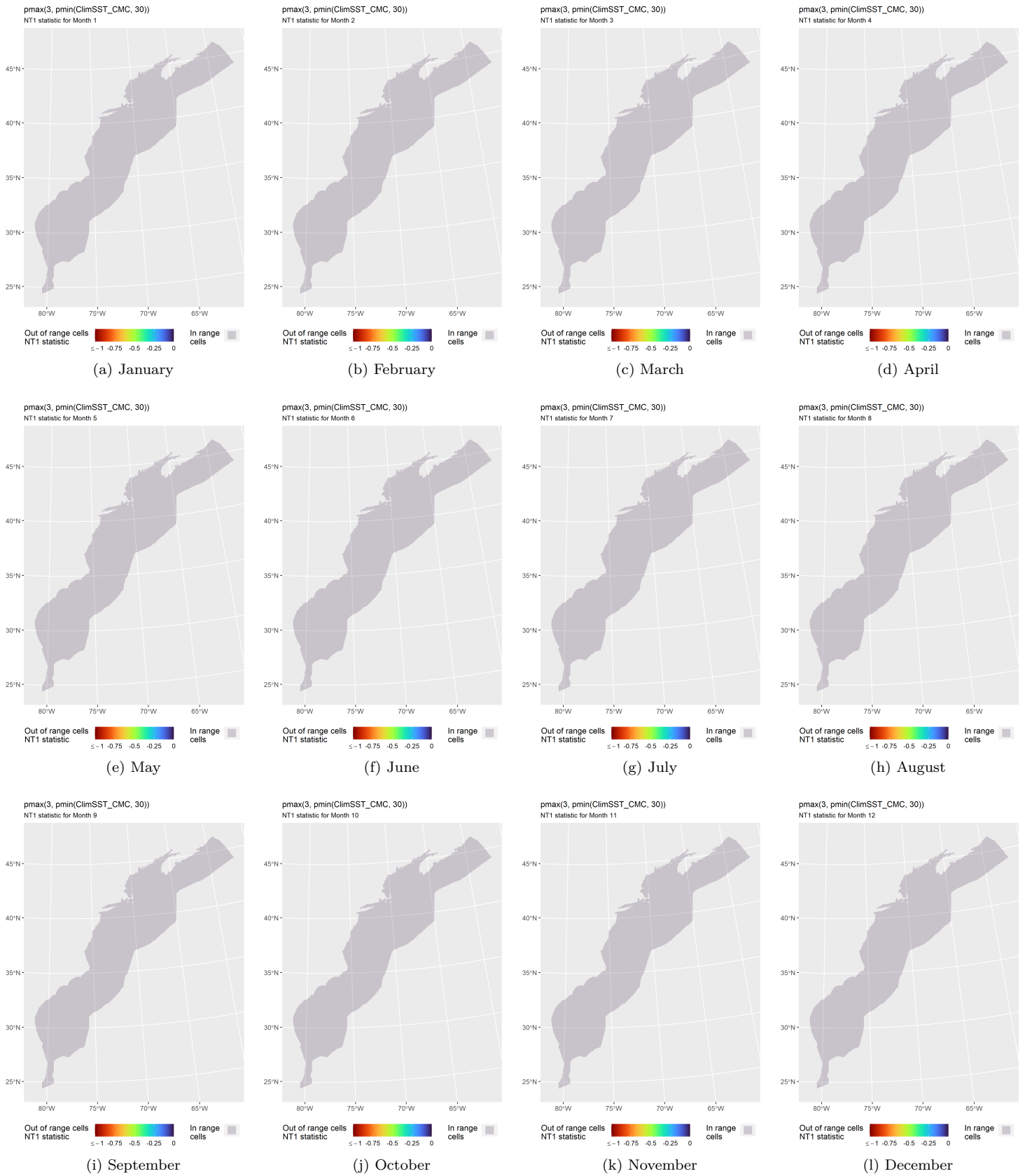


Figure 74: NT1 statistic (Mesgaran et al. (2014)) for the ClimSST\_CMC covariate in the model. Areas outside the sampled range of a covariate appear in color, indicating univariate extrapolation of that covariate occurred there during the month. Areas within the sampled range appear in gray, indicating it did not occur.

### 5.3.2 Multivariate Extrapolation

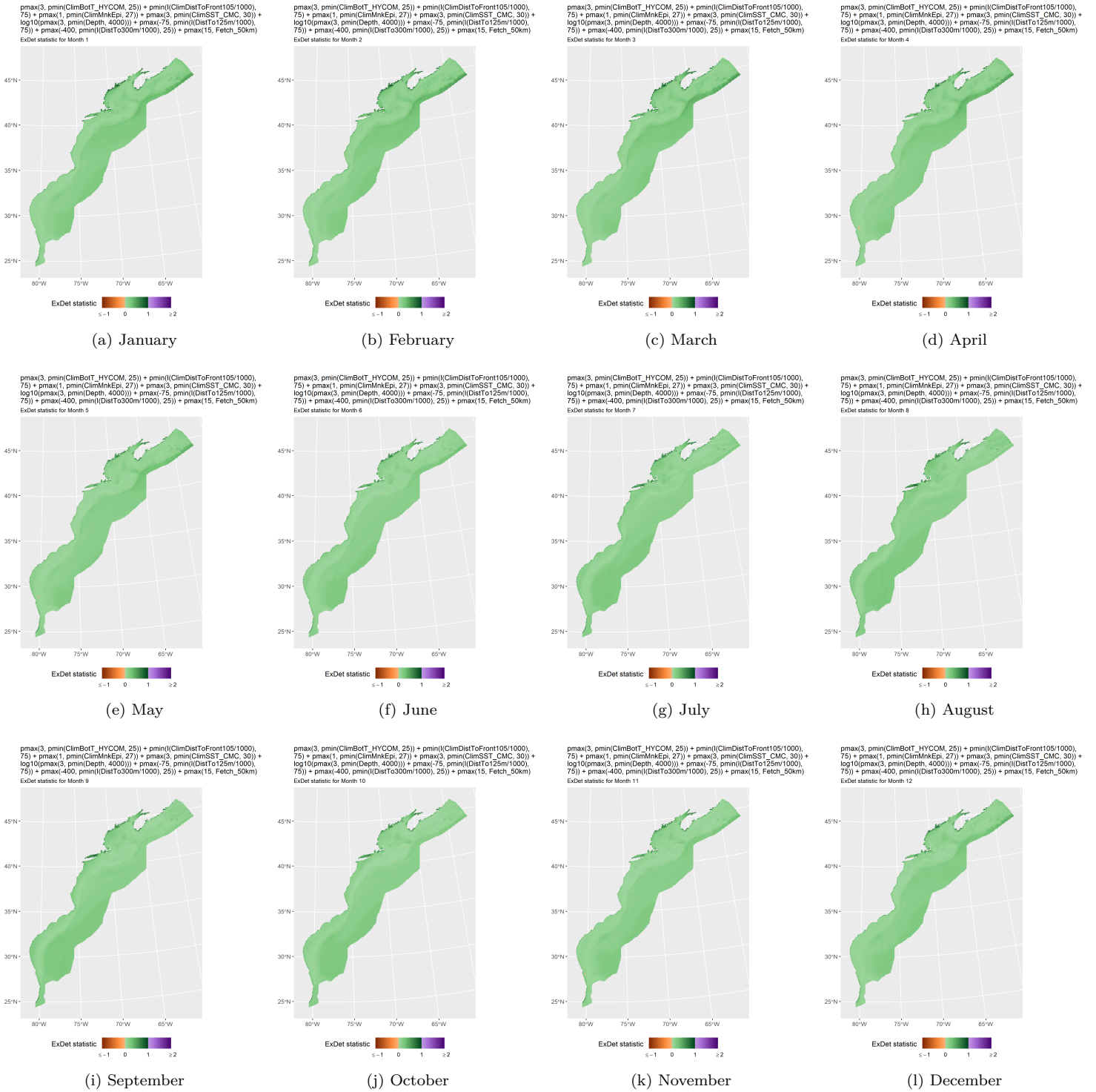


Figure 75: ExDet statistic (Mesgaran et al. (2014)) for all of the covariates used in the model. Areas in orange ( $\text{ExDet} < 0$ ) required univariate extrapolation of one or more covariates (see previous section). Areas in purple ( $\text{ExDet} > 1$ ), did not require univariate extrapolation but did require multivariate extrapolation, by virtue of having novel combinations of covariates not represented in the survey data, according to the NT2 statistic (Mesgaran et al. (2014)). Areas in green ( $0 \geq \text{ExDet} \leq 1$ ) did not require either type of extrapolation.



## 6 Predictions

Based on our evaluation of this model in the context of what is known of this species (see Section 7), we summarized its predictions into monthly climatological density and uncertainty surfaces, shown in the maps below.

### 6.1 Summarized Predictions

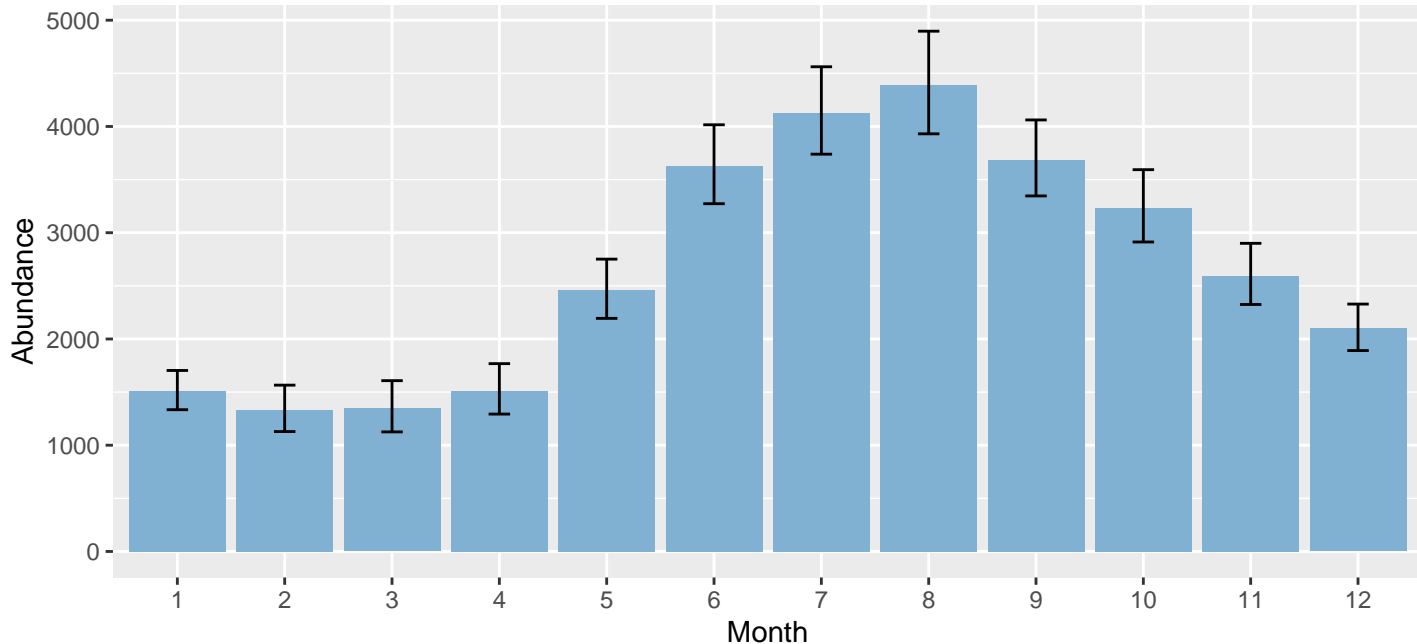


Figure 76: Mean monthly abundance for the prediction area for 1998-2020. Error bars are a 95% interval, made with a log-normal approximation using the prediction’s CV. The CV was estimated with the analytic approach given by Miller et al. (2022), Appendix S1, and accounts both for uncertainty in model parameter estimates and for temporal variability in dynamic covariates.

Table 26: Mean monthly abundance and density for the prediction area for 1998-2020. CV and intervals estimated as described for the previous figure.

Month	Abundance	CV	95% Interval	Area (km <sup>2</sup> )	Density (individuals / 100 km <sup>2</sup> )
1	1,508	0.062	1,334 - 1,704	1,272,925	0.118
2	1,329	0.084	1,129 - 1,565	1,272,925	0.104
3	1,345	0.091	1,126 - 1,608	1,272,925	0.106
4	1,512	0.080	1,293 - 1,768	1,272,925	0.119
5	2,457	0.058	2,194 - 2,751	1,272,925	0.193
6	3,625	0.052	3,273 - 4,016	1,272,925	0.285
7	4,130	0.051	3,739 - 4,562	1,272,925	0.324
8	4,387	0.056	3,931 - 4,897	1,272,925	0.345
9	3,686	0.049	3,346 - 4,061	1,272,925	0.290
10	3,235	0.054	2,913 - 3,593	1,272,925	0.254
11	2,596	0.056	2,325 - 2,900	1,272,925	0.204
12	2,098	0.053	1,891 - 2,328	1,272,925	0.165

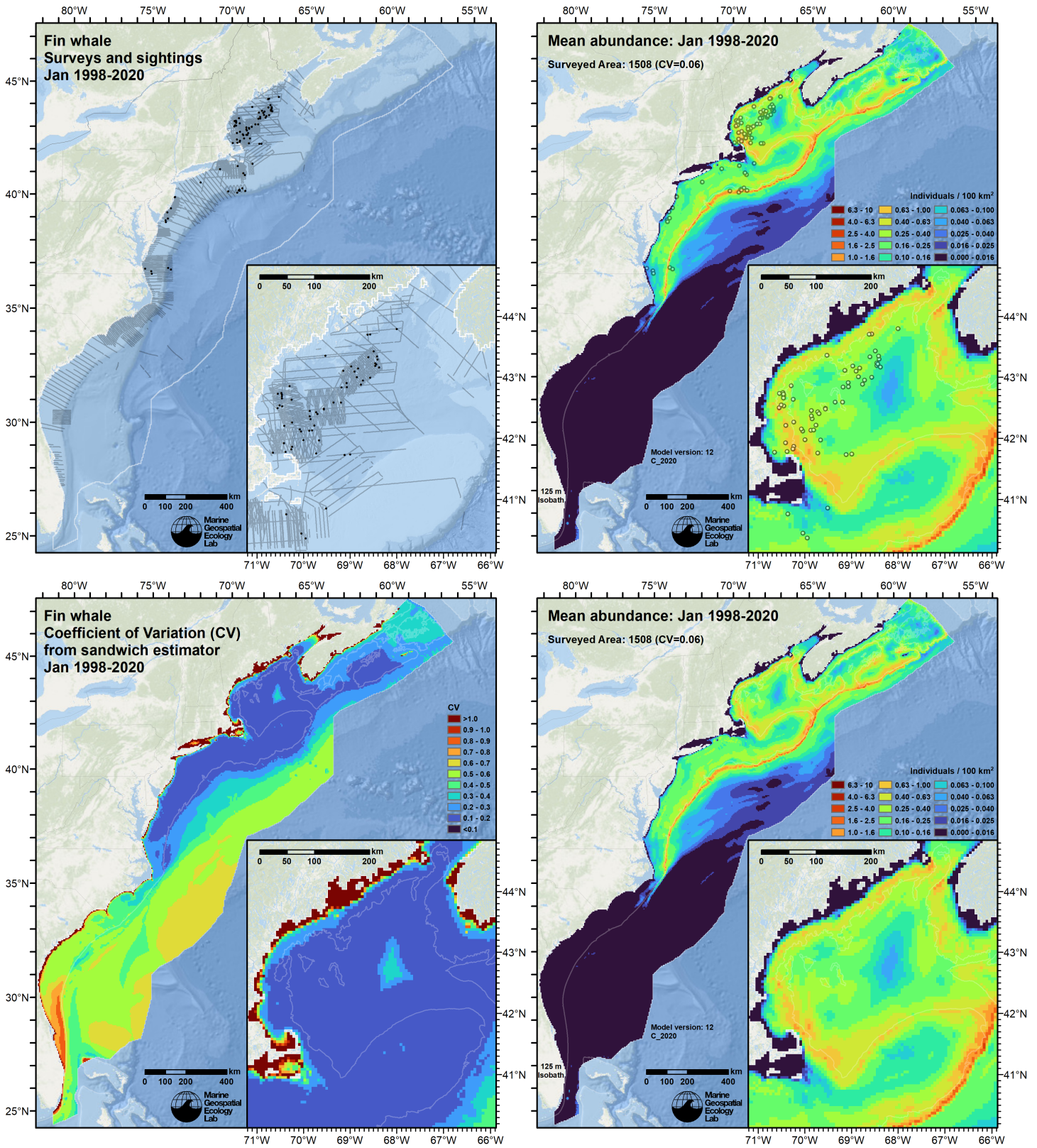


Figure 77: Survey effort and observations (top left), predicted density with observations (top right), predicted density without observations (bottom right), and coefficient of variation of predicted density (bottom left), for the month of January for the given era. Variance was estimated with the analytic approach given by Miller et al. (2022), Appendix S1, and accounts both for uncertainty in model parameter estimates and for temporal variability in dynamic covariates.



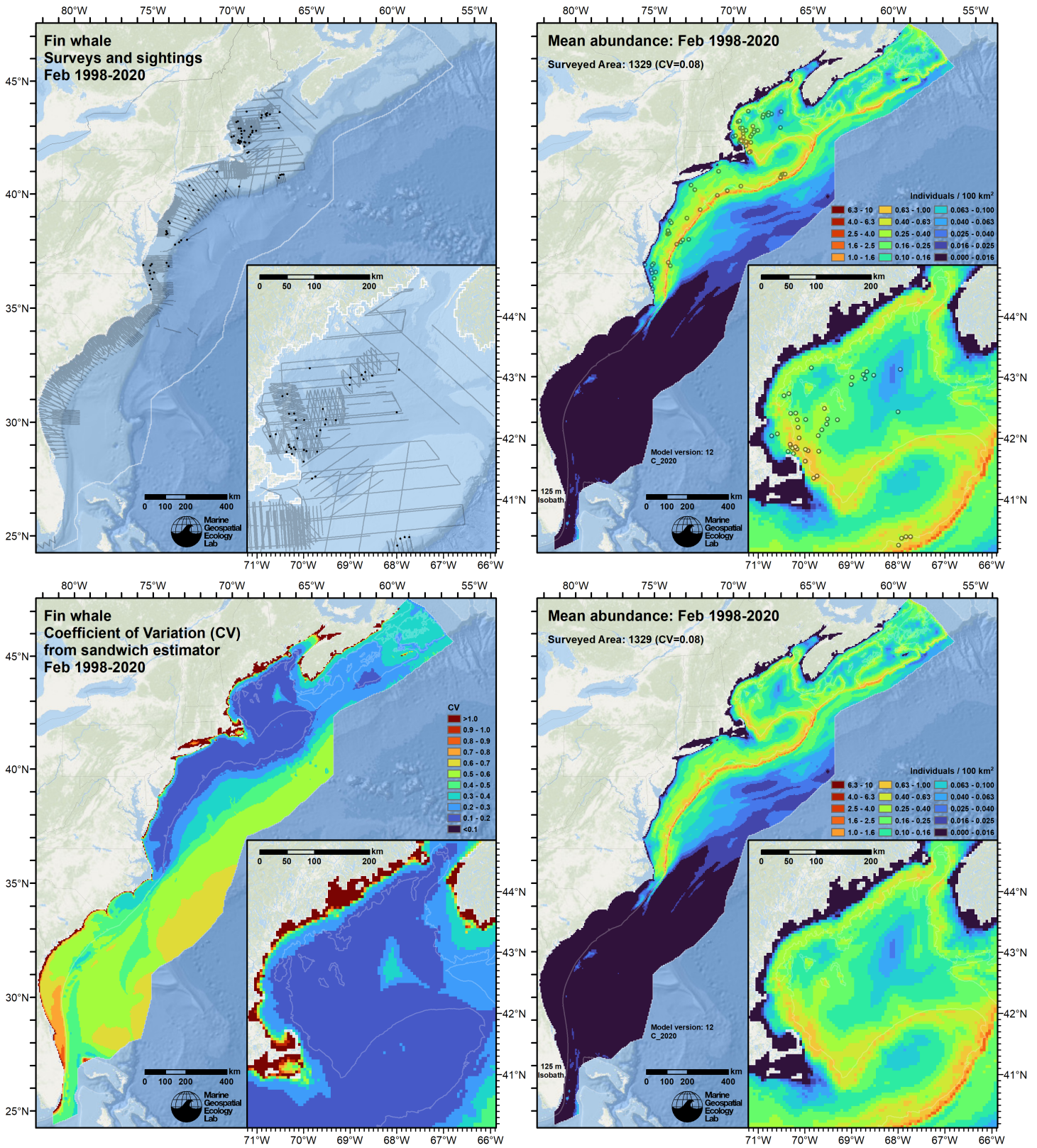


Figure 78: Survey effort and observations (top left), predicted density with observations (top right), predicted density without observations (bottom right), and coefficient of variation of predicted density (bottom left), for the month of February for the given era. Variance was estimated with the analytic approach given by Miller et al. (2022), Appendix S1, and accounts both for uncertainty in model parameter estimates and for temporal variability in dynamic covariates.



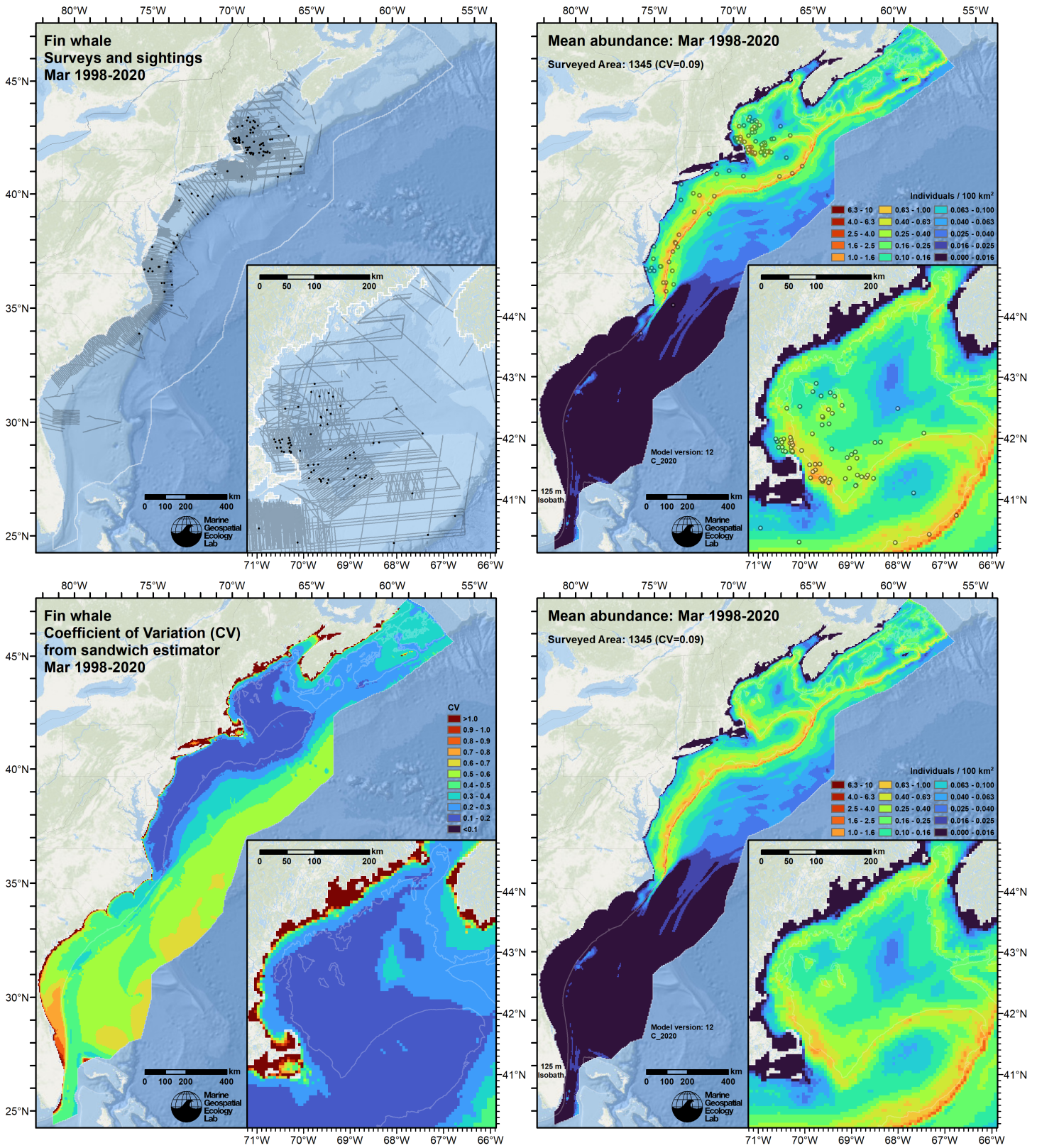


Figure 79: Survey effort and observations (top left), predicted density with observations (top right), predicted density without observations (bottom right), and coefficient of variation of predicted density (bottom left), for the month of March for the given era. Variance was estimated with the analytic approach given by Miller et al. (2022), Appendix S1, and accounts both for uncertainty in model parameter estimates and for temporal variability in dynamic covariates.



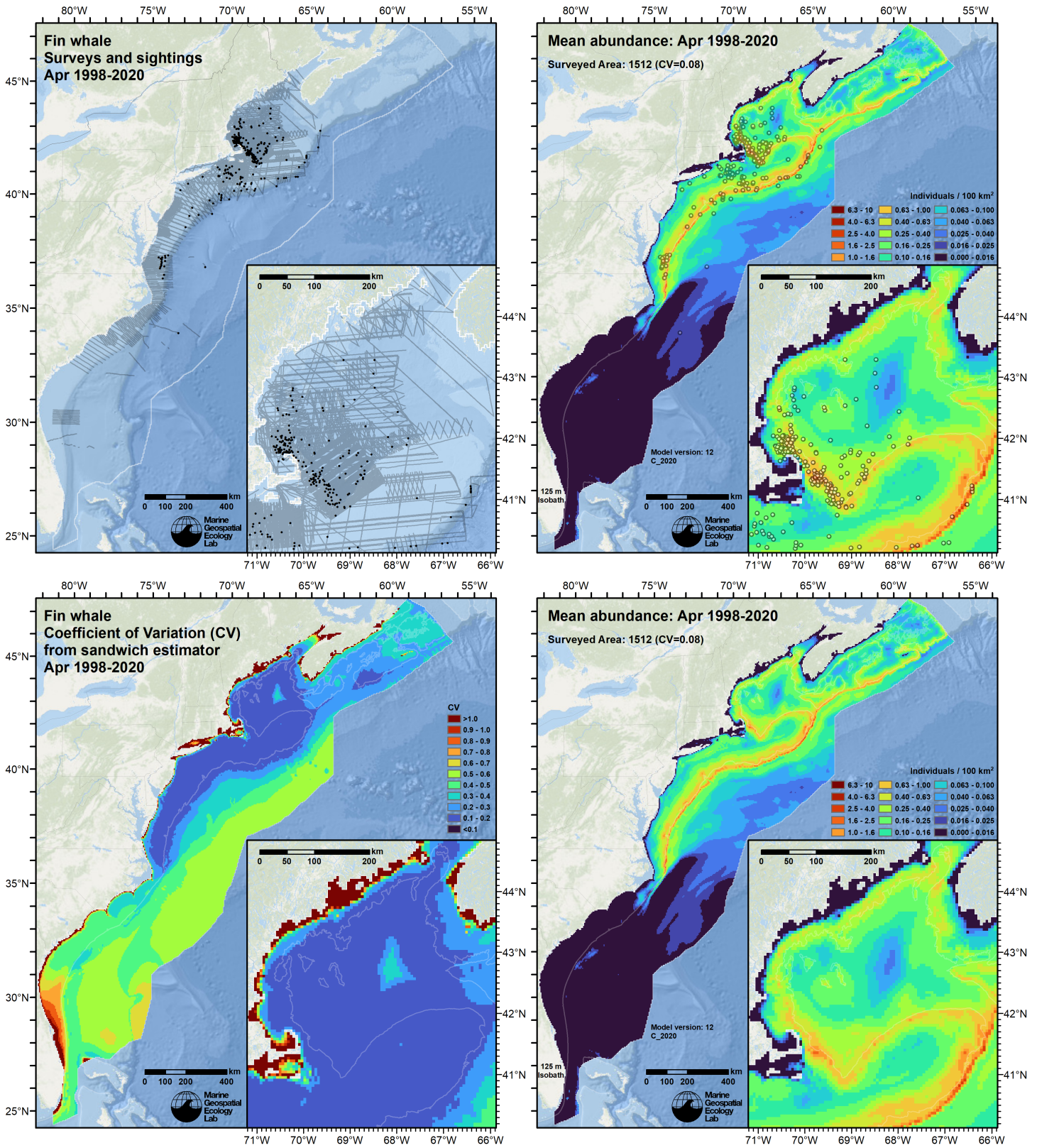


Figure 80: Survey effort and observations (top left), predicted density with observations (top right), predicted density without observations (bottom right), and coefficient of variation of predicted density (bottom left), for the month of April for the given era. Variance was estimated with the analytic approach given by Miller et al. (2022), Appendix S1, and accounts both for uncertainty in model parameter estimates and for temporal variability in dynamic covariates.



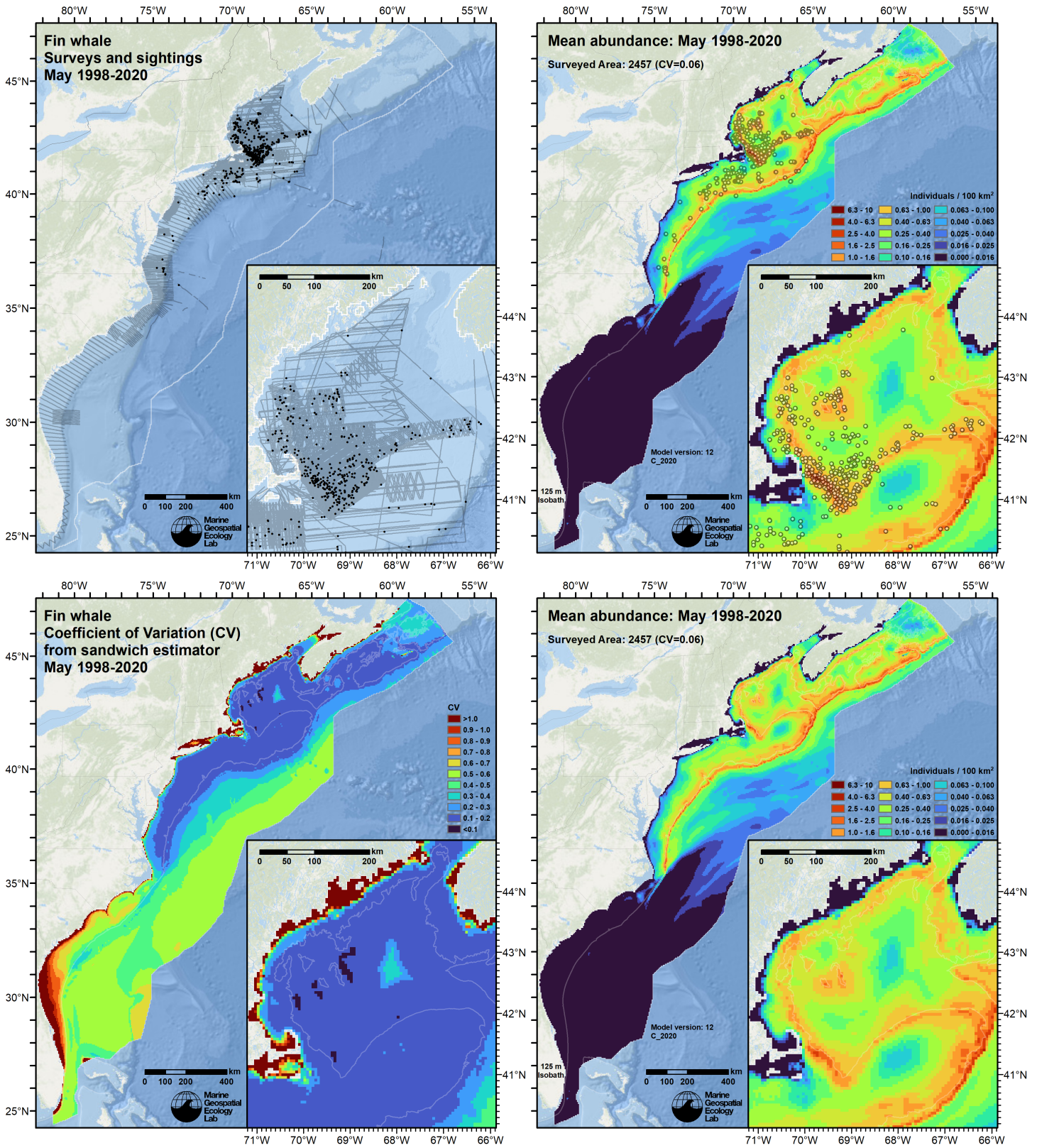


Figure 81: Survey effort and observations (top left), predicted density with observations (top right), predicted density without observations (bottom right), and coefficient of variation of predicted density (bottom left), for the month of May for the given era. Variance was estimated with the analytic approach given by Miller et al. (2022), Appendix S1, and accounts both for uncertainty in model parameter estimates and for temporal variability in dynamic covariates.



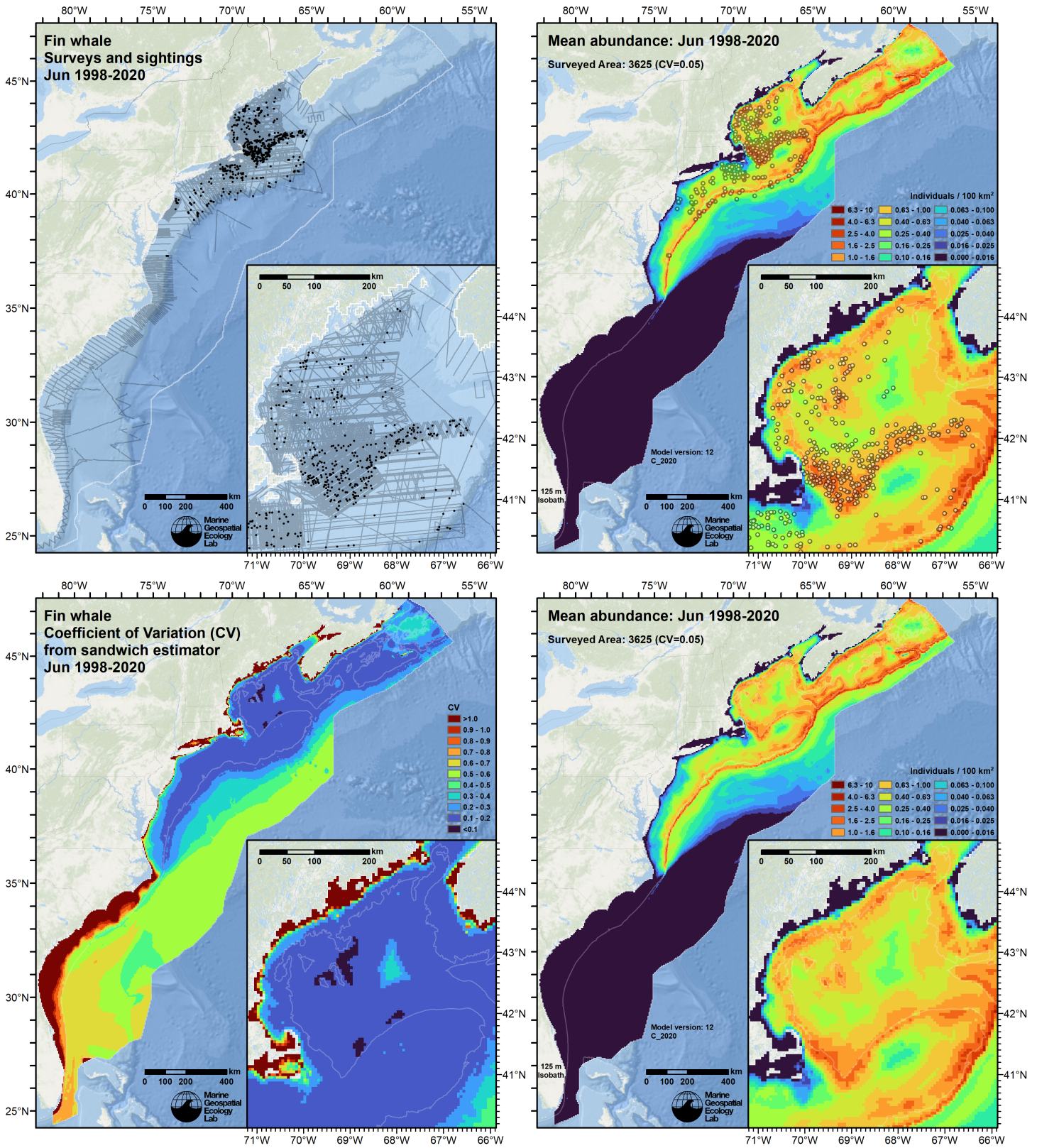


Figure 82: Survey effort and observations (top left), predicted density with observations (top right), predicted density without observations (bottom right), and coefficient of variation of predicted density (bottom left), for the month of June for the given era. Variance was estimated with the analytic approach given by Miller et al. (2022), Appendix S1, and accounts both for uncertainty in model parameter estimates and for temporal variability in dynamic covariates.



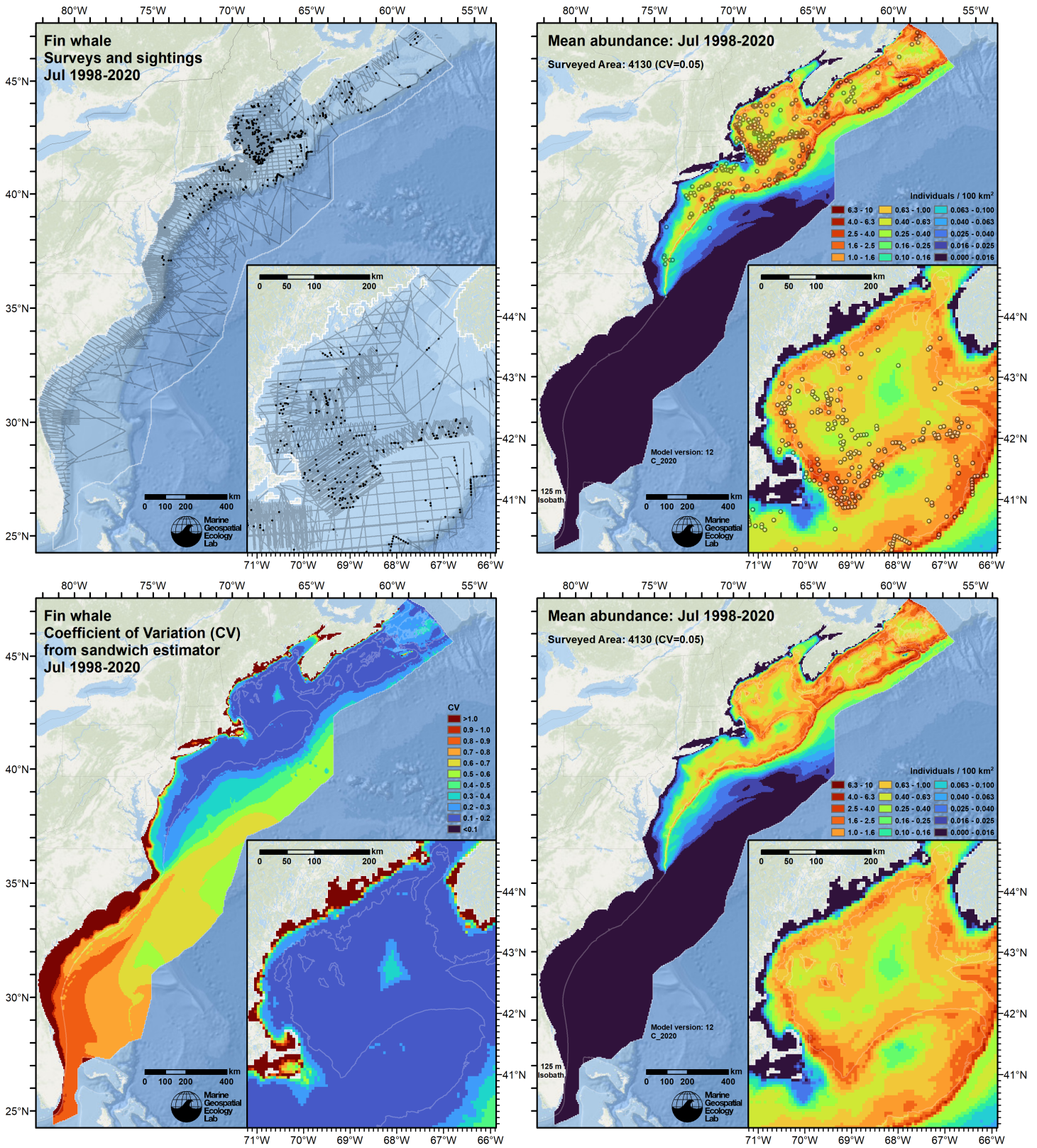


Figure 83: Survey effort and observations (top left), predicted density with observations (top right), predicted density without observations (bottom right), and coefficient of variation of predicted density (bottom left), for the month of July for the given era. Variance was estimated with the analytic approach given by Miller et al. (2022), Appendix S1, and accounts both for uncertainty in model parameter estimates and for temporal variability in dynamic covariates.



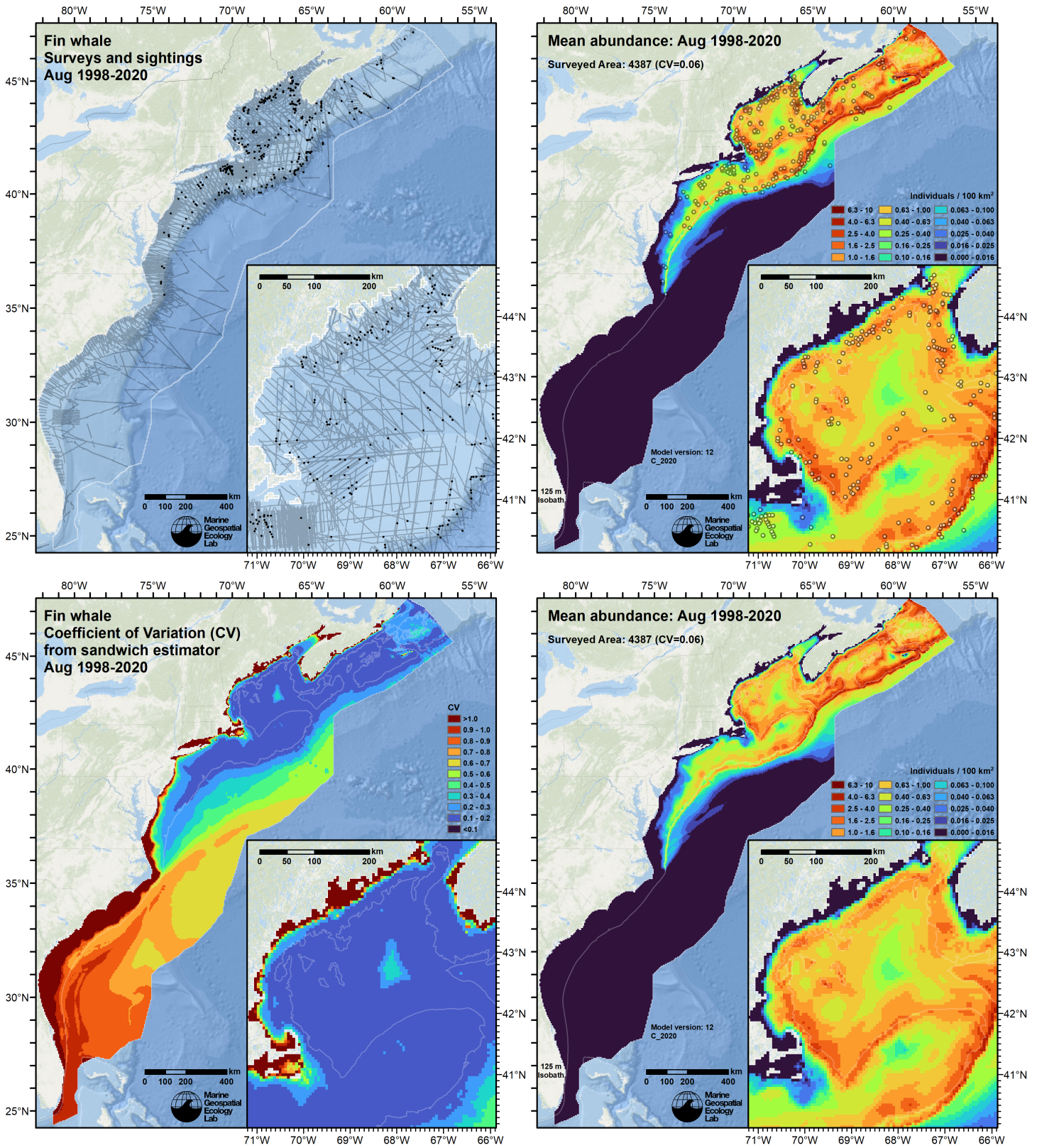


Figure 84: Survey effort and observations (top left), predicted density with observations (top right), predicted density without observations (bottom right), and coefficient of variation of predicted density (bottom left), for the month of August for the given era. Variance was estimated with the analytic approach given by Miller et al. (2022), Appendix S1, and accounts both for uncertainty in model parameter estimates and for temporal variability in dynamic covariates.



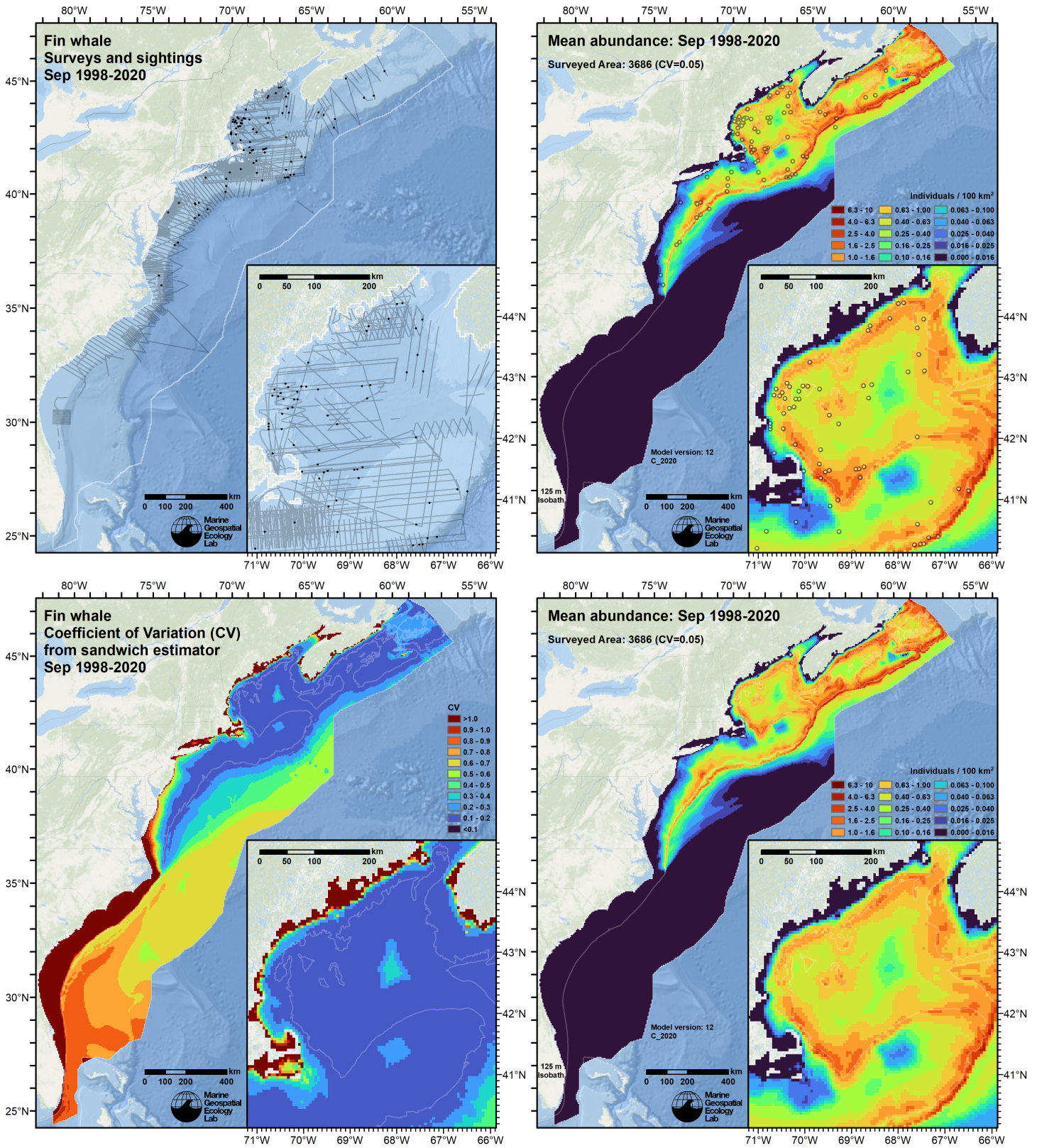


Figure 85: Survey effort and observations (top left), predicted density with observations (top right), predicted density without observations (bottom right), and coefficient of variation of predicted density (bottom left), for the month of September for the given era. Variance was estimated with the analytic approach given by Miller et al. (2022), Appendix S1, and accounts both for uncertainty in model parameter estimates and for temporal variability in dynamic covariates.



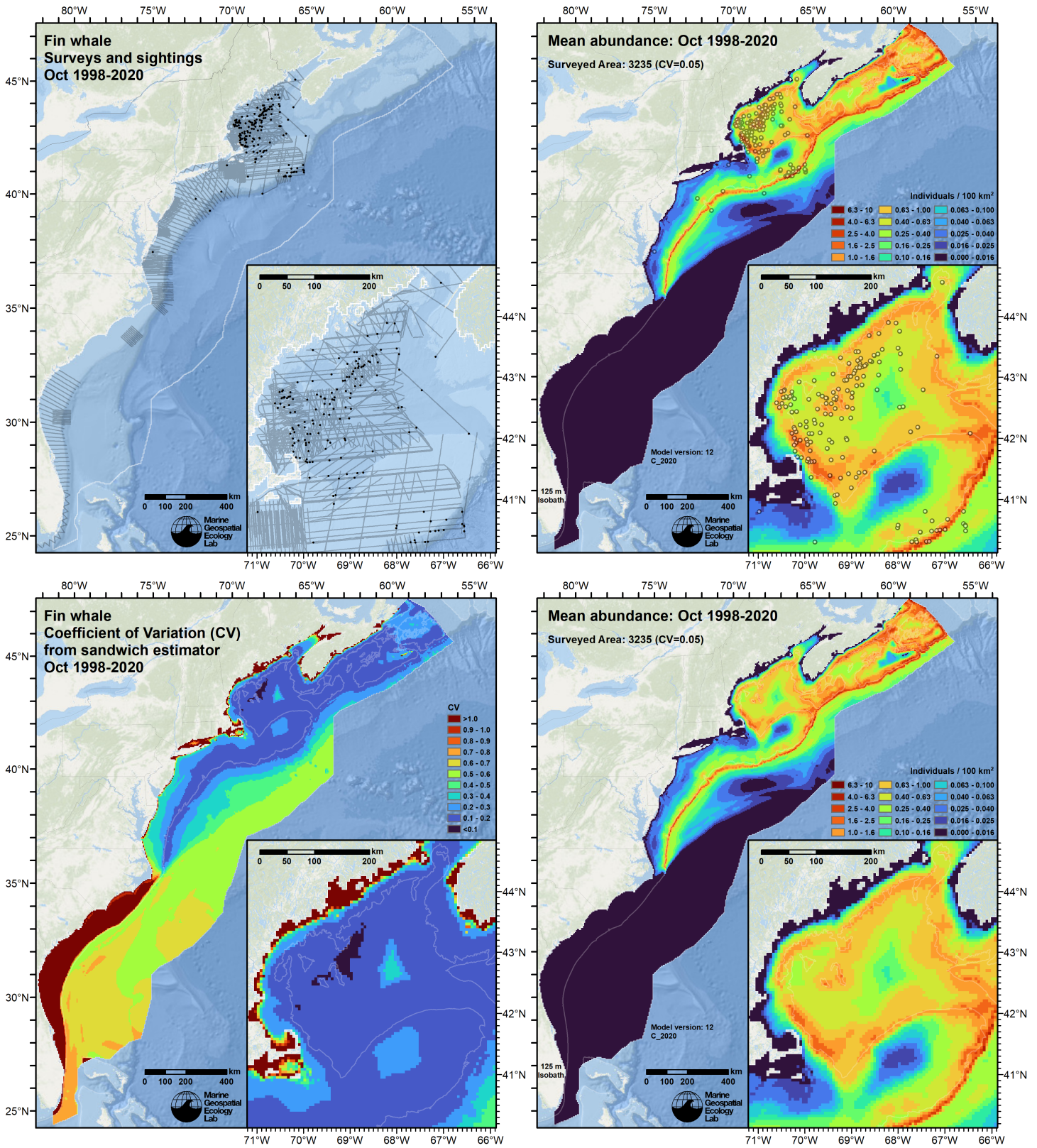


Figure 86: Survey effort and observations (top left), predicted density with observations (top right), predicted density without observations (bottom right), and coefficient of variation of predicted density (bottom left), for the month of October for the given era. Variance was estimated with the analytic approach given by Miller et al. (2022), Appendix S1, and accounts both for uncertainty in model parameter estimates and for temporal variability in dynamic covariates.



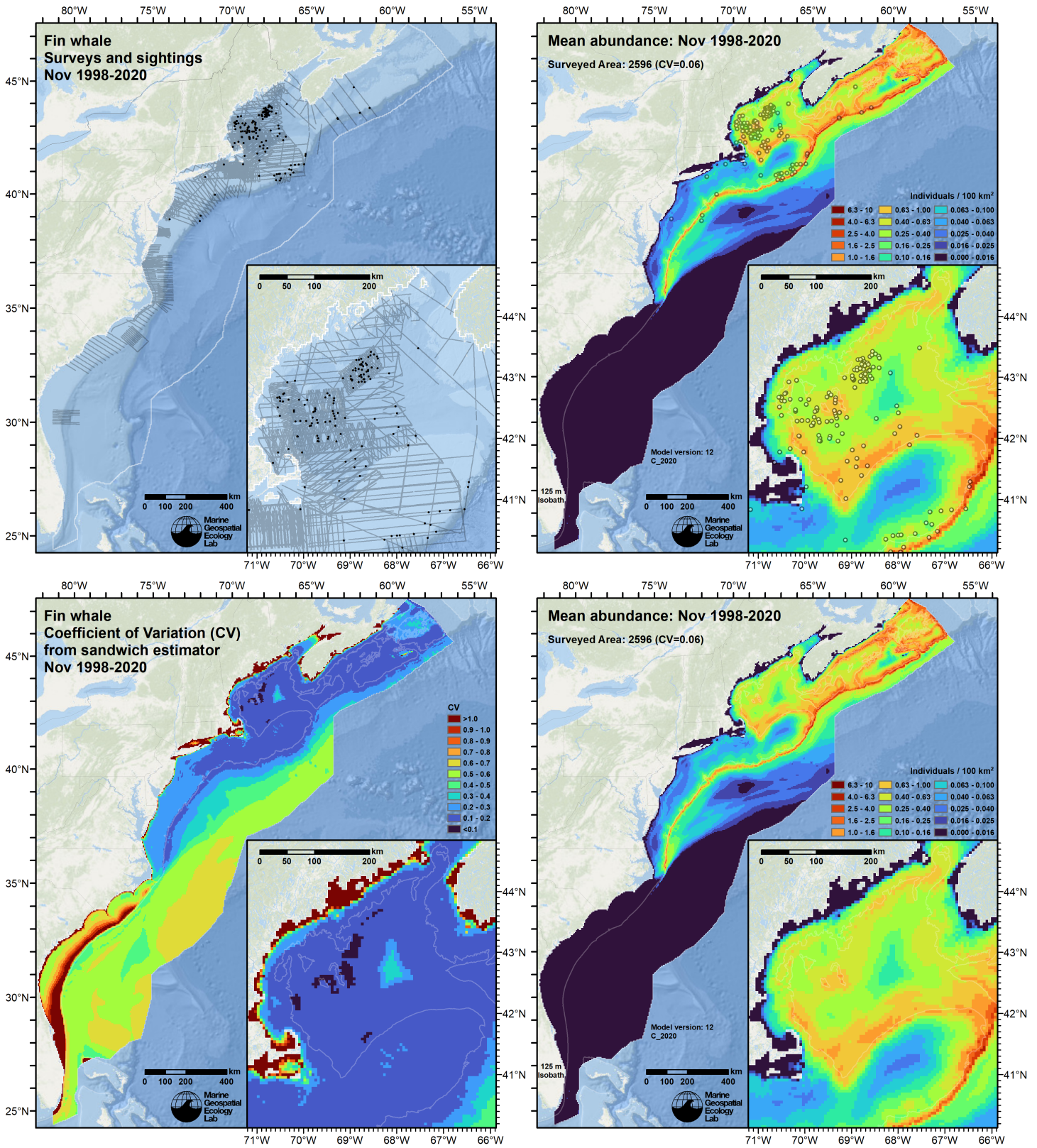


Figure 87: Survey effort and observations (top left), predicted density with observations (top right), predicted density without observations (bottom right), and coefficient of variation of predicted density (bottom left), for the month of November for the given era. Variance was estimated with the analytic approach given by Miller et al. (2022), Appendix S1, and accounts both for uncertainty in model parameter estimates and for temporal variability in dynamic covariates.



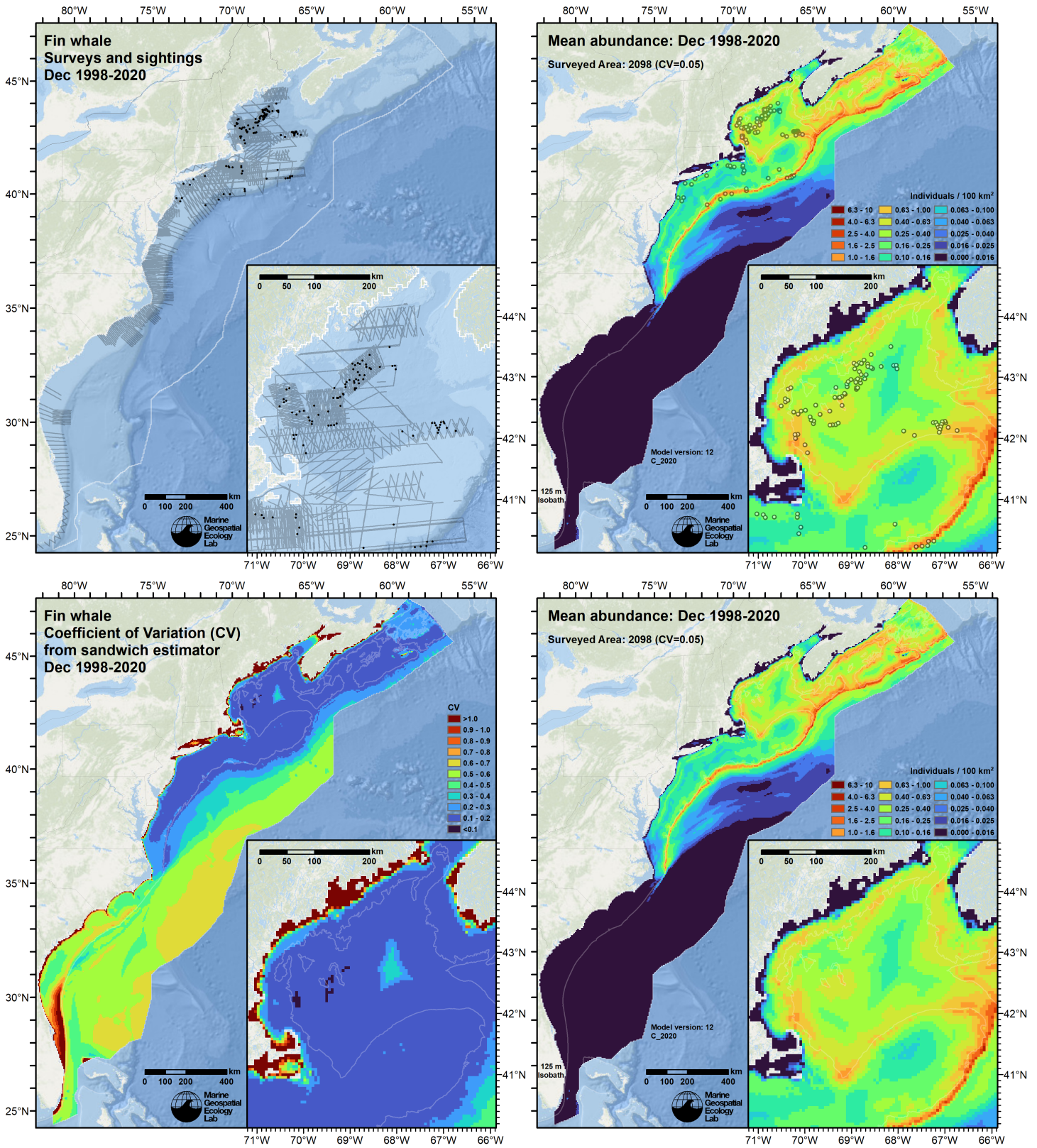


Figure 88: Survey effort and observations (top left), predicted density with observations (top right), predicted density without observations (bottom right), and coefficient of variation of predicted density (bottom left), for the month of December for the given era. Variance was estimated with the analytic approach given by Miller et al. (2022), Appendix S1, and accounts both for uncertainty in model parameter estimates and for temporal variability in dynamic covariates.

## 6.2 Abundance Comparisons

### 6.2.1 NOAA Stock Assessment Reports

Table 27: Comparison of regional abundance estimates from the 2021 NOAA Stock Assessment Report (SAR) (Hayes et al. (2022)) to estimates from this density model extracted from roughly comparable zones (Figure 89 below). The SAR estimates were based on a single year of surveying, while the model estimates were taken from the multi-year mean density surfaces we provide to model users (Section 6.1).

2021 Stock Assessment Report			Density Model		
Month/Year	Area	$N_{est}$	Period	Zone	Abundance
Jun-Sep 2016	Florida to lower Bay of Fundy <sup>a</sup>	2,390	Jun-Sep 1998-2020	NEFSC+SEFSC	1,525
Aug-Sep 2016	Bay of Fundy/Scotian Shelf <sup>b</sup>	2,235	Jun-Sep 1998-2020	Canada	2,431
Jun-Sep 2016	Total	4,625	Jun-Sep 1998-2020	Total	3,956

<sup>a</sup> The SAR combined the NEFSC zone, which had an estimate of 2390 by Palka (2020), and the SEFSC zone, which had an estimate of 0 by Garrison (2020). The latter actually made three fin whale sightings, but two were off effort and the third was truncated during detection modeling.

<sup>b</sup> Estimate originally from Lawson and Gosselin (2018).

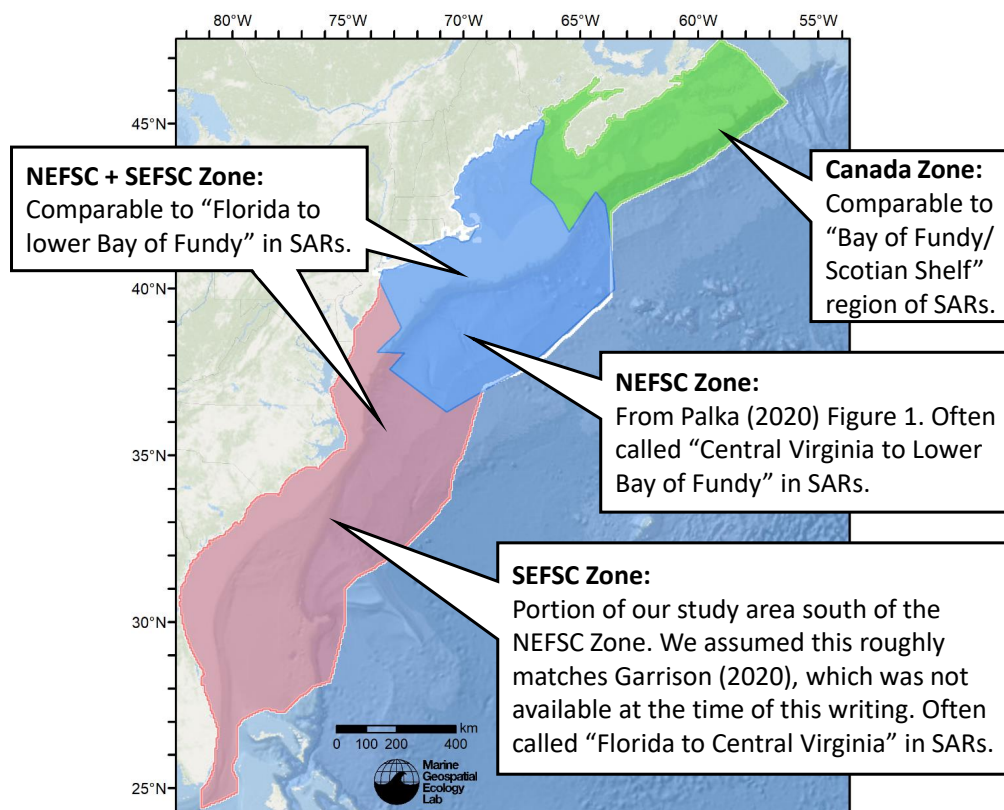


Figure 89: Zones for which we extracted abundance estimates from the density model for comparison to estimates from the NOAA Stock Assessment Report.



## 6.2.2 Previous Density Model

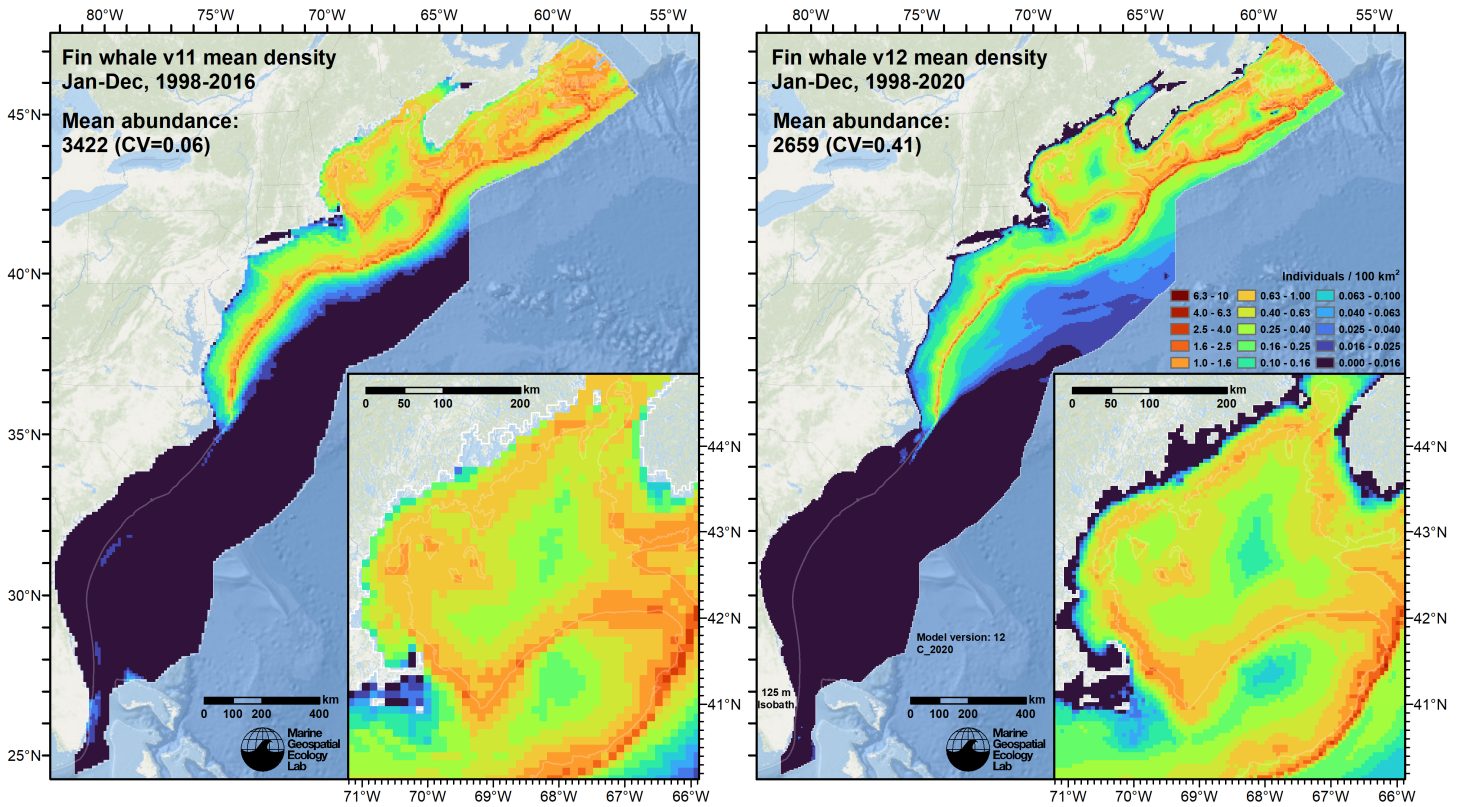


Figure 90: Comparison of the mean density predictions from the previous model (left) released by Roberts et al. (2018) to those from this model (right).

## 6.3 Comparison to Passive Acoustic Monitoring

To facilitate qualitative comparison of passive acoustic monitoring (PAM) detections to visual sightings and density predictions, we overlaid PAM results from Davis et al. (2020) on maps of visual segments and sightings and of density predictions. In each figure below, red circles and white dots represent PAM stations. White dots indicate that at that station, there were no days in which Davis et al. determined the species was acoustically present. Red circles indicate that the species was acoustically present, with the size of the circle indicating the percentage of days of the month it was present. The maps underlying the acoustic data are the effort segments and sightings (left side) used to fit the model, and the mean density prediction (right side), for the given month.

Note that each PAM station was usually only deployed for one of the years in the range listed. If a deployment was repeated in a subsequent year, it was treated as a separate station and allocated its own symbol. At such locations, the map may contain several different symbols, such as a white dot inside a red circle, or several red circles of different sizes, indicating interannual variability in acoustic presence at that location. Because both visual and acoustic surveys were very patchy across time, with multi-year coverage only occurring in a small number of specific areas, we urge caution in drawing firm conclusions about the species' distribution from the points and circles without considering the degree of interannual replication in coverage.

We gratefully acknowledge G. Davis and coauthors for making these data available for this comparison.

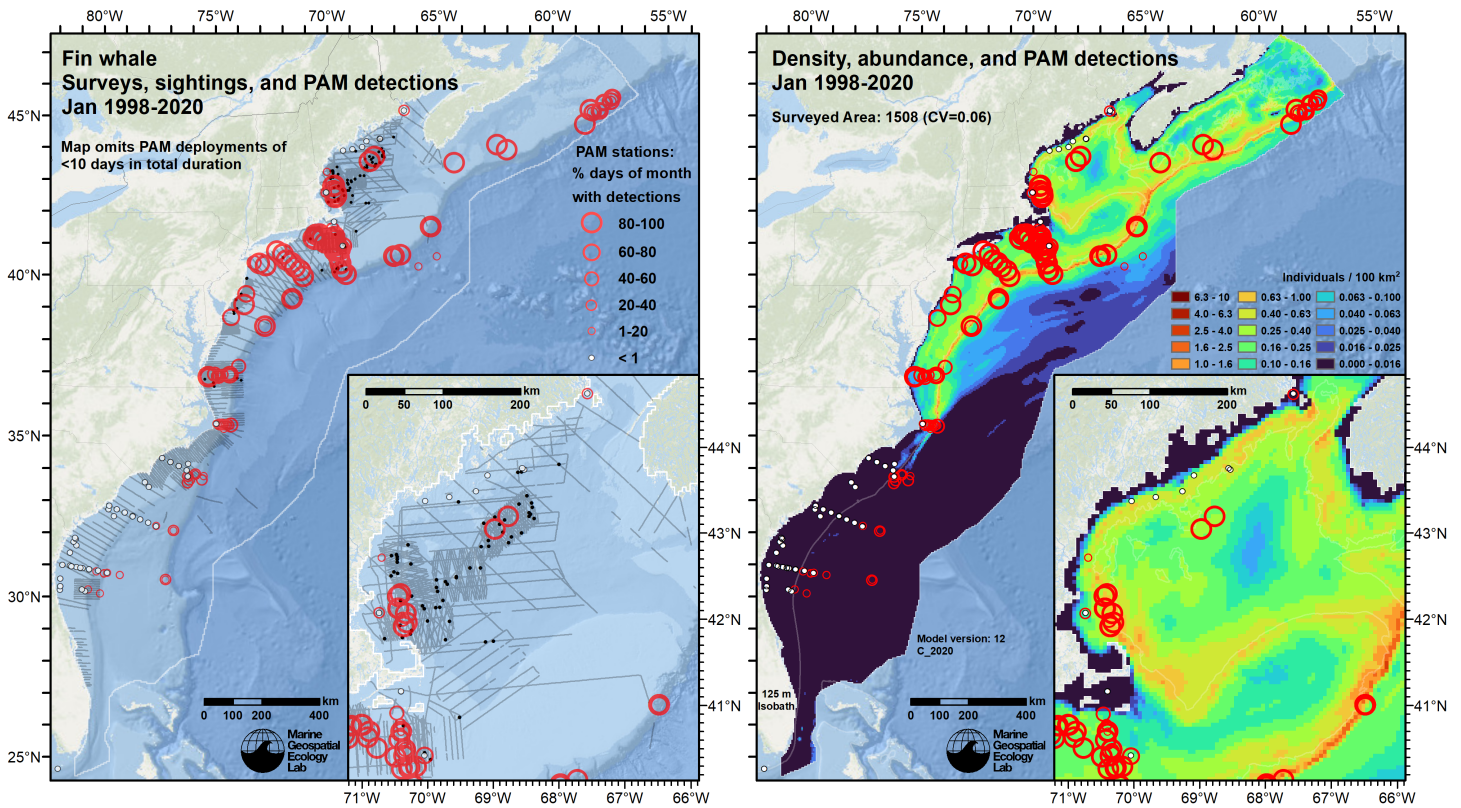


Figure 91: Passive acoustic monitoring stations (red circles and white dots) symbolized by detection rate, overlaid on visual segments and sightings (left) and predicted density (right), for the month of January for the given era.

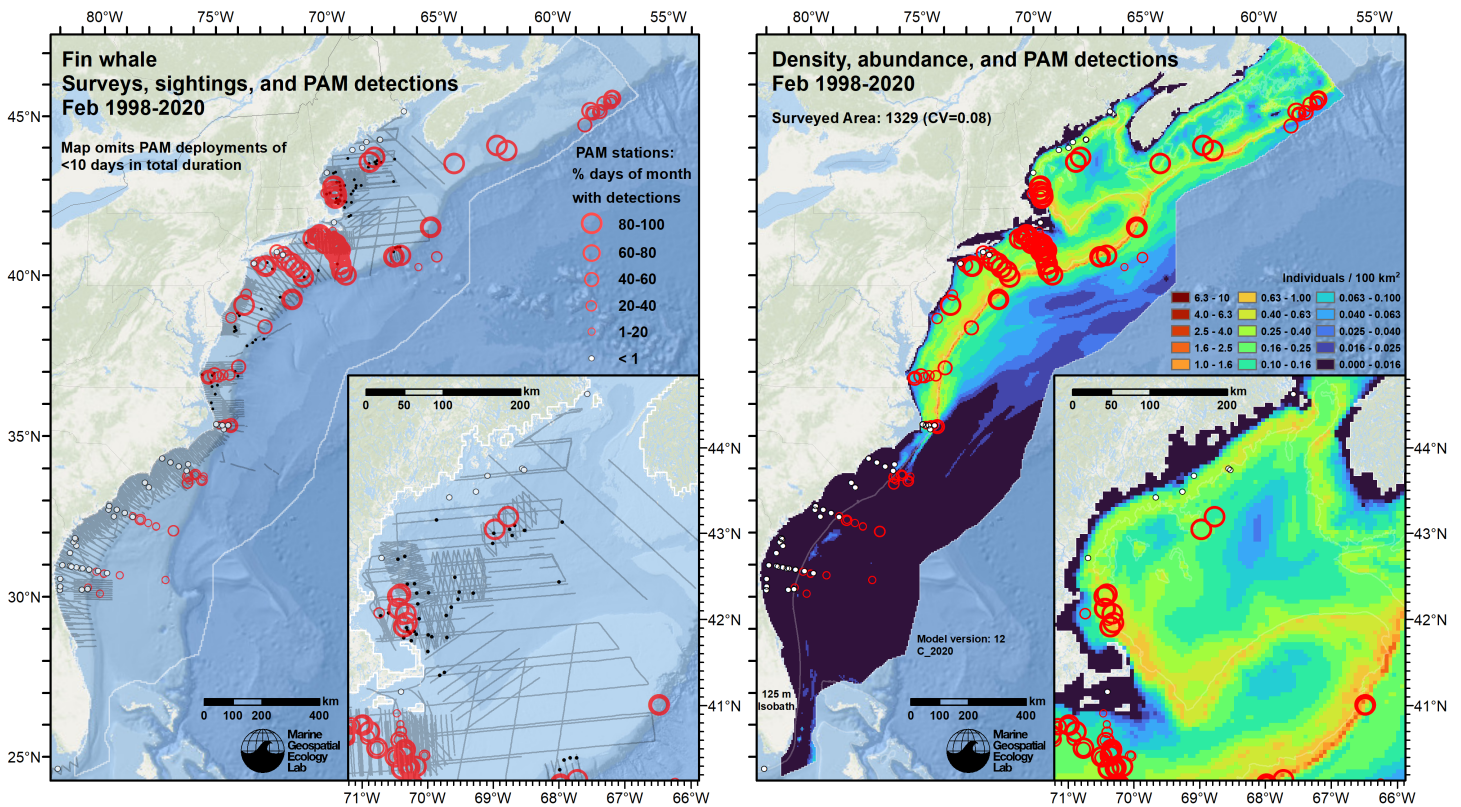


Figure 92: Passive acoustic monitoring stations (red circles and white dots) symbolized by detection rate, overlaid on visual segments and sightings (left) and predicted density (right), for the month of February for the given era.



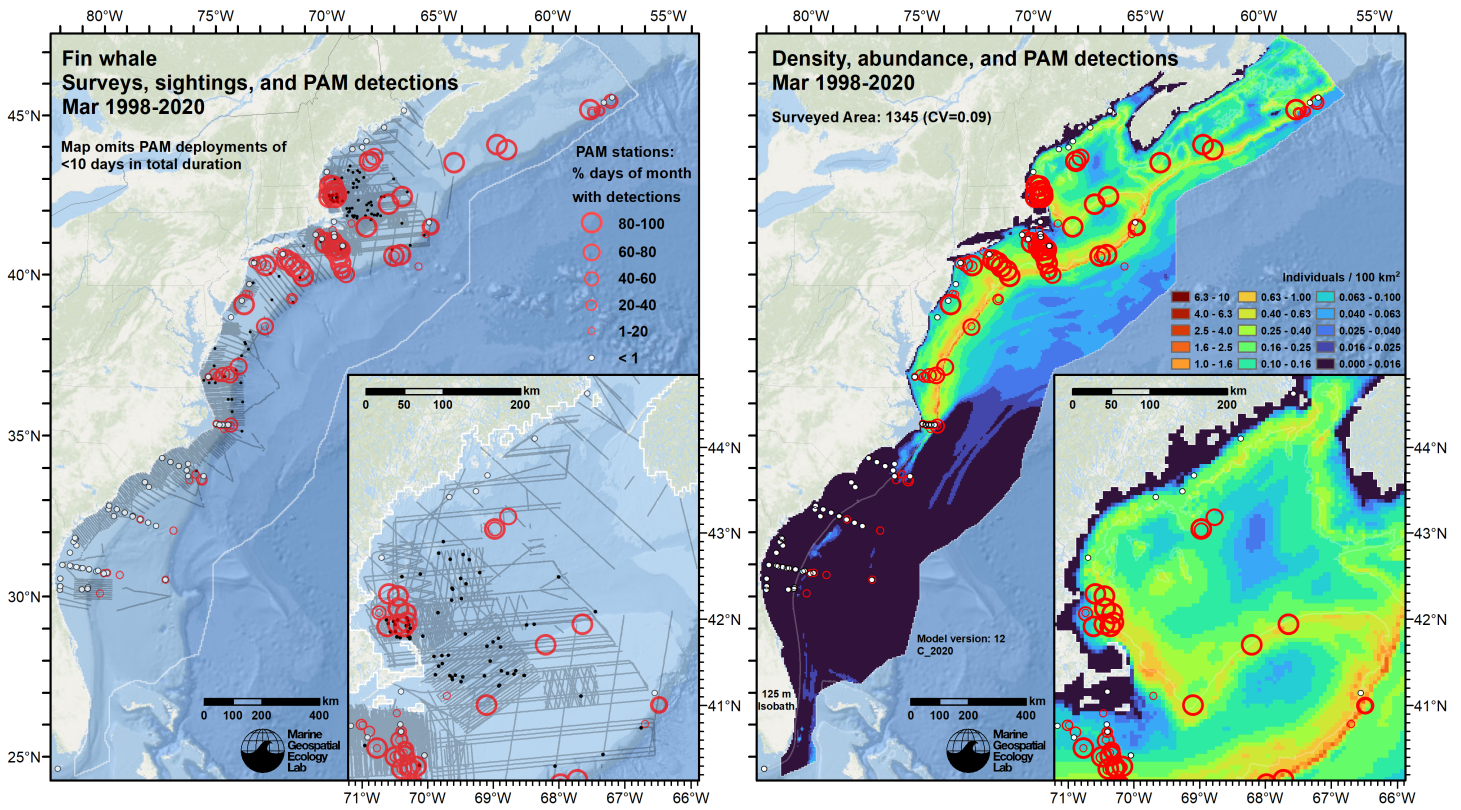


Figure 93: Passive acoustic monitoring stations (red circles and white dots) symbolized by detection rate, overlaid on visual segments and sightings (left) and predicted density (right), for the month of March for the given era.

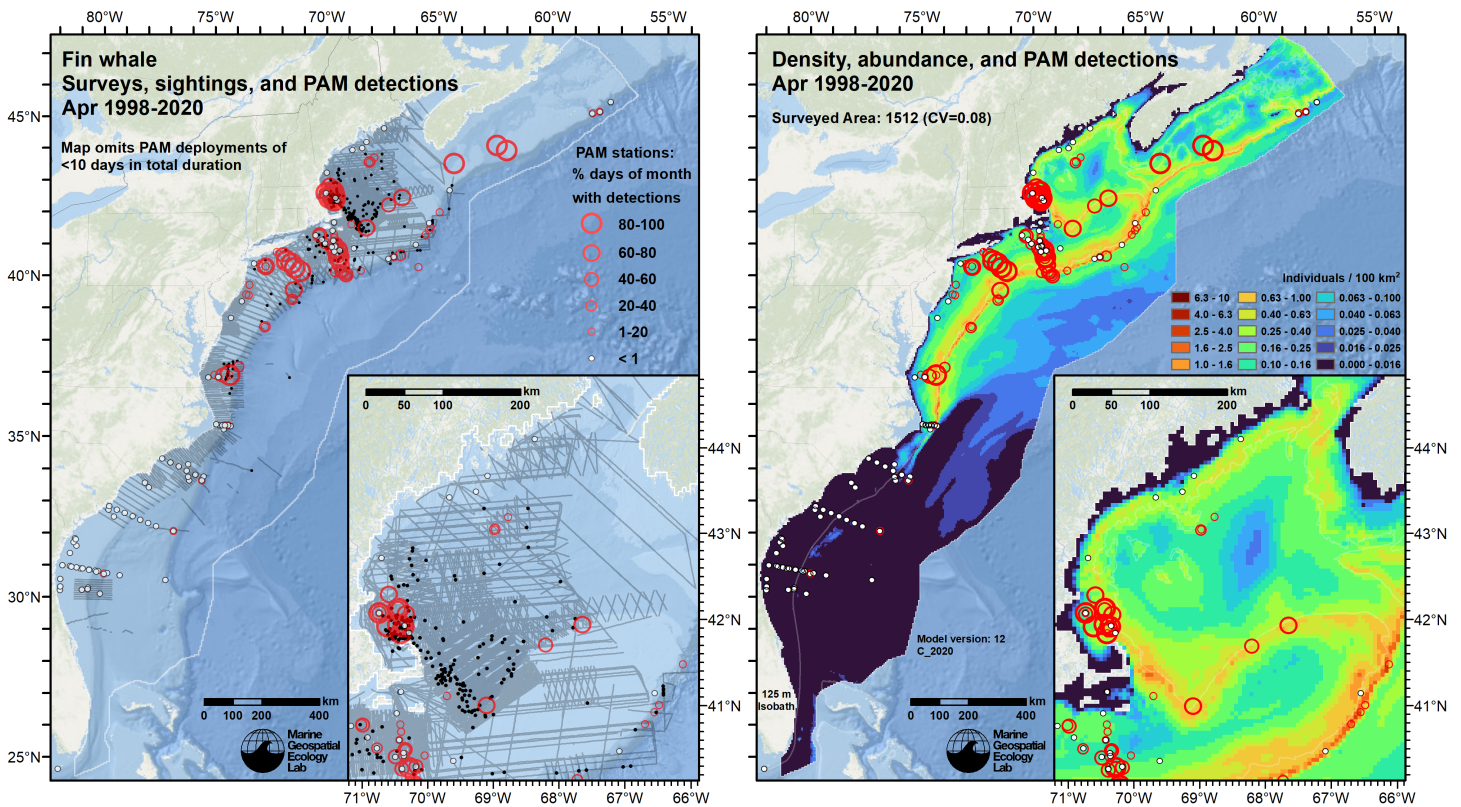


Figure 94: Passive acoustic monitoring stations (red circles and white dots) symbolized by detection rate, overlaid on visual segments and sightings (left) and predicted density (right), for the month of April for the given era.



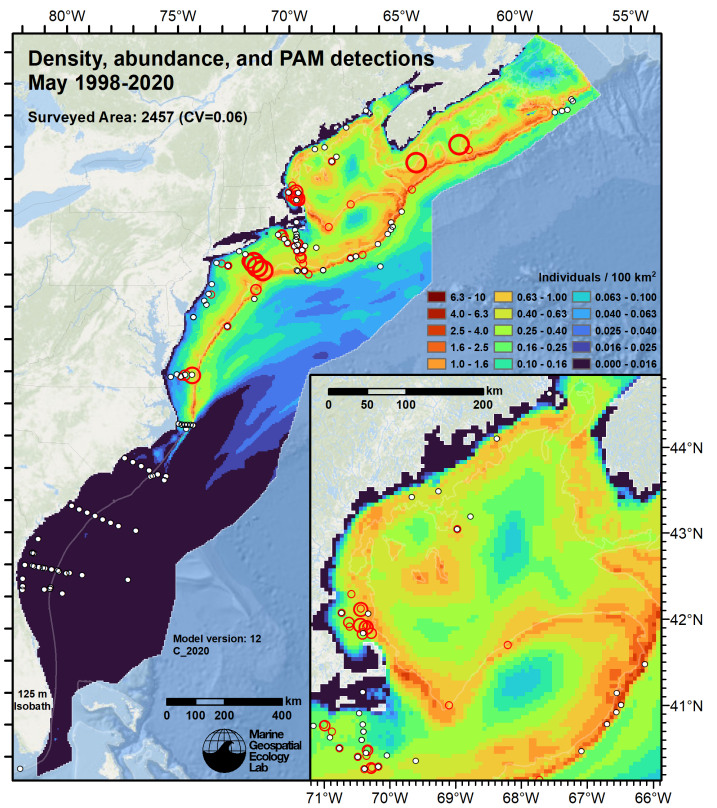
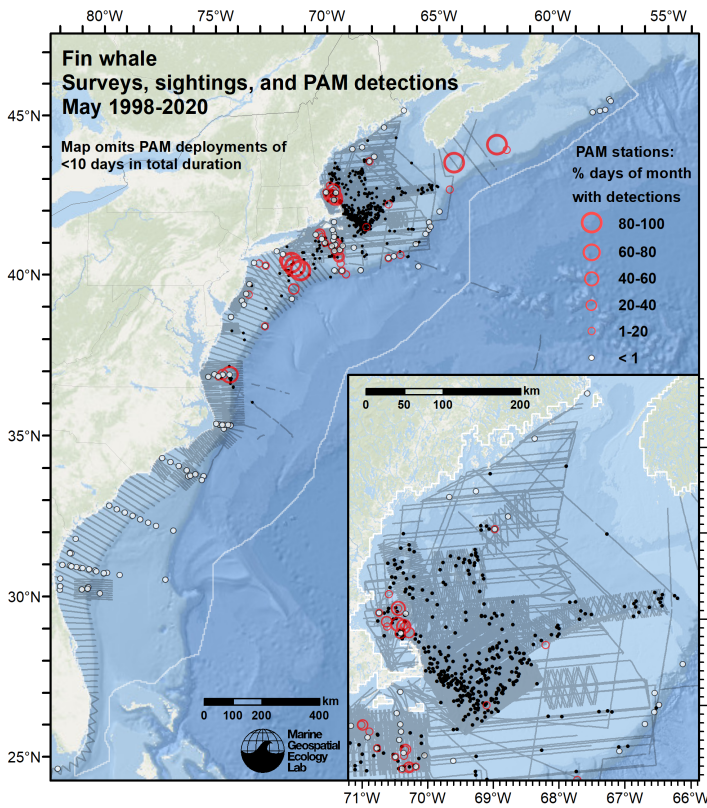


Figure 95: Passive acoustic monitoring stations (red circles and white dots) symbolized by detection rate, overlaid on visual segments and sightings (left) and predicted density (right), for the month of May for the given era.

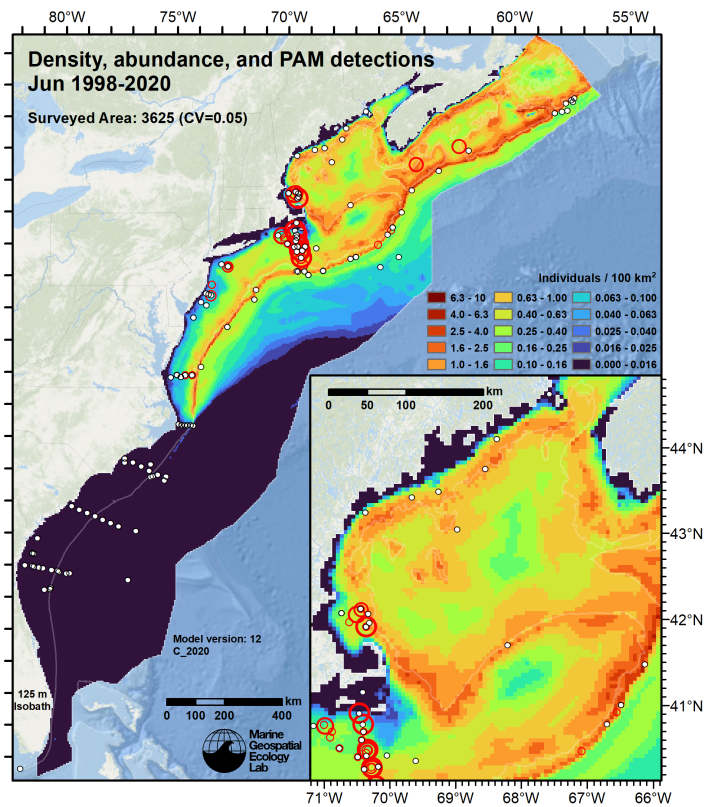
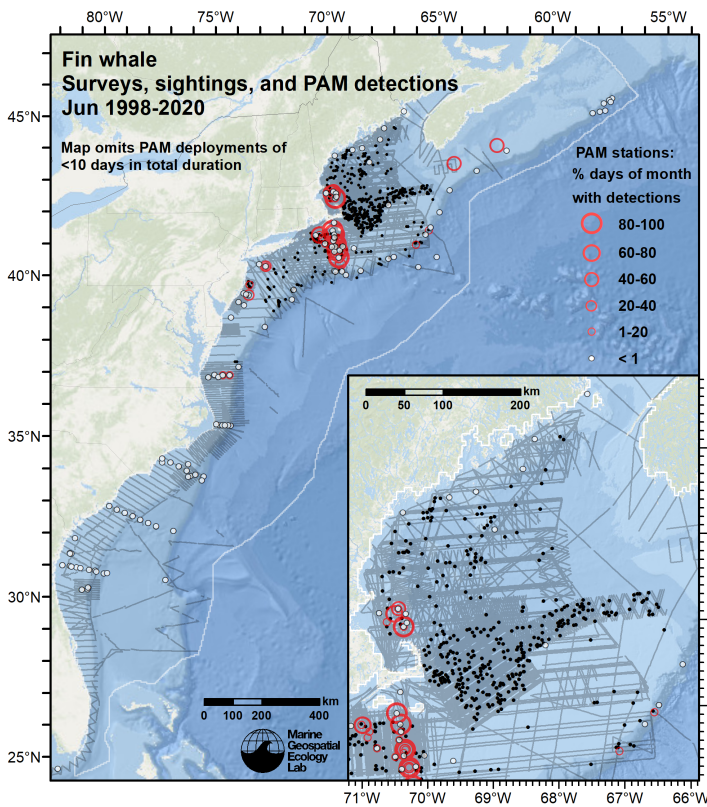


Figure 96: Passive acoustic monitoring stations (red circles and white dots) symbolized by detection rate, overlaid on visual segments and sightings (left) and predicted density (right), for the month of June for the given era.



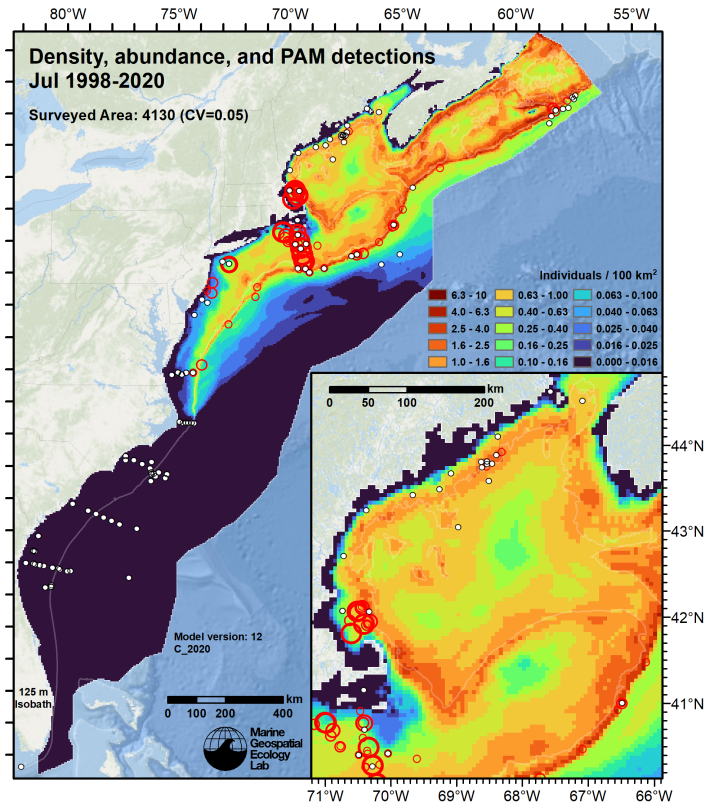
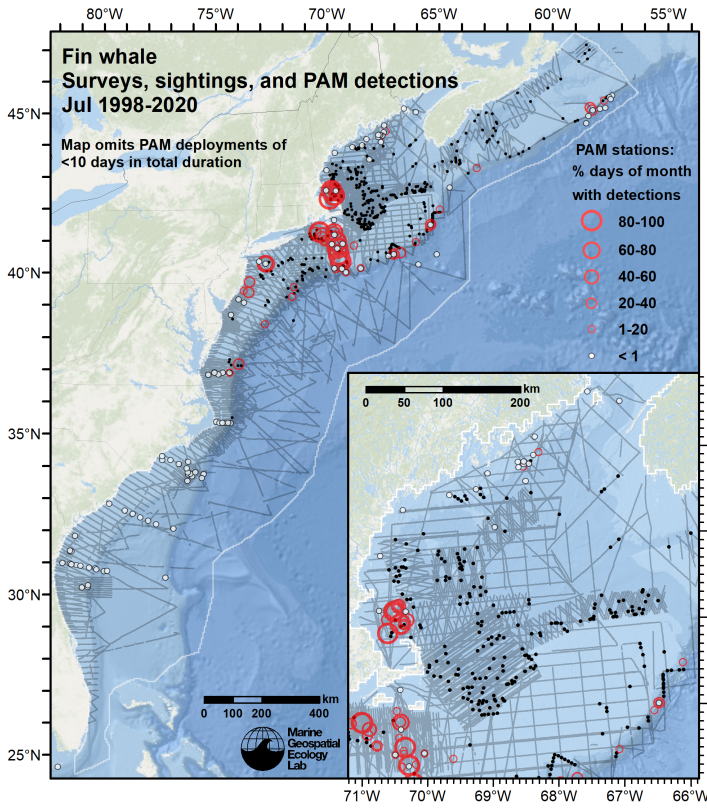


Figure 97: Passive acoustic monitoring stations (red circles and white dots) symbolized by detection rate, overlaid on visual segments and sightings (left) and predicted density (right), for the month of July for the given era.

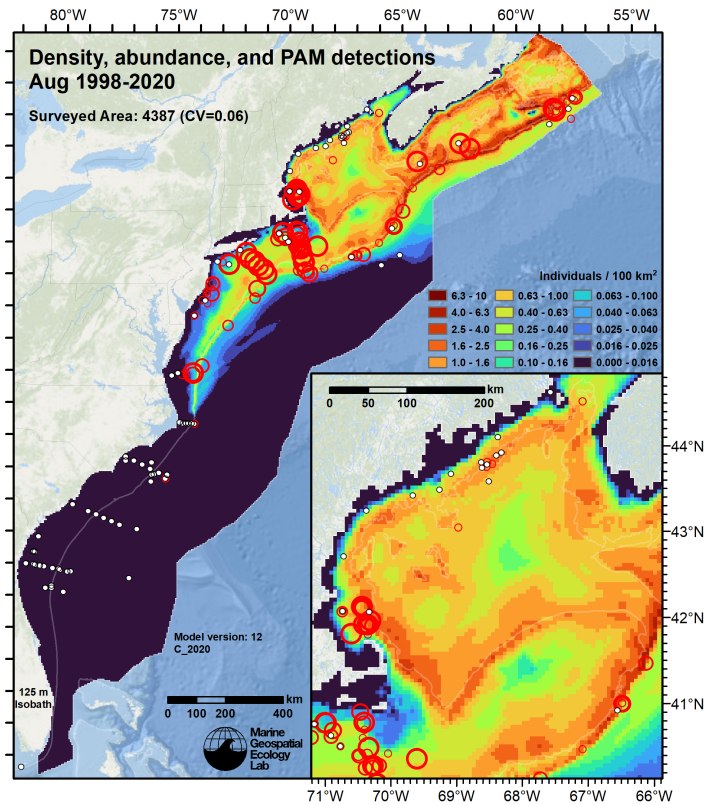
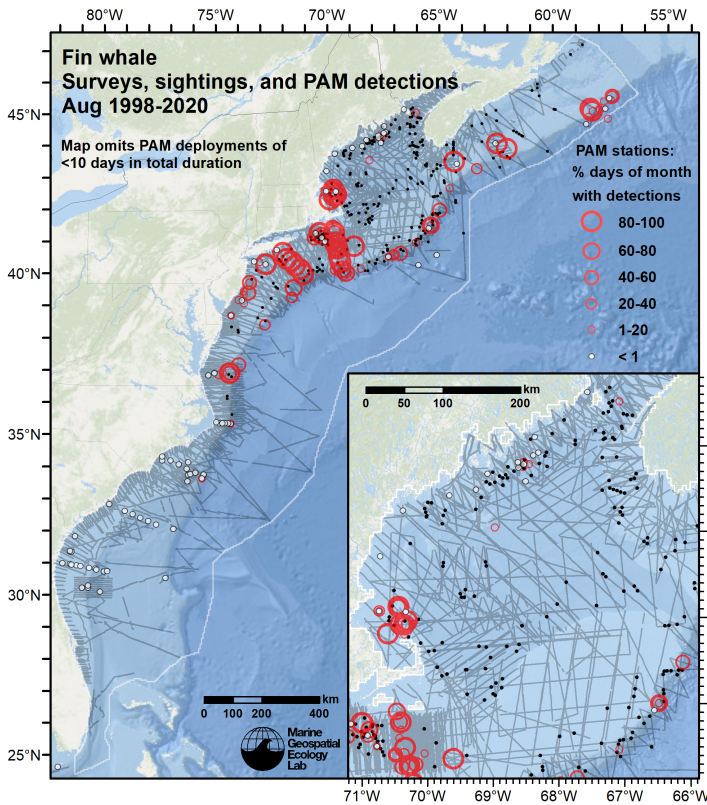


Figure 98: Passive acoustic monitoring stations (red circles and white dots) symbolized by detection rate, overlaid on visual segments and sightings (left) and predicted density (right), for the month of August for the given era.



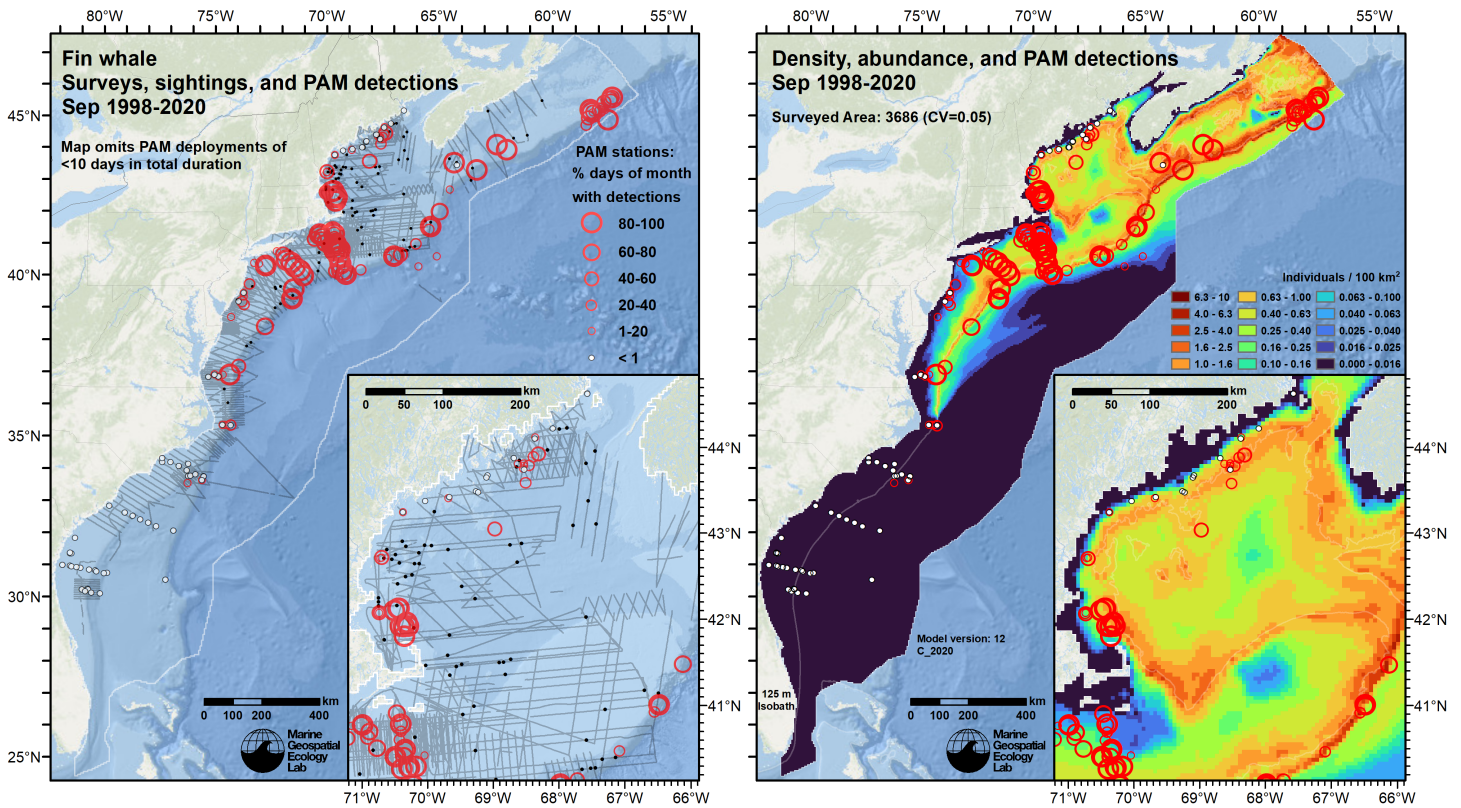


Figure 99: Passive acoustic monitoring stations (red circles and white dots) symbolized by detection rate, overlaid on visual segments and sightings (left) and predicted density (right), for the month of September for the given era.

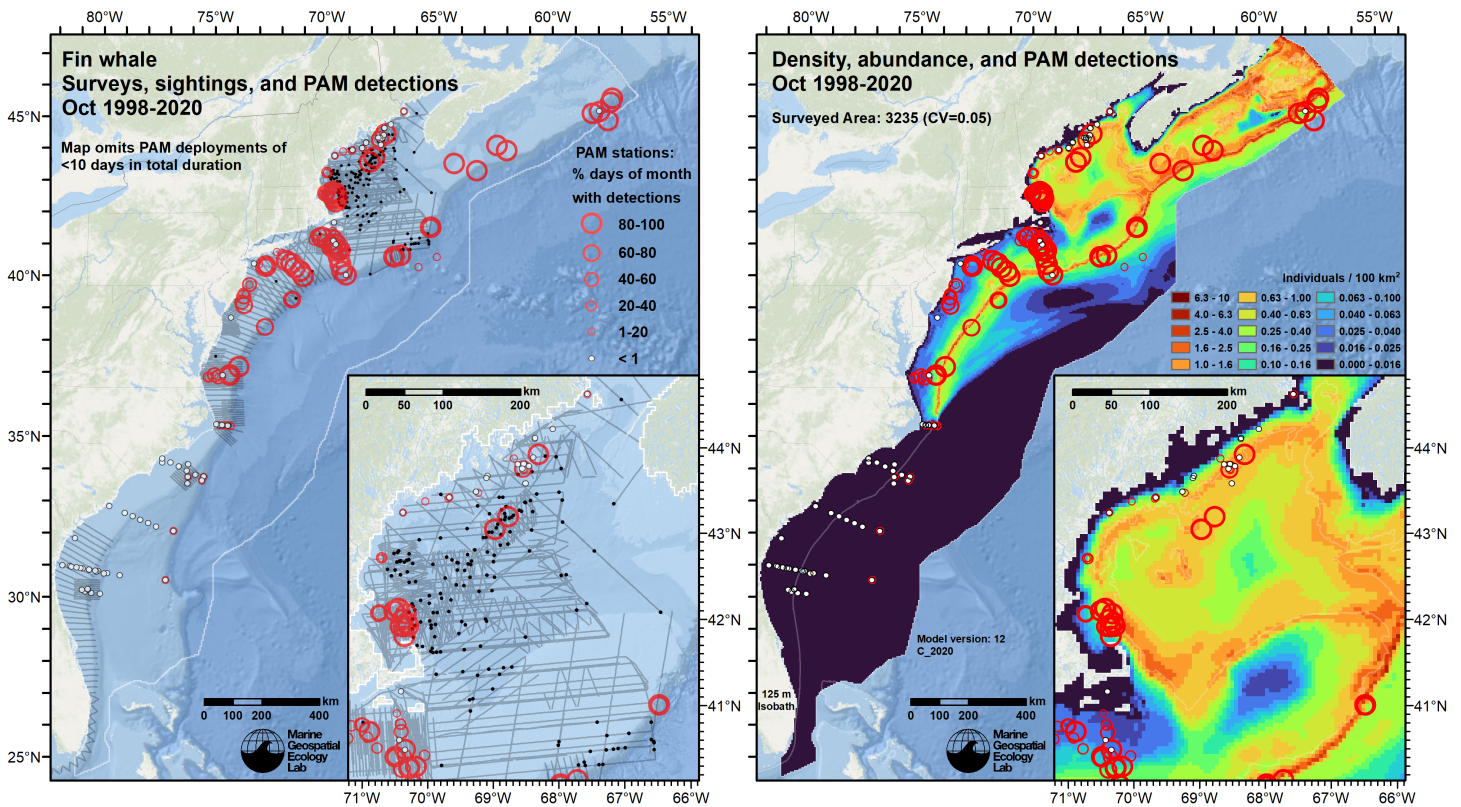


Figure 100: Passive acoustic monitoring stations (red circles and white dots) symbolized by detection rate, overlaid on visual segments and sightings (left) and predicted density (right), for the month of October for the given era.



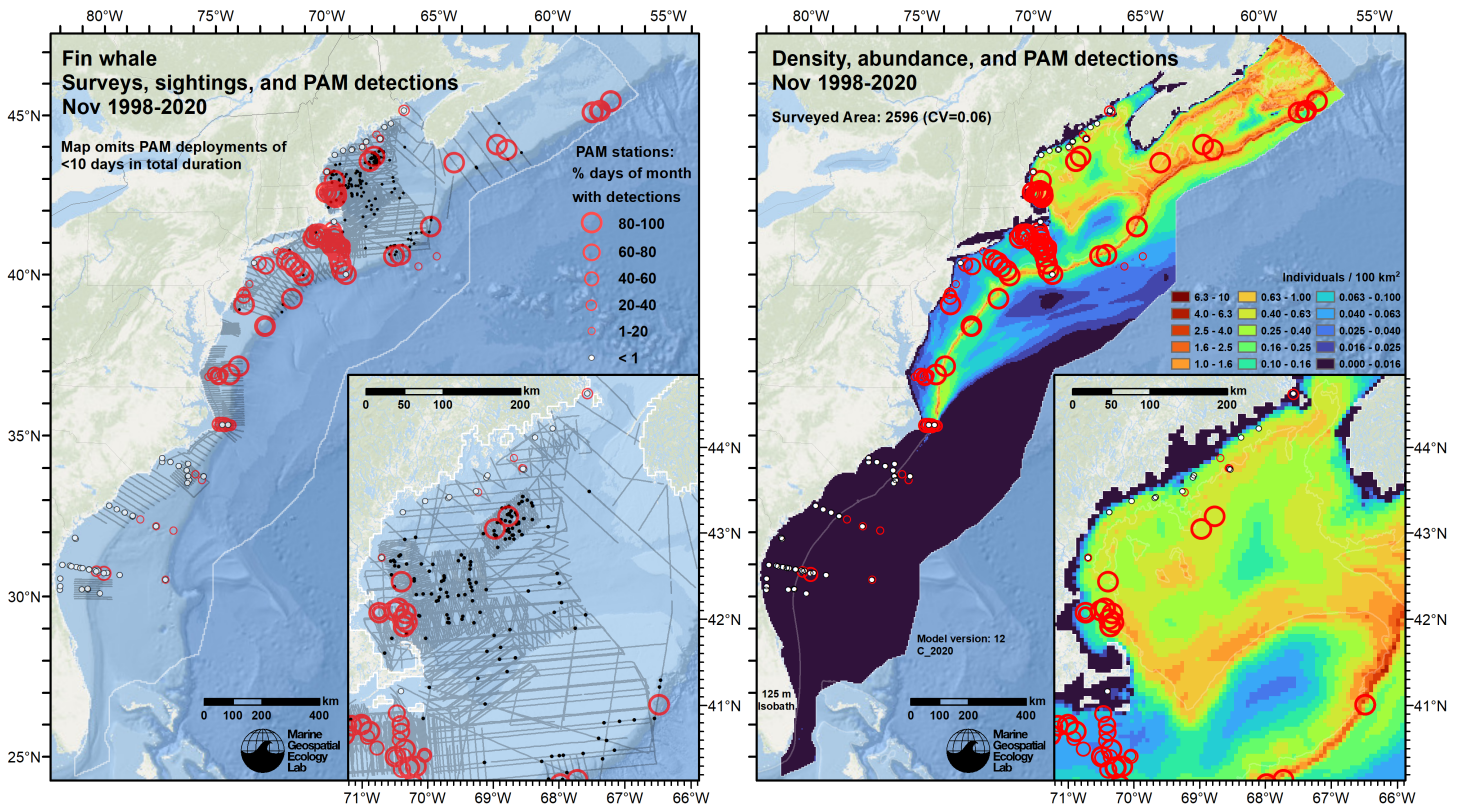


Figure 101: Passive acoustic monitoring stations (red circles and white dots) symbolized by detection rate, overlaid on visual segments and sightings (left) and predicted density (right), for the month of November for the given era.

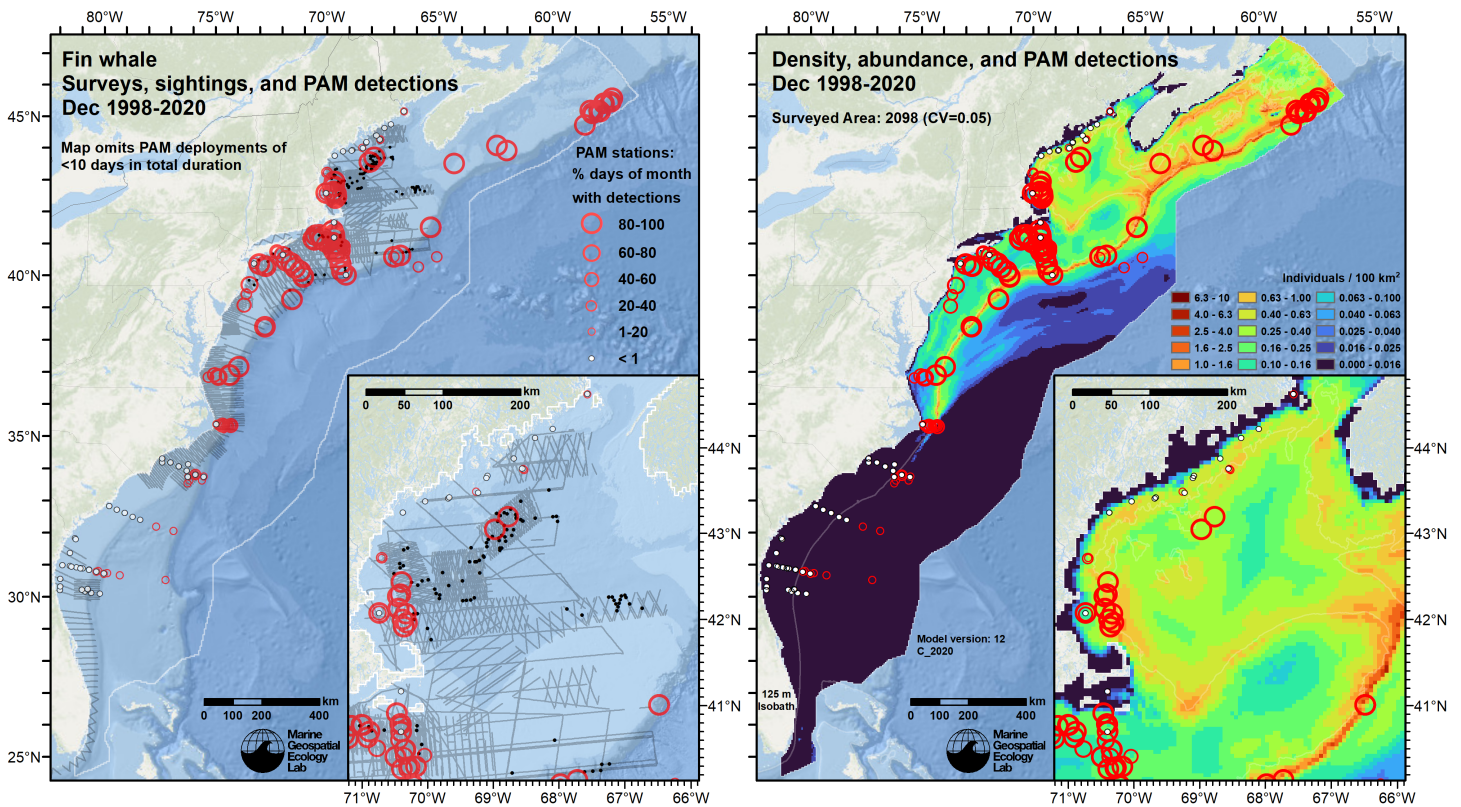


Figure 102: Passive acoustic monitoring stations (red circles and white dots) symbolized by detection rate, overlaid on visual segments and sightings (left) and predicted density (right), for the month of December for the given era.

## 7 Discussion

When summarized across the modeled period (1998-2020), mean monthly density maps (Figures 77-88) broadly agreed with the overall distribution and seasonal pattern described in the literature. The model predicted widespread density across the continental shelf north of Cape Hatteras, with highest densities along the continental shelf break and the deep side of the 125 m isobath, and lowest densities within enclosed inshore areas. Strong seasonal variability was predicted, with abundance ranging from a low in February of about 1329 to a high in August of 4387 (Figure 76; Table 26), but appreciable density occurring from Cape Hatteras through the Scotian Shelf throughout all months of the year, consistent with the view that some fin whales remain at high latitudes year-round, while others may make short seasonal migrations (Edwards et al. 2015). This year-round presence was supported by similar results reported by recent passive acoustic monitoring studies (Davis et al. 2020; Delarue et al. 2022). Given the general match between the model's predictions and what has been reported in the literature, we elected to offer density predictions for this species at monthly temporal resolution.

The model predicted very low but non-zero density south of Cape Hatteras in December-May. These scattered predictions were supported by occasional acoustic detections reported for these months across the Blake Plateau (Figures 102 and 91-95). Very infrequent acoustic detections were also reported south of Cape Hatteras in August-November (Figures 98-101) but no density was predicted; we therefore urge caution during these months across the Blake Plateau.

The model predicted moderate density in northerly distant off-shelf waters except in summer months, when density was generally restricted to the shelf and shelf-break. This prediction should be considered speculative until more off-shelf surveying can be completed in non-summer months, but is supported by acoustic detections at the New England seamounts (Figures 91-102) and by sightings archived in OBIS-SEAMAP (<https://seamap.env.duke.edu/species/180527>) (Halpin et al. 2009) that were not utilizable in this model.

Our model's estimated abundance for the months of June-September (3,956) was 16% lower than that (4,625) of the most recent NOAA Stock Assessment Report (Table 27). Our model's year-round abundance (2,659) was 22% lower than that (3,422) of our prior model (Figure 90). This latter difference was mainly attributable to lower densities close to shore, which we consider an improvement in model accuracy, and to a focusing of density more closely along the shelf break and 125 m isobath. Our prior model predicted near zero density in distant off-shelf waters; we consider the new model's prediction of non-zero density there to be an improvement, but speculative.

Finally, we note that the prior model's CV of mean abundance (0.06) was substantially lower than that (0.41) of the new model. The CV of the prior model was unrealistically low because that model only accounted for uncertainty in model parameter estimates, while the new model also accounts for seasonal variability in predictions. However, because the new model utilized climatological covariates, which provided better goodness of fit than contemporaneous covariates, the new model's uncertainty statistics do not account for interannual variability.

## References

- Barco SG, Burt L, DePerte A, Digiovanni R Jr. (2015) Marine Mammal and Sea Turtle Sightings in the Vicinity of the Maryland Wind Energy Area July 2013-June 2015, VAQF Scientific Report #2015-06. Virginia Aquarium & Marine Science Center Foundation, Virginia Beach, VA
- Becker JJ, Sandwell DT, Smith WHF, Braud J, Binder B, Depner J, Fabre D, Factor J, Ingalls S, Kim S-H, Ladner R, Marks K, Nelson S, Pharaoh A, Trimmer R, Von Rosenberg J, Wallace G, Weatherall P (2009) Global Bathymetry and Elevation Data at 30 Arc Seconds Resolution: SRTM30\_PLUS. *Marine Geodesy* 32:355–371. doi: [10.1080/01490410903297766](https://doi.org/10.1080/01490410903297766)
- Brasnett B (2008) The impact of satellite retrievals in a global sea-surface-temperature analysis. *Quarterly Journal of the Royal Meteorological Society* 134:1745–1760. doi: [10.1002/qj.319](https://doi.org/10.1002/qj.319)
- Breiman L (2001) Random Forests. *Machine Learning* 45:5–32. doi: [10.1023/A:1010933404324](https://doi.org/10.1023/A:1010933404324)
- Buckland ST, Anderson DR, Burnham KP, Laake JL, Borchers DL, Thomas L (2001) *Introduction to Distance Sampling: Estimating Abundance of Biological Populations*. Oxford University Press, Oxford, UK
- Burt ML, Borchers DL, Jenkins KJ, Marques TA (2014) Using mark-recapture distance sampling methods on line transect surveys. *Methods in Ecology and Evolution* 5:1180–1191. doi: [10.1111/2041-210X.12294](https://doi.org/10.1111/2041-210X.12294)
- Canada Meteorological Center (2012) GHRSSST Level 4 CMC0.2deg Global Foundation Sea Surface Temperature Analysis Version 2.0. PODAAC, CA, USA. doi: [10.5067/GHCMC-4FM02](https://doi.org/10.5067/GHCMC-4FM02)
- Canada Meteorological Center (2016) GHRSSST Level 4 CMC0.1deg Global Foundation Sea Surface Temperature Analysis Version 3.0. PODAAC, CA, USA. doi: [10.5067/GHCMC-4FM03](https://doi.org/10.5067/GHCMC-4FM03)



- Cañadas A, Roberts JJ, Yack TM, Halpin PN (2021) Development of Exploratory Marine Species Density Models in the NAVEUR/C6F Study Area. Report prepared for Naval Facilities Engineering Command, Atlantic under Contract No. N62470-15-D-8006, Task Order 18F4048. Duke University Marine Geospatial Ecology Lab, Durham, NC
- Canny JF (1986) A computational approach to edge detection. *IEEE Transactions on Pattern Analysis and Machine Intelligence* 8:679–698. doi: [10.1016/B978-0-08-051581-6.50024-6](https://doi.org/10.1016/B978-0-08-051581-6.50024-6)
- Chassignet E, Hurlburt H, Metzger EJ, Smedstad O, Cummings J, Halliwell G, Bleck R, Baraille R, Wallcraft A, Lozano C, Tolman H, Srinivasan A, Hankin S, Cornillon P, Weisberg R, Barth A, He R, Werner F, Wilkin J (2009) US GODAE: Global Ocean Prediction with the HYbrid Coordinate Ocean Model (HYCOM). *Oceanog* 22:64–75. doi: [10.5670/oceanog.2009.39](https://doi.org/10.5670/oceanog.2009.39)
- Cole T, Gerrior P, Merrick RL (2007) [Methodologies of the NOAA National Marine Fisheries Service Aerial Survey Program for Right Whales \(\*Eubalaena glacialis\*\) in the Northeast U.S., 1998–2006](#). U.S. Department of Commerce, Woods Hole, MA
- Cotter MP (2019) Aerial Surveys for Protected Marine Species in the Norfolk Canyon Region: 2018–2019 Final Report. HDR, Inc., Virginia Beach, VA
- Davis GE, Baumgartner MF, Corkeron PJ, Bell J, Berchok C, Bonnell JM, Bort Thornton J, Brault S, Buchanan GA, Cholewiak DM, Clark CW, Delarue J, Hatch LT, Klinck H, Kraus SD, Martin B, Mellinger DK, Moors-Murphy H, Nieukirk S, Nowacek DP, Parks SE, Parry D, Pegg N, Read AJ, Rice AN, Risch D, Scott A, Soldevilla MS, Stafford KM, Stanistreet JE, Summers E, Todd S, Van Parijs SM (2020) Exploring movement patterns and changing distributions of baleen whales in the western North Atlantic using a decade of passive acoustic data. *Glob Change Biol* gcb.15191. doi: [10.1111/gcb.15191](https://doi.org/10.1111/gcb.15191)
- Delarue JJ-Y, Moors-Murphy H, Kowarski KA, Davis GE, Urazghildiiev IR, Martin SB (2022) Acoustic occurrence of baleen whales, particularly blue, fin, and humpback whales, off eastern Canada, 2015–2017. *Endang Species Res* 47:265–289. doi: [10.3354/esr01176](https://doi.org/10.3354/esr01176)
- Edwards EF, Hall C, Moore TJ, Sheredy C, Redfern JV (2015) Global distribution of fin whales *Balaenoptera physalus* in the post-whaling era (1980–2012). *Mammal Review* 45:197–214. doi: [10.1111/mam.12048](https://doi.org/10.1111/mam.12048)
- Foley HJ, Paxton CGM, McAlarney RJ, Pabst DA, Read AJ (2019) Occurrence, Distribution, and Density of Protected Species in the Jacksonville, Florida, Atlantic Fleet Training and Testing (AFTT) Study Area. Duke University Marine Lab, Beaufort, NC
- Garnesson P, Mangin A, Fanton d’Andon O, Demaria J, Bretagnon M (2019) The CMEMS GlobColour chlorophyll *a* product based on satellite observation: Multi-sensor merging and flagging strategies. *Ocean Science* 15:819–830. doi: [10.5194/os-15-819-2019](https://doi.org/10.5194/os-15-819-2019)
- Garrison LP (2020) [Abundance of cetaceans along the southeast U.S. East coast from a summer 2016 vessel survey. PRD Contribution # PRD-2020-04](#). NOAA National Marine Fisheries Service, Southeast Fisheries Science Center, Miami, FL
- Garrison LP, Martinez A, Maze-Foley K (2010) [Habitat and abundance of cetaceans in Atlantic Ocean continental slope waters off the eastern USA](#). *Journal of Cetacean Research and Management* 11:267–277.
- Geo-Marine, Inc. (2010) [New Jersey Department of Environmental Protection Baseline Studies Final Report Volume III: Marine Mammal and Sea Turtle Studies](#). Geo-Marine, Inc., Plano, TX
- Hain JH, Ratnaswamy MJ, Kenney RD, Winn HE (1992) The fin whale, *Balaenoptera physalus*, in waters of the northeastern United States continental shelf. *Reports of the International Whaling Commission* 42:653–669.
- Halpin P, Read A, Fujioka E, Best B, Donnelly B, Hazen L, Kot C, Urian K, LaBrecque E, Dimatteo A, Cleary J, Good C, Crowder L, Hyrenbach KD (2009) OBIS-SEAMAP: The World Data Center for Marine Mammal, Sea Bird, and Sea Turtle Distributions. *Oceanography* 22:104–115. doi: [10.5670/oceanog.2009.42](https://doi.org/10.5670/oceanog.2009.42)
- Hayes SA, Josephson E, Maze-Foley K, Rosel PE, Wallace J, Brossard A, Chavez-Rosales S, Cole TVN, Garrison LP, Hatch J, Henry A, Horstman SC, Litz J, Lyssikatos MC, Mullin KD, Murray K, Orphanides C, Ortega-Ortiz J, Pace RM, Palka DL, Powell J, Rappucci G, Soldevilla M, Wenzel FW (2022) [US Atlantic and Gulf of Mexico Marine Mammal Stock Assessments 2021](#). NOAA National Marine Fisheries Service, Northeast Fisheries Science Center, Woods Hole, MA
- Hothorn T, Hornik K, Zeileis A (2006) Unbiased Recursive Partitioning: A Conditional Inference Framework. *Journal of Computational and Graphical Statistics* 15:651–674. doi: [10.1198/106186006X133933](https://doi.org/10.1198/106186006X133933)
- Kowarski KA, Martin SB, Maxner EE, Lawrence CB, Delarue JJ-Y, Miksis-Olds JL (2022) Cetacean acoustic occurrence on the US Atlantic Outer Continental Shelf from 2017 to 2020. *Marine Mammal Science* mms.12962. doi: [10.1111/mms.12962](https://doi.org/10.1111/mms.12962)
- Laake JL, Calambokidis J, Osmek SD, Rugh DJ (1997) Probability of Detecting Harbor Porpoise From Aerial Surveys: Estimating  $g(0)$ . *Journal of Wildlife Management* 61:63–75. doi: [10.2307/3802415](https://doi.org/10.2307/3802415)

- Lawson JW, Gosselin J-F (2018) Estimates of cetacean abundance from the 2016 NAISS aerial surveys of eastern Canadian waters, with a comparison to estimates from the 2007 TNASS. NAMMCO SC/25/AE/09. In: Proceedings of the NAMMCO 25th Scientific Committee (SC). North Atlantic Marine Mammal Commission, Bergen-Tromsø, Norway,
- Lehodey P, Senina I, Murtugudde R (2008) A spatial ecosystem and populations dynamics model (SEAPODYM)–Modeling of tuna and tuna-like populations. *Progress in Oceanography* 78:304–318. doi: [10.1016/j.pocean.2008.06.004](https://doi.org/10.1016/j.pocean.2008.06.004)
- Lehodey P, Conchon A, Senina I, Domokos R, Calmettes B, Jouanno J, Hernandez O, Kloser R (2015) Optimization of a micronekton model with acoustic data. *ICES Journal of Marine Science* 72:1399–1412. doi: [10.1093/icesjms/fsu233](https://doi.org/10.1093/icesjms/fsu233)
- Leiter S, Stone K, Thompson J, Accardo C, Wikgren B, Zani M, Cole T, Kenney R, Mayo C, Kraus S (2017) North Atlantic right whale *Eubalaena glacialis* occurrence in offshore wind energy areas near Massachusetts and Rhode Island, USA. *Endang Species Res* 34:45–59. doi: [10.3354/esr00827](https://doi.org/10.3354/esr00827)
- Mallette SD, Lockhart GG, McAlarney RJ, Cummings EW, McLellan WA, Pabst DA, Barco SG (2014) Documenting Whale Migration off Virginia’s Coast for Use in Marine Spatial Planning: Aerial and Vessel Surveys in the Proximity of the Virginia Wind Energy Area (VA WEA), VAQF Scientific Report 2014-08. Virginia Aquarium & Marine Science Center Foundation, Virginia Beach, VA
- Mallette SD, Lockhart GG, McAlarney RJ, Cummings EW, McLellan WA, Pabst DA, Barco SG (2015) Documenting Whale Migration off Virginia’s Coast for Use in Marine Spatial Planning: Aerial Surveys in the Proximity of the Virginia Wind Energy Area (VA WEA) Survey/Reporting Period: May 2014 - December 2014, VAQF Scientific Report 2015-02. Virginia Aquarium & Marine Science Center Foundation, Virginia Beach, VA
- Mallette SD, McAlarney RJ, Lockhart GG, Cummings EW, Pabst DA, McLellan WA, Barco SG (2017) [Aerial Survey Baseline Monitoring in the Continental Shelf Region of the VACAPES OPAREA: 2016 Annual Progress Report](#). Virginia Aquarium & Marine Science Center Foundation, Virginia Beach, VA
- Marsh H, Sinclair DF (1989) Correcting for Visibility Bias in Strip Transect Aerial Surveys of Aquatic Fauna. *The Journal of Wildlife Management* 53:1017. doi: [10.2307/3809604](https://doi.org/10.2307/3809604)
- McAlarney R, Cummings E, McLellan W, Pabst A (2018) Aerial Surveys for Protected Marine Species in the Norfolk Canyon Region: 2017 Annual Progress Report. University of North Carolina Wilmington, Wilmington, NC
- McLellan WA, McAlarney RJ, Cummings EW, Read AJ, Paxton CGM, Bell JT, Pabst DA (2018) Distribution and abundance of beaked whales (Family Ziphiidae) Off Cape Hatteras, North Carolina, U.S.A. *Marine Mammal Science*. doi: [10.1111/mms.12500](https://doi.org/10.1111/mms.12500)
- Meissner T, Wentz FJ, Scott J, Vazquez-Cuervo J (2016) Sensitivity of Ocean Surface Salinity Measurements From Spaceborne L-Band Radiometers to Ancillary Sea Surface Temperature. *IEEE Trans Geosci Remote Sensing* 54:7105–7111. doi: [10.1109/TGRS.2016.2596100](https://doi.org/10.1109/TGRS.2016.2596100)
- Mesgaran MB, Cousens RD, Webber BL (2014) Here be dragons: A tool for quantifying novelty due to covariate range and correlation change when projecting species distribution models. *Diversity Distrib* 20:1147–1159. doi: [10.1111/ddi.12209](https://doi.org/10.1111/ddi.12209)
- Miller DL, Becker EA, Forney KA, Roberts JJ, Cañadas A, Schick RS (2022) Estimating uncertainty in density surface models. *PeerJ* 10:e13950. doi: [10.7717/peerj.13950](https://doi.org/10.7717/peerj.13950)
- Mullin KD, Fulling GL (2003) [Abundance of cetaceans in the southern U.S. North Atlantic Ocean during summer 1998](#). *Fishery Bulletin* 101:603–613.
- O’Brien O, Pendleton DE, Ganley LC, McKenna KR, Kenney RD, Quintana-Rizzo E, Mayo CA, Kraus SD, Redfern JV (2022) Repatriation of a historical North Atlantic right whale habitat during an era of rapid climate change. *Sci Rep* 12:12407. doi: [10.1038/s41598-022-16200-8](https://doi.org/10.1038/s41598-022-16200-8)
- Palka D (2020) [Cetacean Abundance in the US Northwestern Atlantic Ocean Summer 2016](#). *Northeast Fish Sci Cent Ref Doc. 20-05*. NOAA National Marine Fisheries Service, Northeast Fisheries Science Center, Woods Hole, MA
- Palka D, Aichinger Dias L, Broughton E, Chavez-Rosales S, Cholewiak D, Davis G, DeAngelis A, Garrison L, Haas H, Hatch J, Hyde K, Jech M, Josephson E, Mueller-Brennan L, Orphanides C, Pegg N, Sasso C, Sigourney D, Soldevilla M, Walsh H (2021) [Atlantic Marine Assessment Program for Protected Species: FY15 – FY19 \(OCS Study BOEM 2021-051\)](#). U.S. Department of the Interior, Bureau of Ocean Energy Management, Washington, DC
- Palka DL (2006) [Summer abundance estimates of cetaceans in US North Atlantic navy operating areas \(NEFSC Reference Document 06-03\)](#). U.S. Department of Commerce, Northeast Fisheries Science Center, Woods Hole, MA
- Palka DL, Chavez-Rosales S, Josephson E, Cholewiak D, Haas HL, Garrison L, Jones M, Sigourney D, Waring G, Jech M, Broughton E, Soldevilla M, Davis G, DeAngelis A, Sasso CR, Winton MV, Smolowitz RJ, Fay G, LaBrecque E, Leiness JB, Dettloff K, Warden M, Murray K, Orphanides C (2017) [Atlantic Marine Assessment Program for Protected Species:](#)



- 2010-2014 (OCS Study BOEM 2017-071). U.S. Department of the Interior, Bureau of Ocean Energy Management, Washington, DC
- Perkins NJ, Schisterman EF (2006) The Inconsistency of "Optimal" Cutpoints Obtained using Two Criteria based on the Receiver Operating Characteristic Curve. *American Journal of Epidemiology* 670–675.
- Quintana-Rizzo E, Leiter S, Cole T, Hagbloom M, Knowlton A, Nagelkirk P, O'Brien O, Khan C, Henry A, Duley P, Crowe L, Mayo C, Kraus S (2021) Residency, demographics, and movement patterns of North Atlantic right whales *Eubalaena glacialis* in an offshore wind energy development area in southern New England, USA. *Endang Species Res* 45:251–268. doi: [10.3354/esr01137](https://doi.org/10.3354/esr01137)
- Read AJ, Barco S, Bell J, Borchers DL, Burt ML, Cummings EW, Dunn J, Fougères EM, Hazen L, Hodge LEW, Laura A-M, McAlarney RJ, Peter N, Pabst DA, Paxton CGM, Schneider SZ, Urian KW, Waples DM, McLellan WA (2014) [Occurrence, distribution and abundance of cetaceans in Onslow Bay, North Carolina, USA](#). *Journal of Cetacean Research and Management* 14:23–35.
- Redfern JV, Kryc KA, Weiss L, Hodge BC, O'Brien O, Kraus SD, Quintana-Rizzo E, Auster PJ (2021) Opening a Marine Monument to Commercial Fishing Compromises Species Protections. *Front Mar Sci* 8:645314. doi: [10.3389/fmars.2021.645314](https://doi.org/10.3389/fmars.2021.645314)
- Roberts JJ, Best BD, Dunn DC, Treml EA, Halpin PN (2010) Marine Geospatial Ecology Tools: An integrated framework for ecological geoprocessing with ArcGIS, Python, R, MATLAB, and C++. *Environmental Modelling & Software* 25:1197–1207. doi: [10.1016/j.envsoft.2010.03.029](https://doi.org/10.1016/j.envsoft.2010.03.029)
- Roberts JJ, Best BD, Mannocci L, Fujioka E, Halpin PN, Palka DL, Garrison LP, Mullin KD, Cole TVN, Khan CB, McLellan WA, Pabst DA, Lockhart GG (2016) Habitat-based cetacean density models for the U.S. Atlantic and Gulf of Mexico. *Scientific Reports* 6:22615. doi: [10.1038/srep22615](https://doi.org/10.1038/srep22615)
- Roberts JJ, Mannocci L, Schick RS, Halpin PN (2018) Final Project Report: Marine Species Density Data Gap Assessments and Update for the AFTT Study Area, 2017-2018 (Opt. Year 2), Document Version 1.2. Duke University Marine Geospatial Ecology Lab, Durham, NC
- Roberts JJ, Yack TM, Halpin PN (2023) Marine mammal density models for the U.S. Navy Atlantic Fleet Training and Testing (AFTT) study area for the Phase IV Navy Marine Species Density Database (NMSDD), Document Version 1.3. Duke University Marine Geospatial Ecology Lab, Durham, NC
- Robertson FC, Koski WR, Brandon JR, Thomas TA, Trites AW (2015) [Correction factors account for the availability of bowhead whales exposed to seismic operations in the Beaufort Sea](#). *Journal of Cetacean Research and Management* 15:35–44.
- Ryan C, Boisseau O, Cucknell A, Romagosa M, Moscrop A, McLanaghan R (2013) [Final report for trans-Atlantic research passages between the UK and USA via the Azores and Iceland, conducted from R/V Song of the Whale 26 March to 28 September 2012](#). Marine Conservation Research International, Essex, UK
- Silsbe GM, Behrenfeld MJ, Halsey KH, Milligan AJ, Westberry TK (2016) The CAFE model: A net production model for global ocean phytoplankton. *Global Biogeochemical Cycles* 30:1756–1777. doi: [10.1002/2016GB005521](https://doi.org/10.1002/2016GB005521)
- Stone KM, Leiter SM, Kenney RD, Wikgren BC, Thompson JL, Taylor JKD, Kraus SD (2017) Distribution and abundance of cetaceans in a wind energy development area offshore of Massachusetts and Rhode Island. *J Coast Conserv* 21:527–543. doi: [10.1007/s11852-017-0526-4](https://doi.org/10.1007/s11852-017-0526-4)
- Torres LG, McLellan WA, Meagher E, Pabst DA (2005) [Seasonal distribution and relative abundance of bottlenose dolphins, \*Tursiops truncatus\*, along the US mid-Atlantic coast](#). *Journal of Cetacean Research and Management* 7:153.
- Whitt AD, Powell JA, Richardson AG, Bosyk JR (2015) [Abundance and distribution of marine mammals in nearshore waters off New Jersey, USA](#). *Journal of Cetacean Research and Management* 15:45–59.
- Winn HE (1982) CeTAP: A Characterization of Marine Mammals and Turtles in the Mid- and North Atlantic Areas of the U.S. Outer Continental Shelf: Final Report. University of Rhode Island Graduate School of Oceanography, Kingston, RI
- Wood SN (2011) Fast stable restricted maximum likelihood and marginal likelihood estimation of semiparametric generalized linear models. *Journal of the Royal Statistical Society: Series B (Statistical Methodology)* 73:3–36. doi: [10.1111/j.1467-9868.2010.00749.x](https://doi.org/10.1111/j.1467-9868.2010.00749.x)
- Zoidis AM, Lomac-MacNair KS, Ireland DS, Rickard ME, McKown KA, Schlesinger MD (2021) Distribution and density of six large whale species in the New York Bight from monthly aerial surveys 2017 to 2020. *Continental Shelf Research* 230:104572. doi: [10.1016/j.csr.2021.104572](https://doi.org/10.1016/j.csr.2021.104572)